Novel Methods in Helicopter Performance Flight Testing

Arush, I.

DOI
10.4233/uuid:3ffd0639-a889-4882-8537-2f81a6671e8e

Publication date
2023

Document Version
Final published version

Citation (APA)
Arush, I. (2023). *Novel Methods in Helicopter Performance Flight Testing*. [Dissertation (TU Delft), Delft University of Technology]. https://doi.org/10.4233/uuid:3ffd0639-a889-4882-8537-2f81a6671e8e

NOVEL METHODS IN HELICOPTER PERFORMANCE FLIGHT-TESTING

Dissertation

for the purpose of obtaining the degree of doctor
at Delft University of Technology
by the authority of the Rector Magnificus prof.dr.ir. T.H.J.J. van der Hagen;
Chair of the Board for Doctorates
to be defended publicly on
Wednesday 8 November 2023 at
12:30 o'clock

by

Ilan ARUSH

Master of Science in Industrial and Management Engineering,
Ben-Gurion University, Israel
born in Rehovot, Israel

This dissertation has been approved by the promotors.

Composition of the doctoral committee:

Rector Magnificus,	chairperson
Prof.dr.ir. M. Mulder	Delft University of Technology, promotor
Dr. M.D. Pavel	Delft University of Technology, promotor

Independent members:

Prof.dr.ir. G. Jongbloed	Delft University of Technology
Prof.dr. I. Yavrucuk	München University of Technology, Germany
Prof.dr. M. Gennaretti	Roma Tre University, Italy
Dr. L. Ingham	Sikorsky, a Lockheed Martin company, USA
Prof.dr. A. Gangoli Rao	Delft University of Technology, reserve member

The work described in this thesis has been carried out at the Control and Simulation section at Delft University of Technology and at the National Test Pilot School located in Mojave, California.

Keywords: Multivariable Polynomial, Singular Value Decomposition, Corrected Variables, Non-Dimensional Variables, Helicopter Performance, Flight Testing, Optimization under Constraints

Cover design: Ilan Arush. Photos courtesy of the National Test Pilot School, Mojave California

Printed by: Ipskamp Printing, the Netherlands

ISBN: 978-94-6473-231-3

An electronic version of this dissertation is available at
http://repository .tudelft.nl/.

To my beloved family
Shoshi, Ofek and Maya

CONTENTS

List of Figures

List of Tables

Nomenclature

$\mathbf{A}$	Matrix containing numerical regressors
$\mathbf{A_d}$, $\mathbf{A_{disk}}$	Main-rotor disk area
$\bar{c}$	Averaged chord length (main-rotor blades)
c_{d_0}	Zero-lift drag coefficient (main rotor blades)
$C_P \equiv \frac{P}{\rho_a A_d (\omega R)^3}$	Coefficient of power (non-dimensional)
$C_W \equiv \frac{W}{\rho_a A_d (\omega R)^2}$	Coefficient of weight (non-dimensional)
$CNg \equiv \frac{Ng}{\sqrt{\theta}}$	Corrected engine compressor speed
$CSHP \equiv \frac{SHP}{\delta\sqrt{\theta}}$	Corrected engine output power (shaft horse power)
$CTGT \equiv \frac{TGT}{\theta}$	Corrected engine temperature (turbine gas temperature)
$CW_f \equiv \frac{W_f}{\delta\sqrt{\theta}}$	Corrected engine fuel flow
D	Main rotor blade aerodynamic drag force
$\vec{E}_r\big\vert_i$	Prediction error vector; difference between model (i) to actual measured power
$\overline{E}_{R_{(j)}}$	Mean of absolute power prediction errors for sortie (j)
M	Mach number
Ng	Gas turbine engine compressor speed
P	Total power required for flight
p_a	Ambient air static pressure
p_o	Standard sea-level air pressure (14.7 psi)
R	Main-rotor radius
R_{air}	Specific gas constant for air (=287 J/Kg·K)
SHP	Engine output power (shaft horse power)
S_{x_i}	Standard deviation in sampled variable X_i
S_{ref}	Aerodynamic drag reference area
T	Thrust produced by the main rotor system
T_a	Ambient air static temperature
T_o	Standard sea-level static air temperature (288.15K)
TGT	Engine temperature (turbine gas temperature)
TRQ	Engine output shaft torque
V_{CW}	The main rotor chord wise velocity
V_{ih}	Induced velocity in a hover (average), main rotor disk
Vi(r)	Induced velocity at blade station r
V_T	True airspeed
W	Helicopter gross-weight
W_f	Engine fuel-flow
X_{cg}	Helicopter longitudinal center of gravity location
Z, (Z')	Corrected variables matrix (normalized)
a	Speed of sound

a_i, b_i, c_i	Generic single variable polynomial coefficients
b	Main-rotor number of blades
$\vec{\boldsymbol{b}}$	Vector representing measured CSHP
f_e	Fuselage equivalent flat-plate area for drag
f_i	Engine multivariable regressors, i=1,2,3,…
g_j, h_k	Inequality constraints, Equality constraints
ki	Induced power correction factor
q	Dynamic pressure
$r_{x,y}$	Linear correlation coefficient between two variables x,y
$\boldsymbol{t_i}$	Test-statistics of model (i) prediction errors
$\alpha_j^i, \{\gamma_i\}, \{\beta_i\}$	Generic multivariable polynomial coefficients
γ	Heat capacity ratio for air (=1.4, non-dimensional)
λ_i, η_i	Lagrange multipliers (equality constraints, inequality constraints)
$\boldsymbol{\delta = P_a / P_0}$	Static pressure ratio (non-dimensional)
η_m	Main rotor mechanical efficiency
$\boldsymbol{\theta = T_a / T_0}$	Static temperature ratio (non-dimensional)
Θ	Main rotor blade pitch angle
$\mu \equiv \frac{V_T}{\Omega R}$	Advance ratio (non-dimensional)
μ_i	Mean value of prediction errors, model (i)
$\boldsymbol{\rho_a}$	Ambient air static density
$\boldsymbol{\rho_o}$	Standard sea level static air density (1.225 kg/m^3)
$\Sigma, (\Sigma)$	Singular values matrix of Z (normalized)
$\boldsymbol{\sigma = \rho_a / \rho_0}$	Static density ratio (non-dimensional)
$\sigma_i \quad (i=1,2,...,r)$	Singular values of a generic matrix of rank 'r'
$\boldsymbol{\sigma_R = \frac{b\bar{c}}{\pi R}}$	Main-rotor solidity ratio (non-dimensional)
ψ	Main rotor blade azimuth angle
$\boldsymbol{\psi_i}$, $\boldsymbol{\pi_i}$	Generic non-dimensional (ND) variable
$\boldsymbol{\psi_i^*, \pi_i^*}$	Generic corrected variable (ND for a specific helicopter type)
Ω,ω	Main-rotor angular speed

Abbreviations

BET: Blade Element Theory

BEMT: Blade Element Momentum Theory

CFD: Computational Fluid Dynamics

CMIV: Constant Momentum Induced Velocity

CSHP: Corrected Shaft Horse Power

CTGT: Corrected Turbine Gas Temperature

CV: Corrected Variable

CVSDR: Corrected Variables Screening using Dimensionality Reduction

DL: Disk Loading

EFPA: Equivalent Flat Plate Area

FAA: Federal Aviation Administration

FM: Figure of Merit

FW: Fixed Wing

GTE: Gas Turbine Engine

HIGE: Hover In Ground Effect

HOGE: Hover Out of Ground Effect

HUMS: Health and Usage Monitoring System

ISA: International Standard Atmosphere

KKT: Karush Kuhn Tucker

LSV: Left Singular Vectors

MBB: Messerschmitt Bölkow Blohm

MPOC: Multivariable Polynomial Optimization under Constraints

MR: Main Rotor

NTPS: National Test Pilot School

PD: Principal Dimension

PDF: Probability Density Function

PL: Power Loading

PS: Problem Statement

RQ: Research Question

RSV: Right Singular Vectors

RW: Rotary Wing

SHP: Shaft Horse Power

SSL: Standard Sea Level

SVD: Singular Value Decomposition

TPP: Tip Path Plane

TR: Tail Rotor

Summary

Flight test engineering is an interdisciplinary science that gathers flight-test data and develops methods with the objective of evaluating an aircraft or an airborne system in its operational flight environment. The need for flight testing emanates as a necessary effort that complements ground-based verification activities such as wind-tunnel testing, simulators and computational modelling. Flight testing is a broad field that involves many disciplines. Performance flight testing is one discipline that is responsible of providing answers to questions like: How high can the aircraft fly? How fast can it fly? How much power does the aircraft need in order to sustain specific flight conditions of gross-weight, altitude and ambient air temperature? Or How long can the aircraft remain airborne before it runs out of gas (or electric power)? A profound data base for the performance of any type of aircraft is essential for their safe and efficient operation.

This thesis focuses on performance flight-testing methods for conventionally-configured helicopters, i.e., those that employ a single main rotor to generate lift and thrust, and a single tail rotor to counter-act the torque effect of the main rotor. More specifically, the scope of this research was limited to gas-turbine available power testing and power required for out of ground effect (OGE) hover and power required for level-flight (AKA cruise flight). The research was limited to the execution of up to ten flight test sorties on two types of helicopters; the Bell Jet-Ranger and the MBB BO-105 helicopters, both normally used for training at the National Test Pilot School (NTPS) in Mojave, California.

The goal of this thesis is to develop new and improved flight-test methods to rectify existing problems associated with the conventional methods. The conventional method for the maximum available power of a gas-turbine relies on three independent, single-variable polynomials that often yield poor prediction accuracy that sometimes even defy basic engineering concepts. The conventional method for OGE hover performance is overly simplified and neglects important blade non-linear effects. This results in inaccurate empirical models for hover performance representation. The

conventional flight-test method for level-flight performance incorporates several drawbacks which not only make the execution of flight-test sorties inefficient and time consuming, but also compromise the level of accuracy achieved. This conventional level-flight method fails to specifically address non-linear effects such as blade-tip compressibility and drag-divergence that often results in inaccurate predictions, especially at high altitude and low air temperature conditions.

The research intended to develop new flight-test methods for the available power of a gas-turbine engine and for the power required for hover and level-flight. Both new methods are based on multivariable polynomial approach. The research was initiated with the development of a new method for the maximum available power of a gas-turbine engine. A novel method, referred to as the 'Multivariable Polynomial Optimization under Constraints' (MPOC), was developed. This method seeks for a third order multivariable polynomial to describe the engine output power as a function of the other three variables of the engine (compressor speed, temperature and fuel-flow). The maximum available engine power is realized by solving an optimization problem of maximization under constraints. For this optimization, the Karush-Khun-Tucker (KTT) method was used successfully. For the exemplary BO-105, the standard deviation of the output power estimation error was reduced from 13 hp (conventional method) to only 4.3 hp by using the proposed method. Expanding the flight-test data base to include seven different engines reveals that the multivariable polynomials approach of the proposed method performed much better with all seven engines, as compared to the conventional single-variable approach. The *maximum* average prediction error was only 0.2% as compared to a maximum average prediction error of 1.15%, yielded by the conventional method.

The research effort conducted for the OGE hover performance was concluded successfully with the development of the novel "Corrected Variables Screening using Dimensionality Reduction" (CVSDR) method for hover performance. This novel method combines fundamental dimensional analysis to generate a list of candidate corrected-variables (CVs) to represent the hover performance problem, then screens for the most essential ones by means of dimensionality reduction, implemented by

singular-value-decomposition (SVD). This phase of the research was executed with four sorties on the Bell Jet-Ranger helicopter and produced a total of five conclusions. The most significant conclusion was that power predictions of the CVSDR method were 1.9 times more accurate than the conventional method. At the 95% confidence level, the CVSDR method deviated by an average of only 0.9 hp (0.3% of the maximum continuous power of the example helicopter) from the actual power required to hover, whereas power predictions from the conventional method deviated by an average of 1.7 hp.

The final phase of the research concentrated on developing a new flight-test method for the level-flight regime. This effort spanned over five distinct sorties using the BO-105 helicopter. Similar concepts used for the hover performance testing were expanded and adapted for level-flight performance flight testing. The CVSDR method for level flight performance can be regarded (abstractly) as an expansion of the CVSDR method for OGE hover into a higher dimensional space. This phase of the research was aimed at addressing five research questions and yielded ten conclusions. The top three conclusions were that (1) the power predictions accuracy achieved using the CVSDR method for level-flight was nearly 21% better (on average and at the 95% confidence level), as compared to the prediction accuracy yielded from the conventional method. (2) the CVSDR method made planning and execution of flight-test sorties more efficient and time conserving. It is estimated to reduce flight-time for data gathering by at-least 60%, and (3) the CVSDR method is not restricted by the high-speed approximation, hence is also appropriate for the low-airspeed regime, and can potentially bridge the empirical modelling gap between the hover and level-flight regimes.

The novel flight-test methods developed within this research (the MPOC for the available power of a gas-turbine engine and the CVSDR for OGE hover and level-flight performance) are recommended to be used by the helicopter flight-testing community, as they were shown to increase accuracy and promote execution efficiency.

This thesis produced six recommendations concerning possible future expansion of the work already done during the current research. These include an expansion of the CVSDR method into more areas of performance testing like vertical and forward flight climb, partial power and unpowered descent, etc. Another continued research recommendation relates to the applicability and efficiency of the CVSDR method to relevant vertical-lift aircraft that combine both RW and FW characteristics. It is also recommended that continued research look into the potential and feasibility of employing the CVSDR method for empirical modelling used by Health and Usage Monitoring Systems (HUMS) installed in helicopters.

If you are in trouble, an airplane can fly over and drop flowers, but a helicopter can land and save your life.

Igor Ivanovich Sikorsky

1 INTRODUCTION

1.1 BACKGROUND AND RELEVANCE

Flight test engineering is an interdisciplinary science that gathers flight-test data and develops methods with the objective of evaluating an aircraft or a system in its operational flight environment. The need for flight-testing means that the system or the vehicle under testing requires accurate and efficient assessment of its characteristics and performance while operating in its flight environment, rather than just relying on the results of ground-based verification methods such as wind tunnels, simulators, and software models [1]. There are many disciplines involved in flight testing based on the nature of the questions in search. Such ones include, for example, performance assessment, structural integrity testing, stability, and handling-qualities evaluation, etc. Performance flight-testing is an expensive activity that requires efficient and accurate methods for determining the aircraft performance in its certified flight envelope and under a wide range of atmospheric conditions. Such methods involve careful considerations regarding testing techniques and flight-test data analysis.

Accurate performance prediction of any aircraft is essential for a safe and efficient operation of the air-vehicle. Knowing, in advance and with high level of confidence, the answers to questions like "how high can the aircraft fly under specific atmospheric conditions and gross weights? How fast can the aircraft fly? How long can the aircraft remain airborne before it runs out of gas?" etc., are essential for ensuring safety of flight and mission compliance. Although aircraft manufacturers provide early-stage aircraft performance predictions, those are normally based on

practical engineering simplifications and assumptions. Performance validation through an expensive and lengthy phase of flight-testing is inevitable.

Conducting a performance flight-test campaign is not limited to new aircraft programs. Performance flight-testing programs are also required during the life cycle of an aircraft. It is common-practice for aircraft operators to design and implement modifications that alter the aerial-vehicle baseline performance. These modifications can be limited in scope or even a full-scale upgrade programmes, initiated by either economic, political, or operational reasons. The helicopter is no exception in this regard. This type of 'low and slow' aircraft requires efficient and accurate performance flight-testing methods, either to be used by the manufacturers, or by the common operator (civilian or military) for post productions modifications and upgrades. Moreover, the limited flight envelope of the helicopter, as compared to the fixed-wing airplane, gives its operators the confidence and motivation to implement post-production structural modifications that warrant limited-scope performance flight-test campaign [2-6].

The performance charts and tables published by the helicopter manufacturers are based on a certain available power level. As explained in Subsection 1.2.1 hereinafter, the maximum available power out of the engine(s) deteriorates as the engine(s) matures and accumulates an increasing number of working hours. For this reason, the published performance of the helicopter is based on the minimum allowed level of the available power, i.e., just when it is time for the engine(s) to be overhauled. It is common for borderline missions to evaluate the feasibility of a specific helicopter to execute the specific challenging mission. For this, the operator needs to execute ad-hoc performance flight testing using the specific helicopter in order to conclude about mission performance compliance. Accurate and efficient performance flight testing methods are of high relevance for helicopter operators who wish to know the precise performance of their particular helicopter.

1.2 HELICOPTER PERFORMANCE

One might wonder what does 'helicopter performance' exactly mean? According to Cambridge dictionary, performance is defined as: "how well a person, machine, etc. does a piece of work or an activity". The Collins dictionary defines someone's or something's performance as: "how successful they are or how well they do something". According to Meriam-Webster dictionary: "PERFORM implies action that follows established patterns or procedures or fulfils agreed-upon requirements and often connotes special skill". The previous section has already alluded that 'helicopter performance' has something to do with answering questions like how high can the helicopter fly? How heavy can it hover? How long can it stay airborne? etc. The FAA [7] defines aircraft performance as: "a term which is used to describe the ability of an aircraft to accomplish certain things that make it useful for certain purposes". It continues and provides examples like the ability to carry heavy loads or to fly at high altitudes. Definitely, not a sharp and elegant definition for aircraft performance. Prouty [8] also struggles with this performance definition and provides the following explanation instead; helicopter performance analysis is made to answer the questions: How high? How fast? How far? How long? The results of the analysis may be used in design trade-off studies, in a pilot's handbook, in a set of military standard aircraft characteristics charts, or in a sales brochure. Another explanation for helicopter performance is provided by Gessow & Myers (1967) [9]: "The precise estimation of helicopter performance depends on an accurate determination of the thrust produced and the power required by the rotor in those conditions" (p. 66). Leishman (2006) [10] explains the term 'helicopter performance' in the introduction to the performance chapter as: "the estimation of the installed engine power required for a given flight condition, determination of maximum level flight speed, evaluation of the ceiling (in and out of ground effect), or the estimation of the endurance or range of the helicopter".

The previous definitions and explanations for helicopter performance draw a clear distinction between two parts of this term. One is the amount of ***power available*** for use by the helicopter. The other is the amount of ***power required*** to sustain any

specific flight condition. These two parts constitute the term helicopter performance for flight-testing. The power available is provided by the power-plant installed in the helicopter. This power-plant can be based on a single-engine or on a multi-engine configuration. The power required is the amount of power needed to maintain the helicopter under a specific flight and ambient conditions. The power available and power required are independent of each other and can be visualized as the two hands of a scale, the performance scale. As long as the amount of power generated by the power plant is equal to or larger than the power required for the specific flight conditions, the performance of the mission is feasible.

1.2.1 Available Power

Commercial and military helicopters are powered by mainly two types of engines: reciprocating (piston) engines and gas-turbine (GT) engines. In recent years, few programs were conducted to demonstrate and study the feasibility of use of electric engines in helicopters. The Firefly program introduced by Sikorsky innovations in 2010 is a good example to these types of technology demonstration programs [11]. Although some progress was made with the idea of electric propulsion of helicopters, there is still a way to go before electric propulsion turns into a common way to power helicopters for all their types of missions. The use of gas-turbine engines is far more popular than the use of reciprocating engine in helicopters. The superior ratio of power to weight of the gas-turbine engine, makes it a better choice when it comes to medium to large types of helicopters. For small size and light helicopters, the piston engine might be considered. According to Moon and Yakovlev [12] in 2018 the gas-turbine engine helicopters accounted for 69.1% of all in-operation helicopters worldwide. This unrivalled popularity of the gas-turbine engine, as the preferred propulsion system for helicopters, motivates development of efficient flight-testing methods that facilitate accurate prediction of installed gas-turbine output power under a wide range of atmospheric conditions.

Although all engine manufacturers measure their engine performance ('bench testing') and provide charts that describe the engine output power under various ambient conditions ('engine deck'), there is still a necessity for flight-testing methods to measure the ***actual installed*** gas-turbine engines output power. The following are two main reasons to support this necessity and provide motivation to develop new methods for gas-turbine engine performance flight testing:

1) The performance of a gas-turbine engine once installed in any type of a helicopter, is different from its performance measured by the engine manufacturer on a test-bench. Each helicopter type imposes specific levels of degradation in engine output power as compared to the same exact engine, uninstalled original performance. This is referred-to as the engine ***installation loss***. According to Prouty [8], there are various contributors to this degradation in the output power of an installed engine, as compared to its performance outside of a helicopter. One of them is the engine inlet structure element. The purpose of the inlet on any type of aircraft is to slow-down the air flow prior it enters the engine. This deceleration process in the inlet involves loss in total pressure due to friction and increase in static temperature, due to exhaust re-ingestion [13,14] and installation of various heat-exchange devices. The alteration of the thermodynamic properties of the air enters the engine are a cause for up to 5% of power installation loss. In addition to power loss associated with inlets, many helicopters are fitted with 'particle-separator' systems designed to protect the gas-turbine engine by filtering the air before it gets into the engine. Taslim and Spring (2010) [15] show that 'particle-separator' systems reduce the available power by 3% to 10%. Another system installed on military helicopters and is responsible to high power loss (3-15%) is the infrared suppressor designed to protect the helicopter against IR missiles by lowering the IR signature generated by the engine(s) exhaust [16,17]. Finally for installation loss, is the power drained from the engine(s) via compressor bleed, for the benefit of particular helicopter on-board systems operation. This type of power loss can reach up to 20%. The engine performance as provided by the engine manufacturer, is not sufficient for the task of total helicopter performance determination. Explicit flight-testing of an ***installed*** engine output power is mandatory

for the total performance determination of any specific type of helicopter and even for the determination of engine installation-loss themselves.

2) The gas-turbine engine performance as published by the engine manufacturer represents a new gas-turbine engine. This is referred-to as a specification ('spec') engine or a 'commercial off-the-shelf' (COTS) engine. Any gas-turbine engine is ensured to deliver, as a minimum, the 'spec' engine performance. It is common for gas-turbine engine manufacturers to provide new engines with even better performance than the 'spec' engine. As the engine accumulates flight hours and matures, its performance degrades. This is the natural aging process of the gas-turbine engine. Once the engine performance reaches a well-defined, minimum level of performance it is taken-off from the helicopter and sent for overhaul. This minimum level of performance delivered by the engine is frequently defined as the 'reject-line' of the engine. This aging process of the engine is illustrated in Fig. 1.1. In this figure the available power which is the engine output power is represented as a function of the various engine parameters. The helicopter operator must know at any given phase of the gas-turbine life cycle the actual performance the engine possesses, and more importantly the margin of power it maintains above the minimum acceptable power (the reject-line). For this reason, the helicopter operator needs an explicit flight-testing method for the evaluation of the installed gas-turbine engine output power at any given phase of the life cycle of the engine; either newly installed in the helicopter or just prior for it to be retired and sent for overhaul.

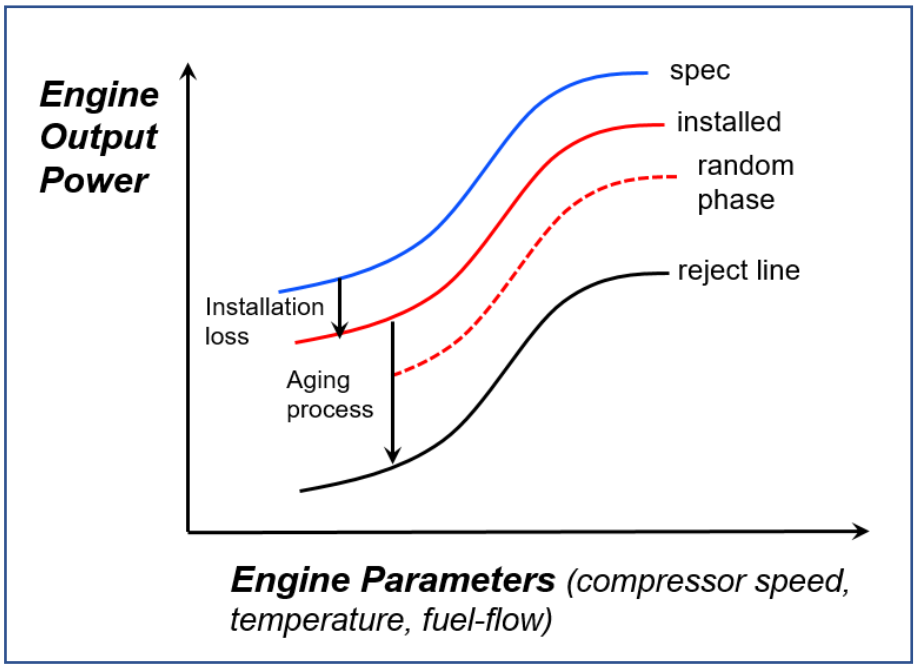

Figure 1.1. Gas-Turbine engine aging process. The engine performance drops once installed in a helicopter. As the engine accumulates flight-hours its performance decreases until it meets the reject line and is taken-off the helicopter to be overhauled.

1.2.2 Power Required

As previously stated, the power required is the amount of power needed to maintain the aircraft under specific flight and ambient conditions. The power required is independent of the available power, although the two are often evaluated simultaneously in flight-test campaigns. It is common practice within the flight-testing community to break down the power required envelope into the following disciplines [18-21]:

1) Hover performance, in and out of ground effect (HIGE/HOGE, respectively);

2) Vertical climb and decent performance;

3) Level flight performance; and

4) Forward flight climb and descent performance.

As stated in the subsequent Section 1.5 (Research Goals and Objectives), the current research is limited to ***only*** two performance disciplines out of the helicopter power required. These are the hover out of ground effect (HOGE) and the level flight, also known as 'cruise flight'. For this reason, only these two-helicopter power required subjects are discussed hereinafter.

1.2.2.1 Hover Performance

Igor Sikorsky, the legendary helicopter developer, was once asked by an anonymous scientist, a friend of his, when will the helicopter go faster than an airplane? In a documented interview Igor Sikorsky replied that it will never go faster than an airplane, but the helicopter will be able to do 'number of jobs no other airplane will be able to do', referring mainly to the remarkable ability of the helicopter to stabilize in a long-term hover. Indeed, the most distinguishing characteristic of a helicopter as stated by Leishman (2006) [22] and by Gessow and Myers (1967) [23] is its ability to steadily hover at any phase of its mission, given it has a sufficient power margin. Knowing the power required to hover throughout all mission phases is crucial for any helicopter flight crew.

For a conventional helicopter, i.e., one which employs a single main-rotor and a single anti-torque tail-rotor, the entire lift force in the hover is generated by the single main rotor. The set of main-rotor blades, referred to as rotary-wings, generate the lift required to hold the helicopter airborne. The main rotor is the helicopter major power consumer in a hover. The actual percentage of power it consumes changes in between types of helicopters and for a given type of helicopter it varies based on the gross weight, external configuration, and atmospheric conditions, but the 'golden-rule' for this power consumption percentage is about 85% [19,20,24]. The remaining ~15% of the hovering power is dissipated by the tail-rotor (5-10%), various accessory drives and transmission loss. Typical values of helicopter transmission loss at nominal rotor speed can be learnt from Lewicki and Coy (1987) [25] and Coy et al. (1988) [26]. The mechanical efficiency of a Black Hawk helicopter transmission at full power (2,828

hp.) was measured between 97.3% and 97.5% (depends on the lubricant oil inlet temperature). For the lower power rated transmission of the OH-58C helicopter (317hp.) measured transmission loss were between 1.2% and 1.7%. This relative portion of the total power consumed by the main rotor is known as the mechanical efficiency of the helicopter, denoted as (η_m). Since the main rotor is responsible for about 85% of the total power required in a hover, much attention is given by helicopter manufacturers for its blades design. Moreover, since the main rotor is the most significant power consumer in a hover, it dictates the conventional flight-test method for hover performance, as initially presented in Subsection 1.3.2 and thoroughly discussed in Chapter 2 of the thesis.

1.2.2.2 Level Flight Performance

The helicopter does not exhibit superior capabilities over other types of aircraft when it comes to level-flight ('cruise flight'). Nevertheless, a typical helicopter spends most of its flying time in the level-flight regime. The relative time while cruising varies based upon the type and the specific mission the helicopter was designed for. Porterfield and Alexander (1970) [44] analysed data from various types of helicopters and proclaimed that, on average, the helicopter spends 71% of its flight-time in level-flight. The FAA (2008) [45] provides different estimates for two exemplary gas-turbine helicopters. The first example is a utility business type which is estimated to spend 61% of its flight time while cruising, and the second example is for a transport helicopter which is estimated to spend 73% of its flight time in level-flight. Regardless of where this value for relative time spent in level-flight truly resides, the helicopter spends most of its airborne time while cruising. This observation makes the evaluation of level-flight performance utterly important in any new or modified helicopter performance flight-test campaign.

The power consumed by a conventional helicopter in level-flight is composed out of three major components as illustrated in Fig. 1.2. These power components are the induced power, the profile power and the parasite (or parasitic) power. The first

two power terms are familiar from the hover domain, although their relative magnitudes significantly change from the hover, based upon the airspeed of the helicopter. The induced power, which is required for the creation of thrust, drops rapidly with the increase of airspeed. From constituting about 85% of the power required for hover, the induced power can drop to about only 10% of the total power required for level flight at a maximum allowed cruising airspeed of a conventional helicopter. The profile power, required to overcome the viscous effects between the blades and the air, increases with airspeed and even becomes the dominant power component, over a certain airspeed section. The parasite power component is due to fuselage drag and it increases rapidly with airspeed (cubic relationship). The parasite power is typically the dominant power component for a cruising helicopter at a high airspeed. The general behaviour of the power required for level flight has the shape of a 'bathtub', i.e., it decreases with airspeed increase until it gets to a minimum power level (referred-to as the 'bucket'), then the power level increases with airspeed, as it is dominated by the parasite and profile power components.

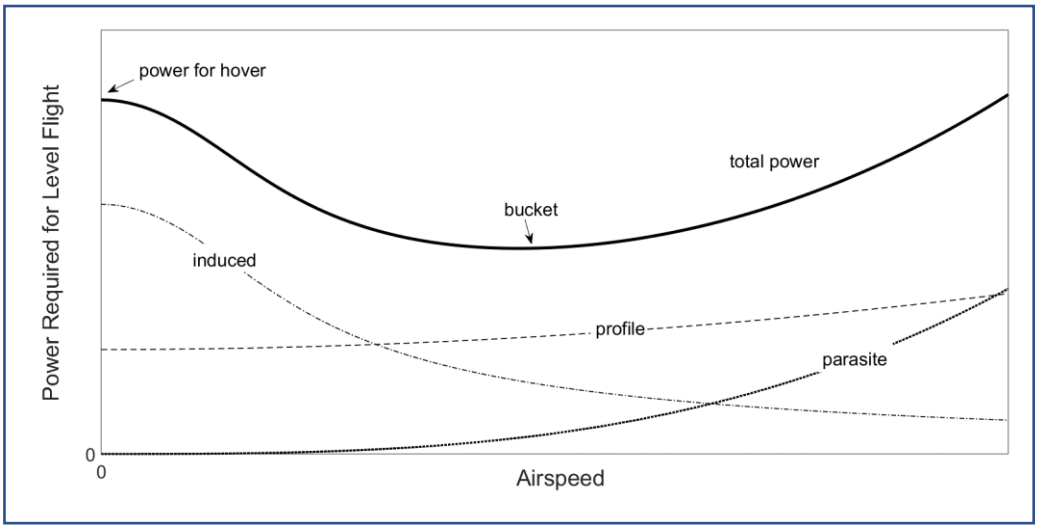

Figure 1.2. Power curve of a conventional helicopter in level flight. The power required in level flight comprises of three main components (induced, profile and parasite). The total power in level flight decreases with airspeed increase until it gets to a minimum ('bucket'). Past the bucket airspeed, the power required for level flight increases with airspeed increase.

A more comprehensive discussion about the power required for a conventional helicopter in level-flight is presented in Chapter 2, Helicopter Performance Theory and Conventional Testing Methods.

Following this brief introduction to the relevant aspects of helicopter performance, a short introduction to the applicable conventional performance flight testing is presented.

1.3 CONVENTIONAL METHODS FOR PERFORMANCE FLIGHT TESTING

The fundamental question troubling the helicopter performance flight-testers has always been how should the performance of the helicopter be tested? This broad question can be further narrowed down to the following set of specific questions; at which particular weights should the performance be measured? Under which combinations of atmospheric conditions? Is it possible to standardize the measurements obtained? Can the performance measurements in a specific flight be used to predict the performance under different flight conditions? These types of questions, which are essentials in performance flight-testing, can be addressed by using tools of dimensional analysis and the Buckingham PI theorem [66] which is commonly regarded as the fundamental theorem of dimensional analysis [67]. Evans [67] also claims that the Buckingham PI theorem is not widely known and that its full generality has not been exploited.

According to the Buckingham PI theorem, any physically meaningful problem with numerous dimensional parameters involved, can be reduced to a lesser number of significant non-dimensional parameters, based on the dimensions involved. The Buckingham PI theorem is used in many walks of science and engineering [68-73]. Zohuri [74] concludes its Chapter 1 by stating that many engineering problems are too complex to find a mathematically closed form of solution for them. In such cases, a type of analysis, which involves the dimensions of the quantities entering the problem may be useful.

The Buckingham PI theorem is no stranger to aerodynamics problems. In fact, this theorem can be used to justify the projection of conclusions from wind-tunnel

tests, performed using reduced size models, onto the actual true-size aircraft. The Buckingham PI theorem can also be used to justify the importance of the Reynolds number in flow dynamics study, or the importance affect the Mach number has on flight performance. Using dimensional analysis in flight-testing allows to collect data under specific atmospheric and flight conditions and to project the data to particular conditions of choice (interpolation and extrapolations). As a ground rule, the flight testers try to refrain, as much as possible, from carrying-out extreme extrapolations to their measured data. Breaking new grounds for the operators is the motto of the flight-testers. Interpolation of flight-test data, on the other hand, is always blessed. The competency of dimensional analysis to reduce the number of affecting variables and to support interpolation and extrapolation of data, has made it a popular tool in performance flight testing. By applying dimensional analysis tools, the flight-tester can answer all performance questions raised above and at the same time, significantly reduce the number of flight-test sorties required to quantify the performance of an aircraft throughout its flight-envelope.

1.3.1 Available Power Flight-Test Method

The current method widely used within the flight-test community for determining the available power any gas-turbine helicopter possess is based on the single-variable analysis [18-21]. According to this method, all four engine performance variables (output power, compressor speed, turbine gas-temperature and fuel-flow), accompanied with their corresponding atmospheric conditions, are recorded during steady engine operation conditions. For this, the helicopter is flown throughout its certified flight-envelope and under diverse atmospheric conditions.

Once a substantial database is gathered, it is analysed with the goal of evaluating the maximum power the engine is able to produce under various atmospheric conditions. This procedure is carried-out in two phases, the first (Phase I) is to generate a convenient mathematical model describing the dependency of the engine output power with all other engine performance variables (typically a third order polynomial).

Phase I can be regarded as uncovering and defining (mathematically) the specific engine 'rules of operation'. The second phase (Phase II) uses the 'rules of operation' to derive the maximum output power of the engine under a wide range of atmospheric conditions, and for the various engine power ratings i.e., the maximum continuous power, the maximum 5-minute take-off rating power, etc.

This conventional flight test method for the available power of a gas-turbine engine (GTE) is further discussed and demonstrated in Chapters 2 and 3 of this thesis. The deficiencies associated with this flight-test method originated the first question of this research (**RQ1**), as presented in Subsection 1.4.1. A comprehensive discussion about the deficiencies of this conventional method is presented in Chapter 3 of the thesis.

1.3.2 Hover Performance Flight Testing

The objective of hover performance flight-testing is to provide a detailed map of the actual power required to sustain the specific type of helicopter at a hover (either in or out of ground effect, IGE/OGE) for all certified gross-weights, external configurations, main-rotor angular speeds and the surrounding atmospheric conditions of air temperature, pressure, and density. This performance 'map' is traditionally presented in a format of a graph, or a set of synchronized graphs and plots. For this objective, the hover performance flight-tester task is to measure the actual power required for hover throughout the flight envelope. Since it is impractical to hover the helicopter in each combination of gross-weight, main-rotor angular speed, atmospheric conditions of pressure altitude and temperature, the flight tester applies means of dimension analysis, as previously discussed in the introduction of this Section (1.3). Applying means of dimensional analysis allows the flight-tester to reduce the number of planned flight test sorties to an achievable and practical number, and at the same time to provide a detailed performance map that covers the entire certified flight envelope of the aircraft.

The conventional, widely used, flight-test method for hover performance is derived from the non-dimensional form of the mathematical relationship that describes the power required for the main-rotor of a hovering helicopter. Since the main-rotor is the principal power consumer in a conventional helicopter hover (about 85%), it justifies enforcement of the ***main-rotor*** power model onto the ***helicopter as a whole***. The flight-test team is required to regress a mathematical model which relates between the power required for hover and the variables of gross-weights, main-rotor angular speeds and atmospheric ambient conditions (pressure, temperature and density). This empirical hovering model retrieved from flight-testing is then used, analytically, to create the detailed performance map mentioned above. This is the estimated power required to hover at any certified gross-weight and main-rotor speed, and under any combination of atmospheric conditions.

The conventional flight-testing method for hover performance is further discussed and demonstrated in Chapters 2 and 5 of this thesis. The deficiencies associated with this flight-test method originated the second question of this research (**RQ2**), as presented in Subsection 1.4.2. A comprehensive discussion about the deficiencies of this conventional hover performance flight-test method is presented in Chapter 5 of this thesis.

1.3.3 Level Flight Performance Flight Testing

The objective of level-flight performance flight testing is to provide a detailed map of the actual power required to maintain the specific type of helicopter at a level flight conditions, for all certified gross-weights, external configurations, main-rotor angular speed range and the surrounding atmospheric conditions of air temperature, pressure, and density. This performance 'map' is traditionally presented in a format of a graph, or a set of synchronized graphs and plots. Moreover, cross-referencing the power required in level flight to the fuel-consumption data base, as evaluated during the available power flight-testing phase (described in Subsections 1.2.1 and 1.3.1 above),

enables to define the helicopter 'best-effort' airspeeds, such as airspeed for maximum range and for maximum endurance. Similarly to the available-power and hover performance flight-testing, the conventional method for level-flight performance flight testing makes use of dimensional analysis concepts in order to reduce significantly the number of planned flight test sorties.

The conventional flight-test method for level-flight performance of a conventional helicopter is thoroughly discussed in the literature [8, 10, 18, 49, 76] and demonstrated in numerous flight test reports [6,77,78]. At its core, this flight-test method seeks for various discrete empirical relationships (for several non-dimensional gross-weights referred-to as coefficient of weight) between the non-dimensional forms of power (coefficient of power) and airspeed (advance ratio). For this, the flight-tester is required to perform many 'speed-runs' while maintaining the coefficient-of-weight at a constant value, a requirement that imposes execution difficulties, and is responsible to one of the method deficiencies. The acquired set of empirical models is then used, analytically, to predict the level flight performance of the tested helicopter at any certified gross-weight and main-rotor speed, and under any combination of atmospheric conditions.

The conventional flight-testing method for level-flight performance is further discussed and demonstrated in Chapters 2 and 6 of this thesis. The deficiencies associated with this flight-test method originated five research questions (RQ3, RQ4, RQ5, RQ6 and RQ7), as presented in Subsection 1.4.3. A comprehensive discussion about these deficiencies of the conventional method for level-flight performance flight-testing is presented in Chapter 6 of this thesis

1.4 PROBLEM STATEMENT

The conventional flight-testing method for the evaluation of conventional helicopter power available and power required for OGE hover and level-flight were briefly presented in the preceding Section 1.3. A comprehensive discussion and

thorough demonstration of these methods, accompanied with authentic flight-test data to highlight deficiencies, is presented in the subsequent Chapters 2, 3, 5 and 6 of this thesis. This section lists seven deficiencies associated with the conventional performance flight-testing method. These seven deficiencies constitute the problem statement (PS's) of this thesis, and derive the corresponding seven research questions (RQ's) this thesis attempts to address.

1.4.1 Available Power

The conventional method which is briefly described in Subsection 1.3.1 and thoroughly demonstrated in Chapter 2 (Subsection 2.3.1) relies on the intrinsic assumption of complete independency between all three limiting parameters of engine output power (compressor speed, turbine gas temperature and fuel-flow). This conventional method uses three independent, single-variable, empirical polynomials for the purpose of predicting the maximum available power of the installed engine, under a wide range of atmospheric conditions and engine power ratings (Eq.(2.34), (2.35) and (2.36)). The available power predictions are frequently inaccurate and can even contradict basic engineering rules. An example for this inaccuracy and fundamental rules contradiction is provided in Chapter 3, Subsection 3.3.2. The poor prediction performance of the conventional method can be mainly attributed to over simplification of the gas-turbine engine output power, as a linear combination of single-variable functions instead of the more realistic engineering problem it is, a multivariable type of a problem. Power prediction based on the simplistic single-variable approach fails to reveal the complex internal relationship between the power limiting parameters of the engine, i.e., the compressor speed, the gas-turbine temperature and the engine fuel-flow.

A designated BO-105 helicopter example presented and analysed in Chapter 3 demonstrates the deficiency of this conventional single-variable method. This BO-105 flight test sortie yielded a physically impossible behaviour that predicts a temperature-limited engine to produce more power under a higher ambient-air temperature.

Moreover, the power prediction errors using the three single-variable polynomials (Eq.(2.34), (2.35) and (2.36)) are substantial and should be reduced (standard deviation of 13hp, which is about 4% of the engine maximum continuous power).

PS1: The current flight-test method for the available power of gas turbine helicopters is based on a simplistic single-variable approach (instead of a multivariable approach) that often results in unacceptable power-prediction errors and physically unrealistic available power modelling.

RQ1: Can a novel flight-test method be developed for the available power of a gas-turbine helicopter, which demonstrates enhanced power prediction accuracy as compared to the conventional method?

1.4.2 Power Required for OGE Hover

The conventional flight-test method for OGE hover performance is based on the combined blade-element momentum theory (BEMT). This method is briefly described in Subsection 1.3.2 and thoroughly demonstrated in Chapter 2 (Subsection 2.3.2), with the supporting theory presented in Section 2.1. This flight-testing method seeks to find an overly simplified empirical model to relate between two non-dimensional variables. These are the coefficient-of-power (C_P) and coefficient-of-weight (C_W) as expressed by Eq.(2.41). The current method fails to explicitly address significant non-linear effects such as blades' compressibility issues and power increase due-to drag-divergence. These non-linear effects are more common for helicopters operating at high-altitude/low air temperature conditions. Any non-linear effects measured during hover performance flight-test sorties, are being averaged into one simplistic empirical model, instead of being handled specifically and exclusively for their effects.

PS2: The conventional flight-test method for OGE hover performance is overly simplified and does not account for rotor-blades non-linear effects. This conventional flight-test method often yields empirical models that fail to

accurately and consistently predict the total power required to hover, under a wide range of helicopter gross-weights and atmospheric conditions.

RQ2: Can a novel flight-test method for OGE hover performance of a conventional helicopter, which demonstrates enhanced prediction accuracy as compared to the conventional OGE hover method, be developed?

1.4.3 Power Required for Level Flight

The conventional flight-test method for helicopter level-flight performance is based on a simplified equation that describes the power required to sustain a helicopter in level-flight (Eq.(2.44)). This flight-test method is briefly described in Subsection 1.3.3 and thoroughly demonstrated in Chapter 2 (Subsection 2.3.3), with the supporting theory presented in Section 2.2. Although widely used and being taught in test-pilot schools around the world, this method incorporates several drawbacks which not only make the execution of flight-test sorties inefficient and time consuming, but also compromises the level of accuracy achieved. The following is a list of the five deficiencies associated with the current level-flight performance flight-test method. This list constitutes five problem statements (PS's) that derive five corresponding research questions (RQ's):

PS3: The conventional flight-test method for level-flight performance fails to specifically address non-linear effects such as blade-tip compressibility and drag-divergence. This often results in inaccurate predictions for the power required for level-flight, especially at high altitude and low air temperature conditions.

RQ3: Can a novel flight-test method be developed for level-flight performance of a conventional helicopter, which accounts for non-linear effects and demonstrates enhanced prediction accuracy as compared to the current level-flight method?

PS4: The conventional flight-test method for level-flight performance entails the executions of 'speed-runs' at constant coefficients-of-weights (Cw). This makes the method inefficient, cumbersome, and time-consuming. Moreover, the resulting empirical model is prone to elevated levels of inaccuracy since it is merely a set of single power curves for constant coefficients-of-weight, rather than a unified empirical model that accounts for the entire range of coefficients-of-weights.

RQ4: Can a novel flight-test method for level-flight performance, which is more convenient, efficient and time-saving than the current one, and produces a unified empirical model for a range of coefficient-of-weights, be developed?

PS5: The conventional flight-test method for level-flight performance is based on Glauert's high-speed approximation, hence making it irrelevant for the low-airspeed regime. The current flight-test method ignores the airspeed regime from the hover to about 40 kts. (depending on the particular helicopter type and configuration).

RQ5: Can a novel flight-test method for helicopter level-flight performance, that also includes the low-airspeed regime, be developed?

PS6: The conventional flight-test method for level-flight performance of a conventional helicopter incorporates no analytical means to account for the helicopter centre-of-gravity location.

RQ6: Can a novel flight-test method for helicopter level-flight performance, which includes analytical means to account for the centre-of-gravity location, be developed?

PS7: The conventional flight-test method for level-flight performance requires the flight-test crew to precisely adjust the main-rotor speed during the test. This requisite makes the method unsuitable for types of helicopter that do not allow for a trivial main-rotor speed manipulation by the flight-test crew.

RQ7: Can a novel flight-test method for helicopter level-flight performance, which does not require adjustment of the main-rotor speed, be developed?

1.5 RESEARCH GOALS AND OBJECTIVES

The general objective of this research is to develop new and improved flight test methods for the available and required power of a conventional helicopter. This general objective is further reduced to form the following set of particular and concise objectives, as imposed by the limitations and the scope of the research.

(1) Develop an enhanced flight-test method to evaluate the available power of a gas-turbine engine installed in a conventional helicopter. The proposed available-power method shall present an improved prediction accuracy, as compared to the current flight-test method. The proposed method shall rectify the identified deficiencies of the current method (PS1), as specified by RQ1 in Subsection 1.4.1 above. The proposed method shall demonstrate an improved prediction accuracy, as compared to the current flight-test method.

(2) Develop an original flight-test method to evaluate the power required for OGE hover of a conventional helicopter. The proposed OGE hover performance method shall address and rectify the identified deficiencies of the current method (PS2), as specified by RQ2 in Subsection 1.4.2 above. The proposed method shall demonstrate an improved prediction accuracy, as compared to the current flight-test method.

(3) Develop an original flight-test method for the level-flight performance of a conventional helicopter. The proposed level-flight performance method shall address and rectify the identified deficiencies of the current method (PS3, PS4, PS5, PS6 and PS7), as specified by RQ3, RQ4, RQ5, RQ6 and RQ7 in Subsection 1.4.3 above. The proposed method shall demonstrate an improved prediction accuracy, as compared to the current flight-test method.

1.6 RESEARCH LIMITATIONS AND SCOPE

The research is limited to gas-turbine engine powered conventional type of helicopters, i.e., those which employ a single main-rotor to generate lift and thrust and a single tail-rotor to counter act the torque effect of the main-rotor. Other types of helicopters that employ a different arrangement of rotors is not covered by this research. The research required planning and execution of flight-test sorties to enable comparison between the conventional and the proposed flight-test methods. Dedicated flight-test sorties were limited to only two types of helicopters, the Bell Jet-Ranger (Fig. 1.3) and the MBB (Messerschmitt-Bölkow-Blohm) BO-105 (Fig. 1.4), normally used for training at the National Test Pilot School (NTPS) in Mojave, California (https:\\www.ntps.edu). The comparison drawn between the proposed and the current flight-test methods is mainly based on flight-test data gathered from these two helicopters. A more detailed description of these two specially instrumented helicopters used for the research is presented in Appendix C. - Research Helicopters Description.

The scope of the research was limited to the execution of ten flight-test sorties, one single sortie for the available-power, four sorties for the hover performance and five sorties for level-flight performance flight-testing. The research sorties were launched from one single geographic location (Mojave) and were conducted under the prevailing atmospheric conditions. These research constraints restricted the varying range of essential parameters affecting helicopter performance, such as ambient air temperature, pressure altitude, centre of gravity location, etc.

The performance flight-test methods that were developed within this research are valid and applicable for any type of a conventional gas-turbine powered helicopter, configured with a single main rotor and a single tail rotor.

Figure 1.3. The Bell-Jet Ranger helicopter used for the research. Photo courtesy of the National Test Pilot School.

Figure 1.4. The MBB BO-105 helicopter used for the research. Photo courtesy of the National Test Pilot School.

1.7 METHODS ACCURACY COMPARISON

The main goal and objective of this thesis, as defined in Section 1.5 above, is to develop new, *more accurate* performance flight-test methods, as compared to the current conventional flight-test method. This section presents the procedure by which the prediction accuracy achieved by each method, is evaluated and compared.

For the ***available power*** method (Chapter 3), the same flight-test data of 34 stabilized engine points are used to establish the empirical models for the engine output power. First, using the conventional single-variable approach then by using the proposed multivariable approach. Power estimation errors result from each method are then compared for a trivial comparison. The more challenging task of the available power testing is the estimation of engine maximum available power under various day conditions. The maximum available power (continuous rating) of the helicopter is estimated for various atmospheric conditions using each method. The physical legitimacy of the two estimated maximum continuous power, under a wide range of atmospheric conditions is then compared.

The prediction accuracy attained by each method for the ***required power*** (Chapters 5, 6) is based on establishing an empirical model by using only a part of the flight-test data. The empirical model is then used to predict the helicopter required power under the conditions of the remaining flight-test data base, the data not used for the empirical model. Power estimation errors arise from each method are compared (literally), and by using hypothesis testing are projected from the particular measured case to the general case. For the OGE hover performance method (Chapter 5) an empirical model based on the first three sorties is used to predict the hover performance of Sortie 4. For the level-flight performance method (Chapter 6) a more elaborated comparison scheme, in two tiers, is executed. The first tier is using flight-test data from each sortie to predict the helicopter performance under conditions of the other three sorties (referred to as the single-sortie approach). The second layer of comparison is accomplished by predicting the helicopter performance in each one of the four sorties by using an empirical model based on data taken from the other three

sorties. This second-tier comparison scheme is referred to as the cluster of sorties approach.

1.8 THESIS OUTLINE

The thesis is structured into seven chapters in order to answer the seven research questions (RQ1 to RQ7 as specified in Section 1.4 above). This process of addressing the seven RQ's is illustrated in Fig. 1.5 and clarified hereinafter. In this Chapter 1 (Introduction) the reader is briefly introduced to helicopter performance theory and the relevant conventional flight-testing methods and their embedded deficiencies. This preliminary description of the relevant helicopter performance and the associated flight-testing methods is merely sufficient to allow the reader understanding the major goals and objectives of this research.

Chapter 2 (Helicopter Performance Theory and Conventional Testing Methods) provides a thorough discussion augmented with examples of the relevant helicopter performance and the associated conventional flight-test methods. This Chapter 2 serves as the literature review for the thesis and is crucial for a full understanding of the succeeding chapters that propose an original and improved flight-test method to address embedded deficiencies with the conventional flight-test methods. The substantial portion of this research effort is presented in Chapters 3 through 6. Chapter 7 concludes the thesis by providing summary remarks, reiterate the fulfilment of all research goals and objectives and offering recommendations for further research. The following is a short description of each chapter (3 through 7) and its role in the big scheme of the thesis:

Chapter 3 - A Multivariable Approach in Gas-Turbine Engine Flight-Testing. This chapter presents an improved flight-test method for the evaluation of the available power of installed gas-turbine engines in helicopters. The method called 'Multivariable Polynomial Optimization under Constraints' (MPOC) is demonstrated using flight-test data from a BO-105 helicopter and exhibits a better prediction

capability, as compared to the conventional flight-test method for the available power. Chapter 2 addresses research goal (1) of Section 1.5 and answers RQ1, as defined in Subsection 1.4.1.

Chapter 4 - A Singular Values Approach in Helicopter Flight-Testing Analysis. This chapter intends to further address research goal (1) of Section 1.5 by elaborating on the process of choosing between empirical models. More specifically, it deals with empirical multivariable polynomials that best represents the available power of a gas-turbine engine. This chapter is intended to complement the MPOC method presented and demonstrated in Chapter 3, and to provide the flight-test team a systematic and repeatable methodology to choose in-between various empirical models for the task of flight-test data representation. The proposed approach is based on the singular-value-decomposition (SVD) concept and is demonstrated by using gas-turbine engine flight-test data gathered from a variety of seven helicopters. One of the several conclusions of this chapter is that although the SVD approach is demonstrated for gas-turbine engine performance, it can and should be used for any type of helicopter performance flight-testing analysis where empirical models are evaluated. The method developed and presented in this chapter for gas-turbine engine performance, undertakes an essential role in the development of new flight-test methods for the hover and level-flight performance, as presented in Chapter 5 and Chapter 6 accordingly.

Chapter 5 – Hover Performance Flight-Testing Using Dimensionality Reduction Approach. This chapter presents an improved flight-test method for the evaluation of the power required to hover OGE. The method is based on concepts of dimensional-analysis and dimensionality-reduction to construct an effective and accurate empirical model for the OGE hover performance. The proposed method called Corrected Variables Screening using Dimensionality Reduction (CVSDR) is demonstrated using flight-test data from an instrumented Bell Jet-Ranger helicopter. The CVSDR method displays a better prediction accuracy, as compared to the conventional flight test method. Chapter 4 addresses research goal (2) of Section 1.5 and answers RQ2 as defined in Subsection 1.4.2.

Chapter 6 - Level Flight Performance Flight-Testing Using Dimensionality Reduction Approach. This chapter presents an improved flight-test method for the evaluation of the power required for level-flight. The method is based on similar concepts used for the improved CVSDR hover flight-test method (Chapter 5) but takes it further to higher dimensional space. The proposed CVSDR flight-test method for level flight performance is demonstrated using flight-test data from an instrumented MBB BO-105 helicopter. The proposed method is proved more accurate and more efficient as compared to the conventional flight-test method for level-flight. Chapter 6 addresses research goal (3) of Section 1.5 and answers RQ3, RQ4, RQ5, RQ6 and RQ7 as defined in Subsection 1.4.3.

Chapter 7 – Conclusions and Recommendations. The last chapter of the thesis opens with a conceptual discussion about the difference between the two flight testing approaches, that of the conventional methods and that of the proposed methods. Next, a concise list of 22 main conclusions drawn from the research is presented in the context of the research goals and objectives. The chapter ends with few recommendations about how this research can be further expanded.

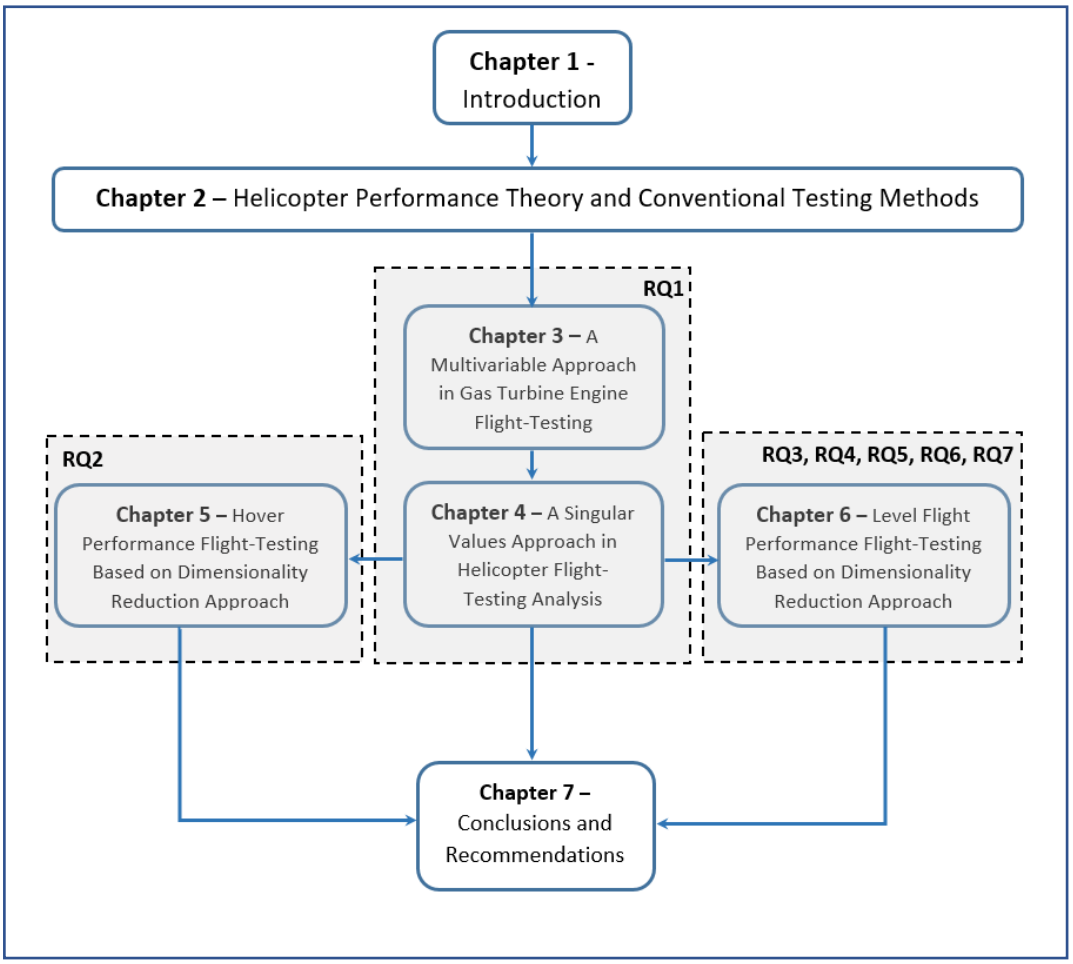

Figure 1.5. Thesis outline illustration. This flow-chart illustrates the structure of the thesis, how the various chapters are interrelated and serve for answering all research questions (RQ's).

1.9 THESIS PUBLICATIONS

The thesis is based on papers that have been (or are to be) published in peer-reviewed scientific journals and conference proceedings. The following is a list of the relevant publications:

Chapter 3 is based on the following papers:

(1) Arush I, and Pavel M.D. "Helicopter Gas Turbine Engine Performance Analysis: A Multivariable Approach." Proceedings of the Institution of Mechanical Engineers,

Part G: Journal of Aerospace Engineering, Vol. 223, No. 3, March 2019. https://doi.org/10.1177/0954410017741329

(2) Arush, I., & Pavel, M.D. (2018). "Flight testing and analysis of gas turbine engine performance: A multivariable approach." In C. Hermans (Ed.), Proceedings of the 44th European Rotorcraft Forum: Delft, The Netherlands, September 2018.

Chapter 4 is based on the following paper:

(3) Arush I, Pavel M.D; and Mulder M. "A Singular Values Approach in Helicopter Gas Turbine Engines Flight Testing Analysis." Proceedings of the Institution of Mechanical Engineers, Part G: Journal of Aerospace Engineering 234, no. 12 (2020): 1851–65. https://doi.org/10.1177/0954410020920060.

Chapter 5 is based on the following paper:

(4) Arush I., Pavel M.D., and Mulder M., "A Dimensionality Reduction Approach in Helicopter Hover Performance Flight Testing." Journal of the American Helicopter Society 67, no. 3 (2022): 129–41. https://doi.org/10.4050/JAHS.67.032010

Chapter 6 is based on the following paper:

(5) Arush I, Pavel M.D., and Mulder M. "A Dimensionality Reduction Approach in Helicopter Level Flight Performance Flight Testing." Journal of the Royal Aeronautical Society, First View 13 July 2023. https://doi.org/10.1017/aer.2023.57

The more you know, the more you know you don't know.

Aristotle

2 HELICOPTER PERFORMANCE THEORY & CONVENTIONAL TESTING METHODS

This chapter elaborates on the relevant two disciplines of the helicopter power required for hover and level-flight. The performance theory is demonstrated using arbitrary helicopter types, making the abstract concepts more practical for the reader to grasp. Once a sound foundation for the hover and the level-flight performance has been laid down, the conventional flight-testing methods are presented and illustrated by using authentic flight-test data.

2.1 HOVER PERFORMANCE

The power consumed by the main-rotor ($P_{M/R}$) of a hovering conventional helicopter is comprised out of two main terms as presented in Eq.(2.1). The relationship given by Eq. (2.1) involves the helicopter gross-weight (W), the ambient air density (ρ_a), the main-rotor disk area (A_d), the main-rotor blade zero-lift drag coefficient (Cd_0), the main-rotor radius (R), the main-rotor angular velocity (Ω) and a non-dimensional term (σ_R), defined as the 'solidity-ratio' of the main-rotor disk. As implied by its name, the solidity ratio describes how solid is the rotor disk, i.e., the relative disk area that is occupied by the blades. The first term of Eq.(2.1) is referred-

to as the induced-power (or the ideal-power) and was derived from the momentum concept. This term which represents the amount of power required to generate lift (or thrust) is comprised from the product of thrust (T), equals the helicopter weight (W) in a hover, and the ***uniform*** induced velocity (V_{ih}) across the disk (Eq.(2.2)). The expression for the constant induced velocity across the disk is based on linear-momentum conservation concept, first presented by Rankine in use of marine propellers in 1865 [27], later refined by Froude in 1878 [28] and generalized by Glauert in 1935 for aeronautical applications [29]. A detailed derivation of the uniform induced velocity through the hovering main-rotor disk (Eq. (2.2)) was presented by Prouty [33].

$$P_{M/R} = \underbrace{\sqrt{\frac{W^3}{2\rho_a A_d}}}_{induced} + \underbrace{\frac{1}{8} C_{d_0} \sigma_R \rho_a A_d \left(\Omega R\right)^3}_{profile} \tag{2.1}$$

$$v_{ih} = \sqrt{\frac{T}{2\rho_a A_{disk}}} = \sqrt{\frac{W}{2\rho_a \left(\pi R^2\right)}} \tag{2.2}$$

The second term in Eq. (2.1) is referred-to as the profile power and it represents the amount of power required to overcome the viscous effects between the main-rotor blades and the surrounding air. This second term is based on principles of blade element theory (BET). One should recognise that Eq. (2.1) relies on few simplifications such as a uniform induced-velocity distribution across the main-rotor disk, a constant zero-lift drag coefficient (Cd_0) and a constant chord length ($\overline{c}$) along the main-rotor blades.

Figure 2.1 (a) illustrates a hovering rotor-blade with a constant chord and length of R, rotating at a constant angular velocity (Ω). An arbitrary blade element distanced 'r' from the centre-of-rotation is subjected to a tangential velocity equals (Ωr), and an induced velocity (V_{ih}) which is assumed, for this preliminary approach, constant across the hovering disk.

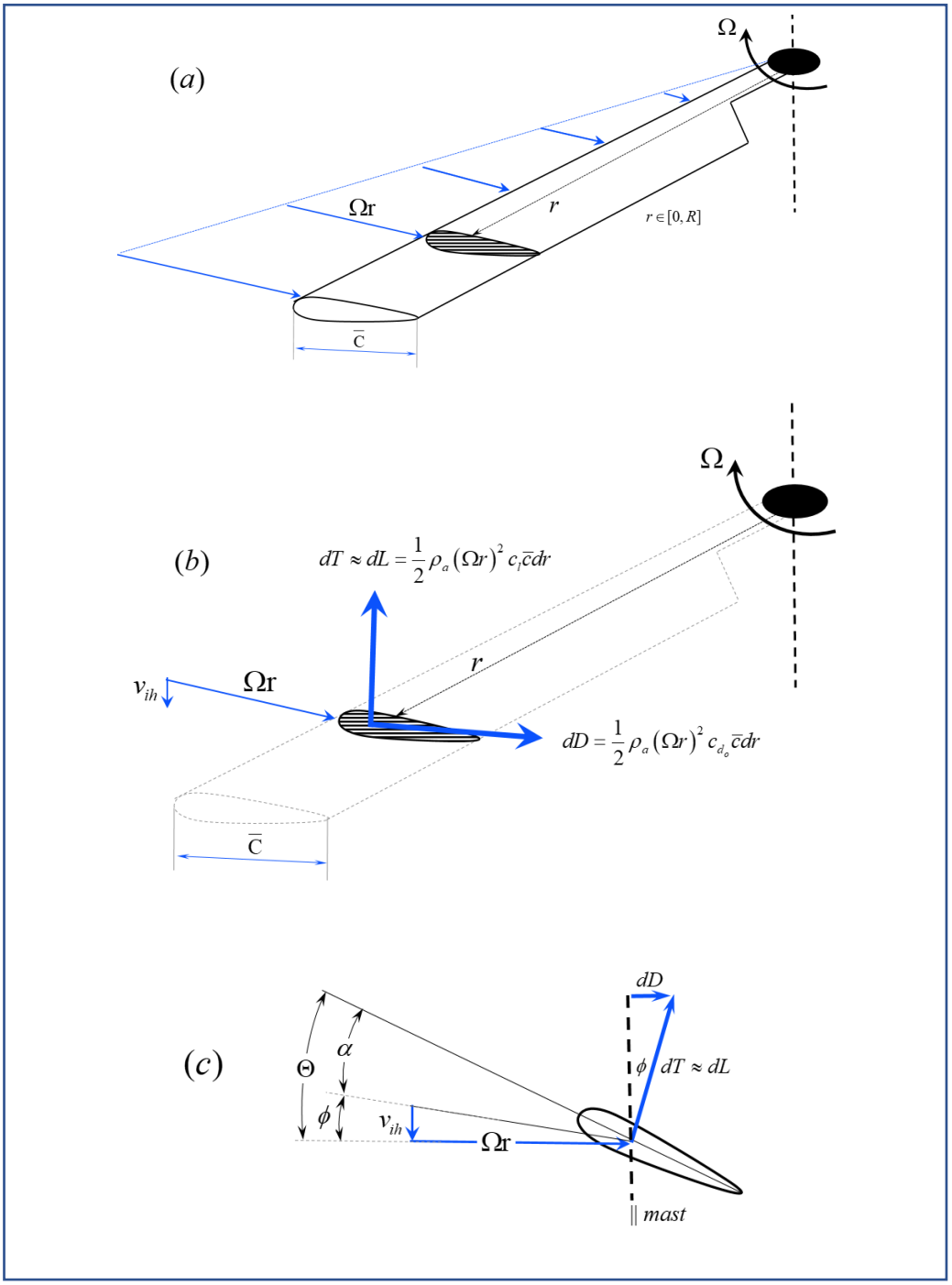

Figure 2.1. The main-rotor blade in a hover flight. The blade is subjected to a tangential velocity due to its rotation. The aerodynamic forces acting on each blade-element are integrated and used to estimate the induced and profile power required by the rotor disk at a hover.

In hover, the aerodynamic forces acting on this blade element are illustrated in Fig. 2.1 (b), (c) and are calculated as per the fundamental lift and drag terms for incompressible flow (Eq.(2.3)).

The power required to overcome the profile-drag is defined as the profile power and can be estimated by the mechanical work done by this profile-drag force per unit of time. This becomes a simple multiplication between the elementary profile-drag force (dD) and the tangential velocity as expressed in Eq. (2.4). Integrating along the span of a single blade (from zero to the blade length, R) yields the profile power of a single blade. The profile power for the whole rotor (Eq. (2.5)) is attained by multiplying the single-blade profile power by the number of blades (b) resulting in the profile power term presented in Eq.(2.1). Note that Eq.(2.5) is expressed by using the solidity ratio of the disk (σ_R).

$$dL = \frac{1}{2}\rho_a (\Omega r)^2 (c_l)(\bar{c}dr) \therefore dD = \frac{1}{2}\rho_a (\Omega r)^2 (c_{do})(\bar{c}dr) \tag{2.3}$$

$$dP_{profile} \equiv dD \cdot (\Omega r) = \frac{1}{2}\rho_a (\Omega r)^3 (c_{do})(\bar{c}dr) \tag{2.4}$$

$$P_{profile} = b\int_0^R dP_{profile}dr = \frac{1}{8}C_{d_0}\sigma_R\rho_a A_{disk}(\Omega R)^3 \therefore \sigma_R \equiv \frac{b\bar{c}}{\pi R} \tag{2.5}$$

Referring back to the induced power term presented in Eq.(2.1), the reader should appreciate it is attained by using a similar approach, as used for the profile power. The elementary induced power is calculated by taking the product of the lift (or thrust) and the induced velocity (V_{ih}). Since this induced velocity is assumed constant (for this simplistic approach where the actuator disk is used), integration along the blade and accounting for the number of blades (b) becomes utterly simple. The thrust generated by the disk which equals the helicopter gross-weight in a hover, is multiplied by the constant induced velocity (Eq.(2.2)). This results in the exact induced power term, as appears in Eq.(2.1).

The induced power term neglects elementary engineering information regarding the number of blades (b) and their shape. The uniform distribution of the induced-velocity across the disk (V_{ih}) represents the minimum possible induced power, or the 'best-case-scenario', as stated by Prandtl's lifting-line theory [30]. According to this 1921 era theory, the necessary and sufficient condition for minimum induced drag (and power) is that the downwash produced by the longitudinal vortices be constant along the entire lifting line, i.e., a constant profile of induced velocity across the rotor disk minimizes the induced power. This best-case scenario can be regarded analogous to the elliptical lift distribution of a fixed-wing aircraft.

A more realistic analysis of the hovering disk, that considers the number of blades (b) and their shape, was first presented by Gessow in 1948 [31]. This analysis, known as the combined blade element momentum theory (BEMT), treats the actuator disk as a combination of infinitesimally thin annuli (rings) of constant induced velocity profile. The practicality of this approach is that the induced velocity through the disk is only considered constant with respect to the blade station (r), regardless of the azimuth angle (ψ). This approach is more accurate compared to the previous analyses [27-29] that assume a uniform induced velocity throughout the disk area.

The quadratic equation in induced velocity (Eq.(2.6)) arises from equating the elementary thrust generated by an infinitesimally thin ring of the disk, using the two analytical approaches of conservation of linear momentum and blade-element theory (BET), illustrated in Fig. 2.1(c). The BET assumes a symmetrical blade cross-section and estimates the angle-of-attack (α) of each blade cross-section as the difference between the pitch angle (Θ) and the induced angle (Φ). This quadratic equation is then solved for a constant-chord blade, providing an explicit expression for the induced velocity through the hovering disk (Eq.(2.7)), for any blade station (r), as measured from the blade centre of rotation.

$$v_i^2 + \frac{bc\Omega c_{l_\alpha}}{8\pi} v_i - \frac{bcr\Theta\Omega^2 c_{l_\alpha}}{8\pi} = 0 \ \therefore \ r \in [0,R] \tag{2.6}$$

$$v_i(r) = \frac{bc\Omega c_{l_\alpha}}{16\pi}\left(-1+\sqrt{1+\frac{32\pi}{cbc_{l_\alpha}}r\Theta}\right) \;\therefore\; r\in[0,R] \tag{2.7}$$

It follows from Eq.(2.7) that maintaining a constant value for the product of the blade station and the pitch angle ($r\cdot\Theta$) along a constant-chord blade, ensures a uniform induced velocity distribution across the hovering disk. This, according to Prandtl's lifting-line theory, guarantees the minimal possible induced power in a hover [30]. One can easily identify the widely known 'ideal' blade twist profile (Eq.(2.8)) is merely this requirement for keeping the product of blade station (r) and blade pitch angle (Θ) constant along the span of the blade. Rotor blades with constant-chord and a variable pitch angle that follow the 'ideal' blade twist profile (Eq.(2.8)) yield a constant induced-velocity across the hovering disk which can be calculated precisely by using Eq.(2.2).

$$\Theta(r) = \frac{R}{r}\Theta_{tip} \;\therefore\; r \le R \tag{2.8}$$

As stated by Prouty [32], it is impractical to manufacture rotor blades with the 'ideal' geometric twist profile due to the pitch angle tends to infinity close to the root. Instead, most conventional blades are made with a variable pitch angle that follows a linear change (angle reduction of Θ_1) from the root to the tip. Although, not the 'ideal-twist' this linear geometric twist defined in Eq. (2.9) offers a practical method to substantially reduce the ***induced*** power of the helicopter at a hover. The other pitch angle (Θ_0) in Eq. (2.9) represents the collective pitch angle, commanded by the pilot. Prouty [32] states that in-general, it is fair to say that high values of main-rotor blade twist (Θ_1) produce good hover performance. This also reflects on the primary mission the helicopter was designed for. When designing blades, variations on the conventional linear twist distribution should be considered only for special reasons [32].

$$\Theta = \Theta_0 + \frac{r}{R}\Theta_1 \therefore \Theta_1 < 0,\; r \le R \tag{2.9}$$

An arbitrary example helicopter is selected for illustration purposes. This hovering helicopter weighs 18,000 lbs., has a 4 bladed main-rotor disk with an area of about 2,262 ft^2 and a blade tip speed of 725 fps. The blades have a constant chord length of 1.73 ft. and a linear pitch ***reduction*** (geometric twist) of 18° ($\Theta_1 = -18°$). The coefficient-of-lift to AOA (α) line slope is approximated as 2π rad^{-1}. The collective angle can be controlled by the pilot in a range between 9.5° to 25.9°. This constitutes the 'collective-stick' range provided to the pilot. Figure 2.2 presents the calculated parameters required to support the hover using the two types of blades twist, the first using the theoretical ideal-twist and the other by using the actual -18° linear twist. Numerical solution suggests that with a linear-twist of -18° the pilot must command a collective pitch angle (Θ_0) of about 22.6° to generate the precise amount of thrust needed for the OGE hover. This collective pitch angle command of the example helicopter is achieved by using about 79% of the total collective-control throw.

As shown in the left graph of Fig. 2.2, there are two crossings in pitch angle between the two types of geometric pitch schedules. The first is at a blade station of about 0.39 and the other at about 0.86. The theoretical pitch angle at the tip of the blade is 6.1° for the ideal-twist profile and 4.6° for the linear-twist. The induced velocity through the disk at the various blade stations is also presented (top-right graph of Fig. 2.2). While the ideal blade twist produces a constant induced velocity of about 41 fps. across the disk, the -18° linear twist profile yields a variable induced velocity, with a maximal value of about 45.4 fps. at the 0.63 blade station. The blade thrust-distribution in each case (ideal and linear) is calculated using Eq.(2.10), and presented in the bottom-right graph of Fig. 2.2. For simplicity, this estimation neglects blade tip loss. While the ideal blade twist yields a triangular thrust distribution, the -18° linear-twist generates a non-linear thrust distribution that peaks at a blade station of 0.8 with a maximal calculated value of 296.6 lbs./ft.

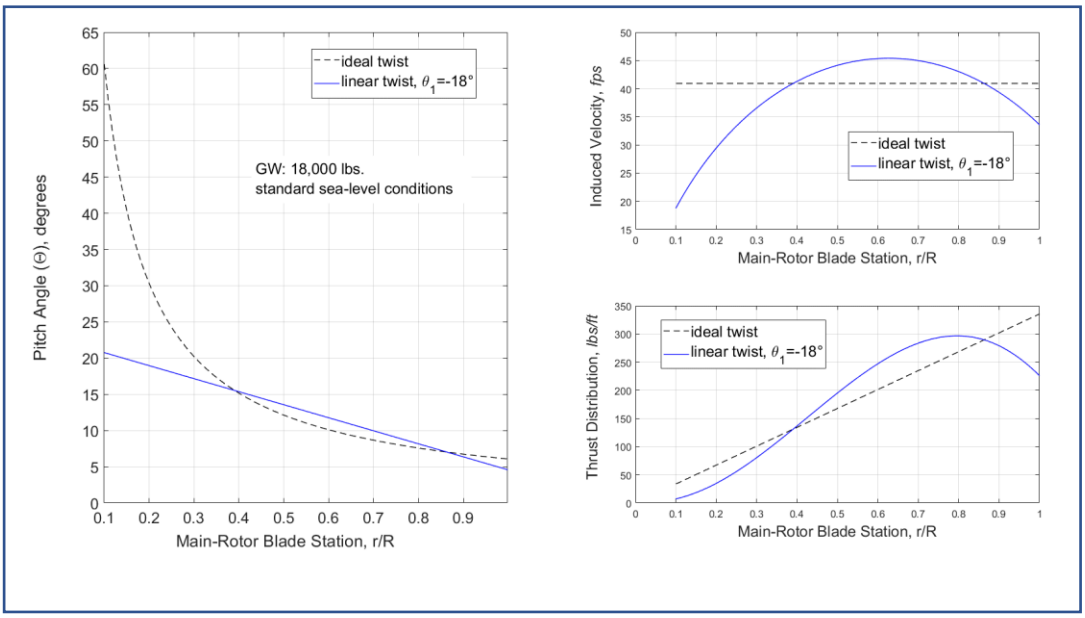

Figure 2.2. The ideal and a -18° linear blade twist in an OGE hover. The two blades pitch schedules are presented in the left. On the top-right a comparison between the induced velocities is calculated. The bottom-right graph provides a comparison between the cross-sectional thrust generated by each type of geometric twist.

$$\left.\frac{dT}{dr}\right|_{blade} = \frac{1}{2}\rho_a c(\Omega r)^2 c_{l_\alpha}\left(\Theta - \frac{v_i}{\Omega r}\right) \tag{2.10}$$

Next, the induced power required for each case of geometric twist is calculated and then compared. The induced power of each blade cross-section is calculated by taking the product of the thrust and the induced velocity for each blade element. Integration along the blade produces the induced power required for a single blade. The induced power for the entire main rotor is attained by accounting for the number of blades (b). This procedure is presented as Eq.(2.11). Notice that for the ideal-twist case, this integral is immediately reduced to a simple multiplication of the (constant) induced velocity by the total thrust produced by the rotor.

Figure 2.3 presents the estimated induced power required to support the specific OGE hover example, using the -18° linear-twisted blades rotor system. The bottom and top right graphs of Fig. 2.3 present, separately, the two factors of the induced power. These are the induced velocity distribution and the thrust distribution

as a function of the blade station. The left graph of Fig. 2.3 presents the induced power distribution which peaks at the 75% blade station with a value of 23.6 hp/ft. Integrating the power distribution along the blade provides an induced power of 342 hp per blade, and a total induced power of 1,368hp for the 4 bladed main rotor. In the case of ideally twisted blades, the required induced power is only 1,339 hp. As expected, a lower value compared to the linear-twist case, but not by much. For the particular hover case illustrated, the -18° linear-twisted blades require an induced-power increase of about 2.2% (29 hp), as compared to the ideal-twisted blades.

$$P_i = b\int_0^R v_i dT \tag{2.11}$$

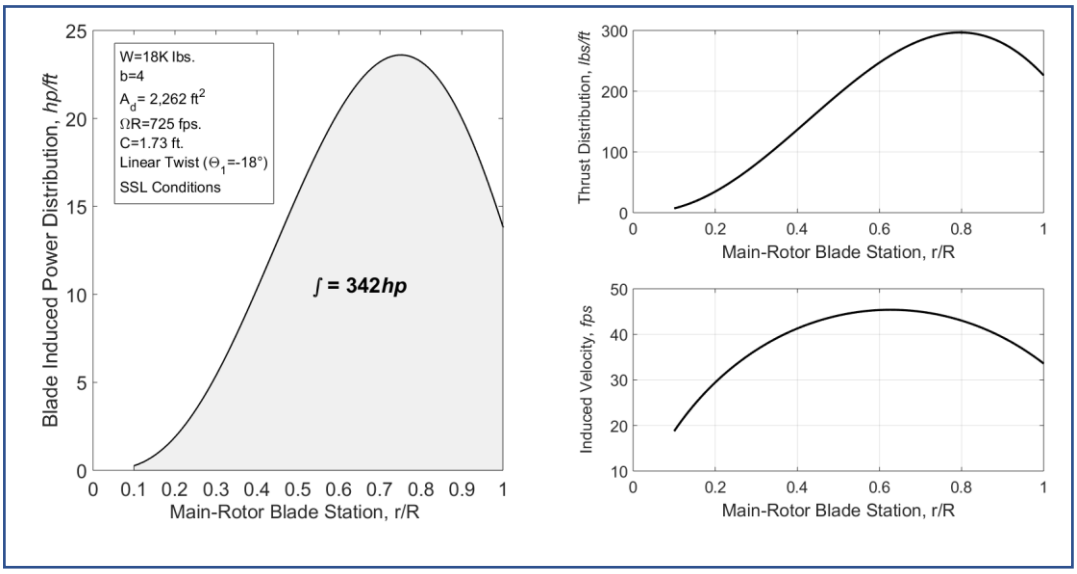

Figure 2.3. Induced power of a -18° linear-twisted blade in an OGE hover. The two factors of the induced power are presented on the right, the thrust distribution along the blade (top graph) and the induced velocity distribution (bottom graph). The left graph presents the induced power distribution along the span of the blade. The area under the curve represents the induced power required by the blade, under the specific OGE hover conditions.

The main rotor induced power in a hover is considerably larger than the profile power required by the blades (more than double). The ratio between the induced and the total power required for the main rotor at a hover is known as the 'Figure of Merit' (FM) of the rotor-system, as presented in Eq. (2.12)[33-35]. The FM, a value bounded

between zero and one, is used by helicopter designers to articulate about the aerodynamic efficiency of the hovering rotor. The higher the value is, the more efficient the rotor is for the hovering conditions. Typical maximum FM values for actual rotor systems at a hover range from 0.75 to 0.8 [36-38].

The relative quantities of induced and profile powers in hover are not constant and vary with altitude. As the hovering altitude increases, the air density decreases resulting in opposite tendencies of the induced and the profile power portions; the induced increases while the profile decreases. Figure 2.4 presents a typical breakdown of the power required to OGE hover by a 22 ft. in radius and 6.5% solidity-ratio (σ_R) main rotor of an arbitrary 8,500 lbs. helicopter. This ***estimated*** power is presented for a standard day condition (ISA), from sea-level to 10,000 ft. of pressure altitude. Mind this power is for the main rotor only. The total power required to hover (for the entire helicopter) can be estimated by accounting for the mechanical efficiency (η_m) of the specific helicopter at a hover. Typical values for conventional helicopter mechanical efficiency at an OGE hover are around 0.85, as stated by Richards [24]. Figure 2.3 also presents the theoretical FM and the induced to profile powers ratio for the entire altitude range between sea-level and 10,000 ft. of pressure altitude (standard day conditions).

$$FM \equiv \frac{P_{induced}}{P_{induced} + P_{profile}} = \frac{1}{1 + \left(P_{profile} / P_{induced} \right)} \tag{2.12}$$

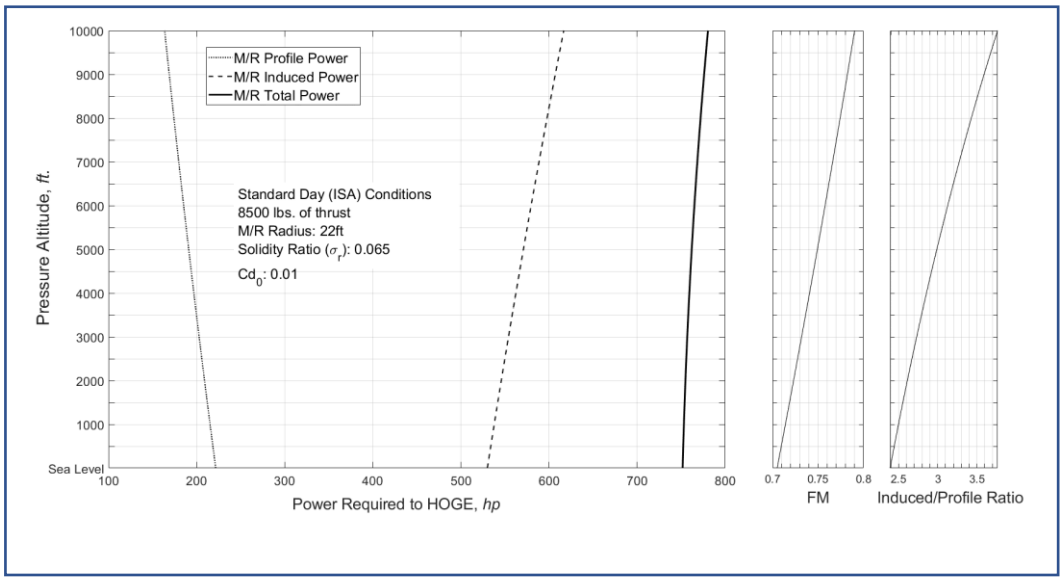

Figure 2.4. Main rotor power components in an OGE hover. Also presented are the theoretical figure-of-merit (FM) and the ratio of the induced to profile powers.

From the data presented in Fig. 2.4, under standard day conditions and for pressure altitude of 5,000 ft., the required induced power is about 571 hp, the required profile power is about 191 hp., total power for the single main rotor is 762 hp and the total power required to hover under the assumption of 85% mechanical efficiency is about 896 hp. The estimated ratio between the induced and the profile powers is 2.99. The main rotor FM under the conditions above is estimated to be 74.9%. The practical interpretation is that 74.9% of the power consumed by the main rotor is directed towards a beneficial purpose of creating lift. The rest 25.1% is just a waste of power since it served to overcome the viscous effects between the blades and the air.

It is worth emphasizing that data presented in Fig 2.4 are a theoretical estimation based on few assumptions and approximations. The precise FM is dependent on the actual induced and profile powers of the main rotor. The induced power used in Fig. 2.4 is based on an ideal main rotor, characterised by constant induced velocity across the disk (Eq.(2.2)) which yields the minimum possible induced power (that is the best-case scenario from an operator standpoint). This estimation serves as a minimum bound for the induced power. Higher values of induced power (profile power remains constant) would increase the actual FM of the rotor system.

Moreover, the estimated profile power for Fig. 2.4 is based on a constant zero-lift drag coefficient (Cd_0) of 1% for all blades. This means that all cross-sections of the main-rotor blades have a constant 0.01 zero-lift drag coefficient. In reality, this value is not constant and increases (much) with both angle of attack and Mach number of the blade cross-sections. An increase of the profile power component (while keeping the induced power constant) would result in FM reduction.

Another ratio with high significance to helicopter hover performance is the disk loading (DL). This dimensional parameter defined in Eq. (2.13) has units of pressure and indicates how loaded the rotor disk is. The higher the DL value is the higher the induced velocity through the rotor disk is. Since, the thrust (T) produced by the main-rotor equals the gross-weight of the helicopter in a hover it can be represented as the ratio of the helicopter gross-weight (W) to the disk area (A_d). It can be shown using the DL definition and the induced velocity through an ideal rotor disk (Eq.(2.2)) that the DL serves as the ***theoretical*** dynamic pressure of the airflow under the disk (the 'down-wash' or 'wake' of the rotor). Actual measurements of non-uniform distributed induced velocity rotor in a hover show the local dynamic pressure may be significantly higher (more than double) than the DL [39]. Nevertheless, an important conclusion that can be drawn from this is that the dynamic pressure underneath a hovering helicopter is related to the DL (helicopter gross-weight and main-rotor disk area), regardless the atmospheric surrounding parameters. Figure 2.5 presents maximum weight DL values of twelve different types of helicopters under standard sea level conditions. The maximum DL values range between 2.8 psf. (small helicopters like the Robinson 22) to about 14.3 psf. for large transport helicopters like the MI-26.

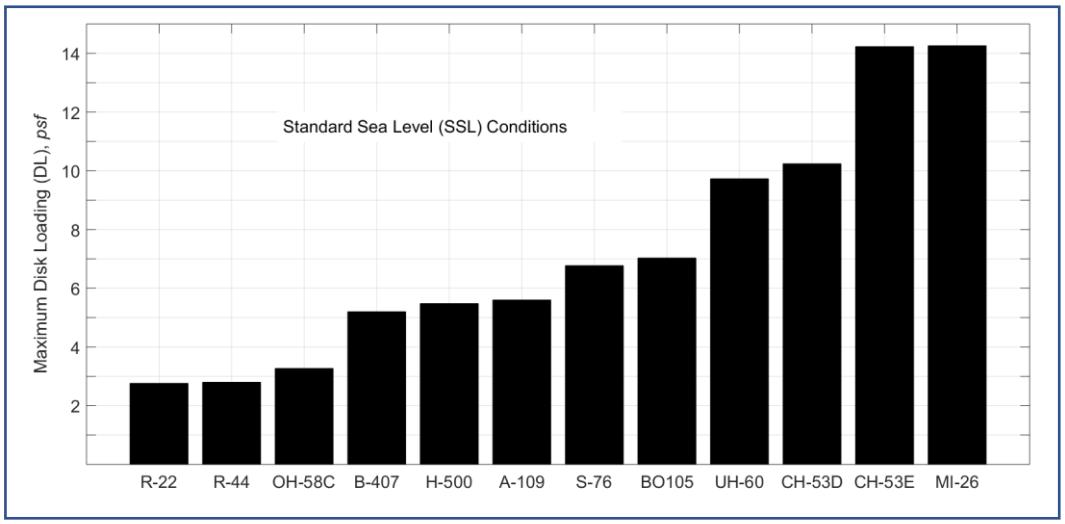

Figure 2.5. Maximal disk-loading values for various helicopters. The maximal disk loading (DL) values of helicopters varies from as low as 2.8 psf. for a Robinson-22 helicopter to high values of over 14 psf. for large and heavy helicopters like the CH-53E and the MI-26.

$$DL \equiv \frac{T}{A_{disk}} = \frac{W}{\pi R^2} \tag{2.13}$$

The power loading (PL) of a hovering disk is defined as the ratio between the thrust produced by the rotor and the power it consumes (Eq.(2.14)). By consolidating information from the three equations, Eq.(2.2), (2.12) and (2.13), the power loading (PL) of the hovering main-rotor disk is expressed in terms of disk loading (DL), figure of merit (FM) and ambient air density (Eq.(2.15)). The PL, yet another significant ratio for hover performance, can be regarded as the power efficiency for hovering. This dimensional ratio provides information about how many thrust units can the hovering rotor produce for a unit of power demanded. More generally, it can be seen from Eq. (2.15) that for a given FM, the power loading and the disk loading are inversely proportional to each other. This means that a highly loaded disk cannot be a power efficient hovering device. The inversely proportional relationship between the PL and the DL is demonstrated in Fig. 2.6 for an imaginary rotor disk under standard sea-level conditions, for three distinct FM values (0.7, 0.75, 0.8) for a range of DL between 3 to 15 psf. The following is a practical interpretation of Fig 2.6; given an arbitrary main rotor with a FM of 0.75 and a disk area of 2,260 ft^2. Using this rotor system to stabilize

a 15,820 lbs. helicopter in a hover (OGE) requires an amount of power of 1,472 hp. to be provided to the main rotor only. This procedure involved calculating the relevant DL value of 7 psf. (15,820 divided by 2,260) and using the 0.75 FM curve of Fig 2.6 to read the corresponding PL value of 10.75 lbs. to hp. The main rotor generates thrust that equals the gross weight at a hover, i.e., a value of 15,820 lbs., therefore the power required for the main rotor is about 1,472 hp. (15,820 divided by 10.75). Mind this amount of power is required for the main rotor only. Projecting from the main rotor onto the entire helicopter, requires information about the mechanical efficiency (η_m) of the helicopter in a hover (OGE). By assuming a mechanical efficiency of 85% an OGE hover power estimation of 1,732 hp. is yielded. A smaller size rotor-system with a similar aerodynamic efficiency (0.75 FM) would require more power to sustain an OGE hover flight. For example, decreasing the disk area by 20% would increase the power to hover by about 11.8%, all other variables are kept constant.

$$PL \equiv \frac{T}{P_{M/R}} \tag{2.14}$$

$$PL = \frac{FM\sqrt{2\rho_a}}{\sqrt{DL}} \tag{2.15}$$

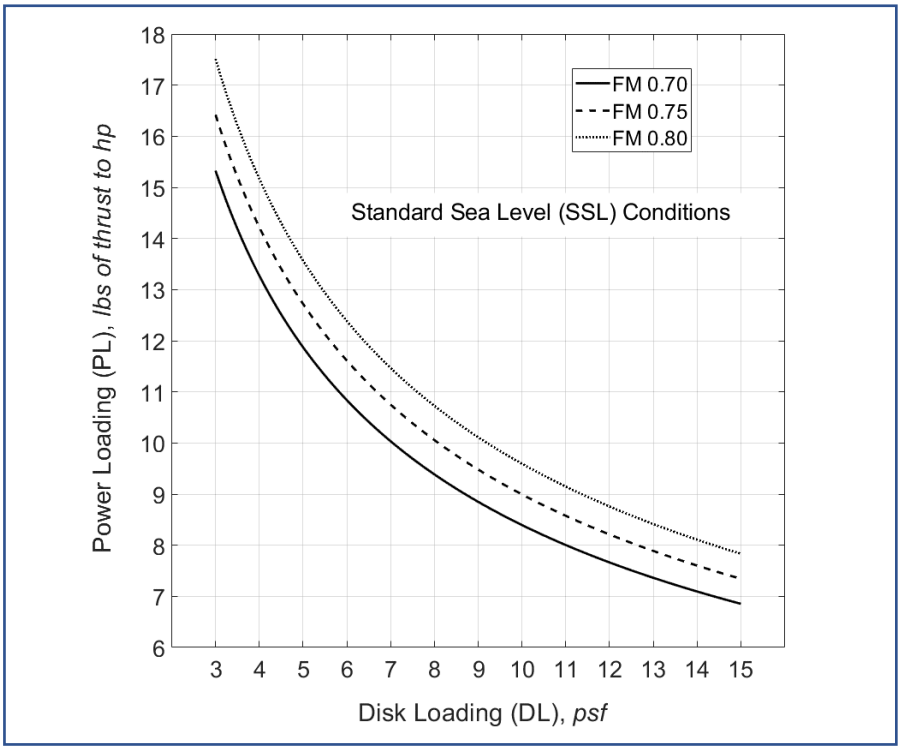

Figure 2.6. The power-loading (PL) and the disk-loading (DL) relationship. The inversely-proportional relationship between the PL and the DL of a rotor system is presented for three distinct values of figure-of-merit (FM) and under standard sea level (SSL) conditions.

It is common practice and knowledge that hovering a helicopter in close proximity to the ground is more efficient in terms of power required to sustain the flight. The ground imposes an external constraint on the induced velocity through the rotor system, which reduces the induced power component of the total power required to hover for the same amount of thrust generated. Cheeseman and Bennett [40] modelled the effect of the ground on the flow through the disk. The ground effect is simplified for the hovering flight and presented as Eq.(2.16). A graphical illustration of Eq. (2.16) is provided in Fig. 2.7. It follows from Eq. (2.16) that hovering at an example height above the ground of 40% of the rotor diameter (distance between the rotor plane and the ground), the induced power required to sustain the hover reduces by 9.8% compared to the out of ground effect case. Moreover, this power reduction estimation, Eq. (2.16)can be used to estimate the ***practical*** hover height for which the helicopter gets out of ground effect. This IGE/OGE transition height is widely considered above 1.2 times the rotor diameter, for which the reduction in the induced

power falls below 1%. This 1% reduction in power is practically undetectable to the flight crew. This practical and useful relationship given by Eq. (2.16) has been validated numerous times in more recent research work and performance flight testing campaigns [41-43].

$$\frac{dv_i}{v_{i_{OGE}}} = \frac{A_{disk}}{16\pi\left(Z_G\right)^2} \tag{2.16}$$

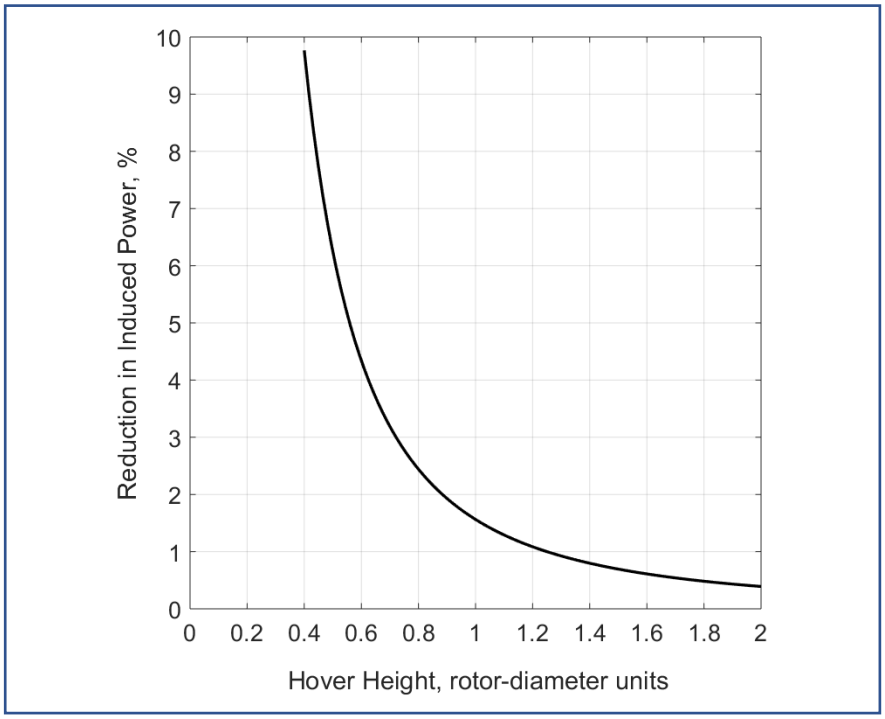

Figure 2.7. The theoretical ground effect on the induced power in a hover. This chart demonstrates the theoretical reduction in the induced power of the rotor system (as compared to the out-of-ground effect case), while hovering in close proximity to the ground. Data presented are based on Eq.(2.16).

2.2 LEVEL FLIGHT PERFORMANCE

The power consumed by a conventional helicopter in level-flight (P_{lvl}) is composed out of three major segments, as presented in Eq.(2.17). This equation can

be regarded as an expansion of the power equation for the hover (Eq.(2.1)), once a forward motion of the helicopter is initiated. The forward velocity of the helicopter (V_T) alters the two power terms already familiar from the hover flight (Induced and Profile) and introduces a new power-term, the parasite power. The induced power terms in Eq.(2.17) is an approximation that is only valid above a certain (vague and unclear) airspeed. It is obvious this induced power term cannot be used for the hover and low airspeed regime, since it will tend to infinity. The parasite power arises from the aerodynamic drag of the helicopter fuselage. The expression 'helicopter-fuselage' in the context of the parasite power means ***any*** helicopter structural element excluding the main and the tail rotors.

Equation (2.17) introduces a new non-dimensional variable (μ) that represents the non-dimensional velocity of the helicopter, also known as the 'advance-ratio'. This non-dimensional variable is defined in Eq.(2.18) as the ratio between the helicopter true airspeed (V_T) projected onto the main-rotor tip path plane (TPP), and the main-rotor blade tip tangential velocity at a hover (ΩR). The main-rotor TPP, also known as the 'plane of no flapping', and the TPP angle of attack (α_{TPP}) are illustrated in Fig. 2.8. The TPP is that plane spanned by the tips of the blades and the TPP angle of attack is defined as the angle between the helicopter velocity vector and the main-rotor tip path plane. By assuming small α_{TPP} and applying the small angle approximation, the TPP projected true airspeed can be used as the true airspeed itself and the advance-ratio (μ) converts into a more practical form as expressed by Eq.(2.19).

$$P_{lvl} = \underbrace{\frac{W^2}{2\rho_a A_{disk} V_T}}_{induced} + \underbrace{\frac{1}{8} C_{d_0} \sigma_R \rho_a A_{disk} \left(\Omega R\right)^3 \left(1 + k_p \mu^2\right)}_{profile} + \underbrace{\frac{1}{2} \rho_a f_e {V_T}^3}_{parasite} \tag{2.17}$$

$$\mu \equiv \frac{V_T \cos(\alpha_{TPP})}{\Omega R} \tag{2.18}$$

$$\mu \approx \frac{V_T}{\Omega R} \therefore \; for \; \cos(\alpha_{TPP}) \approx 1 \tag{2.19}$$

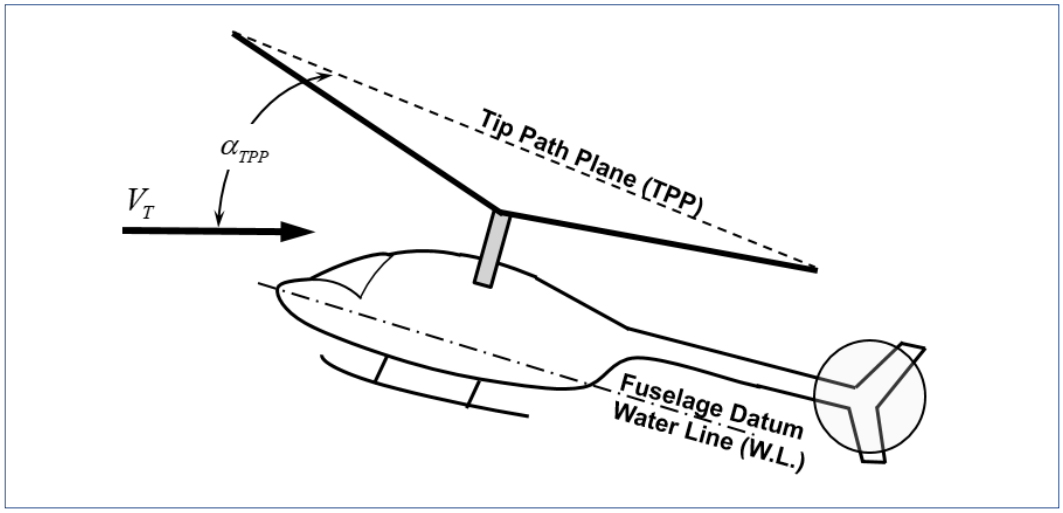

Figure 2.8. The main-rotor tip path plane (TPP). The main rotor TPP is spanned by the tips of the blades. The TPP angle of attack (α_{TPP}) is assumed small enough so that the projection of the helicopter true airspeed (V_T) onto the TPP can be approximated as the true airspeed itself.

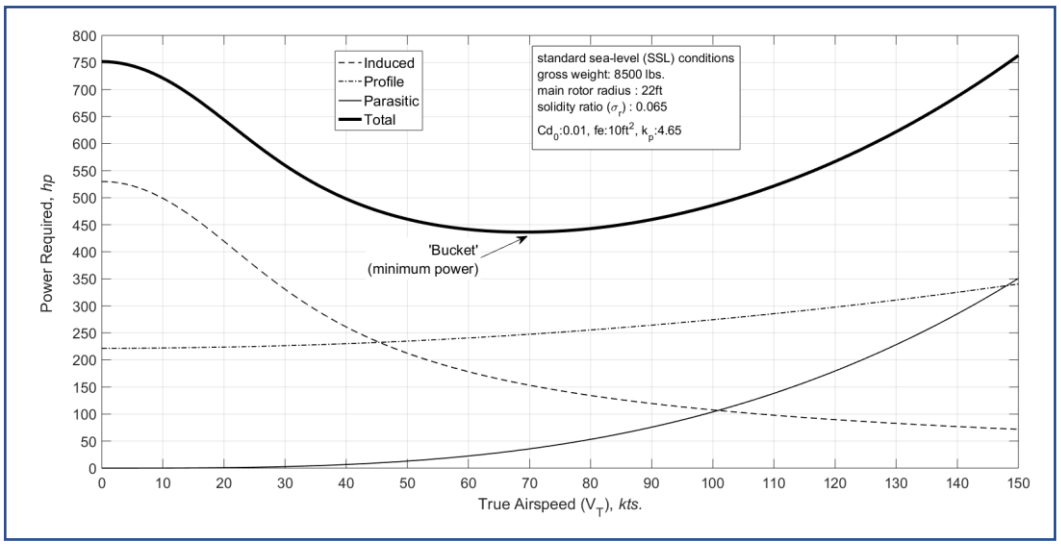

Figure 2.9. The power curve of a helicopter in level-flight. The power required to sustain a conventional helicopter in level-flight is comprised out of three main components, the induced power (reduced with airspeed increase), the profile power (increases moderately with airspeed increase) and the parasitic power which increases rapidly with airspeed increase. The power curve demonstrates a local minimum point, known as the 'bucket', which corresponds to the airspeed for minimum required power for level-flight.

Figure 2.9 presents the general behaviour of all power terms and the total power required against the airspeed of an example helicopter in level flight. Mind this plot is not based on the approximated induced power term of Eq.(2.17) since this high-speed approximation is irrelevant for the low-airspeed regime. The induced power for this plot is based on the induced velocity form of Eq. (2.20) multiplied by the example helicopter gross-weight.

2.2.1 The Induced Power in Level Flight

The first term in Eq. (2.17) is the induced power. This term is based on a simple multiplication of the thrust generated by the rotor-disk, which equals the gross-weight in level-flight, by the induced velocity through the rotor disk. The induced velocity through the cruising disk, as appears in this term, is slightly more obscured than the thrust produced and is based on ***Glauert's 'high-speed' approximation***. Glauert [46] treated the main-rotor as an actuator-disk and by applying concepts of conservation of linear momentum, accompanied with the lenient assumption of a uniformed-profile induced velocity across the disk, the expression for the induced velocity in level-flight was developed (Eq.(2.20)). Notice that Eq. (2.20) is also applicable for the hover case, where the helicopter true airspeed (V_T) is zero. For this case the induced velocity reduces to the induced velocity at a hover (Eq.(2.2)).

This development of the *constant* induced velocity across the disk in level flight is repeated by Leishman and Prouty [34,47] and its outcome (Eq.(2.20)) is known as the ***constant momentum induced velocity*** (CMIV). Prouty [47] comments that a more realistic view of the induced velocity through the disk in level flight should be based on a complex vorticity pattern, consisting of trailing, shed, and bound vortex elements associated with the lift and the change of the lift on each blade element. This type of rigorous approach for the induced velocity across the rotor-disk in cruising flight is presented by Vil'dgrube et al. [48]. That being said, Prouty [47] clarifies this complexity and rigorous approach is of great importance when studying blade loads and vibrations problems, but for performance calculations the use of the constant

momentum induced velocity represents the average of the complex velocity field and provides reasonable accurate results.

$$v_{i\_lvl(CMIV)} = \sqrt{-\frac{V_T^2}{2} + \sqrt{\left(\frac{V_T^2}{2}\right)^2 + \left(\frac{W}{2\rho_a A_{disk}}\right)^2}} \tag{2.20}$$

The constant momentum induced velocity (Eq.(2.20)) can be further simplified for cases where the induced velocity through the disk is negligible compared to the true airspeed the helicopter is flying at (V_T). The same momentum analysis approach is applied, but this time the true airspeed the helicopter flies at is used as the velocity the actuator disk is subjected to, neglecting any alteration caused by the induced velocity. This yields Eq. (2.21) known as the 'Glauert's high-speed approximation' which can be used for cases where the true airspeed the helicopter flies at are 'much' higher than the induced velocity through the cruising rotor. Mind that the first term of Eq. (2.17) is precisely the product of the lift force the rotor disk is generating (equals the gross-weight) and the high-speed approximation for the induced velocity in level-flight (Eq.(2.21)).

$$v_{i\_lvl(HS)} \approx \frac{W}{2\rho_a A_{disk} V_T} = \frac{v_{ih}^2}{V_T} \tag{2.21}$$

One should be asking for a more precise definition for the true airspeed from which the 'high-speed' approximation is valid. The previous loose guidance of when the helicopter true airspeed is 'much' higher than the induced velocity through the rotor disk is vague and impractical. Leishman [34] provides a definite criterion for the practical validity of the high-speed approximation. This criterion is set for the advance ratio (μ) to be larger than 0.1. A brief observation of the two methods for calculating the induced velocity (Eq.(2.20),(2.21)) reveals that by using the advance-ratio value as a criterion for the high-speed approximation validity, the user will be faced with inconsistent approximation errors. The advance-ratio alone cannot be used as a validity-criterion for the high-speed approximation. A particular helicopter can be

flown under a wide range of disk loading (DL) values that alters the relative proportion of the induced velocity calculated in both ways, the CMIV and the high-speed approximation. Figure 2.10 presents a comparison between the two methods for calculating the induced velocity through the main-rotor disk for six example helicopters at their maximum certified disk loadings and under standard sea-level conditions. Leishman's advance-ratio criterion (μ equals 0.1) is shown on all plots. Figure 2.10 shows that applying the same threshold of μ equals 0.1 (translated to a narrow range of true airspeeds between 39 to 43 kts. for the six example helicopters) resulted in erratic differences between the two calculated induced velocities. This is attributed to the different disk loadings of the example helicopters.

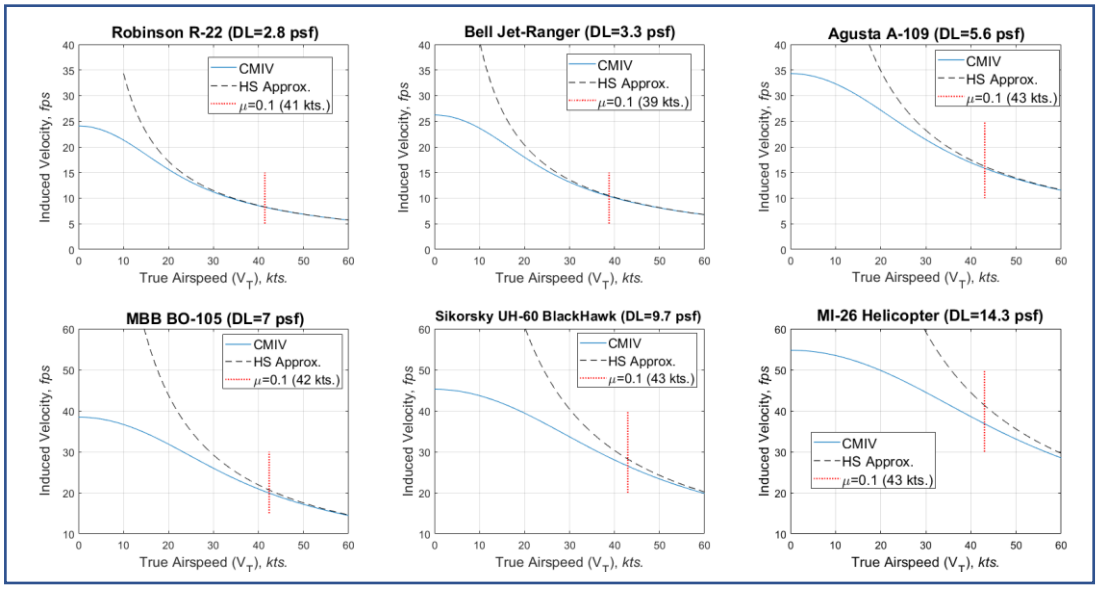

Figure 2.10. The theoretical induced velocity in level flight. Data are presented for six example helicopters. Data are calculated using two methods. One according to the constant momentum induced velocity (CMIV) approach, and the other using the high-speed (HS) approximation.

The estimation-error using Glauert's high-speed approximation as compared to the CMIV approach is calculated per Eq.(2.22) and presented for the six example helicopters in Fig. 2.11. Note the estimation-errors presented in Fig. 2.11 were calculated for standard sea-level conditions. While using μ equals 0.1 as a criterion yielded acceptable estimation errors for few helicopters (below 2.3%), this criterion

was found unacceptable for the BO-105, UH-60 and the MI-26 helicopters. The resulted unacceptable estimation errors for the three helicopters were 3.9%, 6.4% and 12.1%, respectively.

An improved tool to assess the validity (or the level of inaccuracy introduced) of the high-speed approximation under various helicopter conditions was developed and is presented in Fig. 2.12. The estimation error associated with the approximated induced velocity, as calculated by Eq.(2.22), is presented against the helicopter true-airspeed for various discrete disk-loading values, ranging from 2 to 15 psf., and for standard sea-level conditions. Figure 2.12 also includes an illustrated example to assess the minimum airspeed for which the high-speed approximation is valid, given a 5 psf. disk-loading and an allowed estimation error of up to 2%. Using Fig. 2.12 the minimum true airspeed is 42.5 kts. It is clear from Fig. 2.12 that for a given estimation error, the minimum airspeed for the validity of the high-speed approximation is proportional to the helicopter disk-loading. While a true airspeed of 33 kts. is valid for an acceptable 2% estimation error for a low 3 psf. disk-loaded helicopter, the minimum valid airspeed for a 14 psf. disk-loaded helicopter is 71 kts., for the same error budget of 2%. Establishing a legitimacy criterion for the high-speed approximation which is solely based on the advance ratio, as given by Lishman [34], is simply unacceptable. A similar type of graph to Fig. 2.12 but for 10K ft. of pressure altitude (standard day conditions) is provided in Appendix B of this dissertation.

$$Err_{HS} = 100\left(\frac{v_{i\_lvl(HS)} - v_{i\_lvl(CMIV)}}{v_{i\_lvl(CMIV)}}\right) \tag{2.22}$$

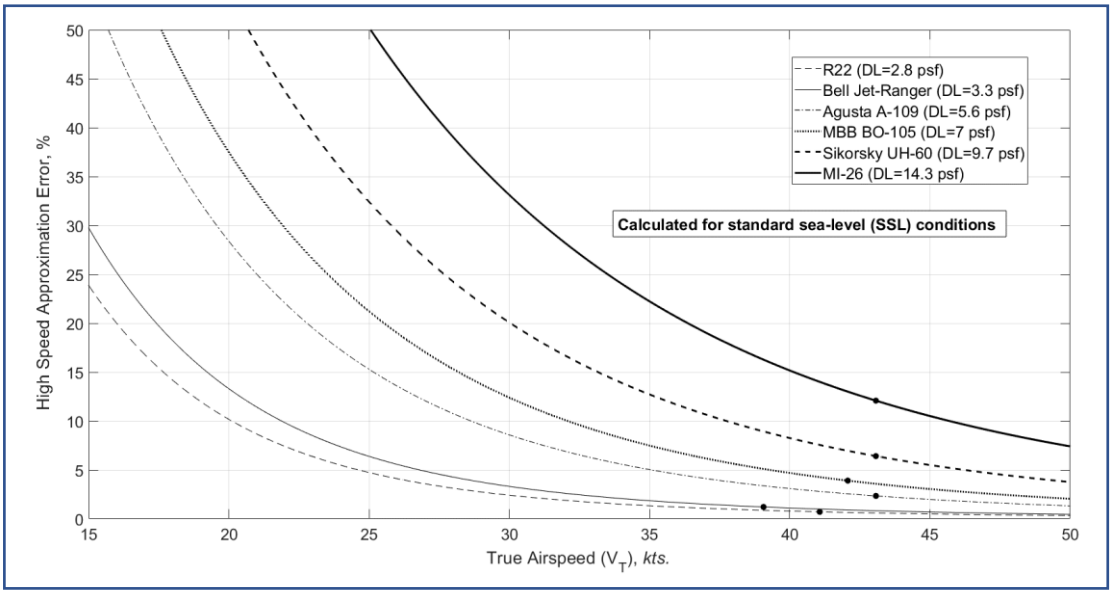

Figure 2.11. The error induced by using the high-speed approximation. This chart demonstrates the percentage of error caused by using Glauert's high-speed (HS) approximation. The error is calculated with respect to the induced velocity based on the constant momentum induced velocity (CMIV) method. Data are presented for six example helicopters and under standard sea-level (SSL) conditions.

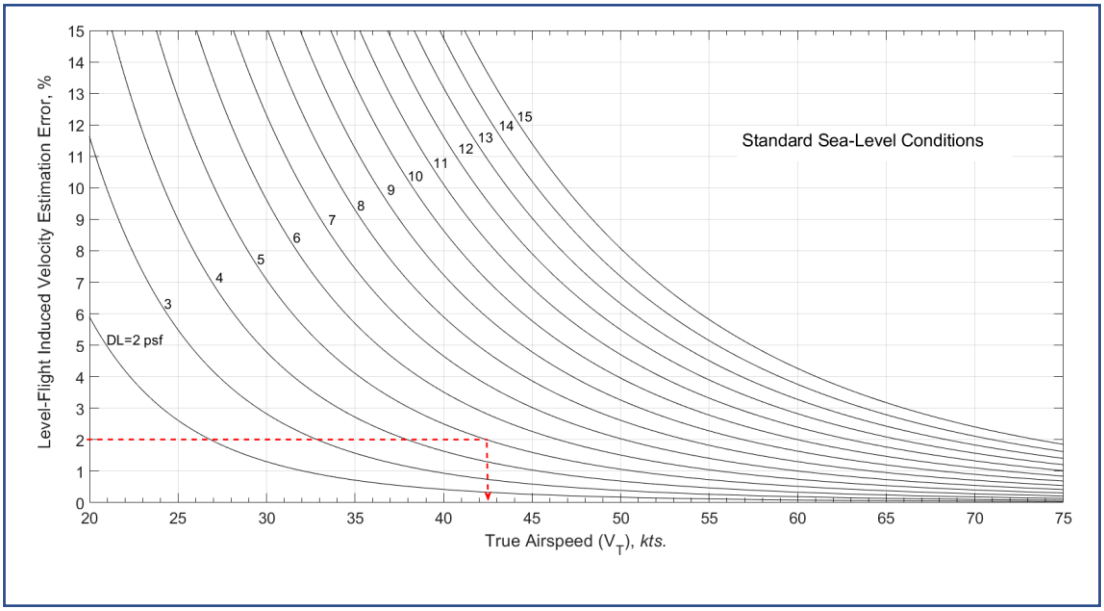

Figure 2.12. High-speed (HS) approximation validation chart. This fan-type chart can be used as a tool for assessing the acceptable minimum true-airspeed for the high-speed approximation, given the disk-loading and the required estimation error. This chart is applicable for standard sea-level (SSL) conditions.

2.2.2 The Profile Power in Level Flight

The second term in Eq. (2.17) is the profile power. This term is merely an extension of the profile power component from the hover (see Eq.(2.1)) but with a correction-term that makes it relevant to the level flight regime. This correction term is based on an empirical coefficient (k_P) multiplied by the advance-ratio squared (μ^2) to represent the proportional rise in profile power with the level-flight airspeed. Since this k_P is an empirical coefficient, it also accounts for the profile power of the tail-rotor. Typical values for k_P vary between 4.65 [8,10,18-20] to a value of 4.7 presented by Stepniewski [49].

Taking the main-rotor from the hover into a forward flight disrupts the symmetric velocity-field surrounded the rotor blades. In the hover, each one of the main-rotor blades senses the same chord-wise velocity profile, regardless of the azimuth angle of the blade (ψ). Once the rotating main-rotor is flooded with the forward flight airspeed, the chord-wise velocity profile of each blade varies based on the azimuth angle of the blade. The chord-wise velocity (V_{CW}) each cross-section of the blade senses is expressed in Eq. (2.23) as a function of the true airspeed of the helicopter (V_T), the azimuth angle (ψ) and the station of the blade (r).

$$V_{CW}(r,\psi) = \Omega r + V_T \sin(\psi) \therefore r = [0, R] \tag{2.23}$$

The main-rotor disk in forward flight can be divided into two halves: the advancing and the retreating sides. For a rotor system rotating in a counter clockwise orientation (as viewed from above), the advancing side (azimuth angles between zero and 180°) is on the right. Rotor blades on the advancing side are exposed to a relative velocity profile which is higher than the tangential velocity, results from the angular motion of the rotor. The advancing side is subjected to higher relative velocities as compared to the retreating side of the disk. The advancing blades are exposed to the tangential velocity resulting from the angular motion of the blade, added with the chord-wise component of the helicopter airspeed. For the retreating blade it is the opposite, the chord-wise component of the helicopter airspeed is subtracted from the

tangential velocity of the blade. This asymmetry is the cause for the formation of three main areas on the main-rotor disk in forward flight. (1) A circular-section area on the advancing side, which is subjected to high Mach number and compressibility issues. This area stretches from the tip of the disk and grows inboard, as the helicopter increases its airspeed. (2) A reverse-flow area in which all blade elements face an air flow from the trailing edge to the leading edge. This reverse flow area, located on the retreating side of the disk, is a perfect circle with a diameter of exactly the product of the advance ratio (μ) and the main-rotor radius (R). The centre of the reverse flow area is always located at an azimuth angle of ψ=270°, regardless of the helicopter airspeed. (3) The blade-stall area on the retreating side of the disk. This area stretches from the edge of the disk inbound and grows with helicopter airspeed increase.

Figure 2.13 presents the theoretical compressibility and reverse flow areas of an example main-rotor disk in level flight. This example uses the formerly 22 ft. in diameter example helicopter for three distinct values of advance-ratio (0.1, 0.3, and 0.5) and two types of atmospheres; standard sea-level and standard-day 10K ft. pressure altitude. All calculations for Fig. 2.13 are based on the example helicopter standard angular speed (Ω) of 324 RPM (33.9 radians per second.). The Mach number each blade cross-section is subjected to (M_{BE}) is calculated from Eq.(2.23) divided by the applicable speed of sound (Eq.(2.24)). The same information is used to annotate the constant Mach lines in Fig. 2.13. For this, the blade station (r) is explicitly expressed as a function of the desired Mach number, the applicable speed of sound, the advance-ratio and the azimuth angle (Eq.(2.25)).

$$a = \sqrt{\gamma_{air} R_{air} T_a} \tag{2.24}$$

$$r = \frac{M_{BE} a}{\Omega} - \mu R \sin(\psi) \tag{2.25}$$

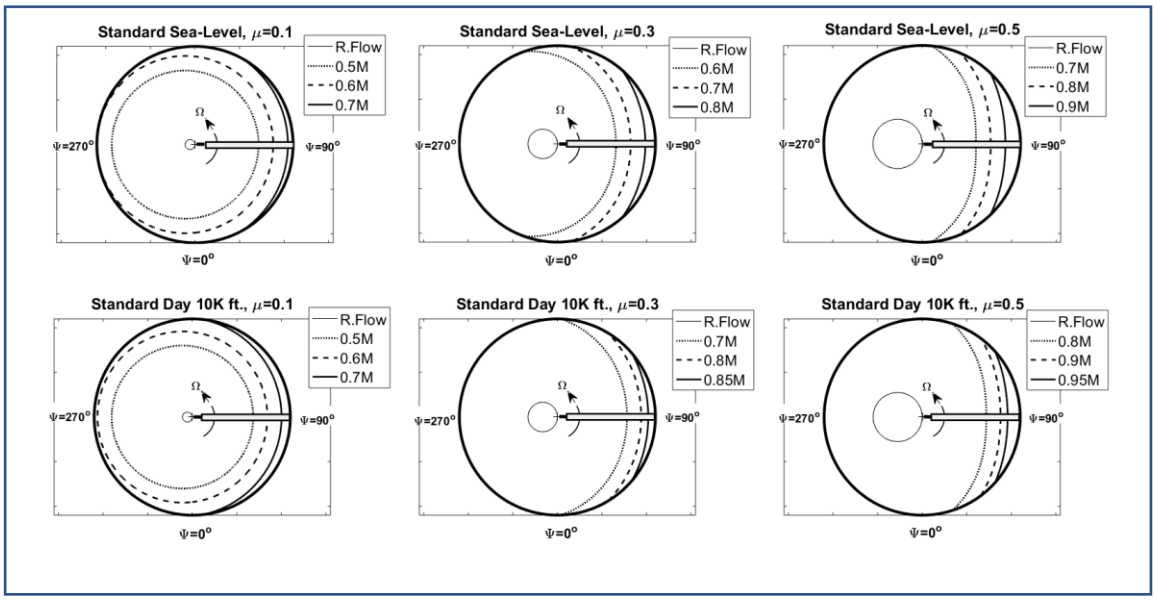

Figure 2.13. An example main-rotor disk in forward flight. An example main-rotor disk is subjected to two atmospheric conditions and three distinct advance ratios. The reverse-flow area grows proportionally to the advance ratio. The advancing side of the disk faces higher Mach numbers with increase in altitude (decrease in speed of sound) and with increase in advance ratio.

The profile power in level-flight (Eq.(2.17)) assumes constant profile drag coefficient (Cd_0). This assumption is valid for an airflow-regime free of compressibility effects, i.e., characterised by Mach numbers below the drag divergence Mach number. Figure 2.13 presents the estimated maximal Mach numbers exist on an example main rotor, under fairly moderate atmospheric conditions. Flying on a standard day, 10K ft. pressure altitude at advance-ratios above 0.3 clearly places a substantial circular section of the main-rotor disk above 0.8M and inside the drag-divergence region of many aerofoils [47,50-53]. This drag-divergence region is characterized by an abrupt increase in the profile drag coefficient due to the formation of shockwaves, responsible for significant drag increase. Flying the helicopter under more extreme conditions of higher altitudes and lower ambient temperatures, would increase the disk area subjected to compressibility issues, resulting in a steep increase in the profile power. As stated by Prouty [47] "if any blade element exceeds the drag divergence Mach

number for its aerofoil, the power required will be higher than that calculated from the closed-form equations" (p. 177).

The two particular zones on the rotor disk, the circular-section infested with compressibility-effects on the advancing side, and the blade-stall area on the retreating side are the reason for the practical (low) airspeed limitation of the conventional helicopter. As the airspeed increases on the advancing blade, certain blade elements on the outbound part of the blade might experience critical Mach values associated with formation of shockwaves on their upper and lower surfaces. This sudden change in the flow regime around those blade element causes a jump in the aerodynamic centre of the relevant cross-sections and a pitch-down moment. Mind this chain of events, formation, and deformation of shock-waves, repeats periodically on a rotating rotor disk. The phenomenon briefly described here is commonly known from fixed-wing airplanes as the 'Mack Tuck'. A flight-test campaign on the Sikorsky NH-3A (modified Sea-King, SH-3A) compound helicopter was aimed to investigate flight characteristics of a helicopter in the high airspeed regime. The flight-test team encountered an unstable blade-twist singularity due-to the Mach Tuck phenomenon. This severe dynamic problem described by Paul [54] was the cause for elevated blade-loads above a tip Mach number of 0.92. This value is commonly considered as the practical limitation for the maximum tip Mach number a main rotor-disk can endure in forward flight. Recalling the maximal Mach number a generic blade section senses is the tip at the 90° azimuth angle, this practical criterion is expressed as Eq.(2.26).

$$M_{tip(\max)} = \frac{V_T + \Omega R}{\sqrt{\gamma_{air} R_{air} T_a}} < 0.92 \tag{2.26}$$

The retreating side of the rotor-disk is subjected to an increasing zone of blade stall. Increasing the helicopter airspeed results in lower relative speeds on the outboard sections of the retreating blades. This combined with the flap-down motion of the retreating blade (ψ between 180° to 270°) makes it more susceptible for stalling. There are many types of stall characteristics based on the shape of the aerofoil (thickness, thickness to chord ratio, symmetry, etc.) and the prevailing non-dimensional variables

of the flow (Reynolds and Mach numbers). A thorough discussion of blade stall is beyond the scope of this dissertation and can be found in Ref [55, 56]. The outboard elements of the retreating blade are subjected to a special type of stall, referred to as the dynamic stall. It was found that when the AOA on an aerofoil is increased rapidly, it can postpone the stall AOA and temporarily generate a higher coefficient of lift, as compared to the static or the quasi-static case. This phenomenon is thoroughly explained and demonstrated in Ref [57-61]. Mind the dynamic aspect of the rotor blades stall can arise from (1) the flapping motion of the blade (defined as 'plunge' motion in the context of dynamic stall. (2) the commanded pitch oscillations. (3) the flap-wise bending structural mode and (4) the torsion structural mode of the blade.

McCroskey et al. [57] provide stall results for seven different helicopter aerofoils oscillating in pitch at 0.3M. All aerofoil sections demonstrated a similar increased maximal coefficient of lift. No significant correlation was found between the amount of increase (between 0.7 and 0.8) and the shape of the aerofoil. Prouty [32] provides a quick and easy guideline for preventing excessive retreating blade stall: "It is also generally accepted that for conventional helicopters at maximum speed, the tip speed ratio limit should not exceed 0.5 to avoid retreating blade stall" (p. 646). This practical criterion is expressed in Eq.(2.27).

$$\mu = \frac{V_T}{\Omega R} < 0.5 \tag{2.27}$$

The two conflicting criteria from Eq. ((2.26),(2.27)) are presented on the V_T, ΩR plane in Fig. 2.14. As the airspeed increases the requirement for restraining the advancing blade compressibility issues results in a decrease of the rotor angular speed, whereas the criteria for preventing excessive retreating blade stall requires an increase in the main-rotor angular speed. The two contradictory requirements meet to define an equilibrium point that represents the maximal-practical airspeed of a conventional helicopter in forward flight and the corresponding main-rotor tip speed. This maximum true airspeed is about 203 kts. (Standard sea-level conditions) and about

196 kts. (Standard-day, 10K ft. pressure altitude). The corresponding main-rotor tip speeds are 685 and 661 fps.

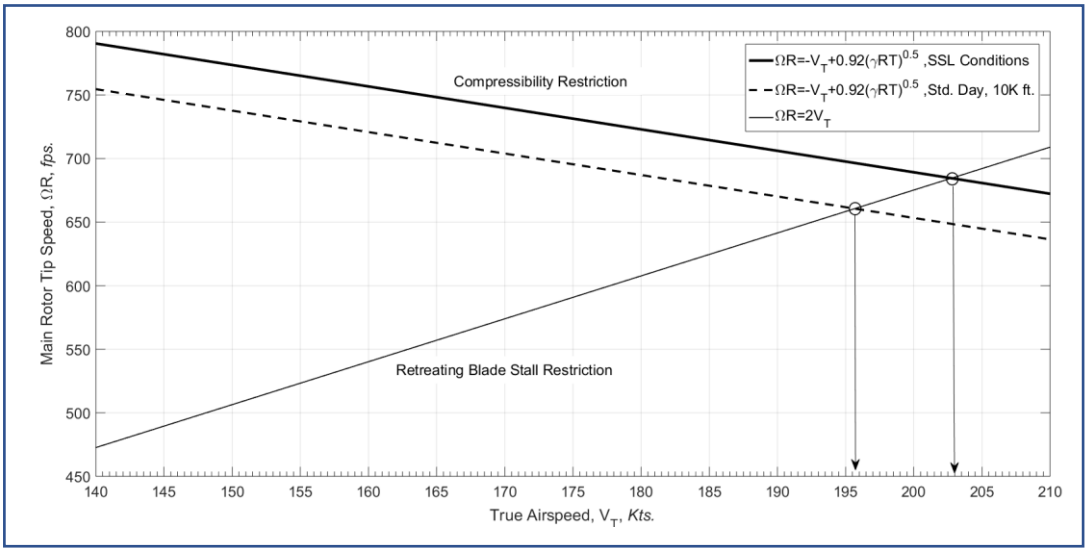

Figure 2.14. Maximum airspeed of a conventional helicopter in forward flight. The two contradicting constraints for restraining compressibility issues on the advancing blade and for preventing excessive retreating blade stall define the practical maximal airspeed for a conventional helicopter in forward flight.

Notice that the two equations can be combined to form an explicit form (Eq.(2.28)) to represent the maximum practical airspeed of a conventional helicopter. This insight relates back to Igor Sikorski's famous quote about the helicopter to never be able to fly faster than the airplane, as already mentioned in the introduction to hover performance in Chapter 1, Subsection 1.2.2.1.

$$V_{T_{MAX}} = \frac{M_{tip(\max)}}{3}\sqrt{\gamma_{air} R_{air} T_a} \tag{2.28}$$

2.2.3 The Parasite Power in Level Flight

The third term in Eq. (2.17) is the parasite power. This power term is required for the support of the aerodynamic drag generated by the helicopter fuselage. This 'fuselage' term holds for any structural element of the conventional helicopter,

excluding the main and tail rotor blades. The main and tail rotor blades are already accounted for in the power equation (Eq.(2.17)) as the profile power. The parasite power term is based on the same fundamental mechanical concept previously used for the induced and profile power components. The mechanical work done by a force on an object is defined by the scalar-multiplication of the two vectors, the force and the object's displacement. The rate of work (power) is then expressed by the evaluation of the work done per unit of time. This ratio of displacement per unit of time is precisely the true airspeed of the helicopter, and when multiplied by the fuselage aerodynamic drag force the parasite power term is attained.

The parasite power term, as appears in Eq.(2.17), is slightly manipulated and is explained hereinafter. Since the conventional helicopter flies at relatively low altitudes and airspeeds characterized by Mach numbers below 0.3, the flow-field surrounding its fuselage can be treated as incompressible flow, as explained by Dommasch et al. [62]. The fuselage aerodynamic drag-force (D_f) is calculated as per Eq. (2.29) which is the product of the dynamic pressure (q), the drag reference area (S_{ref}) and the drag-coefficient based on the drag reference area (C_{Df}). For an incompressible flow the dynamic pressure is calculated as per Eq.(2.30).

$$D_f = qS_{ref}C_{Df} \tag{2.29}$$

$$q = \frac{1}{2}\rho_a V_T^2 \tag{2.30}$$

For reasons of convenience and ease of common-base comparison, the product of coefficient-of-drag (C_{Df}) and drag reference area (S_{ref}) is expressed by a different product, which has the same numerical value. This new product consists of a convenient coefficient-of-drag (equals 1), associated with a new reference drag area, defined as the 'equivalent flat plate area' (EFPA) and depicted by f_e (Eq.(2.31)). By using these new terms, the fuselage aerodynamic drag-force (D_f) is conveniently expressed as Eq.(2.32). The power required to provide against this aerodynamic drag

(D_f) is merely the product of the aerodynamic drag force and the true airspeed of the helicopter, as expressed by (Eq.(2.33)).

$$S_{ref} C_{Df} \equiv f_e \cdot 1 = f_e \tag{2.31}$$

$$D_f = \frac{1}{2} \rho_a V_T^2 f_e \tag{2.32}$$

$$P_{parasite} \equiv D_f V_T = \frac{1}{2} \rho_a V_T^3 f_e \tag{2.33}$$

Helicopter airframes are less aerodynamic than their fixed-wing counterparts, this source of drag can be very significant, as shown by Leishman [10]. According to Leishman [50] the drag of a helicopter fuselage may be up to one order of magnitude higher than that of a fixed-wing aircraft of the same gross weight. As presented by Prouty [47] and Rosenstein et al. [63], typical values for helicopter EFPA range from as low as 5 ft^2, for small and clean designs, up to 60 ft^2 for large flying cranes. Leishman [10] presents data of a variety of helicopter designs as a plot on the EFPA, gross-weight plane. This plot suggests helicopter designs fall into two major categories of 'clean' and 'utility' helicopters (excluding the large flying cranes) and within each category the EFPA value is *approximately* proportional to the square root of the helicopter gross-weight. This empirical observation is referred to as the 'square-cube' law.

According to Sheehy [64] the main-rotor hub and landing gear are the two major contributors to the parasite drag of the helicopter. While, the drag arises from the landing-gear can be significantly reduced by fairings, or even entirely eliminated by retracting the lading-gear into the fuselage, the rotor hub drag contribution cannot be easily reduced and accounts for approximately 20-30% of the total parasite drag. Moreover, fully articulated rotor hub designs can contribute to about 60% of the total parasite drag of a helicopter designed for high-speed operations. Prouty [8] provides parasite drag breakdown estimates for an undisclosed example helicopter (Fig. 2.15), accompanied with the following personal note: "I have never known of an airplane, or

a helicopter drag estimator who was pleasantly surprised by flight-test results showing an overestimation of the drag" (p. 304). For illustration purposes, this estimated EFPA of 19.3 ft^2 converts using Eq. (2.33) to a parasite power of 677 hp, while flying at a true airspeed of 150 kts under standard sea-level (SSL) conditions.

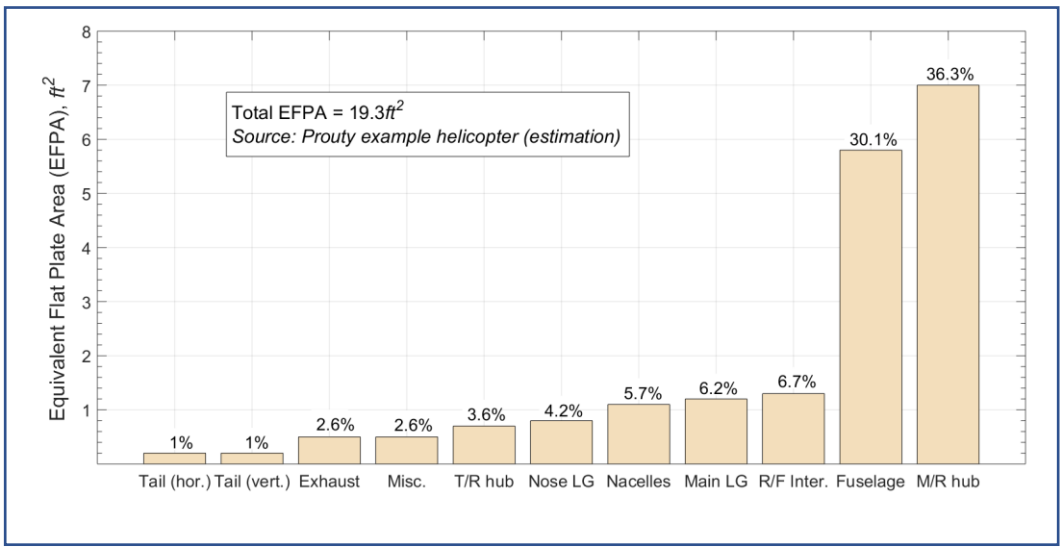

Figure 2.15. Parasitic drag breakdown for an example helicopter. The two main contributors to the parasitic drag of a conventional helicopter are the main-rotor hub with an EFPA of 7 ft² (36.3% of total parasite drag) and the fuselage with an EFPA of 5.8 ft² (30.1%). The landing gear system is the third largest contributor, with a combined main and nose landing gear EFPA of 2 ft² (10.4%).

Maintaining a constant external configuration does not guarantee a permanent parasite drag. The fuselage EFPA varies as the fuselage angle of incidence changes. This variation in the fuselage angle of incidence may be attributed to changes in airspeed or even to migration of the centre-of-gravity (CG). Any change in the fuselage angle of incidence, not only varies the EFPA of the fuselage but also causes for EFPA changes in all components attached to the fuselage, i.e., nacelles, landing gear, stub-wings, and stabilizer surfaces. Notice that changing the angle of incidence on aerodynamic surfaces results in not only skin-friction change but also induced drag change. Flight tests conducted on the prototype OH-58A helicopter with a flat-plate canopy showed [65] that while flying at the cruise airspeed of this helicopter (102 kts.), an aft migration of the longitudinal CG, from the mid-point to the maximum aft

position resulted in 2.2 ft^2 (22%) increase in the EFPA. A forward migration of the CG, from the mid-point to the maximum forward position, resulted in a more subtle EFPA increase of 0.7 ft^2 (7%). The 2.2 ft^2 ERPA increase is equivalent to a power increase of about 24.3 hp (7.7% of available power), under the relevant flight-conditions.

Level flight performance flight testing conducted on the 18K lbs. UH-60A helicopter, equipped with the External Stores Support System (ESSS), demonstrated a strong relationship between the EFPA and the longitudinal CG location of the helicopter [6]. A 15 inches longitudinal CG migration from an aft fuselage station (FS 358") to a forward FS 343" resulted in an EFPA increase of 9.6 ft^2 while flying straight and level at airspeeds between 40 to 140 kts. This 9.6 ft^2 increase in EFPA is equivalent to a power increase of about 274 hp (9.6% of available power) while flying at 140 kts under SSL conditions.

2.3 CONVENTIONAL METHODS FOR PERFORMANCE FLIGHT TESTING

As already mentioned in the introduction to this thesis (Section 1.3), the fundamental question troubling the helicopter performance flight-testers has always been how should the performance of the helicopter be tested? More specifically, at which particular gross-weights? Under which combinations of atmospheric conditions? Can measurements be standardized? Is it possible to use data from a specific flight to predict performance under different and arbitrary flight conditions? These types of questions which are essentials in performance flight-testing can be addressed by using tools of dimensional analysis and the Buckingham PI theorem [66] which is commonly regarded as the fundamental theorem of dimensional analysis, as stated by Evans [67].

The Buckingham PI theorem states that any physically meaning problem with numerous dimensional parameters involved, can be reduced to a lesser number of

significant non-dimensional parameters, based on the dimensions involved. The competency of dimensional analysis to reduce the number of affecting variables and to support interpolation and extrapolation of data, has made it a popular tool in performance flight testing. By applying dimensional analysis tools, the flight-tester can answer all performance questions raised above and at the same time, significantly reduce the number of flight-test sorties required to quantify the performance of an aircraft throughout its flight-envelope.

2.3.1 Available Power Flight-Test Method

The current method widely used within the flight-test community for determining the available power any gas-turbine helicopter possess is based on the single-variable analysis, as presented in few flight testing method text books [18-21] and practicably demonstrated in Belte and Stratton [78] and Benson et al. [86]. This conventional flight test method is further demonstrated, with its major deficiencies emphasized, in Chapter 3 of this thesis. For this, authentic flight test data from a MBB (Messerschmitt-Bölkow-Blohm) BO-105 helicopter are used. According to this flight-test method, all four engine performance variables (output power, compressor speed, temperature, and fuel-flow), accompanied with their corresponding atmospheric conditions, and are recorded during steady engine operation conditions. For this, the helicopter is flown throughout its certified flight envelope and under diverse atmospheric conditions. As demonstrated by Jackson [75], it is essential for multi-engine helicopters to handle data from each engine separately. Each engine is a separate entity with potentially a different level of maximum available power that might be operated under slightly different atmospheric conditions, even if installed on the same helicopter.

Once a substantial database is gathered, it is analysed with the goal of evaluating the maximum power the engine is able to produce under various atmospheric conditions. This procedure is carried-out in two phases. The first (Phase I) is to generate a convenient mathematical model to describe the dependency of the engine output power with all other engine performance variables (compressor speed,

temperature and fuel-flow). Phase I can be regarded as uncovering (mathematically) the specific engine 'rules of operation'. The second phase (Phase II) concentrates on deriving the maximum output power of the specific installed engine under a wide range of atmospheric conditions i.e., performance under hot day or cold day conditions, and for the various engine power ratings i.e., the maximum continuous power, the maximum 5-minute take-off rating power etc.

2.3.1.1 Phase I – The Engine 'Rules of Operation'

The essence of this phase is to derive simple empirical models to represent the dependency between the engine output power and each one of the performance variables of the engine i.e., the engine temperature (TGT), compressor speed (Ng) and fuel-flow (Wf). As already discussed above, dimensional analysis plays a major role in helicopter performance flight-testing. Using the Buckingham PI theorem, the engine performance problem can be simplified to include a set of only four ***corrected*** variables. These corrected variables are essentially non-dimensional magnitudes which bear units and for this reason they are addressed by Knowles [73] as the GT engine corrected variables, rather than non-dimensional. Specifically, these corrected variables are the corrected output power of the engine (CSHP), the corrected compressor speed (CNg), the corrected engine temperature (CTGT) and the corrected fuel-flow into the engine (CWf). The definitions of these non-dimensional variables are presented in the nomenclature and the rigorous procedure to derive these corrected variables is presented as Appendix A in this thesis.

By applying common methods of linear regression, a set of third order single-variable polynomials is retrieved to relate between the corrected output power and each one of the other corrected variables of the GT engine, as given by Eq.(2.34), Eq.(2.35) and Eq.(2.36). Third order polynomials are employed for the reason they are the lowest order that enable modelling an inflection point, a fundamental behaviour of the gas-turbine engine. These polynomials, based on actual flight-test data, serve as empirical models to represent the 'rule of operation' of the specific GT engine, as

installed in the particular type of helicopter and at the specific phase of its life cycle. An example of actual experimental polynomials is presented in Fig 2.16.

$$CSHP = \sum_{n=0}^{3} a_i \left(CNg\right)^n \tag{2.34}$$

$$CSHP = \sum_{n=0}^{3} b_i \left(CTGT\right)^n \tag{2.35}$$

$$CSHP = \sum_{n=0}^{3} c_i \left(CW_f\right)^n \tag{2.36}$$

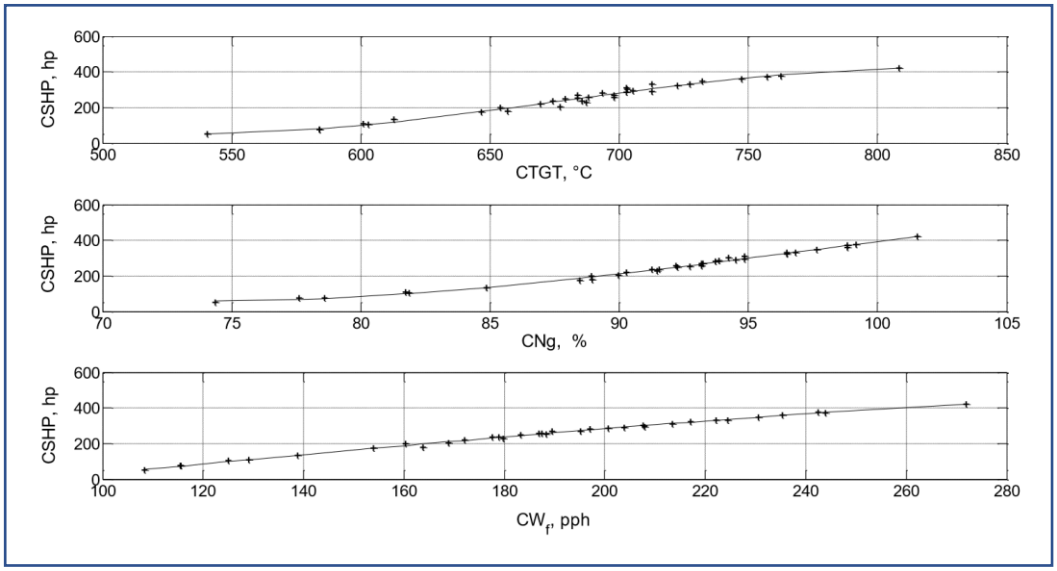

Figure 2.16. Example of 3rd order empirical model of gas-turbine engine. The presented three 3rd order polynomials are derived from actual flight-test data and serve as an empirical model for the installed gas-turbine engine (GTE).

As previously mentioned, the requirement for these polynomials to be of the third order is to ensure the empirical model captures the inflection point of the engine performance. This inflection point represents a fundamental property of any gas-turbine engine for which the rate of change in output power with respect to the engine variables (compressor speed, temperature, or fuel-flow) changes its sign. For the same amount of engine variable increase, the resulted increase in engine output-power is to

be reduced beyond the inflection point, as compared to the output-power increase below this inflection point.

2.3.1.2 Phase II – Maximum Available Power

The second phase of the available power flight-test method uses the empirical models retrieved from Phase I to define the maximum available power the installed engine can generate, for any power rating and under any atmospheric conditions as selected by the flight tester. This phase involves an iterative process, as illustrated by Fig. 2.17 and explained hereinafter. The maximum engine power can be limited by either one of the following parameters: the engine temperature (TGT), the engine compressor speed (Ng), the engine fuel-flow (Wf) or the maximum output shaft torque (TRQ). These limitations are well known to the helicopter operator and their values are typically different for the various power ratings of the engine. The iterative process of evaluating the available power commences by defining the relevant power rating. Is it the continuous power rating with no time limitation? Or is it for the take-off which is limited to only 5 minutes of operation.

Once the power rating is decided, the type of day must be defined. A standard day (ISA) is defined as one with a temperature of 15°C at sea level which decreases by 1.98°C for every 1,000 ft. of climb. Other day conditions are based on the ISA day and are symbolised as the temperature difference from the standard day conditions. For example, ISA+10 represents a day for which the ambient air temperature at sea level is 5°C. The elapsed rate of the temperature with altitude is assumed as 1.98°C per 1,000 ft., although it is seldom the reality. Once a type of day is decided upon, for each pressure altitude selected the relative temperature (θ) and relative pressure (δ) are calculated. For each pressure altitude the three-engine limiting corrected variables can be calculated and plugged into the three flight-test based polynomials retrieved in Phase I. Each one of these polynomials yields a corrected output power which can easily be turned into actual output power and output shaft torque.

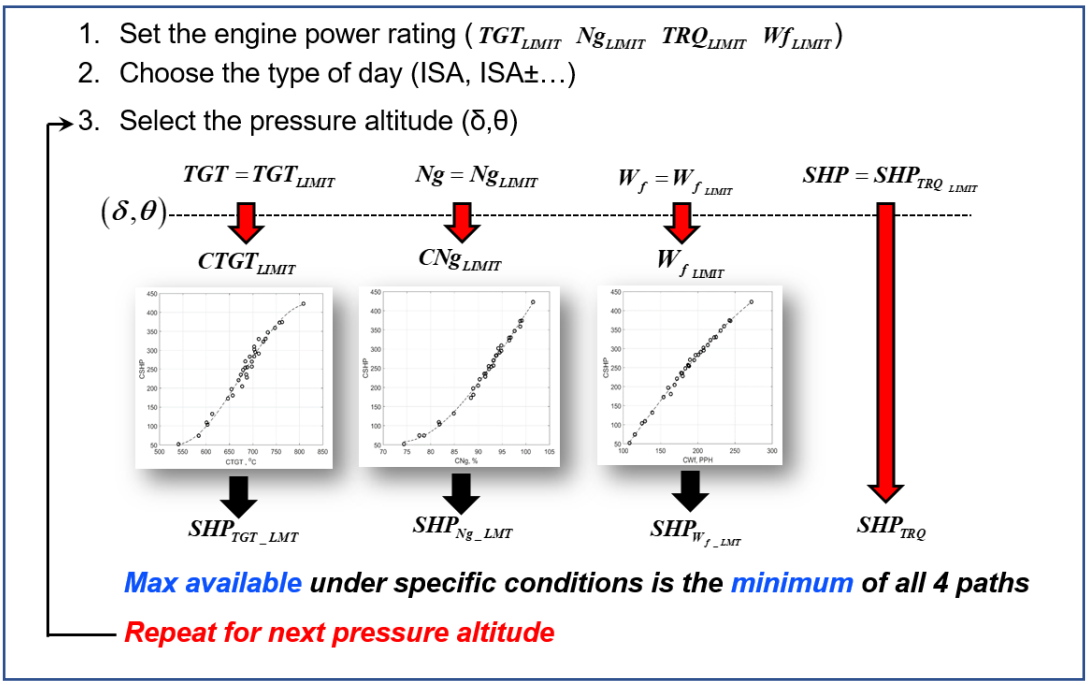

Figure 2.17. The iterative procedure for engine available power disclosure. The maximum available power of an installed gas-turbine engine (GTE) is disclosed by executing an iterative procedure based on the empirical model of the GTE and its operating limitations.

The maximum output power of the engine for the selected pressure altitude would be the ***minimum*** of the three values yielded from the empirical polynomials and the transmission limitation (the output shaft torque limitation). Once the maximum available power for the selected pressure altitude is defined, another iteration for the next pressure altitude is carried out. This procedure is repeated for other types of day and all relevant power ratings of the engine. Figure 2.18 presents an example outcome of this procedure, a plot that specifies the maximum available power an installed GT engine is capable of delivering, for a range of pressure altitudes. Note that Fig. 2.18 is not related to the specific set of polynomials presented in Fig. 2.16. Figure 2.18 specifies the maximum available power of the engine, for a continuous power rating and for two distinct types of day. It shows that for standard day conditions (ISA) this specific installed GT engine is limited by the transmission of the helicopter (569 hp.), from sea level up to a pressure altitude of 3,500 ft. Above 3,500 ft. the engine becomes compressor-speed (Ng) limited. Under hot-day conditions (ISA+25°C), the maximum continuous power is limited by the compressor speed throughout the altitude range

presented, from sea-level up to 10,000 ft. At sea-level the installed engine is capable of continuously producing 486 hp. This continuous maximum power reduces to only 403 hp. at a pressure altitude of 10,000 ft.

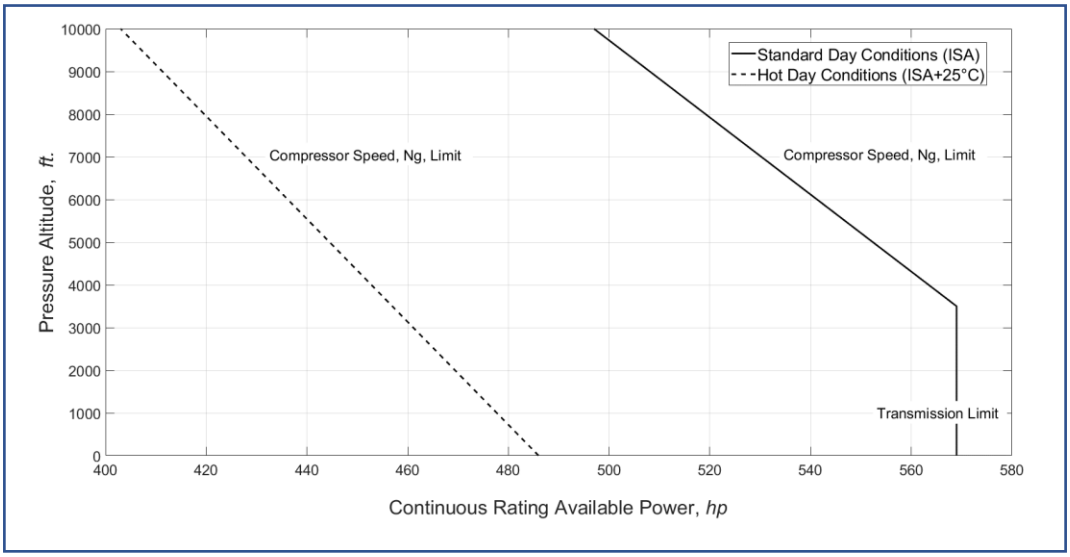

Figure 2.18. Example of an installed engine available power chart. The data represent the available power for continuous operation rating of a GTE, under standard day (ISA) and hot-day (ISA+25°C) conditions.

2.3.2 Hover Performance Flight Testing

As already mentioned in the introduction (Subsection 1.3.2), the objective of hover performance flight testing is to provide a detailed map of the actual power required to sustain the specific type of helicopter at a hover (either in or out of ground effect, IGE/OGE) for all certified gross-weights, external configurations, main-rotor angular speeds and the surrounding atmospheric conditions of air temperature, pressure, and density. This performance 'map' is traditionally presented in a format of a graph, or a set of synchronized graphs and plots. For this objective, the hover performance flight-tester task is to measure the actual power required for hover throughout the flight envelope. Since it is impractical to hover the helicopter in each

combination of gross-weight, main-rotor angular speed, atmospheric conditions of pressure altitude and temperature, the flight tester applies means of dimension analysis as previously discussed in the introduction of this section (2.3). By applying means of dimensional analysis, the flight-tester can both reduce the number of planned flight test sorties to an achievable and practical number, and at the same time to provide a detailed performance map that covers the entire certified flight envelope of the aircraft.

2.3.2.1 Non-Dimensional Hover Performance

The conventional, widely used, flight-test method for hover performance is based on Eq. (2.1) which describes the power required for the main rotor at an OGE hover. The main-rotor system is the principal power consumer in a conventional helicopter hover. Its relative consumption varies between different types of helicopters, and for various flight conditions of a specific type of helicopter, but nevertheless it consumes an immense power portion surrounding 85% [19,20,24]. The remaining ~15% of the hovering power is dissipated by the tail-rotor, all sorts of accessory drives and systems and transmission loss. For this reason, the hover flight test method of the complete helicopter is based on the power of the main-rotor and the applicable Eq. (2.1).

Equation (2.1) is normalized by dividing both of its sides by the term ($\rho_a A_{disk} (\Omega R)^3$) which is a product of the ambient air density, main-rotor disk area and the blade tip tangential speed cubed. This division yields Eq. (2.37) which simply represents the non-dimensional version of Eq. (2.1). The reader should recall that Eq. (2.1) describes the ideal case, or the 'best-case-scenario', of minimum possible induced power in a hover. Leishman [34] compensates for the non-ideal case by implementing an empirical correction factor (k_i) as presented in Eq.(2.38). This (k_i) is called the ***induced power correction factor*** and its typical average value is about 1.15. A power correction value of 1.15 indicates 15% increase in the actual main rotor induced power, as compared to the ideal case of constant induced velocity across the hovering disk.

Mind that Eq. (2.39) merely defines the main-rotor solidity ratio (σ_R), and the two non-dimensional variables known as the 'coefficient-of-power' (C_P), and the 'coefficient-of-weight' (C_W). It is common for applicable textbooks, papers and flight-test reports to interchangeably use either the coefficient-of-weight or the coefficient-of-thrust (C_T) since the thrust equals the weight at a hover, hence C_T equals the coefficient-of-weight (C_W).

$$C_{P_{M/R}} = \frac{\sqrt{2}}{2}\left(C_W\right)^{1.5} + \frac{1}{8}C_{d_0}\sigma_R \tag{2.37}$$

$$C_{P_{M/R}} = k_i\frac{\sqrt{2}}{2}\left(C_W\right)^{1.5} + \frac{1}{8}C_{d_0}\sigma_R \;\; \therefore \; k_i \approx 1.15 \tag{2.38}$$

$$C_{P_{M/R}} \equiv \frac{P_{M/R}}{\rho_a A_{disk}\left(\Omega R\right)^3} \therefore C_W \equiv \frac{W}{\rho_a A_{disk}\left(\Omega R\right)^2} \therefore \sigma_R \equiv \frac{b\bar{c}}{\pi R} \tag{2.39}$$

The conventional flight-test method for hover performance is based on imposing the ***main-rotor*** power onto the ***helicopter as a whole***. This approach is presented as Eq.(2.40), where C_P is the coefficient-of-power based on the total power in hover. The task of the flight-tester is to relate between all ***measured*** coefficient-of-power (C_P) and coefficients of weight (C_W) while hovering under a wide range of gross-weights (W), main-rotor angular speeds (Ω) and ambient air atmospheric conditions. This task can be regarded, mathematically, as Eq. (2.41) for which the flight-tester is required to define the two constants (α_1, α_2) for a particular type of helicopter and/or helicopter external configuration.

$$C_P = \frac{1}{\eta_m}\left(k_i\frac{\sqrt{2}}{2}\left(C_W\right)^{1.5} + \frac{1}{8}C_{d_0}\sigma_R\right) \tag{2.40}$$

$$C_P = \alpha_1 \left(C_W\right)^{1.5} + \alpha_2$$
$$\left\{ \alpha_1 \equiv \frac{\sqrt{2}}{2}\frac{k}{\eta_m} \;:\; \alpha_2 \equiv \frac{1}{\eta_m}\left(\frac{1}{8} C_{d_0} \sigma_R\right) \right\} \tag{2.41}$$

The flight-test team is required to plan and execute numerous hover test-points in order to cover the entire flight envelope of the test article. This includes all certified gross-weights, from minimum to the maximum certified, the entire ambient air temperatures and pressure-altitudes the helicopter is expected to fly at, and throughout the governed range of the main-rotor angular speed (Ω).

There are two fundamental techniques to execute the precise hover sorties for data gathering. The first is the free-flight hover and the second is the tethered hover. The first technique requires the flight-test crew to stabilize the helicopter at a hover and record the essential data to regress the C_P to C_W relationship, as presented in Eq.(2.41). Variation of gross weights is achieved by physical ballast added/removed from the helicopter. Altering the atmospheric conditions is done either by changing testing sites or by hovering in formation to another aerial vehicle, equipped with a low airspeed system capable of establishing a true hover flight.

The second technique of tethered hover is more complicated and requires additional preparation effort. For this technique the helicopter is attached via a tether and an instrumented load-cell device to the ground. The tension in the tether is continuously measured by the load-cell, recorded by the flight-test instrumentation package and presented real time to the flight-test crew. This manner, the thrust generated by the rotor system counter both the physical weight of the helicopter added with the tether tension.

The main advantage of the tethered hover technique over the free-flight technique is that reconfigure the helicopter for different gross-weight is done immediately, just by raising the collective-stick for more thrust. It does not require the flight-test crew to land and to add or remove ballast for the next gross-weight data

planned. Regardless of the hover flight-test technique, whether it is the free-flight or the tethered hover technique, it is utterly important to establish a true and accurate aerodynamically hovering flight. This means that the relative motion between the helicopter and the ambient air is limited to 3 kts. A relative motion that exceeds 3 kts. is outside of the allowed tolerance for this test, since it significantly reduces the induced power, hence deceiving the test results.

A closer look at Eq. (2.41) can provide practical limitations on the empirical values for α_1 and α_2. These limitations allow the flight-tester to perform a basic 'sanity-check' to validate the empirical non-dimensional hover performance equation yielded from the test. As discussed before, typical values for the induced power correction factor (k_i) and the mechanical efficiency (η_m) at hover are 1.15 and 0.85, respectively. This dictates an expected nominal α_1 value of about 0.957. Furthermore, since it is physically impossible for the value of (k_i) to plunge below 1, an established α_1 value below 0.83 should trigger a detailed investigation about either the data analysis process, or the validity of the flight test sorties execution. A possible reason for a lower-than-expected α_1 value can be attributed to hover-data gathering under high relative winds (above the 3 kts. limitation). This will cause for a lower induced power component, hence a lower-than-expected α_1 value. The expected value for α_2 is more trivial and can be easily interpreted from the solidity ratio, zero-lift drag coefficient and the nominal mechanical efficiency at a hover.

Figure 2.19 presents a genuine relationship between the measured coefficient-of-power (Cp) and the coefficient-of-weight (Cw) raised to the 1.5 power, as measured during a limited scope hover performance performed for this research. A linear regression based on minimum squares is performed to retrieve the two coefficients (α_1, α_2). The specific non-dimensional OGE hover performance of the evaluated helicopter is presented in Eq.(2.42). This simple equation is assumed to encapsulate the entire OGE hover performance of the evaluated helicopter. This authentic Bell Jet Ranger (OH-58C) flight-test data are further discussed and analysed in Chapter 5 within the context of deficiencies associated with this current flight-test method.

$$C_P = 1.184\left(C_w\right)^{1.5} + 3.839\times10^{-5} \tag{2.42}$$

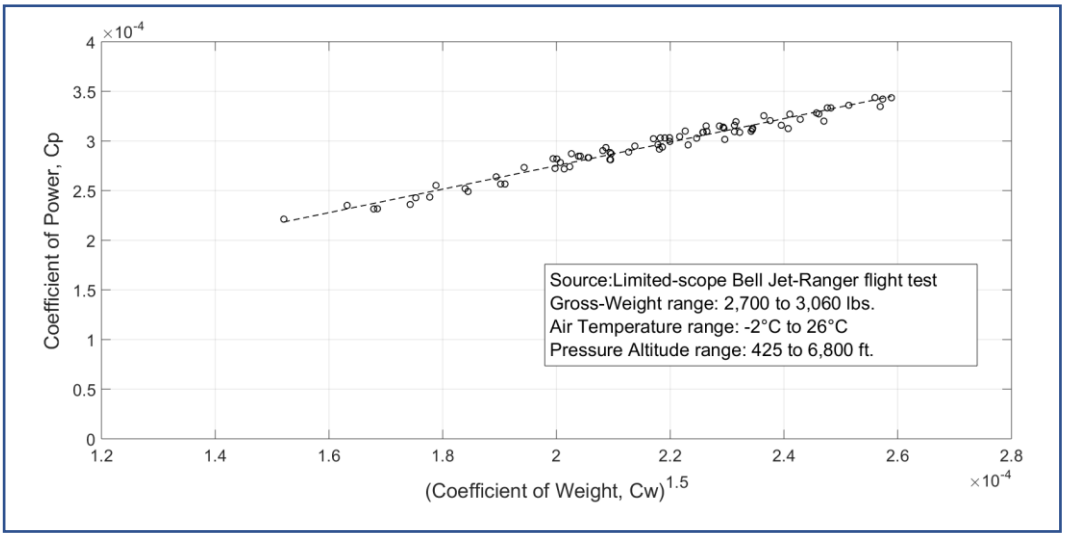

Figure 2.19. Non-dimensional OGE hover performance data. The data represents a limited-scope hover performance flight testing campaign of the Bell Jet-Ranger helicopter that includes 76 stabilized OGE hover points.

2.3.2.2 Un-Referring to Conditions of Choice

For the common helicopter operator this non-dimensional OGE hover performance as presented by Eq. (2.42) does not tell much. It cannot be used explicitly for flight planning purposes. This implicit (or convoluted) OGE hover performance information needs to be simplified and be presented in an accessible manner to the common operator. This simplification procedure, called 'un-referring the data to specific conditions of choice', is discussed and demonstrated hereinafter.

The process starts with reinstituting the explicit definitions of the coefficient-of-power and coefficient-of-weight into the established non-dimensional hover performance (Eq.(2.42)). This back-substitution yields an explicit multivariable function that relates between the power required to hover and the following three independent variables of gross-weight, ambient air density and main-rotor angular

speed (Eq.(2.43)). This allows the flight-tester to generate the performance 'map' mentioned in the introduction of Subsection 2.3.2 above. The power required to sustain a hover flight can be predicted for any arbitrary combination of gross-weight, ambient air density (atmospheric conditions) and main-rotor angular speed. An example OGE hover performance chart based on Eq. (2.43) is presented as Fig. 2.20.

$$\frac{P}{\rho_a A_{disk}\left(\Omega R\right)^3} = 1.184\left(\frac{W}{\rho_a A_{disk}\left(\Omega R\right)^3}\right)^{1.5} + 3.839\times10^{-5} \Rightarrow$$

$$P = 1.184\sqrt{\frac{W^3}{\rho_a A_{disk}}} + 3.839\times10^{-5}\left(\rho_a A_{disk}\left(\Omega R\right)^3\right) \tag{2.43}$$

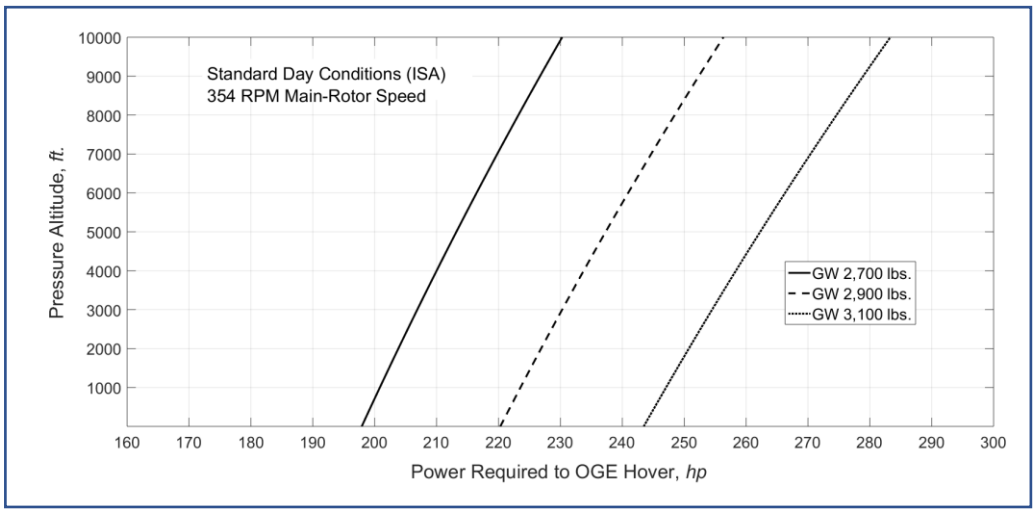

Figure 2.20. Explicit presentation of OGE hover performance. This graph is based on data extracted from the non-dimensional OGE hover performance of the Bell Jet-Ranger helicopter (Eq.(2.43)), and the procedure defined as 'un-referring data to conditions of choice'.

2.3.2.3 Extremum Hover Performance

The previously presented information about the power required to hover a particular helicopter can be combined with the information regarding the available power of the helicopter (Subsection 2.3.1 above) to form what is known as the extremum hover performance of the helicopter. The extremum hover performance

relates to the hover ceiling of the helicopter, i.e., the maximum altitude the helicopter can hover at. Another extremum hover performance aspect is the maximum gross-weight for which the helicopter can establish a hover flight, under various atmospheric conditions. This extremum hover performance evaluation can be accomplished once both the power available, and the power required to hover flight-test campaigns are concluded. Figure 2.21 demonstrates this procedure for a hot-day condition (ISA+20°C). By overlaying the available power on the required power, the extremum hover performance is exposed. On the one hand, the available power of the installed gas-turbine engine reduces with altitude increase (unless limited by the transmission). On the other hand, the power required to hover increases with altitude increase. Both contradicting tendencies reach an equilibrium point which defines the maximum hover altitude (hover ceiling), for a specific gross-weight, specific type of day and a particular engine power rating (continuous, take-off rating, etc.). For clarifying the data presented in Fig. 2.21, the continuous rating OGE hover ceilings of this example helicopter, while operated at standard main-rotor speed (354 RPM) and under ISA+20°C conditions are 9,380, 6,560 and 3,730 ft., for gross-weights of 2,700, 2,900 and 3,100 lbs., accordingly.

The procedure to conclude about the maximum gross-weight the helicopter can hover at for various atmospheric conditions and power ratings, is similar, although not explicitly demonstrated here. For this, Eq.(2.43) should be rearranged to solve for the gross-weight, while all the other variables are treated as known values (P, the ***available*** power, the desired atmospheric conditions expressed by the air density, and the main-rotor angular speed).

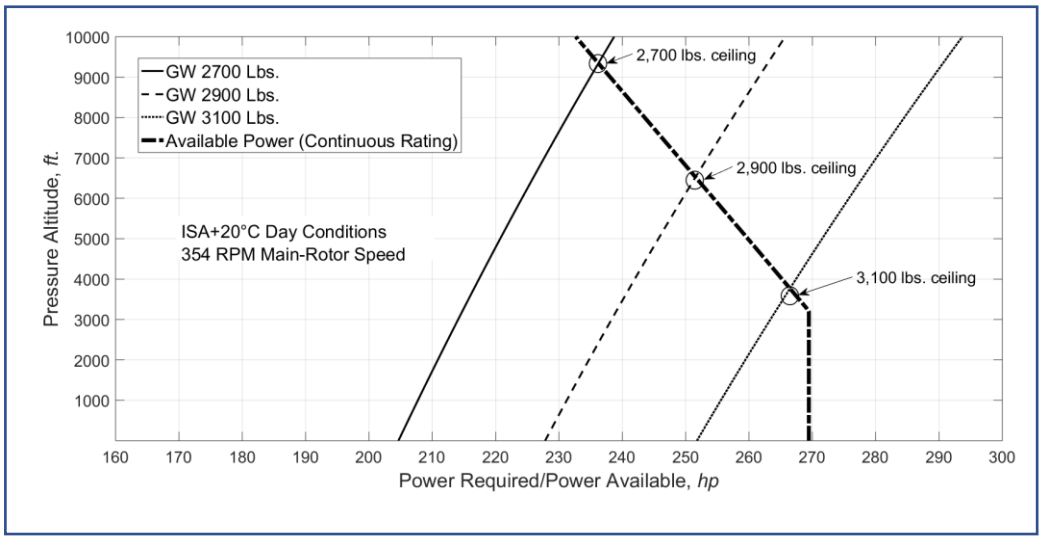

Figure 2.21. Example helicopter OGE hover ceiling determination. The graph shows the hover ceiling of the Bell Jet-Ranger helicopter for three distinct gross-weights, under hot-day conditions (ISA+20°C).

2.3.3 Level Flight Performance Flight Testing

As previously mentioned in the introduction of this thesis (Subsection 1.3.3), the objective of level-flight performance flight testing is to provide a detailed map of the actual power required to maintain the specific type of helicopter at a level flight conditions, for all certified gross-weights, external configurations, main-rotor angular speed range and the surrounding atmospheric conditions of air temperature, pressure, and density. This performance 'map' is traditionally presented in a format of a graph, or a set of synchronized graphs and plots. Moreover, cross-referencing the power required for level flight with the fuel-consumption data base, as evaluated during the available power flight-testing phase (described in Subsections 1.2.1 and 2.3.1 above), enables to define the helicopter 'best-effort' airspeeds, such as airspeeds for maximum range and for maximum endurance. It is impractical for the flight-tester to measure the actual power required for level-flight throughout the flight envelope of the helicopter, and for all possible combinations of configurations and atmospheric conditions. Application of dimensional analysis concepts and means, allows the fight-

tester to both, reduce the number of planned flight test sorties to an achievable and practical number, and to provide a detailed performance map that covers the entire flight envelope of the helicopter.

2.3.3.1 Non-Dimensional Level-Flight Performance

The conventional flight-test method for determining the level-flight performance of a conventional helicopter is thoroughly discussed in the literature [8, 10, 18, 49, 76] and demonstrated in numerous flight-test reports [6, 77, 88]. This method originates from Eq. (2.17) which describes the power required to sustain the helicopter in level flight. Equation (2.17) is converted into a non-dimensional form (Eq.(2.44)) by dividing both sides of the equation by the mathematical-term ($\rho_a A_{disk} \left(\Omega R\right)^3$). The non-dimensional (ND) power required for level-flight equation (Eq.(2.44)) relates between only three variables, the coefficient-of-power (Cp), the advance-ratio (μ) and the coefficient-of-weight (Cw). All other terms in Eq. (2.44) are constants for a specific helicopter and configuration.

$$C_P = \frac{C_W^2}{2\mu} + \frac{1}{8} C_{d_0} \sigma_R \left(1 + k_p \mu^2\right) + \frac{1}{2} \frac{f_e}{A_{disk}} \mu^3 \tag{2.44}$$

The conventional flight-test method for level-flight performance seeks to simplify this rather already simple three-variable relationship. The three-variable relationship described in Eq. (2.44) is further reduced into sets of two-variable mathematical relations that describes the association between the coefficient-of-power (Cp) and the advance-ratio (μ), for discrete values of coefficient-of- weight (Cw). The conventional flight-test method seeks to find this exact empirical relationship (Cp to μ) for the helicopter entire coefficient-of-weight spectrum. For this, the flight-test crew executes numerous 'speed-runs' while maintaining a constant coefficient-of-weight. The method of assuring a constant coefficient-of-weight during the speed run of the helicopter is what defines the flight-test method and can be achieved in two

ways: (1) the constant weight over sigma (W/σ) method; and (2) the constant weight over delta (W/δ) method.

2.3.3.2 Constant Weight over Sigma (W/σ) Method

This flight-test method is the foremost popular and recognized method conducted for the evaluation of the level-flight performance on the conventional helicopter. In this method the flight-test crew maintains the coefficient-of-weight at a certain value by keeping the main-rotor speed constant and maintaining a constant ratio of weight (W) to the air relative density (σ). As presented in Eq.(2.45), the air relative density is defined as the ratio between the ambient air density (ρ_a) and the standard sea level air density (ρ_o). Maintaining a constant ratio of weight to relative density (W/σ) is achieved by a gradual adjustment of the cruise altitude for the speed runs as the helicopter burns fuel and becomes lighter. This constant W/σ method is demonstrated mathematically in Eq.(2.45). The required altitude change in-between test points of the speed-runs is calculated in real time by the test-crew. Typically, the flight-test campaign for a specific helicopter configuration requires the execution of five sorties, each conducted at a different coefficient-of-weight value. The various coefficient-of-weights shall cover the entire certified envelope of the helicopter. Each speed run consists of *at least* eight different airspeeds, beginning at some 'arbitrary' low airspeed to the maximum level flight airspeed defined either by maximum available power (Vh), or by the manufacturer's definition for the 'never-exceed' airspeed (VNE).

$$C_W \equiv \frac{W}{\rho_a A_{disk}\left(\Omega R\right)^2} = \frac{W}{\sigma \rho_o A_{disk}\left(\Omega R\right)^2} = \underbrace{\frac{W}{\sigma}}_{held} \cdot \underbrace{\frac{1}{\Omega^2}}_{fixed} \cdot \frac{1}{\rho_o A_d R^2} \therefore \sigma \equiv \frac{\rho_a}{\rho_o} \qquad (2.45)$$

Figure 2.22 presents a genuine non-dimensional (ND) relationship between the measured coefficient-of-power (Cp) and the advance-ratio (μ) for a *single* coefficient-of-weight (C_W) of 5.79×10^{-3}. Data are gathered for twelve distinct advance-ratios during a dedicated constant W/σ level flight performance flight-test sortie

performed for this research. The presented range of advance-ratio (0.098 to 0.28) translates for the specific helicopter type and test conditions into a true airspeed range in between 42 to 118 kts. A linear regression based on minimum squares is performed to retrieve the four coefficients required to define the particular 3rd order polynomial (Eq.(2.46)). This polynomial represents the non-dimensional level-flight performance of the BO-105 helicopter for the specific coefficient-of-weight ($C_W = 5.79\times10^{-3}$) and for the tested external configuration. This authentic MBB BO-105 helicopter flight-test data is further discussed and analysed in Chapter 6 within the context of deficiencies associated with this current flight test method.

$$C_P = -0.0119\mu^3 + 0.0218\mu^2 - 0.0057\mu + 0.0007 \;\therefore\; C_W = 5.79\times10^{-3} \qquad (2.46)$$

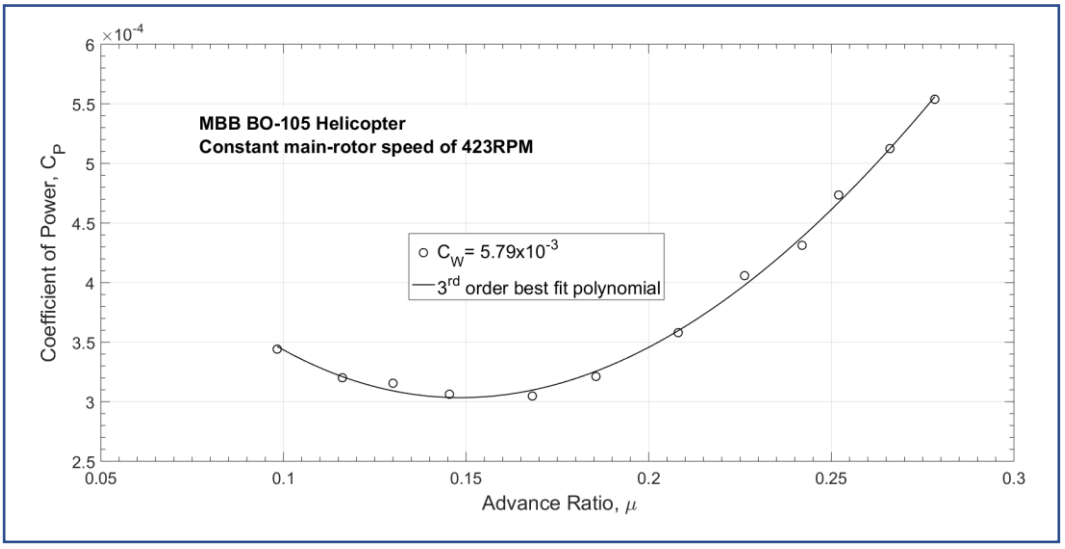

Figure 2.22. Non-dimensional level flight performance. The graph shows the relationship between the coefficient-of-power (Cp) and the advance ratio (μ) for a C_W value of 5.79×10^{-3} as measured on a BO-105 helicopter. Flight test sortie was based on the constant W/σ method.

2.3.3.3 Constant Weight over Delta (W/δ) Method

The second and less common approach of maintaining a constant coefficient-of-weight during the speed run is called the 'weight over delta' method. This method is demonstrated mathematically in Eq.(2.47). Note that the air relative pressure ratio (δ) is defined as the ambient air static pressure (Pa) over the standard sea level air pressure (P_0). By using the equation of state (Eq.(2.48)), the ambient air density is expressed using the ambient static-temperature (Ta) ambient pressure (Pa) and the specific gas constant of the air (R_{air}). It is evident from Eq. (2.47) that by holding a constant ratio of weight over the relative pressure (W/δ) and a constant ratio of static ambient pressure over the angular rotor speed squared (Ta/Ω^2), the flight-test crew assures a constant coefficient-of-weight during the various speed runs. The only advantage this method has over the W/σ method is that by maintaining a constant ratio the flight-test crew can control a particular blade tip Mach number. For flight conditions where compressibility is an issue, the test-crew can avoid gathering flight-test data contaminated with compressibility effects. Nevertheless, level-flight performance is typically required for flight conditions that include compressibility effects. This constant W/δ flight-test method requires even more flight-test sorties than the amount required for the W/σ method. This increased number of sorties is mostly attributed to the complexity and cumbersome associated with the continuous adjustments of the main-rotor angular speed.

$$C_W \equiv \frac{W}{\rho_a A_{disk} (\Omega R)^2} = \frac{W}{\left(\frac{\delta P_o}{R_{air} T_a}\right) A_{disk} (\Omega R)^2} = \frac{W}{\underbrace{\delta}_{held} \underbrace{\Omega^2}_{fixed}} \cdot \frac{T_a}{P_o A_{disk} R^2} \cdot \frac{R_{air}}{}$$
$$\delta \equiv \frac{P_a}{P_o} \therefore \rho_a = \frac{\delta P_o}{R_{air} T_a} \tag{2.47}$$

$$P_a = \rho_a R_{air} T_a \tag{2.48}$$

2.3.3.4 Un-Referring to Conditions of Choice

As stated for the hover performance is Subsection 2.3.2.2 above, this non-dimensional level-flight performance (Eq.(2.46)) will not be appreciated by the common helicopter operator, since it cannot be used explicitly for the task of flight planning. However, this implicit information can be simplified or 'un-referred' to specific conditions of choice. According to this conventional method, the coefficient-of-power (Cp) and the advance-ratio (μ) are interrelated in level-flight as per Eq.(2.46) as long as the coefficient-of-weight of the helicopter equals 5.79×10^{-3}. For a normal operations main-rotor speed of 423 RPM (blade tip speed of 715 fps.), this specific coefficient-of-weight value can be converted into a range of gross-weight and ambient density combinations (Eq.(2.49)). Exhausting the one degree of freedom by choosing an arbitrary gross-weight of 4,850lbs (within the tested range) defines the applicable ambient density of 0.002 slug/ft^3. This ambient air density corresponds to an altitude of 5,744 ft. under standard day conditions. The coefficient-of-power can also be reduced into a dimensional value as expressed by Eq.(2.50). Next, by using the empirical level-flight model retrieved from the flight-test campaign (Eq.(2.46)), the actual power required to sustain a 4,850lbs. BO-105 helicopter in level-flight and under the relevant conditions (5,744 ft. standard day, 423 RPM main-rotor speed) is known. This is expressed as Eq.(2.51) and illustrated in Fig. 2.23. This tedious procedure is repeated for the entire flight envelope covered by the flight-testing sorties.

$$C_W \equiv \frac{W}{\rho_a A_{disk} \left(\Omega R\right)^2} = 5.79\times10^{-3} \xrightarrow[A_{disk}=818\,ft^2]{\Omega R=715\,fps}$$

$$W[lbs.] = 2.422\times10^{6}\,\rho_a[slug/\,ft^3] \tag{2.49}$$

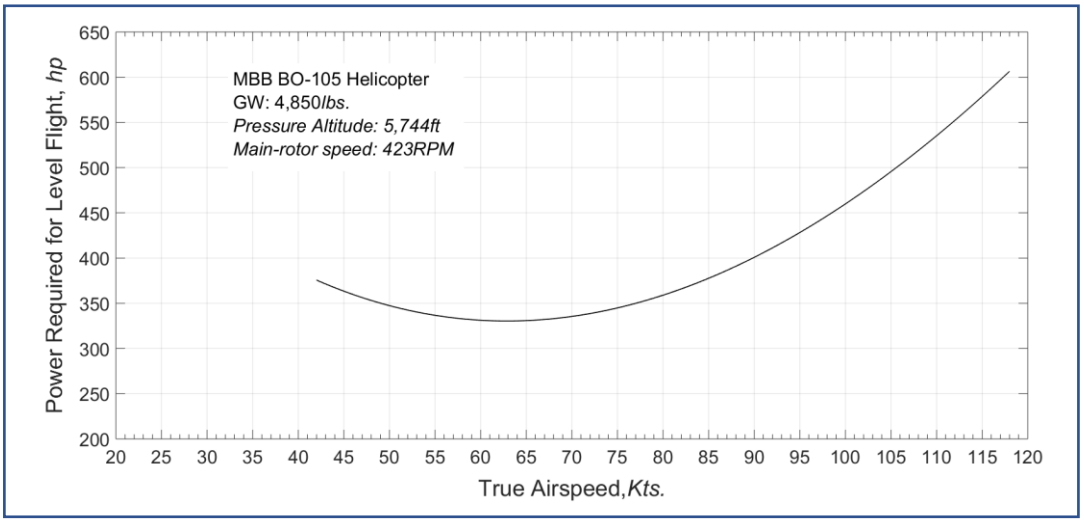

Figure 2.23. Level-flight performance of an example helicopter. The graph is based on extracted data from the ND level-flight performance (Eq.(2.46)) and the procedure discussed in Subsection 2.3.3.4, 'Un-Referring to Conditions of Choice'.

$$C_P \equiv \left.\frac{P}{\rho_a A_{disk}\left(\Omega R\right)^3}\right|_{\substack{\Omega R=715\ fps \\ A_{disk}=818\ ft^2 \\ \rho_a=0.002 slug/ft^3}} \rightarrow P[hp] = 1.089\times 10^6 C_P \tag{2.50}$$

$$P[hp] = 1.089\times 10^6\left(-0.0119\mu^3 + 0.0218\mu^2 - 0.0057\mu + 0.0007\right) \therefore \mu \in [0.098, 0.28] \tag{2.51}$$

Once a theoretical foundation for the relevant sections of helicopter performance and the associated conventional flight test methods have laid down, the substantial portions of the research are presented in the following chapters. Chapter 2 is intendent to provide the crucial theoretical background to allow the reader for a full understanding of the succeeding chapters of the thesis that discuss deficiencies embedded within the conventional flight test method and propose enhanced methods instead.

Nothing takes place in the world whose meaning is not that of some maximum or minimum.

Leonard Euler

3 A MULTIVARIABLE APPROACH IN GAS-TURBINE ENGINE TESTING

3.1 CHAPTER OVERVIEW

Helicopter performance relies heavily on the available output power of the engine(s) installed. A simplistic single-variable approach is often used within the flight-testing community to reduce flight-test data in order to predict the available gas-turbine engine power under various atmospheric conditions. This conventional approach which often results in unrealistic power predictions was previously debated in Subsection 2.3.1. This chapter presents a novel method for analysing flight-test data of a helicopter gas turbine engine. The so-called "Multivariable Polynomial Optimization under Constraints" (MPOC) method is capable of providing an improved estimation of the engine maximum available power. The MPOC method relies on optimization of a multivariable polynomial model subjected to equalities and inequalities constraints. The Karush-Khun-Tucker (KKT) optimization method is used with the engine operating limitations serving as inequalities constraints.

This Chapter 3 was published as a journal paper (i) and as a conference paper (ii):

i. Arush, I., and Pavel, M.D., "Helicopter Gas Turbine Engine Performance Analysis: A Multivariable Approach", Proceedings of the Institute of Mechanical Engineers, Part G: Journal of Aerospace Engineering, Vol. 223, No. 3, March 2019.
ii. Arush, I., & Pavel, M.D., "Flight testing and analysis of gas turbine engine performance: A multivariable approach." In C. Hermans (Ed.), Proceedings of the 44th European Rotorcraft Forum: Delft, The Netherlands, September 2018.

The MPOC method is applied to a set of flight-test data of a Rolls Royce/Allison MTU250-C20 gas turbine, installed on a MBB BO-105M helicopter. It is shown that the MPOC method can predict the engine output power under a wider range of atmospheric conditions and that the standard deviation of the output power estimation error is reduced from 13hp in the single-variable method to only 4.3hp using the MPOC method (over 300% improvement).

3.2 INTRODUCTION

Flight testing is an expensive activity that requires efficient methods for determining correctly the helicopter performance. Such methods involve considerations regarding testing techniques and data reduction of the raw flight-test data. This chapter relates to the flight-test methodology performed for defining the maximum available power of a helicopter gas-turbine engine. Unlike the conventional single-variable method, the novel method presented in this chapter is based on multivariable polynomials defined for the engine parameters, i.e., shaft output power, compressor speed, temperature and fuel-flow. It is shown that this multivariable approach results in more realistic and accurate modelling of the gas-turbine engine output power.

This chapter is structured as follows: following this short introduction, the conventional single-variable method is applied in Section 3.3 to a set of authentic flight test data (34 stabilized test points) of a Rolls Royce/Allison MTU250-C20 gas turbine engine, installed as the left engine on a MBB BO-105 helicopter used for training at the National Test Pilot School in Mojave, California. The two phases of the conventional methodology, as previously presented in Chapter 2 (Subsection 2.3.1), are closely executed to determine the maximum available power of this particular MTU250-C20 gas-turbine engine. In Section 3.4 the novel MPOC methodology is presented and demonstrated by using the same flight test data used for the conventional single-variable method. Final conclusions and recommendation are provided in Section 3.5.

3.3 THE CONVENTIONAL SINGLE-VARIABLE METHOD

The useful performance of any helicopter depends on the amount by which the power available exceeds the power required [79]. The conventional single-variable method widely used by the flight-test community for determining the maximum output power of the helicopter engine is based on gathering stabilized engine(s) parameters (such as temperature, compressor speed, fuel-flow and shaft output power) accompanied by their corresponding atmospheric conditions prevailed during the test [18-21]. These flight-test data are collected while flying the helicopter throughout its certified envelope and collecting engine parameters to their approved operating limitations. Once a substantial data base is gathered it can be analysed with the final goal of deriving the maximum shaft output power that the turbine engine can deliver under various combinations of atmospheric conditions. One should comprehend that the limiting factor for the maximum output power could change under different atmospheric conditions. For example, under hot day conditions the engine maximum output power could be limited by the engine temperature, while under relatively cold day conditions the engine compressor speed could limit the maximum output power the engine can deliver. The flight-test methodology must provide the answer to the following two questions: what is the maximum output power, and what is the related limiting factor. The limiting factor can be either one (or a combination) of the engine temperature, the engine compressor speed or the fuel flow to the engine. Another common power-limiting factor is the maximum transmission torque. Although this limiting factor is not an ***engine*** limitation 'per-se', it has a fundamental effect on maximum output power of the engine.

3.3.1 Phase I – Engine 'Rules of Operation'

The first step in analysing the specific BO105 gas turbine engine data is to 'correct' or 'non-dimensionalize' the raw flight-test data of 34 stabilized test points. The four

engine parameters: shaft output power, compressor speed, temperature and fuel-flow are corrected using the corresponding atmospheric ambient conditions and are converted into, CSHP, CNg, CTGT, and CWf respectively. As previously mentioned in Chapter 2, the definitions of these non-dimensional variables are presented in the nomenclature and the rigorous procedure to derive these corrected variables is provided in Appendix A.

By applying common methods of linear regression, the following set of third order single-variable polynomials is retrieved to relate between the corrected output power and each one of the other corrected variables of the specific gas-turbine engine, as given by Eq.(3.1), Eq.(3.2), and Eq.(3.3). Note that third order polynomials are employed for the reason they are the lowest order that enable modelling an inflection point, a fundamental behaviour of the gas-turbine engine.

$$\left\{\begin{array}{l} CSHP = \tilde{f}_1(CNg) = a_1(CNg)^3 + a_2(CNg)^2 + a_3(CNg) + a_4 \\ \\ (a_1 \quad a_2 \quad a_3 \quad a_4) \equiv (-0.009947 \quad 2.95 \quad -273.47 \quad 8153.2) \end{array}\right\} \tag{3.1}$$

$$\left\{\begin{array}{l} CSHP = \tilde{f}_2(CTGT) = a_1(CTGT)^3 + a_2(CTGT)^2 + a_3(CTGT) + a_4 \\ \\ (a_1 \quad a_2 \quad a_3 \quad a_4) \equiv (-3.328\times10^{-5} \quad 0.068 \quad -43.87 \quad 9256.7) \end{array}\right\} \tag{3.2}$$

$$\left\{\begin{array}{l} CSHP = \tilde{f}_3(CW_f) = a_1(CW_f)^3 + a_2(CW_f)^2 + a_3(CW_f) + a_4 \\ \\ (a_1 \quad a_2 \quad a_3 \quad a_4) \equiv (-9.37\times10^{-6} \quad 0.002 \quad 2.56 \quad -234.32) \end{array}\right\} \tag{3.3}$$

These polynomials, based on actual flight-test data, serve as empirical models to represent the 'rule of operation' of the specific MTU250-C20 gas turbine engine, installed as the left engine on the specific BO-105 helicopter, and at the specific phase of its life cycle. Each polynomial is treated like the 'finger print' of the specific installed engine in the particular helicopter, representing the mathematical relationship between the corrected output power and the separate corrected engine variable (temperature,

compressor speed and fuel-flow). Figure 3.1 presents the 34 stabilized test points of the specific MTU250-C20 gas turbine engine, accompanied by the three best-fit third order polynomials specified in Eq.(3.1), Eq.(3.2) , and Eq.(3.3).

As previously mentioned, the requirement for these polynomials to be of the third order is to ensure the empirical model captures an inflection point of the engine performance. This inflection point represents a fundamental property of any gas-turbine engine for which the rate of change in output power with respect to a particular engine variables (compressor speed, temperature, or fuel-flow) changes its sign. For the same amount of engine variable increase, the resulted increase in engine output-power is to be reduced beyond the inflection point, as compared to the output-power increase below this inflection point.

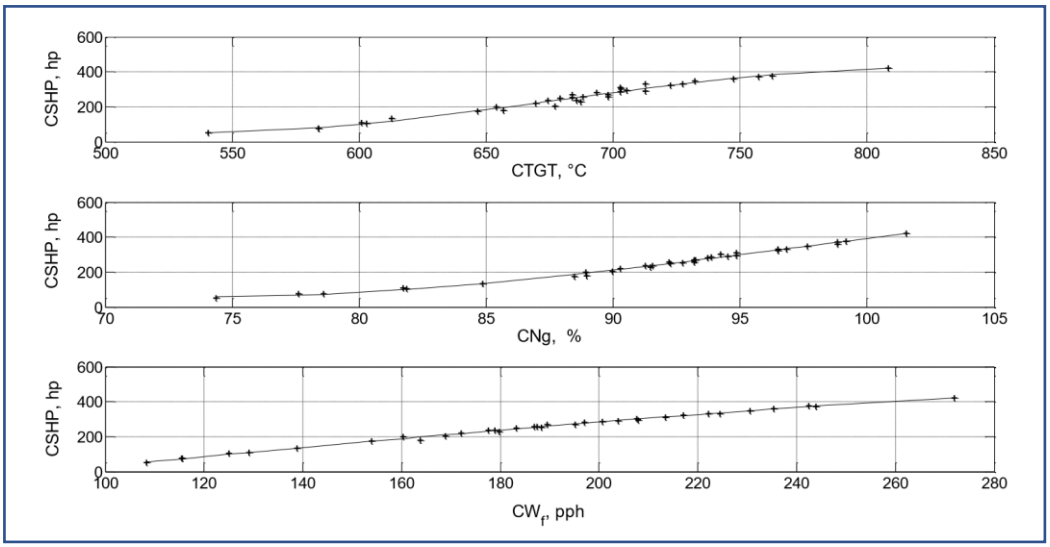

Figure 3.1. Nom-dimensional single variable engine performance. Data represents 34 stabilized engine operation points of a RR/Allison MTU250-C20 engine installed as a left engine on a BO105 helicopter. The corrected engine output power (CSHP) is separately presented against each of the other corrected variables: corrected engine temperature (CTGT), corrected compressor speed (CNg), and corrected fuel-flow (CW_f, presented in pounds per hour units).

3.3.2 Phase II – Maximum Available Power

The second phase of the single-variable method uses the empirical models retrieved from Phase I (Eq.(3.1), Eq.(3.2), and Eq.(3.3)) to define the maximum available power the installed engine can deliver, for any desired power rating and under any atmospheric conditions as selected by the flight tester. This phase involves an iterative procedure, as previously explained in Chapter 2 (Subsection 2.3.1.2) and illustrated by Fig. 2.17. The data presented in Fig. 3.2 were derived by following the relevant iterative procedure with the specific polynomials (Eq.(3.1), Eq.(3.2), and Eq.(3.3)). Figure 3.2 shows the synthesised data for up to 12,000 ft. of pressure-altitude and for five distinct day conditions; a standard day (ISA), 10°C and 20°C hotter than standard, and 5°C and 10°C colder than standard day conditions. Figure 3.2 presents the ***estimated*** maximum continuous output power of the engine based on a set of 34 stabilized engine flight-test data points.

The continuous power rating of this type of engine was set at engine temperature of 738°C and compressor speed of 105%. For the fuel-flow a fictitious limitation (@ 450 pounds per hour) was used. Note that for this specific type of engine and under the atmospheric conditions used for Fig. 3.2, the engine fuel-flow is known to be a non-limiting factor. The maximum continuous power limitation associated with the transmission torque was set at 344 hp. It can be easily seen from Fig. 3.2 that for ISA, ISA-5 and ISA-10 day conditions the helicopter maximum power is limited by the transmission, from sea-level up to 790 ft., 2800 ft. and 3800 ft. above sea-level respectively. For higher pressure-altitudes the limiting factor swaps from the transmission to the engine temperature. As for ISA+10°C and ISA+20°C day conditions, the analysis suggests the engine output power is expected to be temperature limited immediately above sea-level.

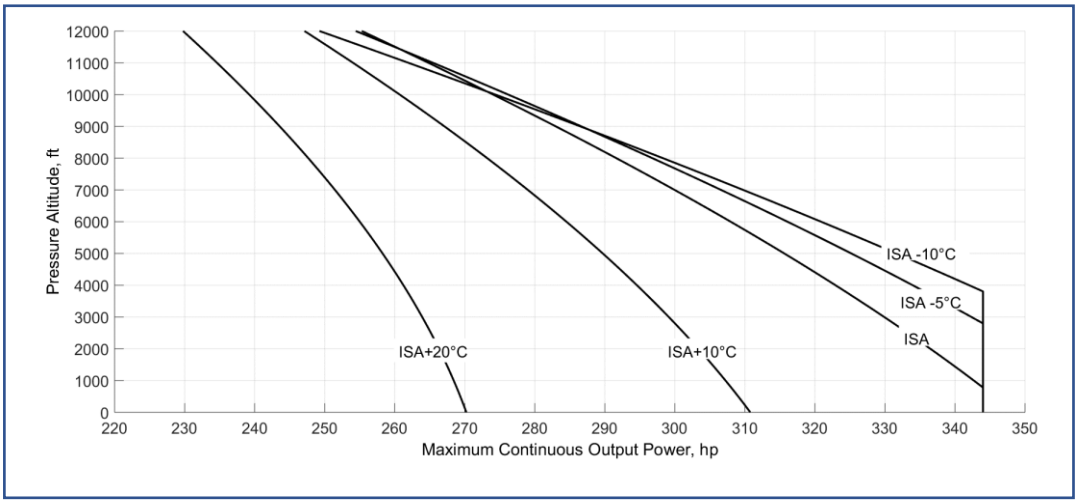

Figure 3.2. Estimated maximum continuous power of the example engine. Note the specific MTU250-C20 engine installed as the left engine on the tested BO105 helicopter is transmission limited for continuous operation under ISA, ISA-5°C and ISA-10°C conditions.

The major disadvantage of this single-variable analysis method lies in the intrinsic assumption of independency between the rules of operation in all three engine limiting factors. This drawback manifests itself by the unrealistic relative behaviour of the three lines of ISA, ISA-5°C and ISA-10°C crossing each other above pressure-altitude of 8,000 ft. as seen in Fig. 3.2. It is physically impossible for a temperature limited engine to deliver more power whilst the ambient temperature is higher.

The absolute errors between the actual measured engine output power and the corresponding predicted values using the reduced polynomials (Eq.(3.1), Eq.(3.2), and Eq.(3.3)) are calculated as per Eq.(3.4),(3.5),(3.6), and are presented in Fig. 3.3.

$$\vec{E}_r\big|_{CNg} = \left\{CSHP_i - f_1\left(CNg_i\right)\right\},\ i = 1,\ldots,34 \tag{3.4}$$

$$\vec{E}_r\big|_{CTGT} = \left\{CSHP_i - f_2\left(CTGT_i\right)\right\},\ i = 1,\ldots,34 \tag{3.5}$$

$$\vec{E}_r\big|_{W_f} = \left\{CSHP_i - f_3\left(W_{fi}\right)\right\},\ i = 1,\ldots,34 \tag{3.6}$$

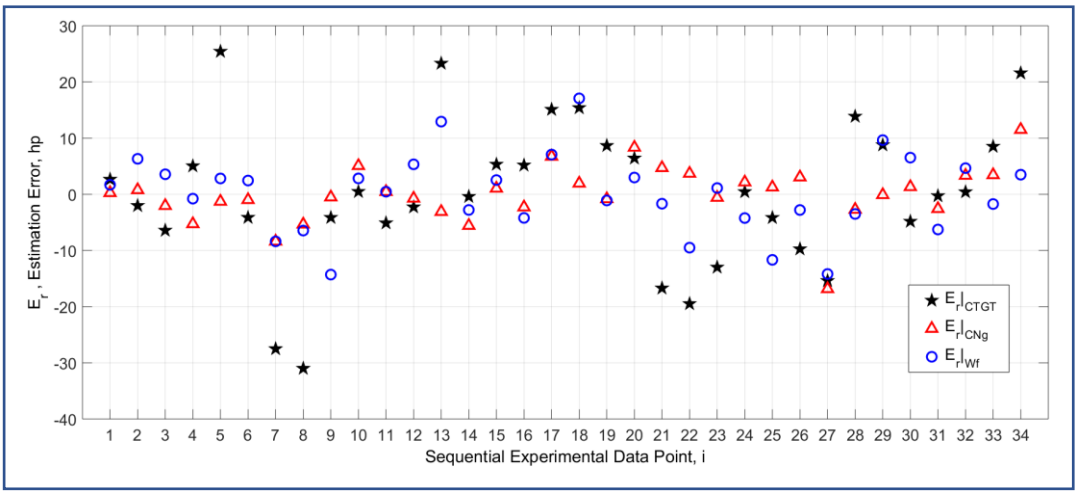

Figure 3.3. The MTU250-C20 engine power estimation errors using single-variable models. Note the relative large estimation errors of up to 30 hp using the engine temperature variable.

These errors were found to be normally distributed about a practically zero mean. Figure 3.4 shows the error standard deviation for each prediction channel plotted against its relevant error mean. This figure also includes a horizontal bar to represent the 95% confidence level interval range for the mean of the error. This bar shows where the mean of the error can be found for the 95% confidence level. Inspecting this figure one can immediately see that the output power prediction, based on engine temperature (Eq.(3.2)) presents the worst performance; the relevant standard deviation of this error is 13 hp. and under 95% confidence level the mean of the estimation could be found anywhere along a range of ±4.6 hp. For the specific engine/helicopter combination tested, a standard deviation of 13 hp is considered a substantial error value for power predictions.

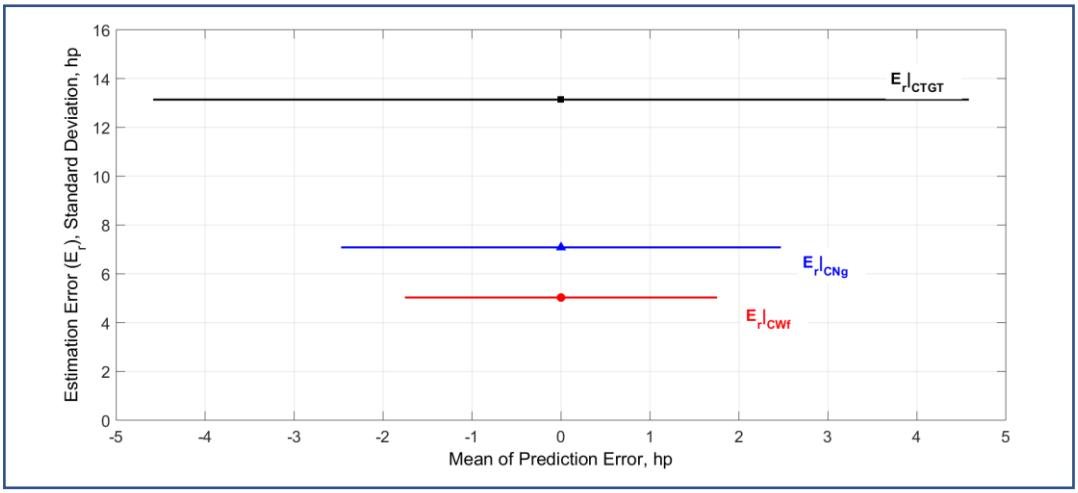

Figure 3.4. Mean and standard deviation of the single-variable estimation errors. The engine temperature based estimation presented the worst performance with an error standard deviation of 13 hp.

Concluding, the conventional single-value method used for determining the maximum output power of the helicopter gas-turbine engine can result in large errors and unrealistic prediction trends. Next section presents a novel, more accurate method for available power determination of a helicopter gas-turbine engine.

3.4 THE MPOC METHOD FOR ENGINE AVAILABLE POWER DETERMINATION

This section presents a novel flight-test method, referred to as 'Multivariable Polynomial Optimization under Constraints' (MPOC), for the task of helicopter gas-turbine engine available power determination. This method requires no change to the way engine performance flight-test sorties are carried out, only to the flight-test data analysis. Using the elegant method of projection onto subspaces a list of mathematical candidate models is derived to best represent the relationship between the engine output power and the engine other variables. The maximum output power of the

engine is assessed as an optimization problem under constraints. The nature of this optimization (maximization) problem has both equalities and inequalities constraints. For this, the Karush-Khun-Tucker (KKT) optimization method which deals with both type of constraints is utilized. The MPOC method presented in this section hereinafter is exemplified with the same MTU250-C20 gas turbine engine flight-test data, used for the conventional single-variable method demonstration in Section 3.3.

The MPOC method is implemented in four phases; phase I is to establish a list of candidate multivariable models to describe the gas-turbine engine rules of operation, Phase II is to fit the candidate models with experimental flight-test data, Phase III concentrates on choosing the right empirical model to represent the gas-turbine engine performance, and in Phase IV the chosen empirical model is used for estimating the maximum available power under a wide range of atmospheric conditions.

3.4.1 Phase I – Multivariable Empirical Models for the Rules of Operation

A convenient mathematical relationship needs to be found for representing the flight-test data. Polynomials serve great role in flight-testing due to their simplicity which makes them suitable candidates for best-fit type models. Various math model search algorithm were developed in the literature of specialty for optimizing regression models of multivariate experimental data obtained in aviation. For examples see Ulbrich [80, 81] and Zhao and Xue [82]. The MPOC method seeks for a multivariable polynomial limited to the third order as in the conventional single-variable method. The first step of the MPOC method is finding candidate multivariable polynomial models to relate between the corrected shaft output power (CSHP), the corrected compressor speed (CNg), corrected engine temperature (CTGT) and corrected fuel flow to the engine (CWf). For simplification and based on common practice, six basic two-variable polynomials of the third order are defined using the three independent engine variables. This results in six different combinations as presented in Table 3.1. Each mathematical term presented in Table 3.1 yields six lower order terms

resulting in a long list of 42 regressors (predictors). However, many of the lower order terms are merely duplicates and can be dismissed. Filtering out repeating terms gives an updated list of regressors as presented in Table 3.2. This table corresponds to a list of 18 candidate regressors to work with for a best fit mathematical expression under the generic expression as given by Eq.(3.7).

Table 3.1. Third order polynomials for GTE performance modeling. This list of third-order polynomials and their lower-order terms yields the empirical model regressors.

#	Mathematical term	List of lower-order terms
1	$(CNg)^3(CTGT)$	CNg, $(CNg)^2$, $(CNg)^3$, CTGT, (CTGT)(CNg), (CTGT)$(CNg)^2$
2	$(CNg)^3(CWf)$	CNg, $(CNg)^2$, $(CNg)^3$, CWf, (CWf)(CNg), (CWf)$(CNg)^2$
3	$(CTGT)^3(CNg)$	CTGT, $(CTGT)^2$, $(CTGT)^3$, CNg, (CNg)(CTGT), (CNg)$(CTGT)^2$
4	$(CTGT)^3(CWf)$	CTGT, $(CTGT)^2$, $(CTGT)^3$, CWf, (CWf)(CTGT), (CWf)$(CTGT)^2$
5	$(CWf)^3(CNg)$	CWf, $(CWf)^2$, $(CWf)^3$, CNg, (CNg)(CWf), (CNg)$(CWf)^2$
6	$(CWf)^3(CTGT)$	CWf, $(CWf)^2$, $(CWf)^3$, CTGT, (CNg)(CTGT), (CNg)$(CTGT)^2$

$$CSHP = f\left(CNg, CTGT, CW_f\right) \approx \alpha_0 + \sum_{i=1}^{n}\left\{\alpha_i f_i\left(CNg, CTGT, CW_f\right)\right\} \therefore n = 18 \qquad (3.7)$$

Table 3.2. Empirical model predictors. An updates list of regressors for best fit hierarchical math regression model.

Single Variable Regressors	Double Variable Regressors
$f_1=(CNg)^3$	$f_{10}=(CNg)(CTGT)$
$f_2=(CNg)^2$	$f_{11}=(CNg)(CW_f)$
$f_3=CNg$	$f_{12}=(CTGT)(CW_f)$
$f_4=(CTGT)^3$	$f_{13}=(CNg)^2(CTGT)$
$f_5=(CTGT)^2$	$f_{14}=(CNg)^2(CW_f)$
$f_6=(CTGT)$	$f_{15}=(CTGT)^2(CW_f)$
$f_7=(CW_f)^3$	$f_{16}=(CNg)(CTGT)^2$
$f_8=(CW_f)^2$	$f_{17}=(CNg)(CW_f)^2$
$f_9=(CW_f)$	$f_{18}=(CTGT)(CW_f)^2$

With the 18 derived regressors one has an enormous amount of possible models to check. The case can be thought as a combination of 1, 2, 3… 18 functions from a set of 18 regressors i.e., 262,143 possibilities as per Eq.(3.8), for which N represents the number of possibilities.

$$N = \binom{18}{1} + \binom{18}{2} + \ldots + \binom{18}{18} = \frac{18!}{1!17!} + \frac{18!}{2!16!} + \ldots + \frac{18!}{0!18!} = 262{,}143 \tag{3.8}$$

The number of possible combinations can be reduced by setting a base model which is a linear combination of the elementary regressors f_1 to f_9 (Eq.(3.10)). The polynomial as given by Eq.(3.10) is addressed in this chapter as model number 1. This way, the problem has been reduced to finding a model which will be constructed from Model 1 superimposed with any combination of the regressors f_{10} to f_{18}. The number of combinations is now reduces to 512 as per Eq.(3.9).

$$N' = 1 + \binom{9}{1} + \binom{9}{2} + \ldots + \binom{9}{9} = 1 + \frac{9!}{1!8!} + \frac{9!}{2!7!} + \ldots + \frac{9!}{0!9!} = 512 \tag{3.9}$$

$$\begin{aligned} CSHP_{M1} = {} & \alpha_1^1 \left(CN_g\right)^3 + \alpha_2^1 \left(CN_g\right)^2 + \alpha_3^1 \left(CN_g\right) + \alpha_4^1 \left(CTGT\right)^3 + \alpha_5^1 \left(CTGT\right)^2 + \\ & + \alpha_6^1 \left(CTGT\right) + \alpha_7^1 \left(CW_f\right)^3 + \alpha_8^1 \left(CW_f\right)^2 + \alpha_9^1 \left(CW_f\right) + \alpha_0^1 \end{aligned} \tag{3.10}$$

This still represents a substantial number of combinations but more manageable. Within the limited scope of this chapter, a performance comparison between ten different models from the 512 is presented. Model 1 presented as Eq.(3.10) is merely being added with the nine regressors (f_{10} to f_{18} of Table 3.2), one at a time. This process of providing candidate multivariable polynomials is presented mathematically as Eq.(3.11). Equation (3.12) presents the suggested model number 4 ($CSHP_{M4}$) as a particular case of the generic formula described by Eq.(3.11).

$$\begin{gathered} CSHP_{MK} = \sum_{i=0}^{9} \alpha_i^K f_i\left(CN_g, CTGT, CW_f\right) + \sum_{j=10}^{K+8} \alpha_j^K f_j\left(CN_g, CTGT, CW_f\right) \\ \left\{ f_0 \triangleq 1, \;\; K = 1,2,\ldots,10 \right\} \end{gathered} \tag{3.11}$$

$$\begin{aligned} CSHP_{M4} = {} & \alpha_1^4 \left(CN_g\right)^3 + \alpha_2^4 \left(CN_g\right)^2 + \alpha_3^4 \left(CN_g\right) + \alpha_4^4 \left(CTGT\right)^3 + \alpha_5^4 \left(CTGT\right)^2 + \\ & + \alpha_6^4 \left(CTGT\right) + \alpha_7^4 \left(CW_f\right)^3 + \alpha_8^4 \left(CW_f\right)^2 + \alpha_9^4 \left(CW_f\right) + \alpha_{10}^4 \left(CN_g\right)\left(CTGT\right) + \\ & + \alpha_{11}^4 \left(CN_g\right)\left(CW_f\right) + \alpha_{12}^4 \left(CTGT\right)\left(CW_f\right) + \alpha_0^4 \end{aligned} \tag{3.12}$$

3.4.2 Phase II – Fitting the suggested models with experimental data

This subsection presents the method used to fit the ten proposed multivariable models (Eq.(3.11), for M=1 to 10) with actual experimental flight-test data. The method used is based on a linear Algebra concept known as projection onto subspaces [83] and is demonstrated hereinafter for Model 1. The 34 flight-test data points of the example MTU250-C20 gas turbine engine considered in this chapter are next substituted in Eq.(3.10). This gives a linear system of 34 equations with ten unknowns (the coefficients α_n^1). This system of equations is compactly represented as Eq.(3.13).

$$\left[A\right] \cdot \vec{\alpha} = \vec{b} \tag{3.13}$$

The matrix A is of size of (34x10) and contains the numerical regressors as columns, α is a column vector (34x1) containing the unknown coefficients and $\vec{b}$ is a column vector (34x1) representing the measured experimental corrected output power of the engine (CSHP). Substituting the regressors of the proposed model number 1 into Eq.(3.13) gives Eq.(3.14).

$$\begin{pmatrix} (CNg_1)^3 & (CNg_1)^2 & CNg_1 & (CTGT_1)^3 & (CTGT_1)^2 & CTGT_1 & (CWf_1)^3 & (CWf_1)^2 & CWf_1 & 1 \\ (CNg_2)^3 & (CNg_2)^2 & CNg_2 & (CTGT_2)^3 & (CTGT_2)^2 & CTGT_2 & (CWf_2)^3 & (CWf_2)^2 & CWf_2 & 1 \\ (CNg_3)^3 & (CNg_3)^2 & CNg_3 & (CTGT_3)^3 & (CTGT_3)^2 & CTGT_3 & (CWf_3)^3 & (CWf_3)^2 & CWf_3 & 1 \\ . & . & . & . & . & . & . & . & . & . \\ . & . & . & . & . & . & . & . & . & . \\ . & . & . & . & . & . & . & . & . & . \\ (CNg_{33})^3 & (CNg_{33})^2 & CNg_{33} & (CTGT_{33})^3 & (CTGT_{33})^2 & CTGT_{33} & (CWf_{33})^3 & (CWf_{33})^2 & CWf_{33} & 1 \\ (CNg_{34})^3 & (CNg_{34})^2 & CNg_{34} & (CTGT_{34})^3 & (CTGT_{34})^2 & CTGT_{34} & (CWf_{34})^3 & (CWf_{34})^2 & CWf_{34} & 1 \end{pmatrix} \times \begin{pmatrix} \alpha_1^1 \\ \alpha_2^1 \\ \alpha_3^1 \\ \alpha_4^1 \\ \alpha_5^1 \\ \alpha_6^1 \\ \alpha_7^1 \\ \alpha_8^1 \\ \alpha_9^1 \\ \alpha_0^1 \end{pmatrix} = \begin{pmatrix} CSHP_1 \\ CSHP_2 \\ CSHP_3 \\ . \\ . \\ . \\ CSHP_{33} \\ CSHP_{34} \end{pmatrix} \tag{3.14}$$

This system of equations is over-determined and does not have an exact solution. However, one can look for the "closest" solution for this system, i.e. the "best-fit" solution. This best-fit solution is denoted as $\{\hat{\boldsymbol{\alpha}}\}$. The matrix constructed from $[A^TA]^{-1}A^T$ is the projection matrix which when multiplied by the vector $\vec{b}$ yields a solution in a subspace of matrix A (Eq.(3.15)). This solution serves as a best-fit or the closest solution one can determine.

$$\{\hat{\alpha}\} = \left[A^T A\right]^{-1} A^T \cdot \vec{b} \tag{3.15}$$

Following the above-described procedure one can immediately solve for the 10 coefficients of model number 1, see Eq.(3.16)

$$\left\{\alpha_i^1\right\} = \left[A^T A\right]^{-1} A^T \cdot \{CSHP\} \tag{3.16}$$

For the numerical set of flight-test data exemplified in this chapter, model number 1 as given in Eq.(3.10) is presented as Eq.(3.17).

$$\left\{\alpha_i^1\right\} \equiv \begin{Bmatrix} \alpha_1^1 \\ \alpha_2^1 \\ \alpha_3^1 \\ \alpha_4^1 \\ \alpha_5^1 \\ \alpha_6^1 \\ \alpha_7^1 \\ \alpha_8^1 \\ \alpha_9^1 \\ \alpha_0^1 \end{Bmatrix} = \begin{Bmatrix} -0.0105 \\ 2.8486 \\ -250.48 \\ 2.386\times10^{-5} \\ -0.046874 \\ 30.406 \\ -8.556\times10^{-5} \\ 0.043963 \\ -5.6956 \\ 945.18 \end{Bmatrix} \tag{3.17}$$

Similar procedure was repeated for all other nine candidate models.

3.4.3 Phase III – selecting the right model for the task

Consider the prediction errors of models number 1 to 10 per an experimental data point as presented in Fig. 3.5 and calculated according to Eq.(3.18).

$$\vec{E}_r\Big|_{MK} = \left\{ CSHP_i - \left(CSHP_{MK} \right)_i \right\} \therefore i = 1,\ldots 34, K = 1,\ldots,10 \tag{3.18}$$

For completeness reasons, Fig. 3.5 includes data obtained from the conventional single-variable analysis method presented in Fig. 3.3. Looking at Fig. 3.5 one can see that, even before any statistical tool is used, each MPOC proposed multivariable polynomial is performing better in predicting the engine output power as compared to the conventional method. However, only one empirical model is required. Since a projection from a limited sample of experimental flight-test data to the entire population needs to be made, inferential statistics tools is utilized. In general, an empirical model is best replicating the experimental data if both the mean and variance of the estimation errors are zero. Obviously, this hypothetical perfect model is not to be found, however the following two approaches look for the closest one.

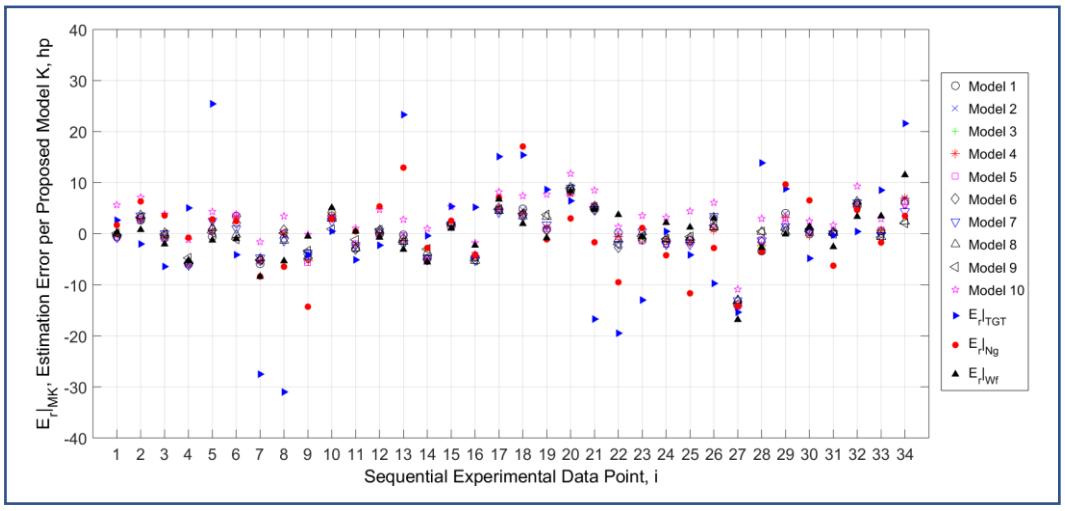

Figure 3.5. Estimation errors for the 10 proposed multivariable models. This figure also includes the estimation errors yielded by the single-variable method. The multivariable empirical models performed far better in estimating the output power of the MTU250-C20 gas turbine engine, as compared with the experimental data.

(1) ***The p-value approach***. The p-value approach ('p' stands for probability) is used to compare between the different ten proposed models. The idea behind the p-value is thoroughly discussed by Guttman et al. [84]. This statistical test concept involves stating two contradicting hypotheses and use the experimental data to either support or to reject the first hypothesis (the Null-Hypothesis, H_0). In our analysis H_0 is set to claim that each of the multivariable models has an array of estimation errors with a zero mean. The level of significance for this statistical analysis was set at 1% (meaning 99% of confidence level). The p-values returned from normal distribution tables represent the smallest significant level that lead to rejecting the Null-Hypothesis. In general, low p-values cast a doubt on the validity of the Null-Hypothesis and once submerge under the significance level of the test, the Null-Hypothesis must be rejected and the Alternative-Hypothesis should be accepted instead. One may think about the p-value as the probability that one would observe a more extreme statistic than actually observed if the Null-Hypothesis were true. All models except for model number 10 strongly supported the Null Hypothesis for the 1% significance level set. All first 5 models returned similar p-values, ranging from 0.999 to 1 with model number 2 being the only one to return a computed p-value of 1. The p-value approach resulted in the elimination of model number 10 from the list.

(2) ***Mean-Variance Plane***. A complementary approach to the p-value concept was to compare the models performance on the mean-variance plane. Figure 3.6 presents the paired values of mean and standard-deviation (square root of the variance) of the estimation prediction errors obtained for the first nine proposed models.

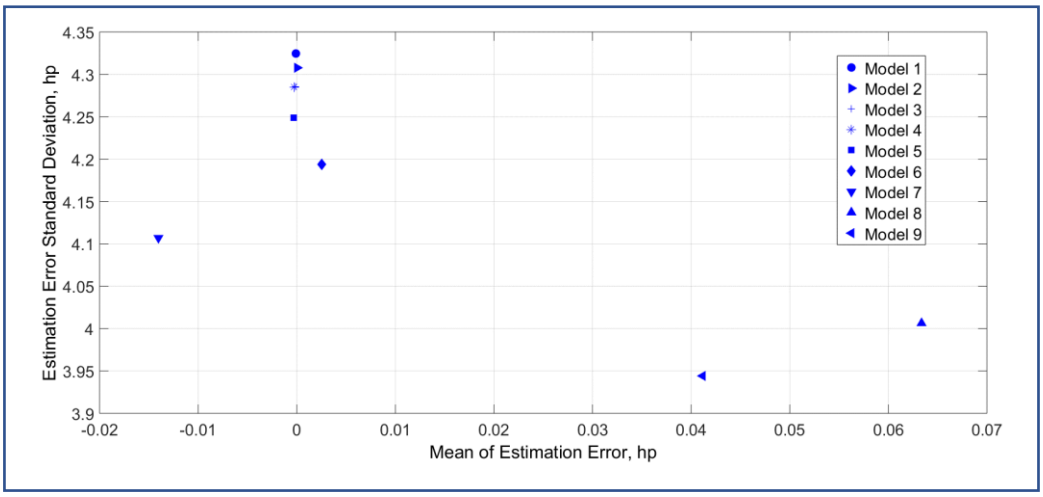

Figure 3.6. Various multivariable empirical models performance. This figure presents the nine multivariable empirical models performance on the mean-standard deviation plane. Model number 10 was omitted from this figure due to an outstanding mean of estimation error of 4 hp.

Concluding from the two approaches and the relative performance of all ten multivariable empirical models involved, model number 2 (Eq.(3.19),(3.20)) was selected as the one to best represent the engine output power. Model number 2 is further used in the subsequent Subsection 3.4.4 for the demonstration of the MPOC method.

$$CSHP_{M2} \approx \alpha_1^2 \left(CN_g\right)^3 + \alpha_2^2 \left(CN_g\right)^2 + \alpha_3^2 \left(CN_g\right) + \alpha_4^2 \left(CTGT\right)^3 + \alpha_5^2 \left(CTGT\right)^2 + \\ + \alpha_6^2 \left(CTGT\right) + \alpha_7^2 \left(CW_f\right)^3 + \alpha_8^2 \left(CW_f\right)^2 + \alpha_9^2 \left(CW_f\right) + \alpha_{10}^2 \left(CTGT\right)\left(CN_g\right) + \alpha_0^2 \tag{3.19}$$

$$\left\{\alpha_i^2\right\} \equiv \begin{Bmatrix} \alpha_1^2 \\ \alpha_2^2 \\ \alpha_3^2 \\ \alpha_4^2 \\ \alpha_5^2 \\ \alpha_6^2 \\ \alpha_7^2 \\ \alpha_8^2 \\ \alpha_9^2 \\ \alpha_{10}^2 \\ \alpha_0^2 \end{Bmatrix} = \begin{Bmatrix} -0.0165 \\ 3.837 \\ -380.69 \\ 3.36\times10^{-5} \\ -0.075 \\ 41.809 \\ -8.35\times10^{-5} \\ 0.043 \\ -5.577 \\ 0.1486 \\ 2242.4 \end{Bmatrix} \tag{3.20}$$

3.4.4 Phase IV – maximum gas-turbine engine output power estimation

Once acquiring a multivariable polynomial to best describe the change in corrected engine output power based on other engine corrected parameters (compressor speed, temperature and fuel-flow), one can look for the maximum available output power of the engine under various atmospheric conditions. The engine output power is limited by reaching one (or more) of its parameters. Determining the maximum output power is equivalent to a mathematical problem of finding an extremum point (maximum output power) under constraints (the engine variables: compressor speed, temperature and fuel-flow). Finding an extremum point of a multivariable function under constraints is of a totally different nature from the case of extremum of a single-variable function. The typical approach for the multivariable case is to use the Lagrange multipliers, but this approach works with equalities constraints only, whereas the problem we have in hand involves both equalities and inequalities constraints.

One applicable method for optimization under both equalities and inequalities constraints is the KKT (Karush-Kuhn-Tucker) thoroughly discussed by Singiresu [85]. According to this KKT approach, Eq.(3.21) provides the general Lagrange equations required for satisfying extremum points of a multivariable function $f(x_i)$ subjected to 'm' number of inequalities constraints, $g(x_i)$, and 'l' number of equalities constraints given by $h(x_i)$. As per Eq.(3.21) η_j represent the Lagrange multipliers associated with the *inequalities* constraints and λ_k represent the Lagrange multipliers associated with the *equalities* constraints.

$$\begin{aligned}
&\frac{\partial f}{\partial x_i}+\sum_{j=1}^{m}\left(\eta_j\frac{\partial g_j}{\partial x_i}\right)+\sum_{k=1}^{l}\left(\lambda_k\frac{\partial h_k}{\partial x_i}\right)=0\therefore i=1,2,3,...,n\\
&x=\left[x_1,x_2,...,x_n\right]\\
&g_j(x)\le 0\therefore\left(j=1,2,...,m\right)\\
&h_k(x)=0\therefore\left(k=1,2,...,l\right)
\end{aligned}\qquad(3.21)$$

The function to be maximized is the empirical model number 2 (Eq.(3.19) ,(3.20)) subjected to several engine operational constraints. For this specific optimization problem to be solvable, at least two equality constraints need to be provided. Those are fulfilled with the engine *internal rule of operation*, as explained hereinafter. Implementing similar approach as described in Subsection 3.4.3 above with the p-value and comparative evaluation on the mean-standard deviation plane, a best-fit surface was calculated to constitute the example MTU250-C20 gas turbine engine multivariable *internal rule of operation*. This type of surface which describes the relationship between the corrected engine temperature (CTGT) and both the corrected compressor speed (CNg) and the corrected fuel-flow (CWf), complemented with the experimental data points, is presented in Fig. 3.7.

The first equality constraint denoted as h_1 and presented in its implicit form as Eq.(3.22) relates between the corrected engine temperature and the corrected compressor speed. The second equality constraint is denoted as h_2 and represents relationship between the corrected compressor speed and the corrected fuel-flow (Eq.(3.23)). Note that h_1 and h_2 constraints are projections of the multivariable rule of operation onto two planes; the CTGT-CNg plane and the CNg-CWf plane, respectively

$$h_1 : CTGT - a_1\left(CNg\right)^3 - a_2\left(CNg\right)^2 - a_3\left(CNg\right) - a_4 = 0 \tag{3.22}$$

$$\begin{Bmatrix} a_1 \\ a_2 \\ a_3 \\ a_4 \end{Bmatrix} = \begin{Bmatrix} 0.0117 \\ -2.9739 \\ 258.49 \\ -7050 \end{Bmatrix}$$

$$h_2 : CNg - b_1\left(CW_f\right)^3 - b_2\left(CW_f\right)^2 - b_3\left(CW_f\right) - b_4 = 0 \tag{3.23}$$

$$\begin{Bmatrix} b_1 \\ b_2 \\ b_3 \\ b_4 \end{Bmatrix} = \begin{Bmatrix} 6.492\times10^{-6} \\ -0.00433 \\ 1.0621 \\ 2.9888 \end{Bmatrix}$$

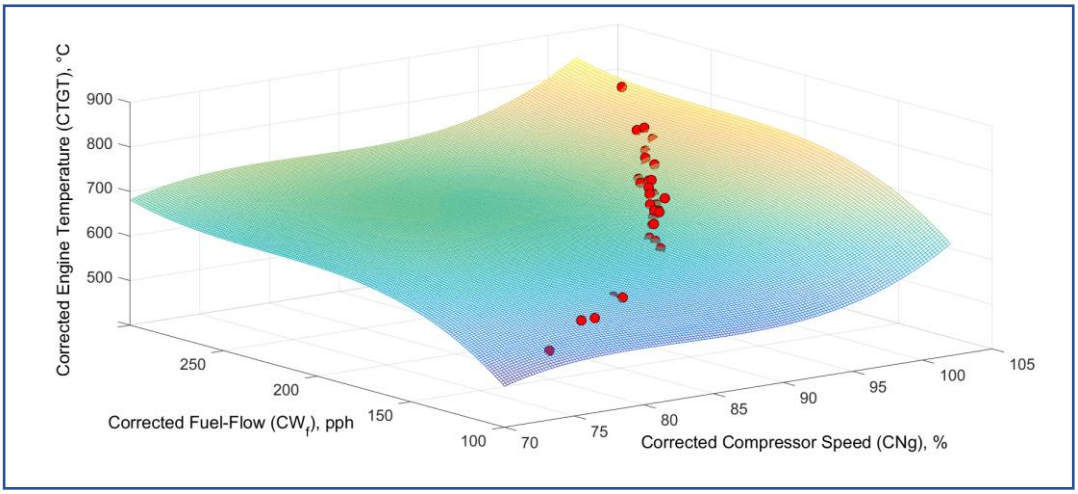

Figure 3.7. The engine internal rule of operation. This figure presents the relationship between the engine corrected temperature and the engine corrected compressor speed and corrected fuel-flow. The circles plotted are the example MTU250-C20 engine data points, which few are obscured by the best-fit surface.

The inequalities constraint for the engine maximum output power are simply the operational limitations imposed on the engine. For the exemplary MTU250-C20 gas turbine engine those are the continuous rating of the engine, denoted as g_1 to g_3 and are presented as equations (3.24) to (3.26).

$$g_1 : CNg - \frac{105}{\sqrt{\theta}} \leq 0 \tag{3.24}$$

$$g_2 : CTGT - \frac{738}{\theta} \leq 0 \tag{3.25}$$

$$g_3 : CW_f - \frac{450}{\delta\sqrt{\theta}} \leq 0 \tag{3.26}$$

The partial differential equations based on Eq.(3.21) and the KKT conditions specified as equations (3.24) to (3.26) for a ***maximization*** problem result in equations (3.27) to (3.29).

$$\frac{\partial(CSHP_{M2})}{\partial(CNg)} - \eta_1 + \lambda_1 \frac{\partial(h_1)}{\partial(CNg)} + \lambda_2 = 0 \tag{3.27}$$

$$\frac{\partial(CSHP_{M2})}{\partial(CTGT)} - \eta_2 + \lambda_1 = 0 \tag{3.28}$$

$$\frac{\partial(CSHP_{M2})}{\partial(CW_f)} - \eta_3 + \lambda_2 \frac{\partial(h_2)}{\partial(CW_f)} = 0 \tag{3.29}$$

Equations (3.27) to (3.29) can be rearranged compactly as presented in Eq.(3.30).

$$\begin{pmatrix} \frac{\partial(CSHP_{M2})}{\partial(CNg)} \\ \frac{\partial(CSHP_{M2})}{\partial(CTGT)} \\ \frac{\partial(CSHP_{M2})}{\partial(CW_f)} \end{pmatrix} = \begin{pmatrix} 1 & 0 & 0 & -\frac{\partial(h_1)}{\partial(CNg)} & -1 \\ 0 & 1 & 0 & -1 & 0 \\ 0 & 0 & 1 & 0 & -\frac{\partial(h_2)}{\partial(CW_f)} \end{pmatrix} \cdot \begin{pmatrix} \eta_1 \\ \eta_2 \\ \eta_3 \\ \lambda_1 \\ \lambda_2 \end{pmatrix} \tag{3.30}$$

The system of partial differential equations (Eq.(3.30)) describes conditions for candidate engine corrected variables representing ***maximization*** of the engine output power. This set of equations does not have a unique solution but a solution with two degrees of freedom for the three distinct cases it represents. The first case (Case I) is when the compressor speed is at its maximum value, i.e., the engine output power is limited by the compressor speed. The second case (Case II) is when the output power is limited by the engine temperature and the last case (Case III) represents a fuel-flow limited engine. Splitting Eq.(3.30) into the three individual cases and applying the KKT conditions on the Lagrange multipliers associated with the inequalities constraints (η_1, η_2, η_3) eliminates the two degrees of freedom and makes each one of these cases to have a unique solution. The three cases are demonstrated hereinafter:

1) Case I – compressor speed limited engine.

Application of the relevant KKT conditions for this case imposes the following conditions on the Lagrange multipliers associated with the inequalities constraints (Eq.(3.31)).

$$\{\eta_1 > 0, \eta_2 = 0, \eta_3 = 0\} \tag{3.31}$$

Combining Eq.(3.31) and Eq.(3.30) results in the following system of equations (Eq.(3.32)):

$$\begin{pmatrix} \frac{\partial(CSHP_{M2})}{\partial(CNg)} \\ \frac{\partial(CSHP_{M2})}{\partial(CTGT)} \\ \frac{\partial(CSHP_{M2})}{\partial(CW_f)} \end{pmatrix} = \begin{pmatrix} 1 & -\frac{\partial(h_1)}{\partial(CNg)} & -1 \\ 0 & -1 & 0 \\ 0 & 0 & -\frac{\partial(h_2)}{\partial(CW_f)} \end{pmatrix} \cdot \begin{pmatrix} \eta_1 \\ \lambda_1 \\ \lambda_2 \end{pmatrix} \therefore \begin{Bmatrix} \eta_1 > 0 \\ CNg = \frac{105}{\sqrt{\theta}} \\ CTGT < \frac{738}{\theta} \\ CW_f < \frac{450}{\delta\sqrt{\theta}} \end{Bmatrix} \tag{3.32}$$

2) Case II – temperature limited engine.

Application of the relevant KKT conditions for this case imposes the following conditions on the Lagrange multipliers associated with the inequalities constraints (Eq.(3.33)).

$$\{\eta_1 = 0, \eta_2 > 0, \eta_3 = 0\} \tag{3.33}$$

Substituting Eq.(3.33) into Eq.(3.30) results in the following system of equations (Eq.(3.34)):

$$\begin{pmatrix} \frac{\partial(CSHP_{M2})}{\partial(CNg)} \\ \frac{\partial(CSHP_{M2})}{\partial(CTGT)} \\ \frac{\partial(CSHP_{M2})}{\partial(CW_f)} \end{pmatrix} = \begin{pmatrix} 0 & -\frac{\partial(h_1)}{\partial(CNg)} & -1 \\ 1 & -1 & 0 \\ 0 & 0 & -\frac{\partial(h_2)}{\partial(CW_f)} \end{pmatrix} \cdot \begin{pmatrix} \eta_2 \\ \lambda_1 \\ \lambda_2 \end{pmatrix} \therefore \begin{Bmatrix} \eta_2 > 0 \\ CNg < \frac{105}{\sqrt{\theta}} \\ CTGT = \frac{738}{\theta} \\ CW_f < \frac{450}{\delta\sqrt{\theta}} \end{Bmatrix} \tag{3.34}$$

3) Case III – fuel-flow limited engine.

Finally, the third case is when the maximum output power of the engine is bounded by reaching the maximum fuel-flow the pump is capable of delivering to the engine. Application of the KKT conditions for this case imposes the following conditions on the Lagrange multipliers associated with the inequalities constraints (Eq.(3.35)).

$$\{\eta_1 = 0, \eta_2 = 0, \eta_3 > 0\} \tag{3.35}$$

Combining Eq.(3.35) with Eq.(3.30) results in the following set of equations (Eq.(3.36)):

$$\begin{pmatrix} \frac{\partial(CSHP_{M2})}{\partial(CNg)} \\ \frac{\partial(CSHP_{M2})}{\partial(CTGT)} \\ \frac{\partial(CSHP_{M2})}{\partial(CW_f)} \end{pmatrix} = \begin{pmatrix} 0 & -\frac{\partial(h_1)}{\partial(CNg)} & -1 \\ 1 & -1 & 0 \\ 1 & 0 & -\frac{\partial(h_2)}{\partial(CW_f)} \end{pmatrix} \cdot \begin{pmatrix} \eta_3 \\ \lambda_1 \\ \lambda_2 \end{pmatrix} \therefore \begin{Bmatrix} \eta_3 > 0 \\ CNg < \frac{105}{\sqrt{\theta}} \\ CTGT < \frac{738}{\theta} \\ CW_f = \frac{450}{\delta\sqrt{\theta}} \end{Bmatrix} \tag{3.36}$$

For demonstration purposes, the specifics of Case II (temperature limited engine) are used with the exemplary MTU250-C20 gas turbine engine flight-test data. Similar methodology can be applied to find the maximum output power for the other

two cases, compressor speed limited engine (Case I) and fuel-flow limited performance (Case III).

The set of equations specified in Eq.(3.34) has a solution if and only if (IFF) the rank of the system matrix is the same as the rank of the auxiliary matrix. This solution would be unique if both ranks equal three (the three unknowns of the problem which are the Lagrange multipliers). This requirement for a unique solution can be stated mathematically as in Eq.(3.37).

$$rank\begin{pmatrix} 0 & -\frac{\partial(h_1)}{\partial(CNg)} & -1 \\ 1 & -1 & 0 \\ 0 & 0 & -\frac{\partial(h_2)}{\partial(CW_f)} \end{pmatrix} = rank\begin{pmatrix} 0 & -\frac{\partial(h_1)}{\partial(CNg)} & -1 & \frac{\partial(CSHP_{M2})}{\partial(CNg)} \\ 1 & -1 & 0 & \frac{\partial(CSHP_{M2})}{\partial(CTGT)} \\ 0 & 0 & -\frac{\partial(h_2)}{\partial(CW_f)} & \frac{\partial(CSHP_{M2})}{\partial(CW_f)} \end{pmatrix} = 3 \qquad (3.37)$$

Instead of pursuing for a pair of corrected compressor speed (CNg) and corrected fuel-flow (CW_f) under a limited corrected temperature ($CTGT_{limit}$) to satisfy Eq.(3.34), one can simplify the process by using the following "back-door" approach: for each and every combination of atmospheric conditions a pair of candidate corrected compressor speed and corrected fuel-flow will be suggested via the engine internal rule of operation (Eq.(3.22) and (3.23)). These candidate pairs complemented with the engine temperature limit will then be evaluated for fulfilment of the KKT conditions required for ***maximization*** of the engine output power. Since the equations specified in Eq.(3.34) have a unique solution, they can be rearranged as in Eq.(3.38). The three engine parameters (candidates for maximum output power) can be used in Eq.(3.38) to solve for the Lagrange multipliers. The three candidate simultaneous engine parameters are then proved valid, as ones that define a maximum output power of a temperature limited engine, if and only if the solution of the system specified as Eq.(3.38) is achieved while coinciding with the KKT conditions required for the case.

$$\begin{pmatrix}\eta_2\\ \lambda_1\\ \lambda_2\end{pmatrix}=\begin{pmatrix}\dfrac{-1}{\left(\partial h_1/\partial CNg\right)} & 1 & \dfrac{1}{\left(\partial h_1/\partial CNg\right)\left(\partial h_2/\partial CW_f\right)}\\ \dfrac{-1}{\left(\partial h_1/\partial CNg\right)} & 0 & \dfrac{1}{\left(\partial h_1/\partial CNg\right)\left(\partial h_2/\partial CW_f\right)}\\ 0 & 0 & \dfrac{-1}{\left(\partial h_2/\partial CW_f\right)}\end{pmatrix}\cdot\begin{pmatrix}\dfrac{\partial\left(CSHP_{M2}\right)}{\partial\left(CNg\right)}\\ \dfrac{\partial\left(CSHP_{M2}\right)}{\partial\left(CTGT\right)}\\ \dfrac{\partial\left(CSHP_{M2}\right)}{\partial\left(CW_f\right)}\end{pmatrix}\therefore KKT:\begin{Bmatrix}\eta_2>0\\ CNg<\dfrac{105}{\sqrt{\theta}}\\ CTGT=\dfrac{738}{\theta}\\ CW_f<\dfrac{450}{\delta\sqrt{\theta}}\end{Bmatrix}\quad(3.38)$$

This "back-door" procedure was executed by using the engine internal rules of operation (Eq.(3.22) and (3.23)) for different type of day conditions (ISA, ISA+10°C, ISA+20°C, ISA-5°C, and ISA-10°C). Figure 3.8 presents the maximum output power of the exemplary MTU250-C20 gas turbine engine alongside with all the KKT requirements as a function of pressure-altitude for an ISA day conditions. It is evident that all of the KKT requirements are met.

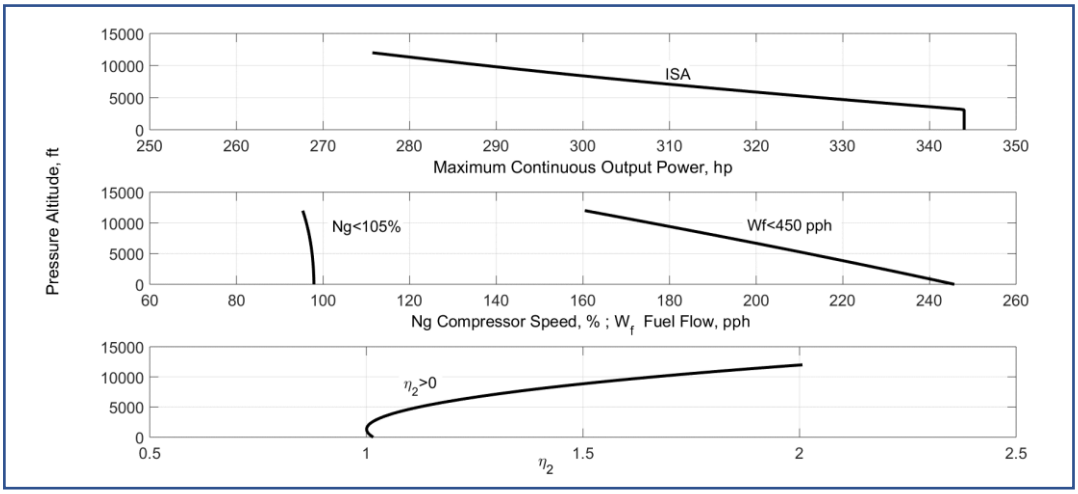

Figure 3.8. A simultaneous presentation of all engine variables. This figure presents the exemplary MTU250-C20 engine parameters between sea level to 12,000 ft. of pressure altitude and under standard day conditions (ISA). The engine maximum continuous output power is limited by its temperature (738°C). Note the fulfilment of all KKT requirements.

The estimated maximum continuous output power of the exemplary MTU250-C20 gas turbine engine as a function of pressure-altitude for different day conditions is presented in Fig. 3.9. The maximum continuous output power of the engine is either transmission limited or temperature limited under all atmospheric conditions

presented in Fig. 3.9. Note the KKT requirements were omitted from Fig. 3.9 although they were all met.

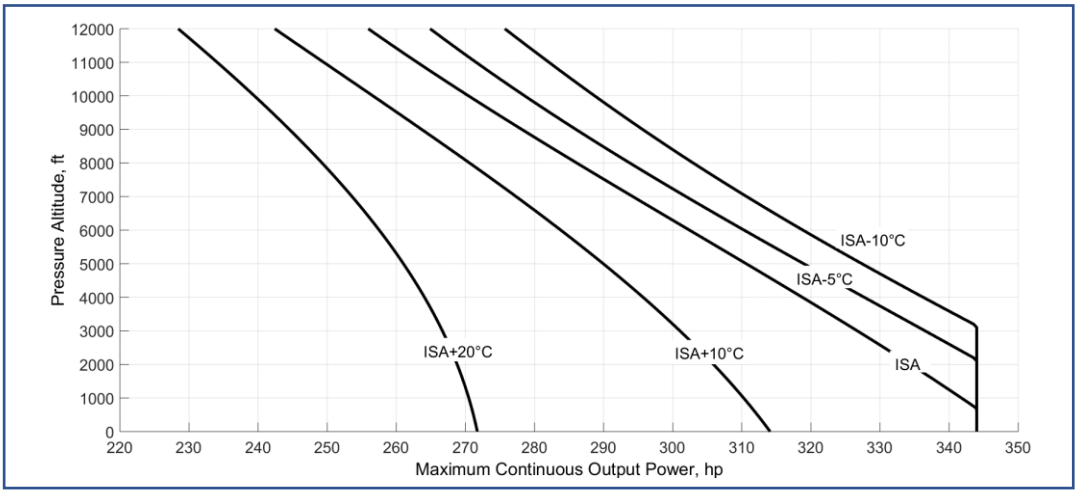

Figure 3.9. A simultaneous presentation of all engine variables. This figure presents the exemplary MTU250-C20 engine parameters between sea level to 12,000 ft. of pressure altitude and under standard day conditions (ISA). The engine maximum continuous output power is limited by its temperature (738°C). Note the fulfilment of all KKT requirements.

3.5 MAXIMUM POWER ESTIMATION COMPARISON

The estimated maximum engine output power was compared using both the conventional single-variable and the MPOC methods. This comparison is presented in Fig. 3.10. From this figure one can observe that both methods demonstrate similar results for atmospheric conditions close to those prevailed during the actual flight-tests (ISA+21°C); however, while the conventional single-variable method completely collapses under standard (ISA) and colder day conditions, the MPOC method predicted reasonable and logical estimations for ISA and colder day conditions. The fundamentally wrong estimation provided by the single-variable method by which a temperature-limited engine delivers more power under higher ambient temperatures, is rectified by the MPOC method.

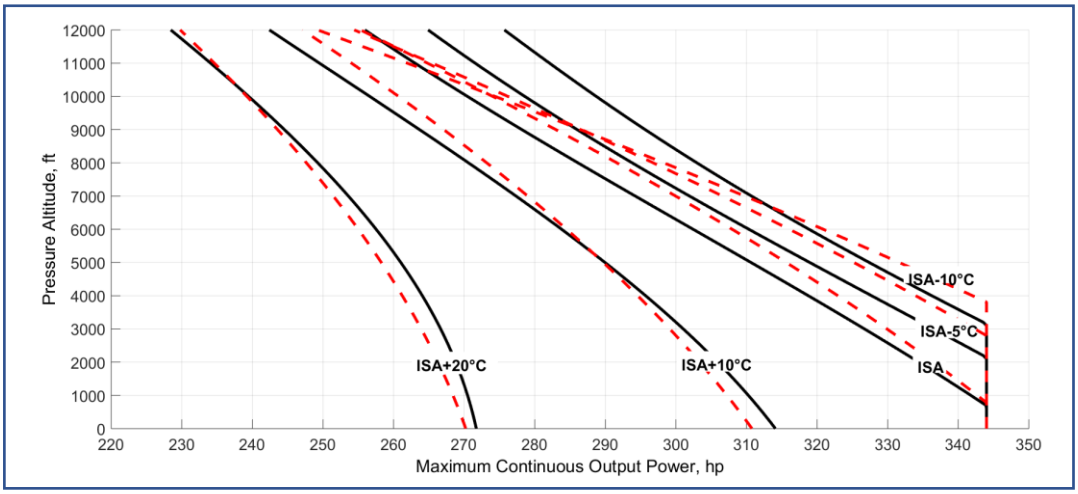

Figure 3.10. MPOC and single-variable methods comparison. This figure shows that while the conventional single-variable method collapses under the estimation for engine maximum continuous output power for standard and colder day conditions, the MPOC method provides logical maximum output power estimations.

3.6 SUMMARY AND CONCLUSIONS

The output power of a helicopter gas turbine engine is a multivariable problem that can be non-dimensionalized as any other physically meaning problem. Over simplification of the problem as linear combination of single-variable models does not provide sufficient accuracy and frequently provides unrealistic estimations for maximum output power under atmospheric conditions different than those prevailed during the test. The novel method presented in this chapter referred to as the Multivariable Polynomial Optimization under Constraints, or MPOC for short, is based on multivariable polynomials. These polynomials demonstrate a substantial better performance in estimating the output power of an exemplary MTU250-C20 gas-turbine engine installed in a MBB BO105 helicopter. The P-value concept complemented with a comparative performance on the mean-standard deviation plane were used successfully as an inferential statistical tool for sorting between various candidate multivariable models to represent the gas turbine engine output power.

The prediction of the maximum output power of the gas-turbine engine can be regarded, mathematically, as an optimization problem of a multivariable function subjected to both equalities and inequalities constraints. The equalities constraints are based on the experimental data and the inequalities are provided by the engine operating limitations. While the conventional single-variable method provides unrealistic estimations for certain atmospheric conditions, the novel MPOC method demonstrates adequate prediction performance for a wider range of atmospheric conditions. Although the conventional single-variable method is simple to use it should be utilized only as a first estimation and not as a formal analysis tool in the process of estimating the maximum output power of a gas turbine engine. The approach presented in this chapter is next expanded in Chapter 4 of this dissertations to include flight-test data of other types of helicopters and engines. This also includes a comparative analysis between a broader base of candidate multivariable polynomials in order to better understand which type of regressors are performing better in modelling the output power of a gas turbine engine.

Algebra is generous. She often gives more than is asked of her.

Jean le Rond D'Alembert

4 A Singular Value Approach in Helicopter Flight Testing Analysis

4.1 Chapter Overview

The process of empirical models evaluation is at the core business of experimental flight-testing data analysis. Accurate and convenient flight-testing of helicopter engine(s) available power is crucial for predicting the total helicopter performance. Common practice in estimation of in-flight helicopter gas turbine engine power consist of a reduction of flight-test data into simplistic single-variable analysis approach. While such an approach is convenient for practical use, it often results in unrealistic predictions of the available engine(s) power. A novel approach for the gas-turbine engine maximum available power problem, referred to as the Multivariable Polynomial Optimization under Constraints (MPOC) method, was introduced in Chapter 3. This chapter is intended to complement the MPOC method and answer the question of which multivariable-polynomial can be generally used in representing helicopter gas-turbine engine performance?

This Chapter 4 was published as the following journal paper: Arush, I., and Pavel, M. D., and Mulder, M., "A Singular Value Approach in Helicopter Gas Turbine Engine Flight Testing Analysis", Proceedings of the Institute of Mechanical Engineers, Part G: Journal of Aerospace Engineering, April 2020. https://doi.org/10.1177/0954410020920060.

In this sense, a variety of seven gas-turbine engines installed on different helicopters are analysed, each one giving 512 possible polynomial models to be used for available-power calculations. While conventional statistical methods of hypothesis-testing failed in providing the answer to the question stated above of which the best general empirical model for representing engine performance is, an alternative approach based on the Singular-Value-Decomposition (SVD) theorem, was proven successful in providing the answer. Moreover, this approach presented in this chapter yielded a short list of ten simple and *convenient* multivariable-polynomials, best representing the performance of all seven engines analysed as a group.

4.2 INTRODUCTION

Flight test engineering is an interdisciplinary science that gathers data and develops methods with the objective of evaluating an aircraft or a system in its operational flight environment. This requisite for flight-testing means that the system or the vehicle under testing requires accurate assessment of its characteristics while operating in its flight environment rather than just relying on the results of ground-based verification methods such as wind tunnels, simulators, and software models [1]. There are many disciplines involved in flight-testing based on the nature of the questions in search. Such ones include, for example, performance assessment, structural integrity testing, handling-qualities evaluation, etc. Regarding helicopter performance assessment, the useful performance of any helicopter is directly derived from the amount by which the engine power (the available-power) surpasses (or falls below) the power required by the main and tail rotor systems, the drag of the fuselage and all other consumers of power for the specific conditions [79].

The "off-the-shelf" engine available power as given by the manufacturer changes once installed in a particular type of helicopter. It typically reduces due to inlet loss. Moreover, the maximum output-power of the installed engine degrades as it matures. Therefore, the actual available-power of the installed engine during a particular phase of its life is of high practicality to helicopter users. This chapter relates

to the methods used in flight-test engineering for measuring helicopter gas turbine engine performance and estimating the maximum available output power under a wide range of environmental conditions.

The conventional flight-test method widely used for determining the maximum power of a helicopter gas turbine engine relies on empirical single-variable polynomials. This method is thoroughly discussed and demonstrated in Chapter 2 (Subsection 2.3.1) and Chapter 3. The method requires the collection of stabilized engine parameters while flying the helicopter throughout its operational envelope. The four main raw engine variables measured in flight (compressor speed, temperature, fuel-flow and the output power) are normalized (or 'corrected') using the surrounding atmospheric conditions. By applying linear regression methods, three third-order single-variable polynomials are defined, representing the empirical relation between the corrected engine power (CSHP) and each one of the three engine corrected variables: corrected compressor speed (CNg), given by Eq.(4.1), corrected temperature (CTGT), given by Eq.(4.2) and corrected fuel-flow (CWf), given as Eq.(4.3).

$$CSHP = \tilde{f}_1\left(CN_g\right) \approx \sum_{i=0}^{n} a_i \left(CN_g\right)^i \therefore n = 3 \tag{4.1}$$

$$CSHP = \tilde{f}_2\left(CTGT\right) \approx \sum_{i=0}^{n} b_i \left(CTGT\right)^i \therefore n = 3 \tag{4.2}$$

$$CSHP = \tilde{f}_3\left(CW_f\right) \approx \sum_{i=0}^{n} c_i \left(CW_f\right)^i \therefore n = 3 \tag{4.3}$$

The maximum available power of the installed engine is next estimated by using these three empirical single-variable polynomials as demonstrated in Chapter 2 (Subsection 2.3.1.2). The three calculated values of the engine output power are first compared with each other and then against the maximum transmission torque (transmission limitation). This comparison is performed through an iterative process executed for various atmospheric conditions. The maximum available power under various atmospheric condition is then prescribed as the minimum value out of all four

values compared. The main advantage of the single-variable method lies in its simplicity. The flight-tester does not need to be confused with which mathematical model to choose, since the method is based on third-order single-variable polynomials. However, this simplicity is also the method's biggest disadvantage since (1) it requires careful analysis of the data especially when the required flight conditions are outside of the limitations of the helicopter; (2) it may not replicate performance limiting factors that depend on actual flight conditions although matching non-dimensional values has been targeted successfully; and (3) it frequently yields poor estimations of the maximum engine output power, especially under atmospheric conditions outside of the actual tested range. A comprehensive demonstration of the poor estimation using the single-variable method is presented in Chapter 3 (Section 3.3).

The novel "Multivariable Polynomial Optimization under Constraints" (MPOC) method to estimate the maximum output power of a helicopter gas turbine engine more accurately and under a wider range of atmospheric conditions is presented in Chapter 3. The main advantages to analysing data using MPOC models over the single-variable method are: (1) it gives the ability to determine the relative influence of one or more predictor variables to the criterion value; (2) it has the ability to identify outliers, or anomalies; and (3) it gives a superior estimation precision. As demonstrated in Chapter 3 for the exemplary MTU250-C20 gas-turbine engine installed in a MBB BO105 helicopter, the MPOC provided a more accurate engine power estimation (in excess of 300%) when compared to the single-variable method. However, the main weakness of the MPOC method is that it struggles with a large number of possible multivariable-polynomials (more exactly 512 polynomials) to choose from without clear and decisive guidelines.

The primary objective of this chapter is to address this disadvantage of MPOC method by developing a systematic and repeatable approach on which specific, pre-defined multivariable-polynomial models shall be used. For this goal the MPOC method is applied to a large set of flight-test data gathered from seven different types of helicopters as presented in Table 4.1. Using the Singular-Value-Decomposition (SVD) approach, the relative performance of 512 different potential models is

compared towards the objective of identifying the best performing multivariable polynomial model to be generally used by the MPOC method.

This chapter is structured as follows: right after the introduction, the MPOC method, as applied to a set of flight-test data gathered from a MBB BO-105 helicopter, is reviewed. The MPOC review in Subsection 4.3.1 also presents the procedure of fitting the candidate multivariable polynomials with the flight-test data. Next in Subsection 4.3.2, the conventional method of hypothesis-testing is used (unsuccessfully) for the task of screening between all 512 candidate multivariable models and choosing the best-performing empirical model, with respect to a group of seven distinct engines (Table 4.1). This unsuccessful screening attempt is then rectified in Section 4.4 which presents a novel method based on the Singular-Value-Decomposition (SVD) theorem. This novel screening method was used successfully with the seven gas-turbine engines in producing a short list of accurate and convenient multivariable-polynomial models. This list is provided in Table 4.4. Section 4.5 draws a short comparison between this chapter findings and other similar studies. A summary and conclusions portion in Section 4.6 completes this chapter.

Table 4.1. Gas-turbine engines used for the analysis. The following table lists the seven different gas-turbine engines used for the MPOC analysis.

Engine No.	Engine Model	Helicopter Installed	Rated Pwr. [hp.]	Installation Config.
1	RR MTU250-C20B	MBB BO-105M	420	Twin
2	Turbomeca Arriel 1E2	Eurocopter EC-145	740	Twin
3	Allison T63-A-700	Bell OH-58C	420	Single
4	Turbomeca Arriel 1C2	Aerospatiale SA365-N2	700	Twin
5	PW-207E	MD-902 Explorer	710	Twin
6	Turbomeca Arriel 1M1	Eurocopter AS-565	780	Twin
7	GE T700-GE-701A	Sikorsky UH-60A	1700	Twin

4.3 GAS-TURBINE ENGINE PERFORMANCE FLIGHT TESTING

4.3.1 Principles of MPOC Method

Unlike the conventional single-variable polynomial method, the MPOC method is seeking for a multivariable-polynomial model representing the engine power while capturing the interrelation between the engine variables. The maximum engine power can then be assessed as an optimization problem of a multivariable-function under constraints. Such a multivariable approach applied to engine analysis results in a more accurate and realistic available power prediction as it contains the intrinsic couplings between all engine variables. Chapter 3 demonstrates that the empirical model for the engine output power (Eq.(4.4)) should rely on a basic model, superimposed with any possible combination of nine regressors (f_1 to f_9), as listed in Table 4.2.

$$CSHP_{M(i)} = CSHP_{M(1)} + f(CN_g, CTGT, CW_f)\Big|_{(i-1)} \quad i = 1,2,3,...,512 \therefore \textit{Model number } i \qquad (4.4)$$

Table 4.2. List of MPOC engine predictors. The following table lists nine engine regressors to be superimposed on Model 1.

$f_1=(CNg)(CTGT)$	$f_4=(CNg)^2(CTGT)$	$f_7=(CNg)(CTGT)^2$
$f_2=(CNg)(CW_f)$	$f_5=(CNg)^2(CW_f)$	$f_8=(CNg)(CW_f)^2$
$f_3=(CTGT)(CW_f)$	$f_6=(CTGT)^2(CW_f)$	$f_9=(CTGT)\ (CW_f)^2$

The basic model, referred to as Model 1 and denoted hereinafter as $CSHP_{M(1)}$, is a third-order multivariable-polynomial in all engine variables given as Eq.(4.5). One should acknowledge there are 511 different combinations of choosing from regressors f_1 to f_9 of Table 4.2, as demonstrated by Eq.(4.6). Adding the basic model 1 with the 511 possible combinations sets the total number of candidate models to be as large as

512. Having a list of 512 candidate models is impractical as the flight-tester still needs to undertake a tedious task of evaluating the performance of each candidate model (Eq.(4.4)) against the actual flight-test data.

$$\begin{aligned} CSHP_{M(1)} &= \alpha_1^1 CN_g^3 + \alpha_2^1 CN_g^2 + \alpha_3^1 CN_g + \alpha_4^1 CTGT^3 + \alpha_5^1 CTGT^2 + \alpha_6^1 CTGT + \\ &+ \alpha_7^1 CW_f^3 + \alpha_8^1 CW_f^2 + \alpha_9^1 CW_f + \alpha_0^1 \qquad \textit{Model number } 1 \end{aligned} \tag{4.5}$$

$$N = \binom{9}{1} + \binom{9}{2} + \ldots + \binom{9}{9} = \frac{9!}{1!\cdot 8!} + \frac{9!}{2!\cdot 7!} + \ldots + \frac{9!}{0!\cdot 9!} = 511 \tag{4.6}$$

4.3.2 Hypothesis testing and P-values

All 512 proposed polynomial models can be fitted with actual experimental flight-test data, yielding the specific coefficients for the best-fit solution. A practical method to solve for the best-fit coefficient, based on linear concept known as projection onto subspaces, is thoroughly described by Strang [83] and demonstrated in Chapter 3 (Subsection 3.4.2). The best-fit solution obtained for any candidate polynomial model can be used to evaluate how precisely this model predicts the actual measured flight-test data. The corrected engine power (CSHP) is estimated by substituting the *measured* independent variables in the model, i.e., corrected engine compressor speed (CNg), corrected engine temperature (CTGT) and corrected engine fuel-flow (CWf). The prediction errors of the arbitrary chosen model 122 for each measured data point of the exemplary MTU250-C20B gas turbine engine of Chapter 3 are then calculated using Eq.(4.7) and presented graphically in Fig. 4.1. The prediction errors of model 122 are *approximately* normally distributed about a practically zero mean (actual mean is $-4\text{x}10^{-10}$ hp).

$$\vec{E}_r\Big|_{122} = \left\{ CSHP_i - \left(CSHP_{122}\right)_i \right\} \therefore i = 1,\ldots 34 \tag{4.7}$$

The conventional approach in flight-testing assessing prediction goodness is based on hypothesis testing and the associated p-values assigned. This approach

follows from the Central Limit Theorem and is thoroughly discussed in literature [84,87]. In a nutshell, one can set-up a hypothesis ('the null hypothesis') with regards to the mean value of the prediction errors and by using the actual measured data, the probability of falsely rejecting this hypothesis (making a 'type-I' error) is calculated. This probability numeral is known as the p-value and once it falls under a predefined value (the statistical significance level) it raises doubts about the statistical validity of the null hypothesis.

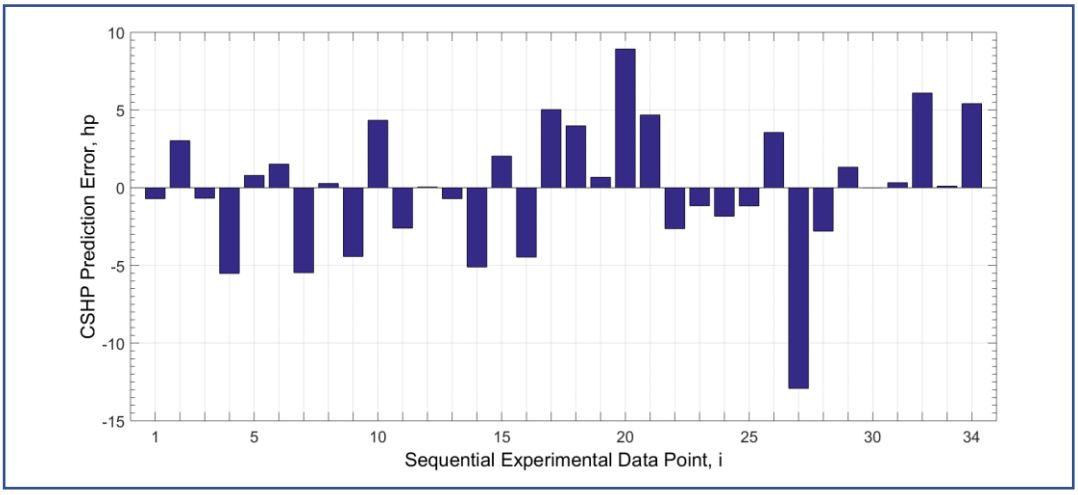

Figure 4.1. Corrected output power prediction errors. This figure shows the MTU250-C20B gas turbine engine corrected output power (CSHP) prediction errors using the arbitrary polynomial Model 122.

Once again, the process is demonstrated by using the exemplary MTU250-C20B engine data and the arbitrary chosen, Model 122. The hypothesis assigned claims all of model 122 prediction errors have a mean of zero. The test-statistic of this two-sided case is calculated as per Eq.(4.8) to be an extremely low value of -5.47×10^{-10}.

$$t_{122} = \frac{\overline{\left(\vec{E}_r\big|_{122}\right)}}{S/\sqrt{n}} \tag{4.8}$$

In Eq.(4.8) the symbol 'n' represents the number of measured test-points and 'S' stands for the sample standard deviation with respect to the estimation errors of the engine power. One should realize for this particular case, low test-statistics values

return large p-values and vice versa. This extremely low test-statistic value returns a calculated p-value of 1 (the maximum available due to software rounding errors). There is no statistical data to support rejection of the null hypothesis, meaning that model number 122 predicts the MTU250-C20B engine performance with zero mean errors. Theoretically, this makes Model 122 an excellent multivariable model for the available power prediction.

4.3.3 Prediction goodness comparison between candidate models

Assuming the arbitrary-chosen model number 122 is the "perfect" multivariable-polynomial model to represent the output power of the BO-105 engine, how will all other 511 candidate models perform? Repeating the previous analysis presented in Subsection 4.3.2 for all other candidate models returned far too many *calculated* p-values of 1. The immediate conclusion one can draw is that the p-value by itself is not an effective screening tool. Since in our case the p-value and the absolute-value of the test-statistic are inversely proportional to each other, it is reasonable to use the test-statistic value itself as an indicator for prediction goodness. The screening process should be based then on minimum values of the test-statistics in lieu of a maximum p-values.

Figure 4.2 presents a wide perspective of the test-statistics, mean of prediction errors and errors standard deviations for all 512 candidate models. Figure 4.3 presents a closer look ("zooming") at the test-statistic of a group of only 84 candidate models, those involving the base model (Eq.(4.5)) superimposed with any combination of three predictors out of the list of the nine (f_1 to f_9 in Table 2). Note that each one of those 84 models returned a perfect *computed* p-value of 1, including models number 62, 88, 107 and 112 which seem to stand out from the group. The conclusion arising from Fig. 4.3 is that the conventional approach of screening models using the p-value is not practical for the specific task of finding the best empirical model to represent gas-turbine engine performance.

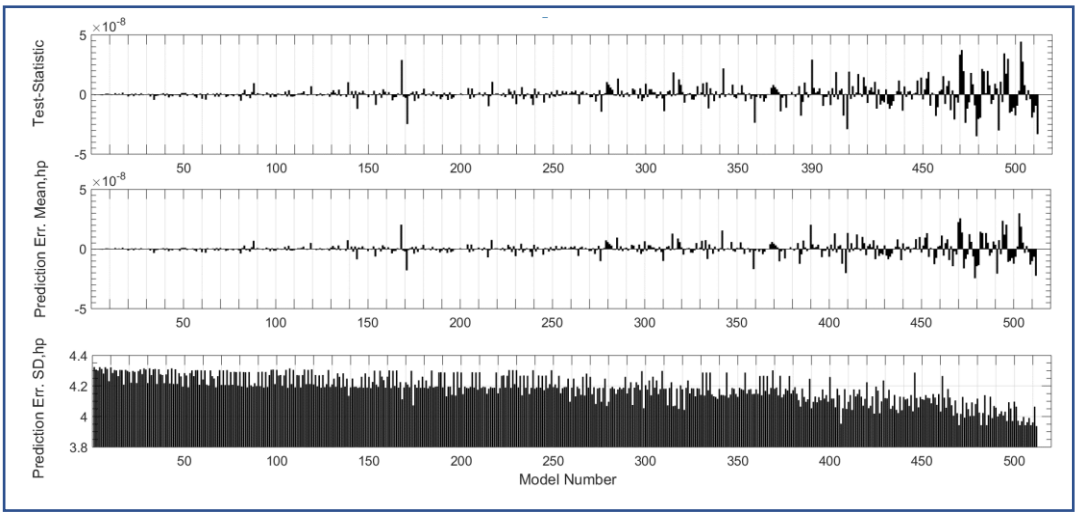

Figure 4.2. Output power prediction performance. This figure shows a wide perspective of all 512 candidate models performance in predicting the exemplary MTU250-C20B engine output power.

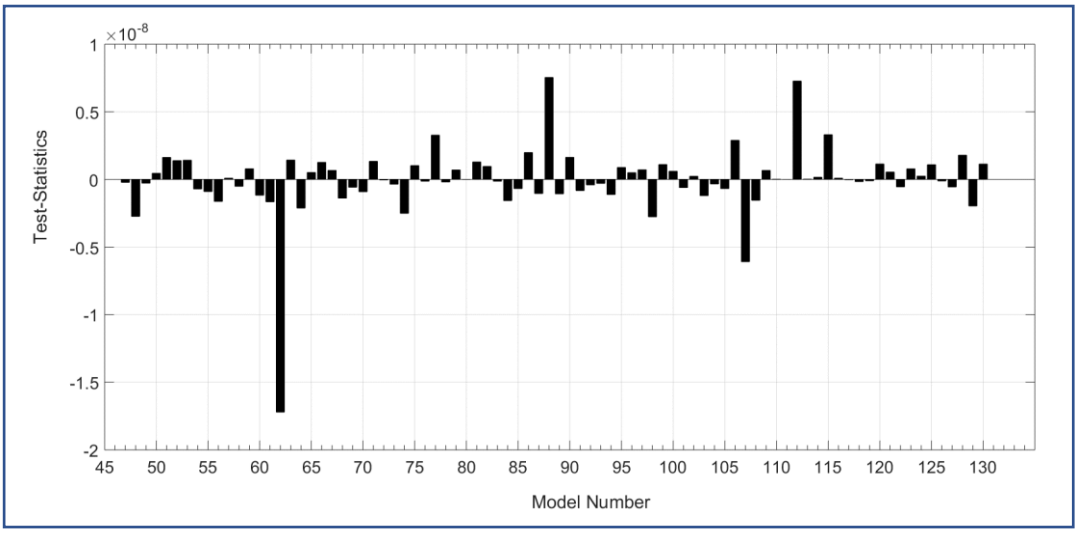

Figure 4.3. Test-statistics of models number 47-130. This figure shows the test-statistics of 84 candidate models (models number 47-130) involving the base Model 1 (Eq.(4.5)) superimposed with any combination of three regressors from Table 4.2.

The absolute-values of the test-statistics are then used instead of the *p-values*. Figure 4.4 presents the test-statistics (absolute-value) of the top ten performing models for the MTU250-C20B engine. Table 4.3 specifies these models in details. Examining Table 4.3, no obvious pattern can be detected with respect to which regressors yield the best prediction performance. Nevertheless, the number of regressors used in the

model has no immediate obvious effect on the prediction performance. Within the set of ten top-performing models there are models which involve additional one, two, three or four regressors to be superimposed over the basic model number 1. The trivial question to be asked next is do these 10 top performing models also excel when applied to ***different gas-turbine*** engines? Can findings from the MTU250-C20B engine installed in the BO-105 helicopter be generalized to other types of helicopter gas-turbine engines? These enquiries are addressed hereinafter.

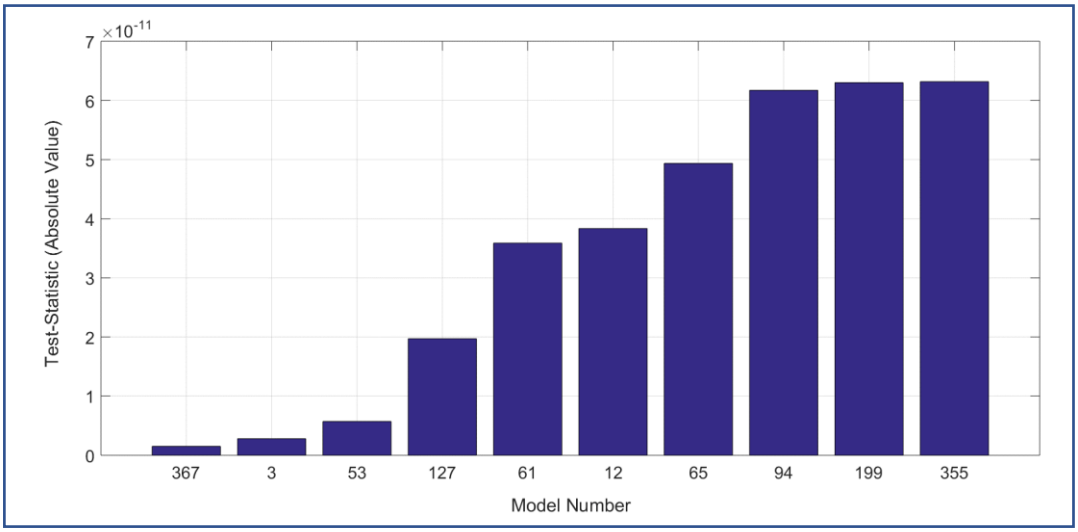

Figure 4.4. Top ten performing models. This figure shows the test-statistics (absolute value) of the top ten performing models for the MTU250-C20B engine installed in the BO-105 helicopter.

Table 4.3. List of 10 top-performing models for the BO-105 helicopter.

Auxiliary Regressors	**Model Number**									
Involved †	***367***	***3***	***53***	***127***	***61***	***12***	***65***	***94***	***199***	***355***
$f_1=(CNg)(CTGT)$			x		x	x	x			
$f_2=(CNg)(CW_f)$		x	x					x	x	X
$f_3=(CTGT)(CW_f)$	x					x			x	
$f_4=(CNg)^2(CTGT)$	x				x					x
$f_5=(CNg)^2(CW_f)$	x						x			
$f_6=(CTGT)^2(CW_f)$				x	x		x			x
$f_7=(CNg)(CTGT)^2$				x				x	x	
$f_8=(CNg)(CW_f)^2$	x			x					x	x
$f_9=(CTGT)(CW_f)^2$	x		x					x		x

† Regressors to be superimposed over the basic Model 1 (Eq.(4.5)).

Consider next a different type of gas-turbine engine (Engine 2 as per Table 4.1) installed on a different type of helicopter and a new set of flight-test data. Performing similar analysis reveals completely different findings from the BO-105 case. Figure 4.5 presents test-statistics of the 10 top-performing models for engine number 2. Further analysis was undertaken to include flight-test data from five other types of gas-turbine engines installed on different helicopters, as presented in Table 4.1. Results merely confirmed the previously stated conclusion that the best performing model to describe helicopter gas-turbine power, if it exists, cannot be found using a conventional approach of screening between models using hypothesis testing, neither based on the p-value nor on the test-statistics. Concluding this section, an alternative *general* approach needs to be taken. The alternate approach for screening between empirical models relates to the Singular-Value-Decomposition (SVD) theorem and is discussed and demonstrated in the next section of this chapter.

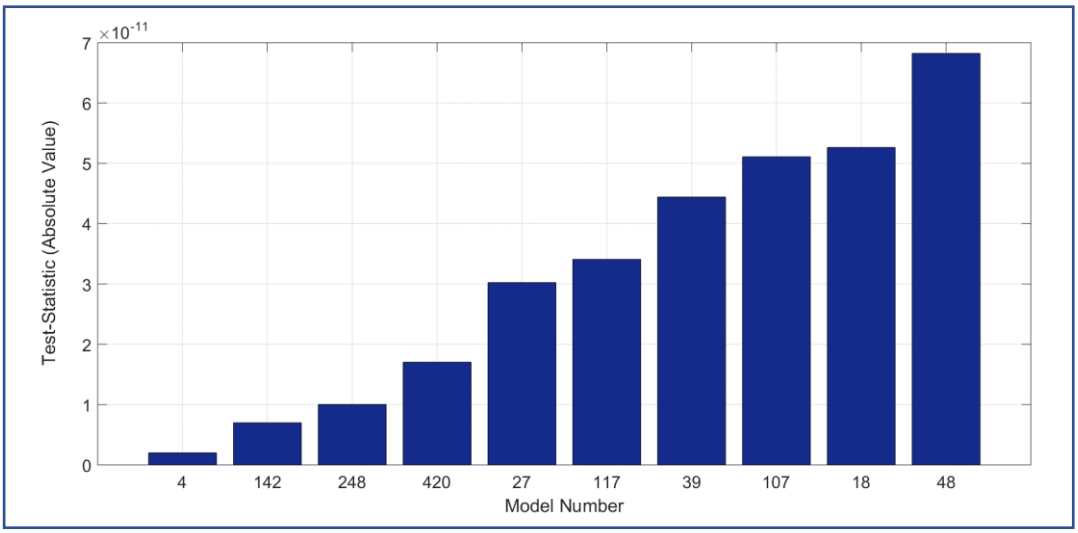

Figure 4.5. Top ten performing models for the EC-145 engine. This figure shows the test-statistics (absolute value) of the top ten performing models for the Turbomeca Arriel 1E2 engine installed in the EC-145 helicopter.

4.4 SINGULAR VALUES APPROACH FOR MODEL SCREENING

The singular values approach for screening between various engine output power model candidates is derived from a mathematical theorem known as the Singular-Value-Decomposition (SVD). This theorem which relates to the field of linear algebra is *briefly* introduced in the following subsection, before it is applied for the task of candidate models screening.

4.4.1 The SVD Theorem

The theory and mechanics of the SVD are thoroughly discussed in Strang [88]. In a nutshell, this theorem states that any matrix from any size which holds real numbers as entries can be decomposed as a product of 3 ***unique*** and special matrices as shown in Eq.(4.9). One should view this decomposition as a way of finding convenient orthogonal bases for both the column-space and the row-space of an arbitrary real matrix.

$$Z = U\Sigma V^T = \begin{bmatrix} u_{1,1} & u_{1,2} & \cdot & u_{1,n} \\ u_{2,1} & u_{2,2} & \cdot & u_{2,n} \\ \cdot & \cdot & \cdot & \cdot \\ \cdot & \cdot & \cdot & \cdot \\ u_{m,1} & u_{m,2} & \cdot & u_{m,n} \end{bmatrix} \begin{bmatrix} \sigma_1 & & & \\ & \sigma_2 & & \\ & & \cdot & \\ & & & \sigma_r \end{bmatrix} \begin{bmatrix} v_{1,1} & v_{2,1} & \cdot & v_{n,1} \\ v_{1,2} & v_{2,2} & \cdot & v_{n,2} \\ \cdot & \cdot & \cdot & \cdot \\ v_{1,r} & v_{2,r} & \cdot & v_{n,r} \end{bmatrix} \tag{4.9}$$

$$\sigma_1 > \sigma_2 > ... > \sigma_r \geq 0$$

Consider a real matrix Z to be of size 'm' by 'n' (denoted (m,n)) and rank 'r'. Matrix Z can then be expressed as a product of the three ***unique*** matrices:

(1) Matrix U called the "left-singular-vectors" (LSV) is an orthonormal matrix of size (m,r). The columns of this matrix are unity-norm vectors which are orthogonal to each other. This set of vectors serves as a basis for the column-space of matrix Z.

(2) Matrix Σ is a diagonal matrix (size (r,r)) which holds the singular-values of Z as entries along its diagonal. The singular-values are non-negative real numbers which can be arranged along the diagonal in a descending order.

(3) Matrix V called the "right-singular-vectors" (RSV) is an orthonormal matrix of size (n,r). The columns of this matrix (or the rows of the transposed matrix, V^T) are unity-norm vectors which are orthogonal to each other. The set of these vectors serves as a basis for the row-space of matrix Z.

The SVD of a real matrix can alternatively be regarded as a linear combination of 'r' rank-one matrices (Eq.(4.10)). This complementary manner to look at the SVD is referred-to as the ***spectral decomposition*** of the matrix Z. With this approach, any real matrix Z of rank 'r' can be "approximated" as a lower ranked matrix (lower than rank 'r'). This reduction in the rank of a matrix is the essence of the dimensionality reduction of matrix Z.

$$Z = \sigma_1 \begin{bmatrix} u_{1,1} \\ u_{2,1} \\ \cdot \\ \cdot \\ u_{m,1} \end{bmatrix} \begin{bmatrix} v_{1,1} & v_{2,1} & \cdot & v_{n,1} \end{bmatrix} + \sigma_2 \begin{bmatrix} u_{1,2} \\ u_{2,2} \\ \cdot \\ \cdot \\ u_{m,2} \end{bmatrix} \begin{bmatrix} v_{1,2} & v_{2,2} & \cdot & v_{n,2} \end{bmatrix} + \\ + \ldots + \sigma_r \begin{bmatrix} u_{1,r} \\ u_{2,r} \\ \cdot \\ \cdot \\ u_{m,r} \end{bmatrix} \begin{bmatrix} v_{1,r} & v_{2,r} & \cdot & v_{n,r} \end{bmatrix} \qquad (4.10)$$

$$\sigma_1 > \sigma_2 > \ldots > \sigma_r \geq 0$$

4.4.2 SVD implementation for model screening

The SVD theorem can be implemented to identify latent dimensions or concepts in the gas-turbine engine flight-test data. For this, matrix Z is defined with its elements

to indicate measures of excellence (scores) for each *specific* multivariable-polynomial model in predicting performance of each *specific* engine tested (see Eq.(4.11)).

$$Z \equiv \begin{pmatrix} \zeta_{1,1} & \zeta_{1,2} & \zeta_{1,3} & \zeta_{1,4} & \zeta_{1,5} & \zeta_{1,6} & \zeta_{1,7} \\ \zeta_{2,1} & \zeta_{2,2} & \zeta_{2,3} & \zeta_{2,4} & \zeta_{2,5} & \zeta_{2,6} & \zeta_{2,7} \\ \zeta_{3,1} & \zeta_{3,2} & \zeta_{3,3} & \zeta_{3,4} & \zeta_{3,5} & \zeta_{3,6} & \zeta_{3,7} \\ \cdot & \cdot & \cdot & \cdot & \cdot & \cdot & \cdot \\ \cdot & \cdot & \cdot & \cdot & \cdot & \cdot & \cdot \\ \cdot & \cdot & \cdot & \cdot & \cdot & \cdot & \cdot \\ \zeta_{511,1} & \zeta_{511,2} & \zeta_{511,3} & \zeta_{511,4} & \zeta_{511,5} & \zeta_{511,6} & \zeta_{511,7} \\ \zeta_{512,1} & \zeta_{512,2} & \zeta_{512,3} & \zeta_{512,4} & \zeta_{512,5} & \zeta_{512,6} & \zeta_{512,7} \end{pmatrix} \therefore \zeta_{i,j} = \frac{1}{\left| t_{i,j} \right|} \qquad (4.11)$$

This matrix Z is of size (512, 7) with its rows representing all 512 candidate multivariable-polynomial models and its columns representing the various engines/helicopters tested. For example, engine number 1 is represented by the most left column and engine number 7 by the most right column of matrix Z.

Next step is to assign scores as elements of matrix Z to quantify level of precision each model predicts a specific engine. As explained before, these scores are based on the absolute-values of the relevant test-statistics (Eq.(4.11)). Since prediction goodness and test-statistics (absolute-value) are inversely proportional to each other, that is the smaller the test-statistic absolute-value is the better the model represents the experimental data, the reciprocals of all test-statistics (absolute-value) are used as elements in matrix Z. The variable $t_{i,j}$ as appears in Eq.(4.11) represents the test-statistic calculated for model number (i) using the flight-test data of engine number (j). Note that matrix Z encapsulates the entire flight-test data base.

Equation (4.9) displays the SVD decomposition of matrix Z into its three unique matrices as defined above. The idea of linearly-independent vectors to span a base in space can be regarded as an exposure of hidden dimensions in the data. The conceptual interpretation of the SVD of matrix Z is illustrated in Fig. 4.6 and further explained hereinafter:

The rank of matrix Z represents the number of independent hidden Principal Dimensions (PDs). The diagonal singular-values matrix (Σ) has all PDs represented by elements along its main diagonal. These elements are arranged in a descending order and indicate the relative 'strength' of appearance of each PD in the flight-test data.

The left singular-vectors (LSV) matrix has seven columns, each with 512 elements. These seven columns are orthonormal vectors which represent the level of correspondence between each one of the 512 models and an identified PD in the data. As illustrated in Fig. 4.6 the first column vector indicates correspondence between each one of the 512 models to the first *(and the most significant)* PD identified in the data. The second column vector specifies level of correspondence between all 512 models to the second most significant PD, and so on. Figure 4.6 explicitly notates one element of the left-singular vector matrix (third row and sixth column) as an example to indicate the level of correspondence between model number 3 and PD number 6.

The right singular vectors (RSV) matrix has seven rows (the rank of matrix Z) with seven elements each (the seven engines in the flight-test data base). As illustrated in Fig. 4.6, these rows of V^T (or the columns of V) represent the level of correspondence between each specific engine (denoted by the column number of V^T) and a Principal Dimension (denoted by the row number of V^T). The first row vector indicates relative levels of correspondence between all 7 engines and the first ***(and the most significant)*** PD. The second row specifies the relative strength between all engines and the second most significant PD, and so on. Figure 4.6 specifies one element of the right-singular vector matrix (7th row and 2nd column) as an illustration of the level of correspondence between engine number 2 and PD number 7 (the least significant PD exposed in the data).

The ***relative*** strength of each PD which is indicated by the corresponding singular-value is then normalized as per Eq.(4.12).

$$\hat{\sigma}_i = \frac{\sigma_i}{\sum_{k=1}^{r} \sigma_k} \therefore r \triangleq rank(Z) \tag{4.12}$$

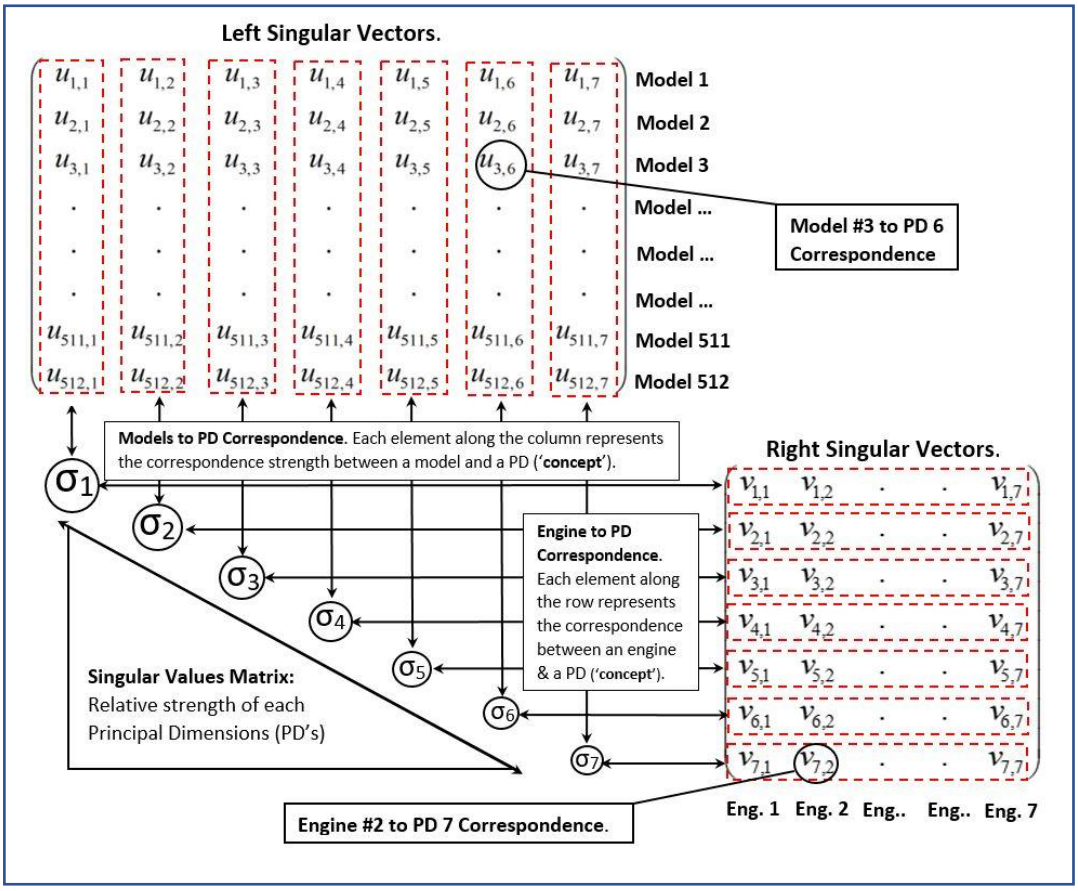

Figure 4.6. The conceptual interpretation of SVD of matrix Z. This matrix decomposition is used as a tool for screening between 512 distinct empirical models based on their relative prediction performance using flight-test data from seven distinct gas-turbine engines.

Figure 4.7 presents the normalized seven PDs singular-values. One can observe that the major PD detected in the data holds a relative strength of 36%, while the following two PDs (PD2 and PD3) share an almost similar relative strength of 23% and 22%, respectively. The combination of the first four PD's encapsulates about 96% of the PDs representation in the data.

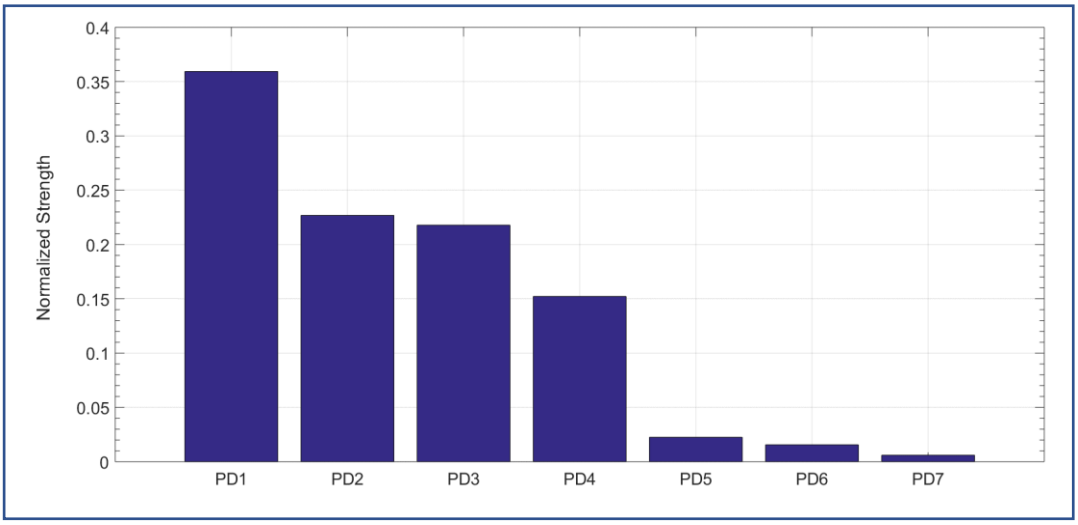

Figure 4.7. The relative strength of the seven Principle Dimensions (PDs). This figure presents the normalized strength of each identified PD as demonstrated by the normalized Singular-Values (SV's) of matrix Z (Eq.(4.12)).

4.4.2.1 The LSV – Models to PDs correspondences

The absolute-value of each element along a *column* vector of the LSV indicates the level of correspondence between a specific model (row number of the vector) and the relevant PD. Each element along the column vectors is normalized as per Eq.(4.13).

$$\hat{U}(i,j)=\frac{|U(i,j)|}{\sum_{i=1}^{512}|U(i,j)|}\ ,\ j=1,2,...,r\ \therefore r=rank(Z) \tag{4.13}$$

Figure 4.8 presents a collage of seven plots to indicate the normalized elements along the seven columns of the LSV as level of correspondence between each one of the 512 candidate models and the seven PDs. The first plot represent correspondences between each candidate model and the first and most significant PD (PD1). It is evident from this plot that Model 320 demonstrates the strongest correspondence to PD1. The other plots on Fig. 4.8 are broadening the spectrum of models to PD's correspondence. Model 125 demonstrates the strong correspondence to PD2, model

367 to PD3, model 4 to PD4, models 49 and 226 to PD5, model 7 to PD6 and model 282 to PD7.

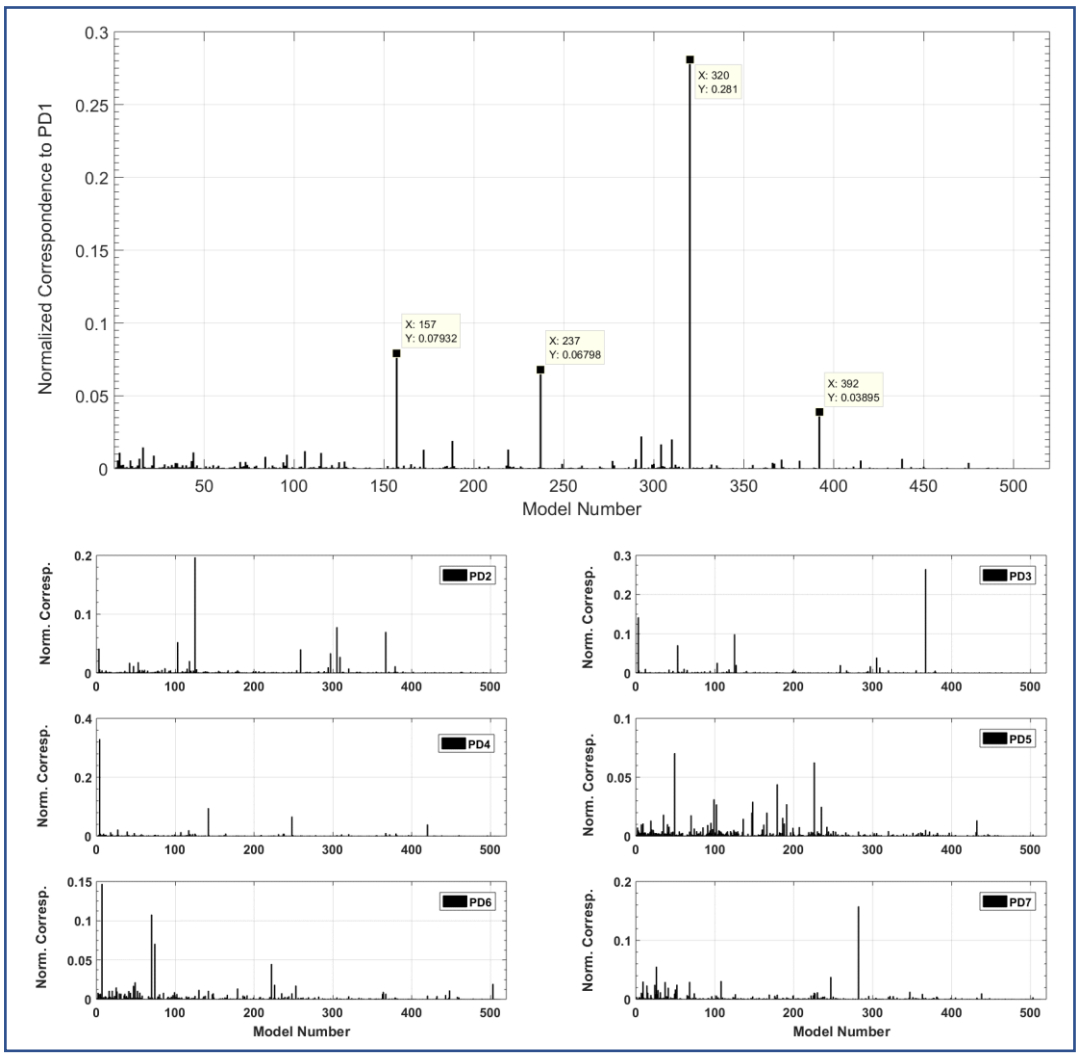

Figure 4.8. Models to PDs correspondences (LSV). This figure presents the normalized correspondences (Eq.(4.13)) between all 512 candidate models and the seven identified PDs.

4.4.2.2 The RSV – Engines to PDs correspondences

The absolute-value of each element along a row vector indicates the level of correspondence between a specific engine (column number of the row-vector) and the relevant PD. Each element along a row is normalized as per Eq.(4.14).

$$\hat{V}(i,j) = \frac{|V(i,j)|}{\sum_{j=1}^{7} |V(i,j)|} \ , \ i = 1,2,...,r \ \therefore r = rank(Z) \tag{4.14}$$

Figure 4.9 presents a collage of seven plots to indicate the normalized elements along the seven row-vectors as level of correspondence between engines and PDs. It follows from the first plot in Fig. 4.9 that PD2 is mainly driven by two engines; engine number 1 and engine number 4. In a more general context, these two engines share a substantial similarity with respect to performance models through the second most significant PD (PD2). This demonstrates the capability of the SVD decomposition to detect latent dimensions in the data, hence to expose hidden similarities between different types of engines.

The other six plots in Fig. 4.9 continue to expose the similarity shared between engines 1 and 4 through PD3. The most significant PD1 is mostly driven by engine number 7, PD4 by engine number 2, PD5 by engine number 5 and PD7 by engine number 6.

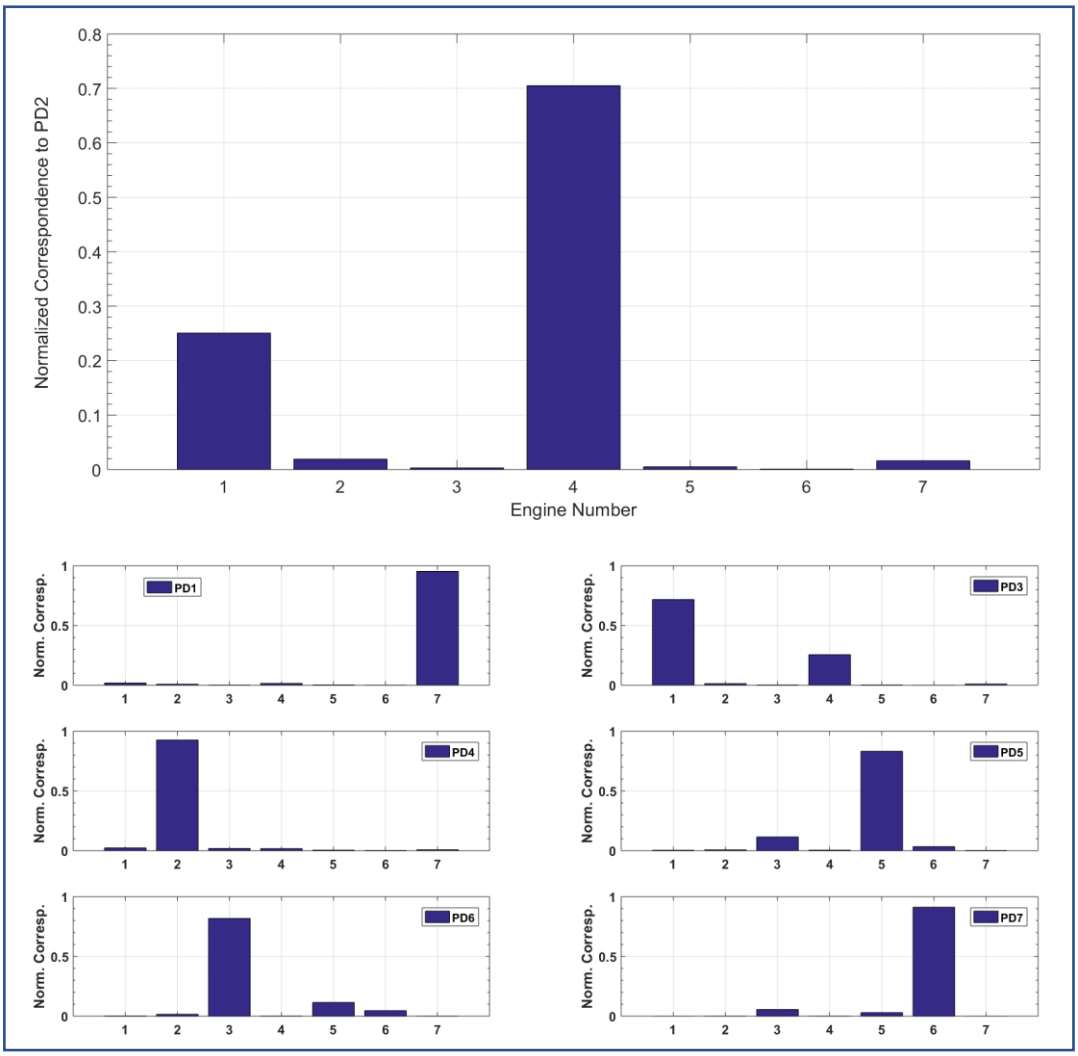

Figure 4.9. Engines to PDs correspondences (RSV). This figure presents the normalized correspondences (Eq.(4.14)) between all seven engines and the principal dimensions (PDs).

4.4.3 Selection of the best multivariable polynomial model

Once the SVD theorem and its practical interpretation for flight-test data analysis has been demonstrated, the fundamental question raised in this chapter can be readdressed, namely, is it practicable to find a general approach to the MPOC method for best prediction of the gas turbine engine available power? Can the flight-test data recommend a short list of multivariable polynomial models best describing the

helicopter gas-turbine engine performance? As concluded in Subsection 4.3.3 above, the conventional method of hypothesis-testing provided confusing and incoherent results. For this a new matrix (W) is defined as per Eq.(4.15).

$$[W]=\left[\hat{U}\right]\left[\hat{\Sigma}\right] \;\therefore\; \left[\hat{\Sigma}\right]\triangleq\begin{pmatrix}\hat{\sigma}_1 & & 0\\ & \ddots & \\ 0 & & \hat{\sigma}_r\end{pmatrix} \tag{4.15}$$

Matrix W is the product of the normalized LSV matrix and the normalized singular-values matrix. This matrix is of the same size of matrix Z, i.e. 512 rows and 7 columns. Each column of W represents the relative correspondence of the 512 models to the relevant PD (the column number). Adding all column vectors of matrix W to each other results in a single column vector {S} with 512 elements (Eq.(4.16)).

$$\{S\}=\sum_{i=1}^{r}\left(\{w_i\}\right)\therefore[W]\triangleq\left[\{w_1\}\quad\{w_2\}\quad .\quad .\quad\{w_r\}\right] \tag{4.16}$$

Practically, each element of the column-vector {S} holds a normalized value for the overall/combined performance of each model in predicting the output power of the "generic" engine, a hypothetical engine that represents all engines tested. The elements of the column-vector {S} can be regarded as the Combined Normalized Scores (CNSs) of each one of the 512 models used in predicting the performance of a gas-turbine engine *in general*. Figure 4.10 presents the CNS for all 512 candidate multivariable polynomial models. Based on the highest CNS achieved, the best empirical model describing the gas-turbine engine performance is model number 320.

This outcome can be expanded to provide a short list of the ten top-performing multivariable polynomial for the seven engines tested (see Table 4.4). From Table 4.4 one can find the similarities between this list and the one formulated for Engine 1 (Fig. 4.4) and for Engine 2 (Fig. 4.5). Although engines number 1 and 2 'sent' few of their top 10 performing models as "representatives" to the final ten top-performing models list, neither one nor the other shared the best final model proposed based on their level of correspondence to the most significant PD1. The engine that

demonstrates the maximum correspondence to PD1 was Engine 7 (Fig. 4.9) and its top-performing model comes leading in the final list. As presented in Table 4.4, model number 320 involves the basic ten predictors as given by Eq.(4.5), superimposed with five other predictors: f_1, f_4, f_6, f_8 and f_9. One should notice that adding more predictors to the basic model, Model 1 (Eq.(4.5)), does not necessarily correlate with prediction performance improvement. The final top-ten list actually includes two models which are using only one extra predictor to the basic Model 1. These are models number 4 and number 3. Model number 4 (Eq.(4.17))) uses f_1 as the auxiliary predictor and Model 3 (Eq.(4.18)) uses f_2. When analysis requires simple model to use, either one of the two is suitable. Another point worth addressing is how well the basic model performs in the bigger scheme of all seven engines? It appears that model number 1 attains the 173rd place, at the top of the second trimester of the pack of all 512 models.

$$CSHP_{M_{(4)}} = \alpha_1^4 \left(CN_g\right)^3 + \alpha_2^4 \left(CN_g\right)^2 + \alpha_3^4 \left(CN_g\right) + \alpha_4^4 \left(CTGT\right)^3 + \alpha_5^4 \left(CTGT\right)^2 + \\ + \alpha_6^4 \left(CTGT\right) + \alpha_7^4 \left(CW_f\right)^3 + \alpha_8^4 \left(CW_f\right)^2 + \alpha_9^4 \left(CW_f\right) + \alpha_{10}^4 \left(CTGT \cdot CW_f\right) + \alpha_0^4 \tag{4.17}$$

$$CSHP_{M_{(3)}} = \alpha_1^3 \left(CN_g\right)^3 + \alpha_2^3 \left(CN_g\right)^2 + \alpha_3^3 \left(CN_g\right) + \alpha_4^3 \left(CTGT\right)^3 + \alpha_5^3 \left(CTGT\right)^2 + \\ + \alpha_6^3 \left(CTGT\right) + \alpha_7^3 \left(CW_f\right)^3 + \alpha_8^3 \left(CW_f\right)^2 + \alpha_9^3 \left(CW_f\right) + \alpha_{10}^3 \left(CN_g \cdot CW_f\right) + \alpha_0^3 \tag{4.18}$$

Table 4.4. List of 10 top-performing models for helicopter gas turbine engines.

Auxiliary Regressors Involved*	Model Number									
	320	***367***	***125***	***4***	***3***	***157***	***305***	***237***	***53***	***103***
f_1=(CNg)(CTGT)	x					x	x		x	
f_2=(CNg)(CW_f)		x			x				x	
f_3=(CTGT)(CW_f)		x		x		x	x	x		x
f_4=$(CNg)^2$(CTGT)	x	x								
f_5=$(CNg)^2$(CW_f)		x	x			x	x	x		x
f_6=$(CTGT)^2$(CW_f)	x					x				
f_7=(CNg)$(CTGT)^2$			x				x			
f_8=(CNg)$(CW_f)^2$	x	x					x	x		x
f_9=(CTGT)$(CW_f)^2$	x	x	x					x	x	

***** Regressors to be superimposed to the basic-model expressed as Model 1 (Eq.(4.5))

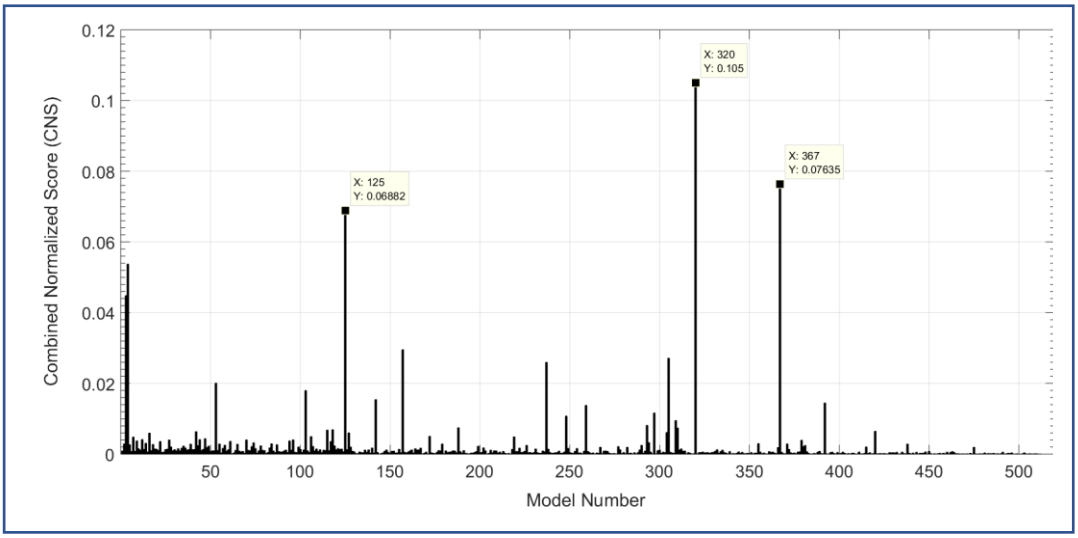

Figure 4.10. The Combined Normalized Scores (CNSs) for all 512 engine models. This figure presents the CNS values for all 512 multivariable engine models based on data from the seven engines. Model number 320 outperforms all other empirical models in predicting the output power of the seven gas-turbine engines tested.

4.5 COMPARISON TO CONVENTIONAL METHODS AND APPLICATIONS

The conventional method for estimating helicopter *installed* gas turbine engine output power is based on single-variable analysis method. The innovative MPOC method, based on multivariable polynomial models, was shown in Chapter 3 to significantly improve prediction of maximum available power under a wider range of atmospheric conditions. The main weakness of the MPOC method is that it struggles with a large number of candidate multivariable polynomial models to choose from. Table 4.4 addresses this shortcoming by providing a brief list of 10 best-performing multivariable polynomial models to be used with the MPOC method. Figure 4.11 presents the mean of the prediction error of all these multivariable polynomial models using the seven engines of Table 4.1.

The mean of the prediction errors presented in Fig 4.11 were calculated as per Eq.(4.19). In this equation the variable CSHPi represents the measured engine power

for data point "i" and CSHPj is the engine output power as estimated by sequential model number "j". The parameter "n" represents the number of measured data points.

$$\mu_j = \frac{1}{n}\sum_{i=1}^{n}\left(\frac{100\left(CSHP_i - CSHP_j\big|_i\right)}{CSHP_i}\right) \tag{4.19}$$

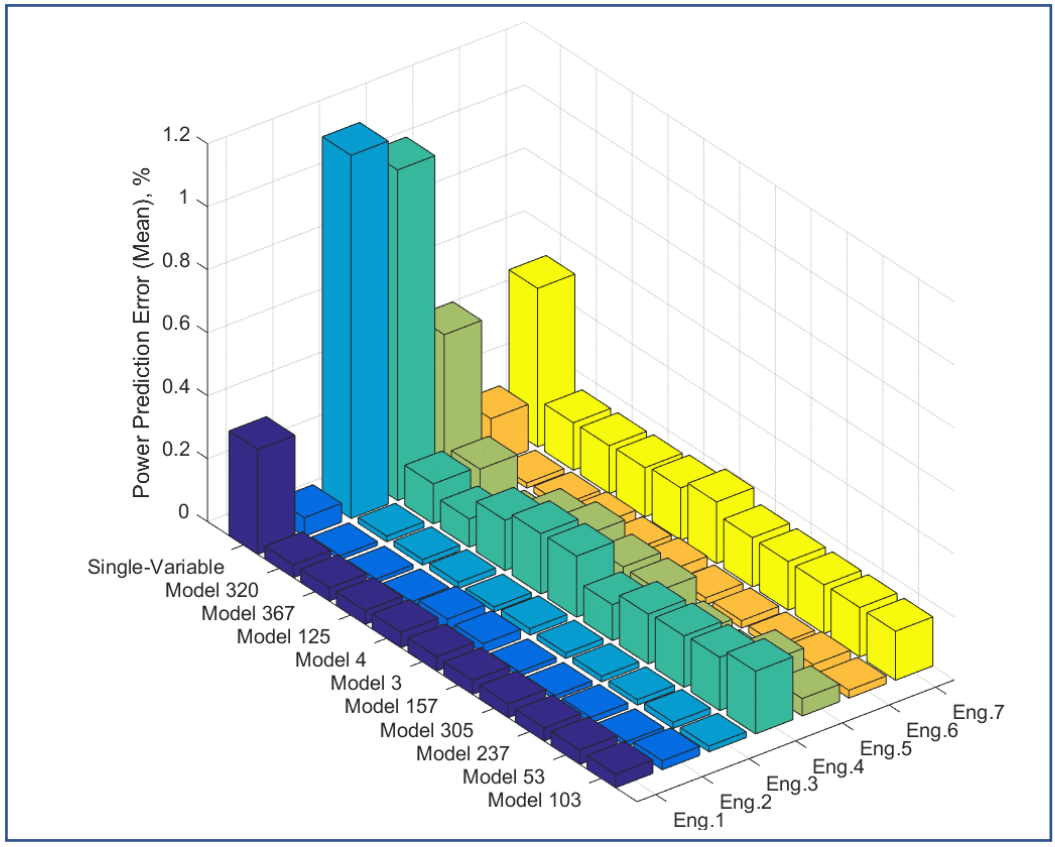

Figure 4.11. The mean errors of engines output power estimations. This figure presents the mean of output power prediction errors for all seven engines tested using the top-ten multivariable models listed in Table-4.4 and the conventional single-variable model.

Figure 4.11 also presents the prediction performance of the seven engines of Table 4.1 using the conventional method based on the single-variable models (Eq.(4.1) -(4.3)). One can notice that the multivariable polynomial models performed much better in predicting all seven engine output-power. The maximum average prediction-error using a multivariable model was measured to be only 0.2%. This relatively low prediction error belongs to the two models 3 and 4 whilst predicting the output power

of Engine 4 (as per Table 4.1). Comparing the prediction performance of the multivariable polynomial models to those achieved using single-variable models disclose a clear advantage for the multivariable models. The single-variable models returned much higher prediction errors for all seven engines tested. One can see in Fig. 4.11 these prediction errors reached up to 1.15% (for Engine 3).

A different multivariable approach for helicopter engine performance determination is presented by Gomez et al. [89]. Although prediction accuracy achieved is not specifically discussed in Gomez [89], the method presented completely ignores the engine temperature as a predictor for the engine performance model. The engine temperature is essential for the determination of maximum available power, since the engine output power is often limited by this variable reaching the maximum allowed. Discarding the engine temperature from the performance model, makes this approach useless for the MPOC method. Another fundamental difference between the MPOC method and the one presented by Gomez [89] is the order of the polynomials used to describe the engine output power. The MPOC method is based on third-orders, while Gomez [89] uses second-orders. Limiting the engine performance model to a second-order only, prevents an inflection point and therefor fails from modelling an important physical characteristic of the engine that the rate of power increase with engine temperature increase must reduce, while operating the engine close to its limitations.

All multivariable models presented in Table 4.4 were found to estimate the output power of the seven different engines tested with an average accuracy of no more than 0.2% for each model tested. The absolute prediction error for a single measured point never exceeded 4.1% for all seven different engines tested. Similar analysis, based on conventional single-variable models, returned best estimation errors of only 8%. Putting the work presented in this chapter in the larger context of gas turbine engine performance and comparing the prediction accuracy achieved using the multivariable polynomial with prediction accuracy of commonly used research simulation tools, such as Turbomatch [90] reveals similar or better results. Goulos et al. [91] uses Turbomatch to predict helicopter gas-turbine performance for their work. Chapter 3 of Goulos et

al. [91] reports that the model has been matched at design point conditions with public domain data in terms of specific fuel consumption (SFC) with an accuracy of 0.3%.

Heng et al. [92] presents a method of calculating gas-turbine engine output power based on flow-field simulation and aerodynamics modelling. The engine output-power estimation is based on the engine outlet temperature. Predictions for engine outlet temperature were validated against five measured steady-state engine operating data points (output power between 340 to 1,394 hp) using five similar-type but different helicopter gas turbine engines tested on a bench. The reported temperature estimation errors ranged between 2.4% and 4.1% for all 25 data points measured.

Simple and accurate mathematical models that represent the available output power of the engine, such as presented in Table 4.4, can efficiently be used not only for the immediate prediction of a specific helicopter performance, but also in relevant adjacent research which requires a gas-turbine engine power model. Examples of such are improvement of existing gas-turbine engine technologies, where current performance is needed for comparison (see Zhang and Gummer [93]). Other examples can be improvement and validation of helicopter performance where the engine output power is needed as a module in the big scheme of total helicopter performance as presented by Savelle and Garrard [94], and Yeo et al. [95].

4.6 CONCLUSIONS AND SUMMARY

The process of empirical models evaluation is at the core business of experimental flight-testing data analysis. A commonly used technique in experimental flight testing to sort between candidate models is the one based on hypothesis-testing and the associated P-values. The hypothesis-testing method is thoroughly demonstrated in Subsection 4.3.2 above for the purpose of selecting the best empirical multivariable-polynomial model to represent the BO-105 engine. After applying minor adjustments, the hypothesis-testing method was implemented successfully in ranking all 512 candidate multivariable-polynomial models based on their relative performance.

However, the hypothesis-testing approach became completely ineffective once the experimental data-base was expanded to include six more engines. The method failed providing a clear answer to the question of which is the best-performing model when the entire experimental data from all seven engines is analysed as a whole.

The Singular-Value-Decomposition (SVD) approach was used successfully where the hypothesis-testing method failed and produced a list of top-performing multivariable polynomial models to describe gas turbine engine performance in general. The SVD approach was also used for exposing latent similarities between different engines with respect to their performance models.

Analysis showed no correlation between the number of auxiliary predictors used in the multivariable-polynomial model and the power prediction accuracy. The fourth and fifth best-performing models out of the 512 evaluated incorporated only 11 predictors, making either one of them a great choice, if analysis simplicity is paramount.

Although the SVD approach is demonstrated in this chapter using engine data, it is not bounded only to gas-turbine engine testing and available power flight-testing. In the following chapters of this dissertation, the SVD approach is implemented for other disciplines of helicopter performance flight-testing, for which empirical models are being evaluated.

It does not matter how beautiful your theory is. If it does not agree with experiments, it's wrong.

Richard P. Feynman

5 HOVER PERFORMANCE TESTING BASED ON DIMENSIONALITY REDUCTION

5.1 CHAPTER OVERVIEW

The power required to hover a helicopter is fundamental to any new or modified helicopter performance flight-testing effort. The conventional flight-test method that was previously discussed in Chapters 1 and 2 (Subsections 1.3.2 and 2.3.2) is based on relating two non-dimensional variables (coefficient of power and coefficient of weight). This single-variable method is overly simplified and neglects compressibility effects in the power required to hover under a wide range of gross weight and atmospheric conditions. This chapter presents an alternative flight test method for hover performance that addresses the deficiencies of the conventional method, as stated in Subsection 1.4.2 (PS2). This novel hover performance testing method is referred-to as the 'Corrected-Variables Screening using Dimensionality Reduction' (CVSDR). The method uses an original list of 15 corrected-variables derived from fundamental dimensional analysis.

This Chapter 5 was published as the following journal paper: Arush I., Pavel M.D., and Mulder M., "A Dimensionality Reduction Approach in Helicopter Hover Performance Flight Testing", Journal of the American Helicopter Society 67, No. 3 (2022): 129–41. https://doi.org/10.4050/JAHS.67.032010.

This list is further reduced by means of dimensionality reduction to include only the essential and effective hover performance predictors. The CVSDR method is demonstrated and tested in this chapter using flight-test data of a Bell Jet-Ranger and shows that at the 95% confidence level; the averaged prediction error is only 0.9hp (0.3% of the helicopter maximum continuous power). Using the same set of flight-test data, the conventional method yields a much larger average prediction error of 1.7 hp. Although demonstrated in this chapter with a specific type of helicopter, the CVSDR method is applicable for hover performance flight-testing of any type of a conventional helicopter configured with a main rotor and a tail rotor.

5.2 INTRODUCTION

The most distinguishing characteristic of a helicopter is its ability to steadily hover at any phase of its mission given it has a sufficient power margin [22,23]. Knowing the power required to hover is fundamental to any new or modified helicopter flight-test effort. As already discussed in Chapter 2, the conventional flight-test method for hover performance is based on the combined blade-element momentum (BEM) theory and is overly simplified. This simplification often yields empirical models that fail to accurately and consistently predict the total power required to hover under a wide range of helicopter gross weight and atmospheric conditions. Bousman [96] demonstrates this drawback by using Out-of-Ground Effect (OGE) hover performance testing of five different flight test programs and reporting inconsistency in OGE hover performance of up to 5% of which the source of the error could not be explained.

As already mentioned in Chapter 1 (Subsection 1.4.2), a major disadvantage of the conventional OGE hover flight-test method is that it does not address main rotor blade compressibility effects as those are often assumed to have negligible effect on the hover performance. An example of this frequently taken assumption can be found in the study on uncertainty quantification in helicopter performance by Siva et al. [97]. The ability to account for compressibility effects, mostly related to blade tip Mach

number and shape, is essential for accurate hover performance predictions. This relation is well illustrated by computational fluid dynamic (CFD) simulations used to predict hover performance of rotor systems. Jacobson and Smith [98] presents hover performance comparison between predictions from a hybrid CFD methodology and measured hover performance of a rotor with three different blade tip configurations at three different tip Mach numbers (0.55, 0.6 and 0.65). They state that future work is needed to understand why CFD models do not predict the same impact of the tip shape as measured in the experiment. Moreover, one of Jacobson and Smith [98] conclusions states that hover performance predictions from the hybrid methodology CFD improve as tip Mach numbers reduce. This conclusion solidifies the significance compressibility effects have on hover performance. Garcia and Barakos [99] provide another example to show compressibility effects should not be neglected from hover performance predictions. Their work, which focuses on accurate rotors hover performance predictions using modern CFD methods with modest computer resources, shows the significance the tip shape and Mach number have on hover performance of a rotor system.

Measuring compressibility effects in flight-testing of a full-scale helicopter and not just a rotor system requires the hover trials to be performed in high altitude and low air temperatures. Whereas in the past, these kind of high altitude hover trials were challenging since they required high-ground reference points, recent technological developments show potential to make these trials more practical in the future. Matayoshi et al. [100] present results from a flight-test evaluation of a helicopter airborne LiDAR (Light Detection and Ranging) system. This system can measure accurately three-axis true airspeed which is crucial for high altitude hover performance trials. Boirun [101] attempts to rectify the disadvantage of the conventional hover flight-test method by including compressibility effects into the empirical performance model of the helicopter. However, his approach does not determine a definitive single empirical model to include compressibility effects. Instead, various curves for different values of main-rotor tip speeds are offered.

Obtaining an accurate single empirical model to predict the hover performance is highly beneficial since it can also be used for real-time applications. A single empirical hovering model can be used in conjunction with existing algorithms that predict the gross weight of the helicopter for real time hovering performance. Abraham and Costello [102] present such a practical algorithm to estimate the gross weight and center of mass of a helicopter in flight and report the algorithm works well in hover.

Chapters 3 and 4 present an alternative and more accurate approach to helicopter performance flight-testing, using multivariable polynomials as empirical models. This approach was proven in Chapter 3 more accurate in the prediction of the available power of a helicopter under a wide range of atmospheric conditions as compared to the conventional single-variable flight-test method. Chapter 4 provides a systematic method for screening between candidate multivariable predictors. This multivariable polynomial approach is next applied in this chapter (Chapter 5) to the power required to sustain a helicopter in an OGE hover, without taking any lenient assumptions such as negligible compressibility effects.

This Chapter 5 is structured as follows: after a short introduction, the conventional method for hover performance testing is briefly reminded and demonstrated using flight-test data from a Bell Jet-Ranger helicopter. Flight-test data from three distinct sorties, totalling 56 data points are used to obtain an empirical single-variable model for the power required to OGE hover. The expected level of accuracy is then evaluated while using this empirical model to predict the power required to hover, under condition of the 20 hover points of Sortie 4. Unsatisfied with the level of prediction accuracy, an alternative method referred to as the "Corrected-Variables Screening using Dimensionality Reduction" (CVSDR), is presented and discussed in Section 5.4. The CVSDR method is applied to the same Jet-Ranger flight-test data and yields an alternative empirical multivariable model for power required to OGE hover. The level of prediction accuracy expected from the CVSDR driven model is discussed in Sections 5.5 and compared with the conventional method in Section 5.6. The later Section 5.6 also provides possible reasoning to explain the different

prediction accuracy between the two methods. Section 5.7 presents the conclusions and summary and concludes this chapter.

5.3 CONVENTIONAL METHOD FOR HOVER PERFORMANCE TESTING

The conventional single-variable flight-test method for determining the power a helicopter required for a hovering flight is thoroughly discussed in Chapter 2 (Subsection 2.3.2), and demonstrated in many helicopter hover performance papers [77,103-105]. In a nutshell, this method seeks to uncover the linear relation between the coefficient of power (C_p) and the coefficient of weight raised to the 1.5 power $(C_w)^{1.5}$, i.e., to realize the two coefficients $\alpha_1$and α_2 of Eq.(5.1) for a particular type of helicopter.

$$C_P = \alpha_1 \left(C_W\right)^{1.5} + \alpha_2$$
$$\left\{ C_P \equiv \frac{P}{\rho_a A_d \left(\omega R\right)^3} \;,\; C_W \equiv \frac{W}{\rho_a A_d \left(\omega R\right)^2} \right\} \tag{5.1}$$

The flight-test team is required to plan and execute numerous hover test points in order to cover the entire flight envelope of the helicopter under test. This includes all certified gross-weights (W), the entire atmosphere the helicopter is expected to fly at (which defines the ambient air density, ρ_a), and throughout the governed range of the main-rotor angular speed (ω,Ω). As already discussed in Chapter 2, there are two fundamental techniques to execute the precise hover sorties for data gathering. The one is the free-flight hover and the other, which requires more preparation efforts and coordination, is the tethered hover. The pros and cons of each technique are discussed in Chapter 2 (Subsection 2.3.2.1).

Next, the conventional method is demonstrated using free-flight OGE hovering flight-test data obtained during from four distinct sorties of a Bell Jet-Ranger

helicopter. The four sorties were conducted under different atmospheric and gross-weight conditions, as summarized in Table 5.1.

Table 5.1. Summary of OGE hover conditions. This table presents the ambient conditions and range of Bell Jet-Ranger parameters during the free-flight OGE hovers.

Sortie	W [lbs.]	C_W [x10^{-3}]	Pressure Altitude [ft.]	Ta [°C]	M_{tip}
1	2900 - 3000	3.298 – 4.032	2200 - 6600	11 to 18	0.59 – 0.62
2	2850 - 2960	2.986 – 4.046	3100 - 6100	10 to 15	0.59 – 0.61
3	2850 - 2980	3.161 – 3.739	700 - 6350	-2 to 3	0.61 – 0.64
4	2700 - 3060	3.043 – 4.062	425 - 6800	20 to 26	0.59 – 0.61

Figure 5.1 presents the total of 76 matching pairs of coefficient of power (C_p) and coefficient of weight raised to the 1.5 power ((C_w)$^{1.5}$) measured in all four sorties. All 76 OGE hover points were obtained using the free-flight (un-tethered) flight-test technique. Specialty Flight Test Instrumentation (FTI), which was calibrated for the test, sampled relevant parameters at a rate of 10 cycles per seconds. The helicopter was stabilized at each hover point for a duration of at least 20 sec., and sampled data was averaged over this period of time post flight. The power required to hover was reduced from the engine output torque and the free-turbine speed which were both sampled by the FTI. The gross weight (W) of the helicopter was calculated by subtracting the fuel used from the take-off all up weight. All hover points were conducted under the restrict limitation for the relative wind to be less than 3 kts. For ground referenced hover points the relative was measured using a ground based anemometer and for high altitude hover points, an independent helicopter with an independent Low Airspeed Indicator (LAI) was used as a hover reference for the tested Jet-Ranger.

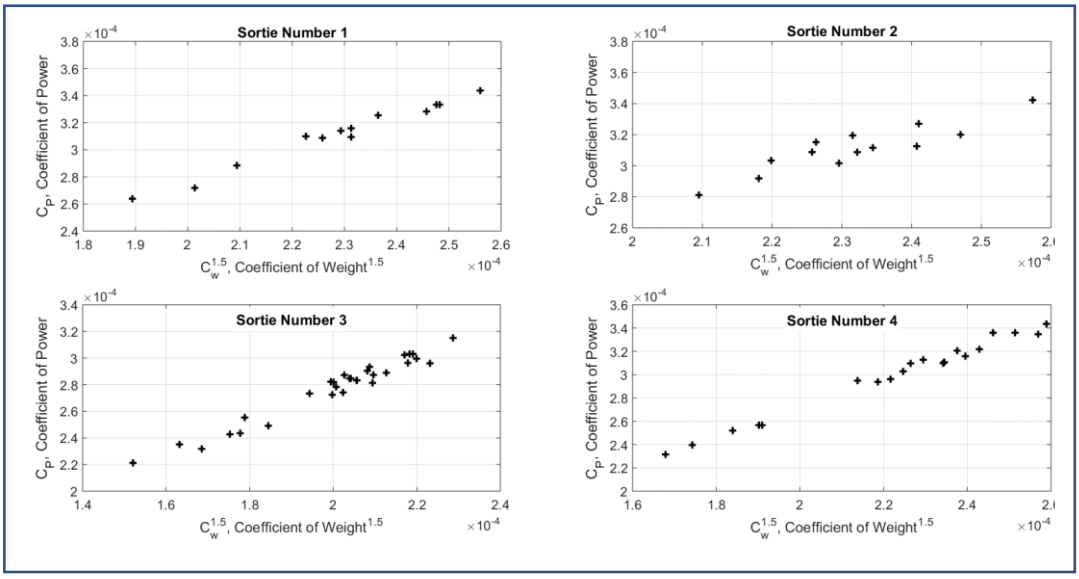

Figure 5.1. Non-dimensional OGE hover performance. This figure shows the non-dimensional OGE hover performance of a Bell Jet-Ranger. The figure is split into four distinct sorties (Sortie 1-4), as per the conditions specified in Table 5.1.

The level of accuracy achieved using the conventional method was assessed by taking the following approach: flight-test data from the first three sorties was used for the derivation of an empirical OGE hover model, obtained from a linear regression. Then, the accuracy and effectiveness of this empirical model was evaluated by comparing its predictions with the actual flight-test data gathered in Sortie 4. The reason for this specific partition of predicting the performance of Sortie 4 by using data obtained from the first three sorties was to challenge the method to the fullest extent possible. It is evident from Table 5.1 that Sortie 4 was executed under a wider range of gross weights and pressure altitudes, not covered by the first three sorties. By applying this specific partition, the empirical hovering model is challenged with an extrapolation task.

Linear regression was executed in order to describe the relationship between the coefficient of power (C_p) and the coefficient of weight raised to the 1.5 power ($(C_w)^{1.5}$). The 56 flight-test hover points of Sorties 1-3 were substituted in Eq.(5.1), yielding a linear system of 56 equations with only two unknowns ($\alpha_1$and α_2). This set of equations is compactly represented as Eq.(5.2).

$$[A]\{\alpha\} = \vec{b} \tag{5.2}$$

The matrix A is of size (56,2) and contains the numeral values of the coefficient of weight (C_w) raised to the 1.5 power as the first column, and a unity vector as the second column. The column vector α is of a size (2, 1) and contains the coefficients (α_1 and α_2). The column vector $\vec{b}$ is of size (56,1) and contains the numerical values of the measured coefficient of power (C_p) for all hover points. The explicit representation of Eq.(5.2) is presented as Eq.(5.3).

$$\begin{bmatrix} C_{w_1}^{1.5} & 1 \\ C_{w_2}^{1.5} & 1 \\ . & . \\ . & . \\ . & . \\ C_{w_{56}}^{1.5} & 1 \end{bmatrix} \begin{bmatrix} \alpha_1 \\ \alpha_2 \end{bmatrix} = \begin{bmatrix} C_{P_1} \\ C_{P_2} \\ . \\ . \\ . \\ C_{P_{56}} \end{bmatrix} \tag{5.3}$$

The system of equations represented by Eq.(5.3) is over-determined and does not have an exact solution. However, one can look for the 'closest' solution of this system, i.e., the "best-fit" solution denoted as $\hat{\alpha}$ (see Strang [83]). The matrix constructed from $[A^TA]^{-1}A^T$ is defined as the ***projection-matrix***, and when multiplied by the vector $\vec{b}$ provides the best-fit solution or the "closest" solution one can look for (Eq.(5.4)). Although this specific example solves for only two coefficients (α_1, α_2), this method is applicable for an over-determined system with any arbitrary number of coefficients.

$$\{\hat{\alpha}\} = \left[A^T A\right]^{-1} A^T \vec{b} \tag{5.4}$$

For the exemplary Bell Jet-Ranger considered in this chapter, the regressed empirical OGE hover model is presented as Eq.(5.5).

$$C_P\big|_{(S_{1-3})} = 1.175\left(C_W\right)^{1.5} + 4.118\times10^{-5} \quad \left(\textit{Base Model}\right) \tag{5.5}$$

Figure 5.2 presents all 56 data points from the first three sorties and the "best-fit" solution (Eq.(5.5)).

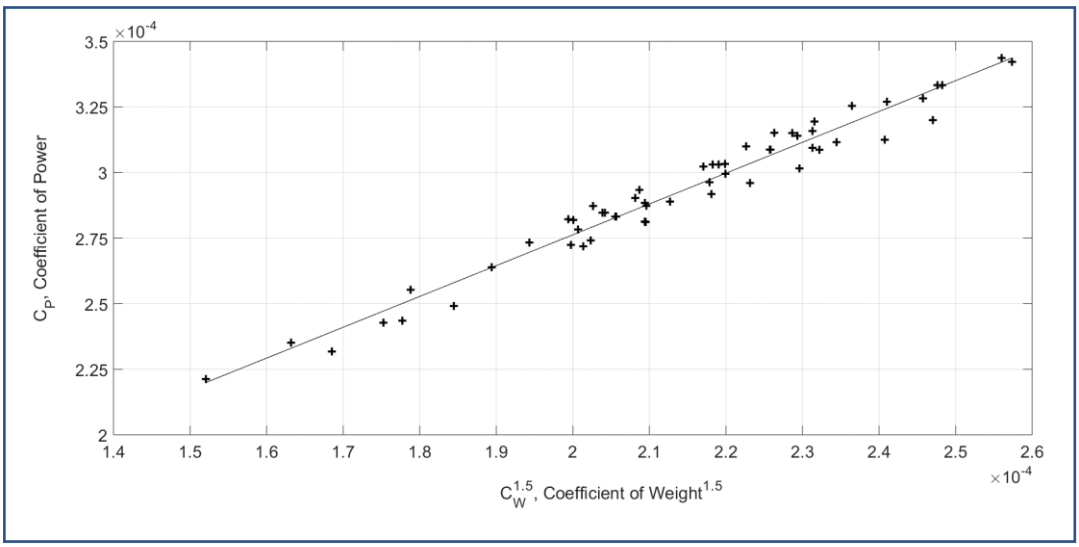

Figure 5.2. Non-dimensional OGE hover performance (Sorties 1-3).

The errors between the measured and the predicted OGE hovering power for Sortie 4 were calculated in accordance with Eq.(5.6) and are presented in Fig. 5.3.

$$\vec{E}_r\Big|_{base} = \left(C_{p_i} - \left(1.175\left(C_{W_i}\right)^{1.5} + 4.118\times10^{-5} \right) \right) \rho_{a_i} A_d \left(\omega_i R\right)^3 \ , i = 1,2,...,20 \qquad (5.6)$$

The prediction errors ranged up to an absolute maximum value of 11.7 hp, a mean of -3.7 hp and a variance of 18.1 hp^2. For the type of helicopter tested, a power deviation of more than 1.6 hp (absolute value) is already noticeable to the aircrew. The averaged prediction error of -3.7 hp (over-estimate) with a variance of 18.1 hp^2 is therefore considered substantial. The conventional approach in flight-testing for assessing how accurate a model predicts the actual performance is based on hypothesis-testing. This approach which follows from the central-limit theorem is thoroughly discussed in the literature [84,87]. In a nutshell, a hypothesis is set (the 'null-hypothesis') and by using the test-statistic (Eq.(5.7))) the validity of the null-hypothesis is assessed against the alternative hypothesis.

$$t_{base} = \frac{\left|\bar{E}_{r_{base}}\right| - \mu_0}{S_{base}/\sqrt{n}} \;,\; \mu_0 = 1.6hp \;:\; n = 20 \tag{5.7}$$

For the specific case presented, the null-hypothesis assigned is that ***on-average*** the power-to-hover predicted by the empirical model obtained (Eq.(5.6)) does not differ from the true measured power by more than ±1.6 hp (deviation mismatch noticeable to the Jet-Ranger aircrew). This null hypothesis is tested against the alternative that ***on-average*** the power to hover from Eq. (5.6) shows an absolute prediction error of more than 1.6 hp.

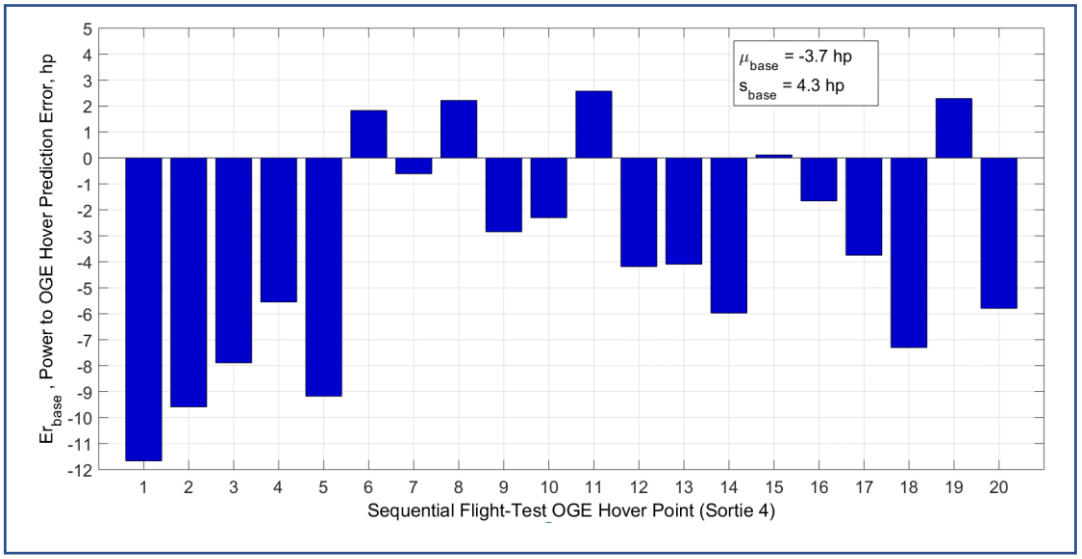

Figure 5.3. Power prediction errors for Sortie 4 (base model). This figure shows the power to OGE hover prediction errors generated by the base model (Eq.(5.6)) for the conditions of Sortie 4.

The relevant test-statistic for this hypothesis testing is calculated per Eq.(5.7). The symbol 'n' represents the number of measured test points of Sortie 4 (n=20) and 'S' stands for the standard deviation of the prediction errors of the empirical hover model (Eq.(5.6)) which are presented in Fig. 5.3. The calculated value for the test-statistic (Eq.(5.7)) was found to be 2.18. Inferential statistical analysis based on the sampled data from Sortie 4 shows the probability for making a type-I error by rejecting the null-hypothesis to be only 4.2%. This low probability for a type-I error is below the 5% significance level accustomed in helicopter performance flight-testing. The

practical meaning of this test is that there is significant statistical evidence at the 95% confidence level to reject the null hypothesis and adopt the alternative hypothesis instead. It can be concluded that ***on-average*** and at the 95% confidence level, the power required to hover predictions (Eq.(5.6)) deviates by more than 1.6 hp from the actual measured power. Complementary statistical analysis shows that on-average and at the 95% confidence level, the hover-power predictions based on Eq.(5.6) deviate by up to 1.7 hp from the actual measured power. This noticeable prediction error of the conventional hovering model is to be expected. One should doubt the linear relation between the coefficient of power and the coefficient of weight raised to the 1.5 power (Cp, $(Cw)^{1.5}$). Merely by looking at Fig. 5.2 one should doubt if the relation is actually linear and whether there are some other latent factors that affect the relation between the data points.

Concluding this subsection, the conventional flight-test method for assessing the OGE power required to hover can result in substantial estimation errors as demonstrated for the prediction of Sortie 4. Statistical analysis at the 95% confidence level shows that on-average the hover-power predictions based on Eq.(5.6) deviate by up to 1.7 hp from the actual measured power. Next, in Sections 5.4 an alternative analysis method with an improved prediction accuracy is proposed.

5.4 CORRECTED-VARIABLE SCREENING USING DIMENSIONALITY REDUCTION

An alternative analysis method for the power required to hover is proposed, referred-to as the 'Corrected-Variables Screening using Dimensionality Reduction' (CVSDR). This method requires no variation to the way flight-test sorties are carried-out, only the analysis method is modified. The method involves three phases. In phase one, an original list of corrected-variables is generated for a multivariable analysis approach. In phase-two, this list of corrected-variables is refined based on concepts of dimensionality reduction. Phase three starts once the bare-essential list of corrected

variables is defined, and an empirical multivariable model is fitted to the flight-test data. The entire derivation process is demonstrated hereafter using the same flight test data from a Bell Jet-Ranger helicopter that was used in Section 5.3.

5.4.1 Phase One - Original list of corrected-variables for hover performance

Phase one of this method starts by proposing the dimensional variables that affect the physical problem of the amount of power needed for a helicopter in a hover. These are the ambient static pressure, Pa, the ambient static temperature, Ta, the helicopter gross-weight, W, the main-rotor disk area, A_d, the main rotor angular speed, ω, and the main-rotor height above the ground, h. The power required to hover, P, can be represented mathematically as Eq.(5.8) and Eq.(5.9) in an implicit form. The dimensions involved are presented in Table 5.2, where 'M' represents mass, 'L' represents length and 'T' represents time.

$$P = f(P_a, T_a, W, A_d, \omega, h) \tag{5.8}$$

$$\hat{f}(P, P_a, T_a, W, A_d, \omega, h) = 0 \tag{5.9}$$

Table 5.2. Variables and dimensions involved in hover performance. This table presents all major variables affecting the OGE hover performance problem and associated dimensions.

#	Physical Variable	Notation	Dimension
1	Power Required to Hover	P	$[M][L]^2[T]^{-3}$
2	Ambient static Pressure	P_a	$[M][L]^{-1}[T]^{-2}$
3	Ambient static Temperature	T_a	$[L]^2[T]^{-2}$
4	Helicopter Gross-Weight	W	$[M][L][T]^{-2}$
5	Main-Rotor Disk Area	A_d	$[L]^2$
6	Main-Rotor Angular speed	ω	$[T]^{-1}$
7	Main-Rotor Height Above Ground	h	[L]

The physical problem of OGE hover performance has seven variables involved with three dimensions (L,M,T). According to the Buckingham Pi-theorem [66] the complexity of the problem can be reduced from the seven dimensional-variables dependent to only four Non-Dimensional (ND) variables. These four ND variables are next defined as products of the dimensional variables. The four ND variables are denoted by π_i. Since there are seven dimensional variables to construct four ND variables, three dimensional variables are used as repeating variables in the ND products (π_i). There are 35 different options to choose three variables out of seven for the case where the order does not matter (combinations). This sets a fairly tedious task of screening between 35 different options, defining the best appropriate manner to describe the ND helicopter hover performance. The derivation is demonstrated for only one of the 35 options available. The following example involves setting the main-rotor disk area, the ambient static pressure and the ambient static temperature as repeating variables. The four ND products are defined in Eq.(5.10).

$$\left\{\begin{aligned}\pi_1 &= \left(A_d\right)^a \left(P_a\right)^b \left(T_a\right)^c \left(P\right) \\ \pi_2 &= \left(A_d\right)^d \left(P_a\right)^e \left(T_a\right)^f \left(W\right) \\ \pi_3 &= \left(A_d\right)^g \left(P_a\right)^h \left(T_a\right)^i \left(\omega\right) \\ \pi_4 &= \left(A_d\right)^j \left(P_a\right)^k \left(T_a\right)^m \left(h\right)\end{aligned}\right\} \tag{5.10}$$

Next, the dimensional analysis procedure requires to replace each of the dimensional variables with its dimensions and to enforce each one of the four π_i parameters to be non-dimensional. This process is demonstrated as per Eq.(5.11).

$$\begin{cases} [\pi_1] = \left[L^2\right]^a \left[\frac{M}{LT^2}\right]^b \left[\frac{L^2}{T^2}\right]^c \left[\frac{ML^2}{T^3}\right] = M^{b+1} L^{2a-b+2c+2} T^{-2b-2c-3} = M^0 L^0 T^0 \\ [\pi_2] = \left[L^2\right]^d \left[\frac{M}{LT^2}\right]^e \left[\frac{L^2}{T^2}\right]^f \left[\frac{ML}{T^2}\right] = M^{e+1} L^{2d-e+2f+1} T^{-2e-2f-2} = M^0 L^0 T^0 \\ [\pi_3] = \left[L^2\right]^g \left[\frac{M}{LT^2}\right]^h \left[\frac{L^2}{T^2}\right]^i \left[\frac{1}{T}\right] = M^h L^{2g-h+2i} T^{-2h-2i-1} = M^0 L^0 T^0 \\ [\pi_4] = \left[L^2\right]^j \left[\frac{M}{LT^2}\right]^k \left[\frac{L^2}{T^2}\right]^m [L] = M^k L^{2j-k+2m+1} T^{-2k-2m} = M^0 L^0 T^0 \end{cases} \quad (5.11)$$

Each one of the π products yields 3 equations with 3 unknowns, which are the exponents. Solving for the exponents of π_1 is demonstrated in Eq.(5.12). The same process is repeated for each one of the other ND variables, π_2, π_3 and π_4.

$$\left.\begin{cases} [M]: b+1=0 \\ [L]: 2a-b+2c+2=0 \\ [T]: -2b-2c-3=0 \end{cases}\right\} \Rightarrow \begin{bmatrix} 0 & 1 & 0 \\ 2 & -1 & 2 \\ 0 & -2 & -2 \end{bmatrix} \begin{Bmatrix} a \\ b \\ c \end{Bmatrix} = \begin{Bmatrix} -1 \\ -2 \\ 3 \end{Bmatrix} \Rightarrow \begin{Bmatrix} a \\ b \\ c \end{Bmatrix} = \begin{Bmatrix} -1 \\ -1 \\ -1/2 \end{Bmatrix} \quad (5.12)$$

Based on Eq.(5.12) the first ND variable, π_1, can be written as Eq.(5.13).

$$\pi_1 = \frac{P}{A_d \cdot P_a \sqrt{T_a}} \quad (5.13)$$

The interest is in developing a method to gather hover performance for a specific helicopter and not in drawing a comparison between different types of helicopters. Therefore, the ND variable (Eq.(5.13)) can be further simplified. The main-rotor disk area (A_d) is constant, and the static pressure (Pa) and temperature (Ta) of the ambient air can be expressed as per their ratio to the standard sea level values (Eq.(5.14)).

$$P_a = P_0 \cdot \delta \ , \ T_a = T_0 \cdot \theta \quad (5.14)$$

This gives a simplified expression for π_1 defined as π_1^* in Eq.(5.15).

$$\pi_1 = \frac{P}{A_d P_a \sqrt{T_a}} = \frac{P}{A_d P_0 \delta \sqrt{T_0 \theta}} = \frac{P}{\left(A_d P_0 \sqrt{T_0}\right) \delta \sqrt{\theta}} = \frac{1}{A_d P_0 \sqrt{T_0}} \frac{P}{\delta \sqrt{\theta}} = Const \cdot \frac{P}{\delta \sqrt{\theta}} \Rightarrow$$

$$\pi_1^* = \frac{P}{\delta \sqrt{\theta}} \tag{5.15}$$

Since this term has dimensions and is not a pure ND, it is better defined as a "corrected" variable (CV) to describe the hover performance of a specific helicopter. It can be used to facilitate the forthcoming analysis.

Similar analysis performed for π_2, π_3 and π_4 yielded the corresponding three corrected-variables (π_2^*, π_3^* and π_4^*). The hover performance of a specific helicopter can now be simplified as presented as Eq.(5.16).

$$\pi_2^* = \frac{W}{\delta} \ , \ \pi_3^* = \frac{\omega}{\sqrt{\theta}} \ , \ \pi_4^* = \frac{h}{\sqrt{A_d}} \tag{5.16}$$

One should be noted that π_4^* is a true ND variable which represents the ND height of the main-rotor above the ground. This ND variable is beneficial only if the hover performance deals with in-ground-effect (IGE). This thesis is limited to the out of ground effect (OGE) only and does not address the ground effect on hover performance.

Identical dimensional analysis was repeated to evaluate all other 34 possibilities of choosing three dimensional variables out of the seven. Ten options were found to not having a unique solution, and few other options returned repeated ND variables. Overall, the analysis yielded 15 different corrected-variables which can be used for the specific hover performance analysis. Table 5.3 summarizes all 15 corrected-variables in an array form that indicates which of the three dimensional-variables (power, weight and main-rotor angular speed) is used in the specific corrected-variable. Three of the corrected-variables (π_{13}^*, π_{14}^* and π_{15}^*) are based on all three dimensional-variables.

Table 5.3. Corrected Variables (CV) to represent the OGE hover performance.

	Power Based	Weight Based	Main-Rotor & angular-speed based	Power, Weight and Main-Rotor angular speed based
Power based	$\pi_1^* = \frac{P}{\delta\sqrt{\theta}}$	$\pi_6^* = \frac{P}{W\sqrt{\theta}}$	$\pi_4^* = \frac{P}{\delta\omega}$	$\pi_{13}^* = \frac{P}{W\omega}$
	$\pi_5^* = \frac{P}{\delta^2\theta}$	$\pi_8^* = \frac{P^4}{W^5\delta}$	$\pi_{10}^* = \frac{P\omega^2\sqrt{\theta^3}}{\delta}$	$\pi_{14}^* = \frac{P\sqrt{\delta}}{\omega\sqrt{W^3}}$
		$\pi_9^* = \frac{P\sqrt{\theta}}{W^2}$	$\pi_{12}^* = \frac{P\omega^2}{\delta\sqrt{\theta^3}}$	$\pi_{15}^* = \frac{P\sqrt{\delta}}{W\omega}$
Weight based		$\pi_2^* = \frac{W}{\delta}$	$\pi_{11}^* = \frac{W\omega^2}{\delta\cdot\theta}$	
Main-Rotor Angular speed based			$\pi_3^* = \frac{\omega}{\sqrt{\theta}}$	
			$\pi_7^* = \frac{\omega}{\sqrt{\delta}}$	

5.4.2 Phase Two - Screening for essential CVs using dimensionality reduction

Phase Two of the proposed CVSDR method is to refine the list of 15 corrected-variables (Table 5.3) generated from fundamental dimensional analysis and to select only the essentials for the task of acquiring an empirical model to represent the OGE hover performance of a helicopter. A power based corrected-variable needs to be expressed as a function of other corrected-variables. It is immediately evident that the three corrected-variables (π_{13}^*, π_{14}^* , π_{15}^*) cannot serve as effective predictors since each one of them simultaneously involves all three major variables of power, weight and angular speed of the main rotor. Even prior to implementing dimensionality reduction tools, the list of candidate corrected variables is reduced to 12 candidate predictors.

The proposed dimensionality reduction approach for hover CVs screening is based on the Singular Value Decomposition (SVD) theorem which is thoroughly presented and discussed in Chapter 4 (Subsection 4.4.1). As a reminder, the SVD theorem states that any generic real matrix can be ***uniquely*** decomposed into a set of three matrices as given in Eq.(5.17). Consider a real matrix Z to be of size (m,n) and rank 'r'. This matrix Z can be expressed as a product of the following three ***unique*** matrices: matrix U, an orthonormal matrix of size (m,r) called the "Left-Singular-Vectors" (LSV); matrix Σ, a diagonal matrix which holds along its diagonal the singular-values of Z; and matrix V, an orthonormal matrix of size (n,r) called the "Right-Singular-Vectors" (RSV).

$$Z = U\Sigma V^T = \begin{bmatrix} u_{1,1} & u_{1,2} & \cdot & u_{1,n} \\ u_{2,1} & u_{2,2} & \cdot & u_{2,n} \\ \cdot & \cdot & \cdot & \cdot \\ \cdot & \cdot & \cdot & \cdot \\ u_{m,1} & u_{m,2} & \cdot & u_{m,n} \end{bmatrix} \begin{bmatrix} \sigma_1 & & & \\ & \sigma_2 & & \\ & & \cdot & \\ & & & \sigma_r \end{bmatrix} \begin{bmatrix} v_{1,1} & v_{2,1} & \cdot & v_{n,1} \\ v_{1,2} & v_{2,2} & \cdot & v_{n,2} \\ \cdot & \cdot & \cdot & \cdot \\ v_{1,r} & v_{2,r} & \cdot & v_{n,r} \end{bmatrix} \quad (5.17)$$

$$\sigma_1 > \sigma_2 > \ldots > \sigma_r \geq 0$$

The SVD theorem can be implemented for refining the corrected-variable (CV) list and to identify those which stand-out from the group of 12 as the most effective predictors for the OGE hover empirical model. A comparable approach is performed in the process of gas-turbine empirical models screening presented in Chapter 4. For this task of screening the most effective CVs for hover performance, matrix Z is filled with numeral entries of the 12 corrected-variables as evaluated for the first three flight-test sorties of the Bell Jet-Ranger helicopter. Matrix Z becomes of size (56,12); 56 rows that each represents a distinct single hover point and 12 columns that represent the 12 CVs (π_1^* to π_{12}^*). Next is to normalize the columns of Z to have a mean of zero and a variance of 1. For this, each entry along the columns of Z is normalized as per Eq.(5.18).

$$\pi_i^{'} = \frac{\pi_i^* - \mu_{\pi_i^*}}{S_{\pi_i^*}} \quad , i = 1,2,\ldots,11,12 \quad (5.18)$$

The normalized Matrix Z (defined as Z') is then decomposed into its unique three matrices as per Eq.(5.17). As expected, the rank of Z' is 12 representing the dimensionality of the flight-test data. The OGE hover performance problem as appears in matrix Z' can be represented by using all 12 CVs (π_1^* to π_{12}^*). However, not all corrected-variables have the same level of significance in representing the variance in the flight-test data held by matrix Z'. The singular-values (σ_i) which are arranged in a descending order along the main diagonal of matrix Σ are key to understanding the level of importance each corrected-variable ('i') holds. The conceptual interpretation of the SVD of Z' for the specific problem of OGE hover performance is illustrated in Fig. 5.4 and is further explained herein.

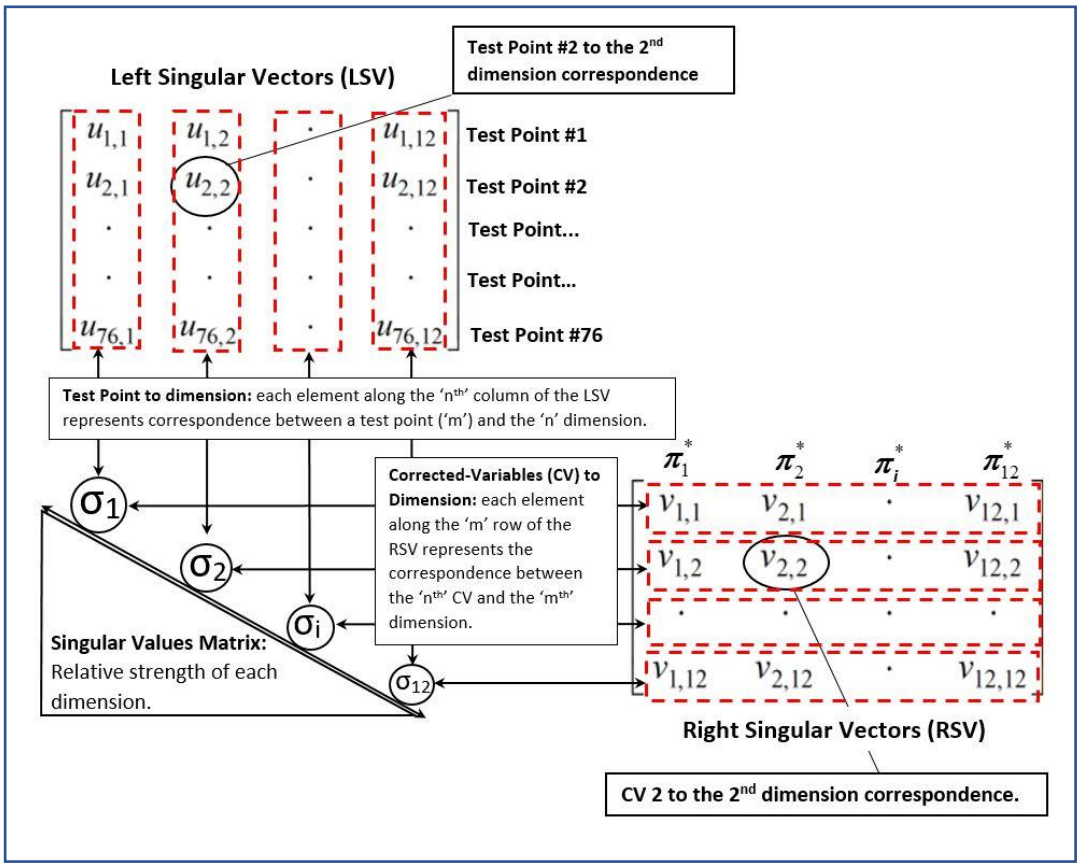

Figure 5.4. The conceptual interpretation of SVD of Z' in OGE hover performance. This figure presents how the abstract SVD of matrix Z' (normalized predictors) should be interpreted for the task of screening out the most effective predictors for OGE hover performance representation.

The 12 singular-values of the diagonal matrix Σ are normalized as per Eq.(5.19)

$$\hat{\sigma}_i = \frac{\sigma_i}{\sum_{k=1}^{12} \sigma_k} \quad ,i = 1,2,3,...,11,12 \tag{5.19}$$

The normalized singular values are presented in Fig. 5.5 along with a cumulative-sum plot of all normalized singular values. The main conclusion one can draw from Fig. 5.5 is that the dimensionality of the general OGE hover problem can be ***practically*** reduced from 12 (the general case) to only five for the specific OGE hover analysed. The empirical model representing the general OGE hover performance can be substantially simplified for the specific case analysed, to include only five CVs, instead of the original 12. The cumulative sum plot presented in Fig. 5.5 indicates that 98% of the variance in the flight-test data stored in matrix Z (or Z') can be captured by using only the first five most significant CVs. Also from Fig. 5.5, it can be noticed that the most significant dimension of the problem is responsible to 52% of variance in the flight-test data, the second dimension explains 19% of variance in the data, and the third, fourth and fifth can explain 13%, 8% and 6%, respectively.

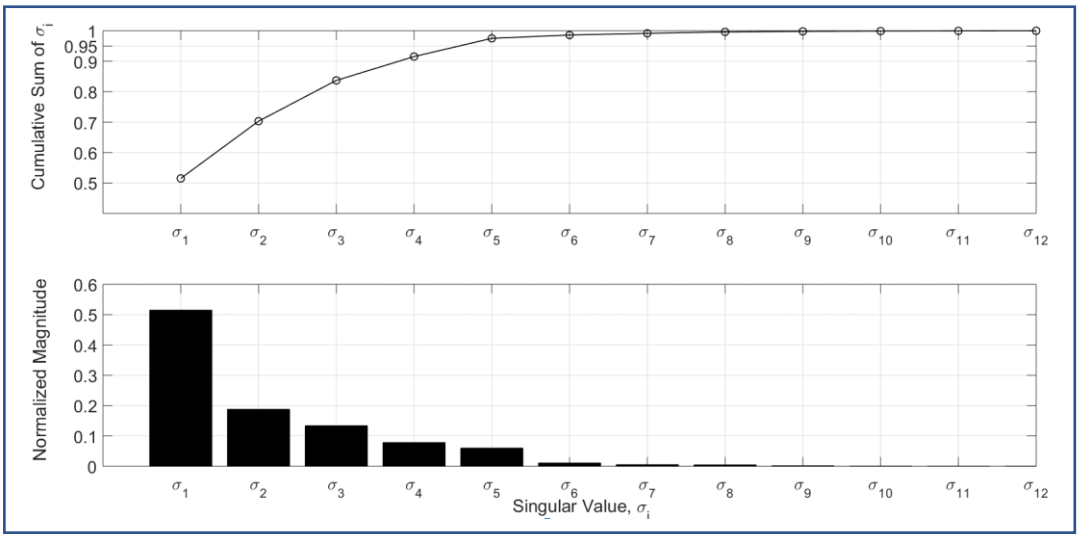

Figure 5.5. The Singular Values (SVs) of Matrix Z'. This figure shows the relative significance of the 12 SVs (or dimensions) involved in the specific OGE hover performance.

The following necessary question one might have is "which are the most significant corrected-variables?" This question is answered by evaluating the absolute values of the entries of the RSV matrix. As illustrated in Fig. 5.4, each row of the RSV indicates the level of correspondence to a specific singular-value (or a dimension) of the problem. For example, the first row of the RSV specifies the level of correspondence each one of the 12 corrected-variables has to the first (and most significant) singular-value. The second row of the RSV indicates the correspondence between all 12 corrected-variables to the second most significant dimension of the problem and so on. Since the dimensionality of the problem was reduced from 12 to 5, it is required to evaluate the first five rows of the RSV matrix in order to expose the most significant CVs of the OGE hover problem. Figure 5.6 presents the significance of each CV to each one of the five substantial dimensions of the OGE hover performance problem by indicating the ***normalized*** values (as per Eq.(5.20)) of the entries along the first five rows of the RSV matrix.

$$\hat{V}(i,j)=\frac{|V(i,j)|}{\sum_{j=1}^{12}|V(i,j)|} \quad ,i=1,2,3,4,5 \tag{5.20}$$

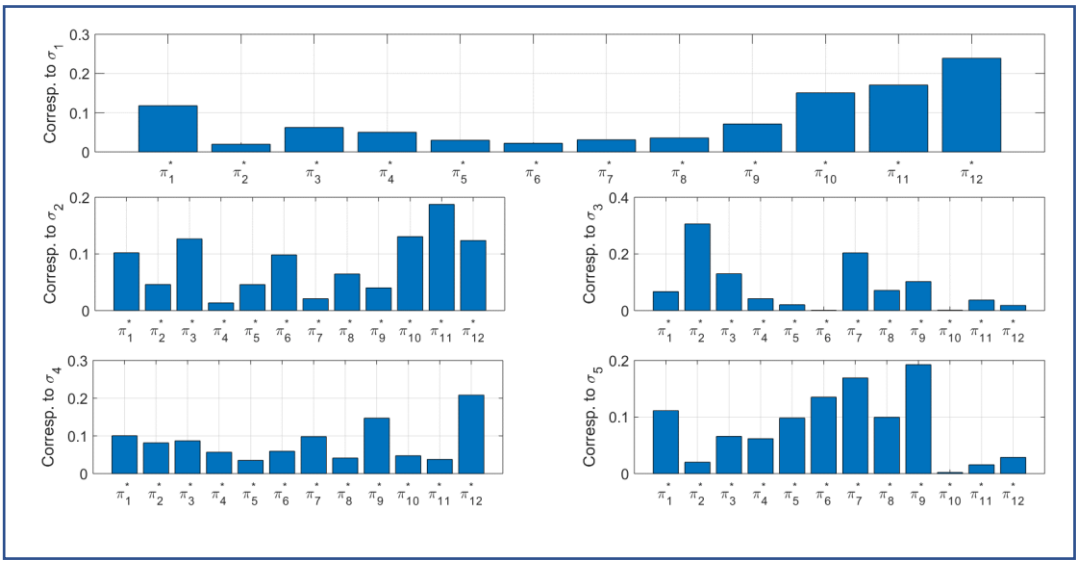

Figure 5.6. Dimensions to CVs correspondence. This figure shows the correspondence between each one the 12 CVs to the detected dimensions of the OGE hover problem.

The left singular vectors (LSV) matrix has no significant role in the type of analysis addressed in this chapter since it only indicates level of correspondence between each one of the 56 OGE hover points and the singular-values of Z. This type of correspondence between particular hover test-points and the various dimensions of the OGE hover performance is deemed irrelevant to the subject of this analysis.

The following five conclusions are drawn from Fig. 5.5 and Fig. 5.6:

(1) The first and most significant dimension of the OGE hover problem holds for 52% of variance in the data, and is best represented by π_{12}^*.

(2) The second most significant dimension of the OGE hover problem holds for 19% of variance in the data, and is best represented by π_{11}^*.

(3) The third dimension of the OGE hover problem holds for 13% of variance in the data, and is best described by π_2^*.

(4) The fourth dimension of the problem holds for 8% of variance in the data, and is best represented by π_{12}^*.

(5) The least significant dimension in the truncated list of 5 dimensions holds for only 6% of variance in the data and is best represented by π_9^*, followed by π_7^*.

Since only one power-based predictor is required for the empirical model in quest and the previous conclusions suggest two (π_{12}^* and π_9^*), it was decided to use the one that shows the highest correspondence with the first dimension which is π_{12}^*. Furthermore, π_9^* is replaced with π_7^* as the predictor which best represents the fifth dimension of the OGE hover problem.

Finally for Phase Two, a conceptual empirical model to represent the OGE hover performance of the example helicopter can be stated as Eq.(5.21). This conceptual relationship is next pursued with a first-order linear model as described in Eq.(5.22).

$$\pi_{12}^{*} = f_1(\pi_{11}^{*}, \pi_2^{*}, \pi_7^{*}) \therefore \frac{P\omega^2}{\delta\sqrt{\theta^3}} = f_1\left(\frac{W\omega^2}{\delta\cdot\theta}, \frac{W}{\delta}, \frac{\omega}{\sqrt{\delta}}\right) \tag{5.21}$$

$$\frac{P\omega^2}{\delta\sqrt{\theta^3}} = \beta_1\left(\frac{W\omega^2}{\delta\cdot\theta}\right) + \beta_2\left(\frac{W}{\delta}\right) + \beta_3\left(\frac{\omega}{\sqrt{\delta}}\right) + \beta_4 \tag{5.22}$$

The numerous steps executed for dimensionality reduction in Phase Two are summarized as a flowchart presented in Fig. 5.7.

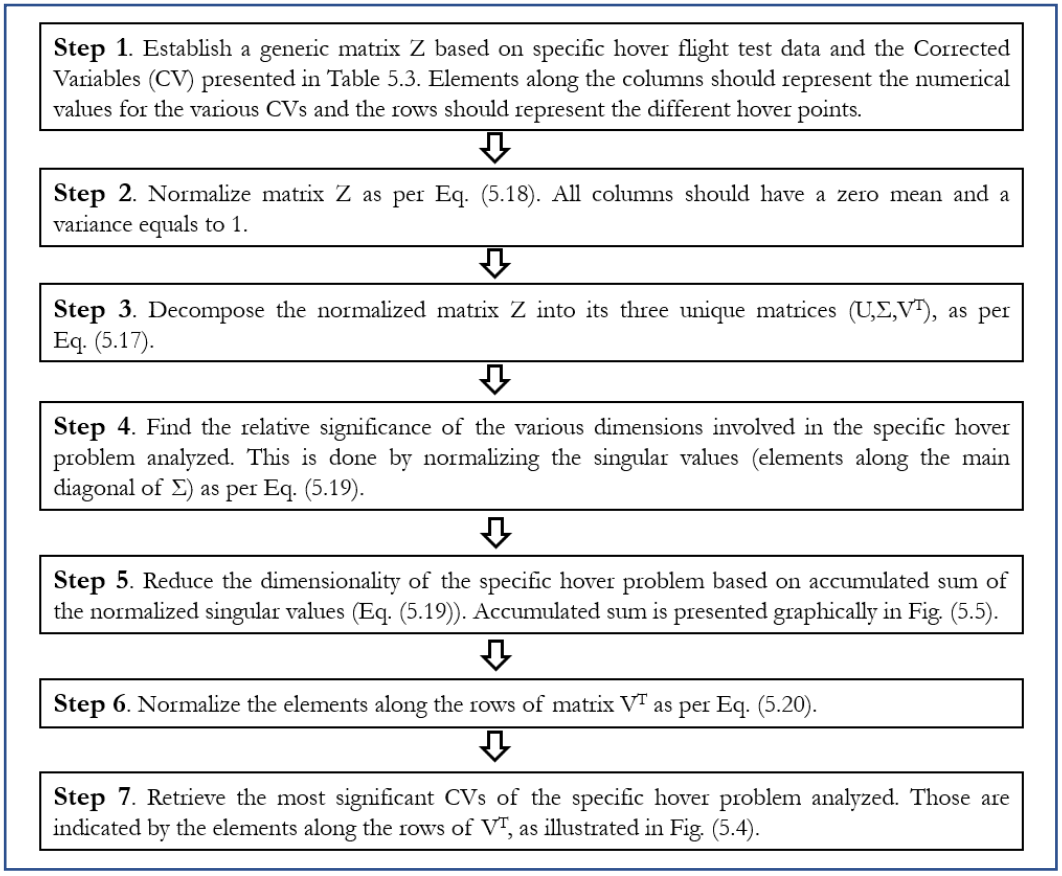

Figure 5.7. Steps required for dimensionality reduction. This figure presents the seven steps required for screening between the various CVs and choosing the most significant ones.

5.4.3 Phase Three - Deriving a practical empirical model

The proposed model (Eq.(5.22)) is fitted with the 56 flight-test OGE hover points from the first three sorties. This regression process is based on the 'least-squares' method as previously explained in Section 5.3. The refined OGE hover model, based on the CVSDR method and the flight-test data from the first three sorties, is presented as Eq.(5.23). This empirical model is addressed hereinafter as Model number 1 and denoted as M1.

$$\frac{P\omega^2}{\delta\sqrt{\theta^3}} = \beta_1\left(\frac{W\omega^2}{\delta\cdot\theta}\right)+\beta_2\left(\frac{W}{\delta}\right)+\beta_3\left(\frac{\omega}{\sqrt{\delta}}\right)+\beta_4\ ,\ \begin{Bmatrix}\beta_1\\ \beta_2\\ \beta_3\\ \beta_4\end{Bmatrix}=\begin{Bmatrix}0.134\\ -7.99\\ 926.5\\ -2\times10^5\end{Bmatrix}\quad \text{(Model 1)} \qquad (5.23)$$

5.5 THE CVSDR MODEL PREDICTION ACCURACY (OGE HOVER)

The OGE hover model generated by the CVSDR method (Eq.(5.23)) is next evaluated for its expected level of accuracy. For this, Model 1 (Eq.(5.23)) is used to predict the power required to OGE hover under the conditions of Sortie 4. The errors between the predicted power and the ***actual*** measured power were calculated in accordance with Eq.(5.24), and are presented in Fig. 5.8.

$$\vec{E}_{r_{M1}} = P_i - \left(\beta_1\left(\frac{W\omega^2}{\delta\cdot\theta}\right)_i+\beta_2\left(\frac{W}{\delta}\right)_i+\beta_3\left(\frac{\omega}{\sqrt{\delta}}\right)_i+\beta_4\right)\frac{\delta_i\sqrt{\theta_i^3}}{\omega_i^2},\ i=1,2,...,20 \qquad (5.24)$$

Prediction errors ranged up to a maximum absolute deviation of 8.5 hp. The mean of the prediction errors for the 20 hover points of Sortie 4 was calculated to be -2.3 hp with a variance of 9.7 hp^2.

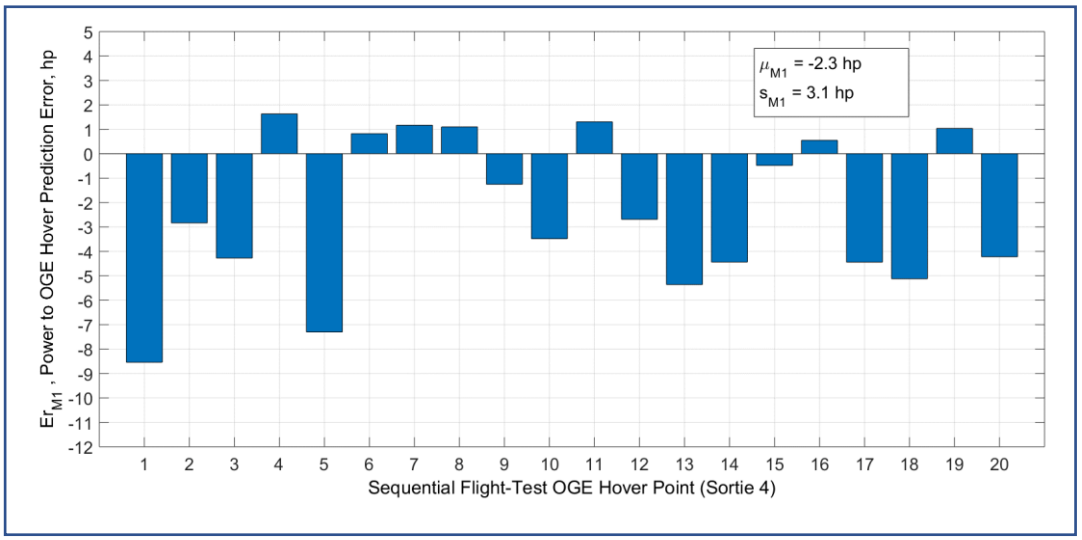

Figure 5.8. Power prediction errors for Sortie 4 (CVSDR model). This figure shows the power to OGE hover prediction errors generated by the CVSDR model (Eq.(5.23)) for the conditions of Sortie 4.

Parallel statistical analysis as discussed in Section 5.3 for the base-model was performed in order to evaluate the level of accuracy to be expected from the CVSDR-based OGE hover model (Model 1, Eq.(5.23)). The applicable test-statistic for the relevant hypothesis testing was calculated per Eq.(5.25).

$$t_{M1} = \frac{\left|\bar{E}_{r_{M1}}\right| - \mu_0}{S_{M1}/\sqrt{n}},\ \mu_0 = 1.6\ hp\ ,n = 20 \tag{5.25}$$

The symbol 'n' represents the number of measured test points of sortie 4 (n=20) and 'S_{M1}' stands for the standard deviation of the prediction errors of Model 1 (the standard deviation of the data presented in Fig. 5.8). Test-statistic was found to be 1.06. Inferential statistical analysis based on the sampled data from Sortie 4 show a significant probability of 30.1% for making a type-I error by rejecting the null-hypothesis. This probability for a type-I error is well above the 5% significance level accustomed in helicopter performance flight-testing. Practically, there is no significant statistical evidence at the 95% confidence level to reject the null hypothesis therefore it has to be accepted. Complimentary statistical analysis shows that at the 95% confidence-level, Model 1 (Eq.(5.23)) predictions deviate ***on-average*** by up to 0.9 hp

from the actual measured power to hover. This value of 0.9 hp is well below the deviation threshold of 1.6 hp noticeable to the Bell Jet-Ranger aircrew.

5.6 A COMPARISON BETWEEN THE CONVENTIONAL AND CVSDR METHODS

As previously noted in Section 5.3, the OGE hover flight-test data obtained from a Bell Jet Ranger helicopter in a course of 4 different sorties were divided into two groups. The first, which consisted of data from the first three sorties, was used to develop an empirical model to represent the power for OGE hover. This model was evaluated for accuracy while used to predict hover points of Sortie 4. Two different models were used, the base-model which relies on the conventional hover flight-testing method (the single-variable, Cp to $(Cw)^{1.5}$ method), and another multivariable empirical model derived from the proposed CVSDR method. Figure 5.9 presents a comparison between the prediction errors of the two OGE hover models, the conventional method (Eq.(5.5)) and the proposed multivariable Model 1 (Eq.(5.23)).

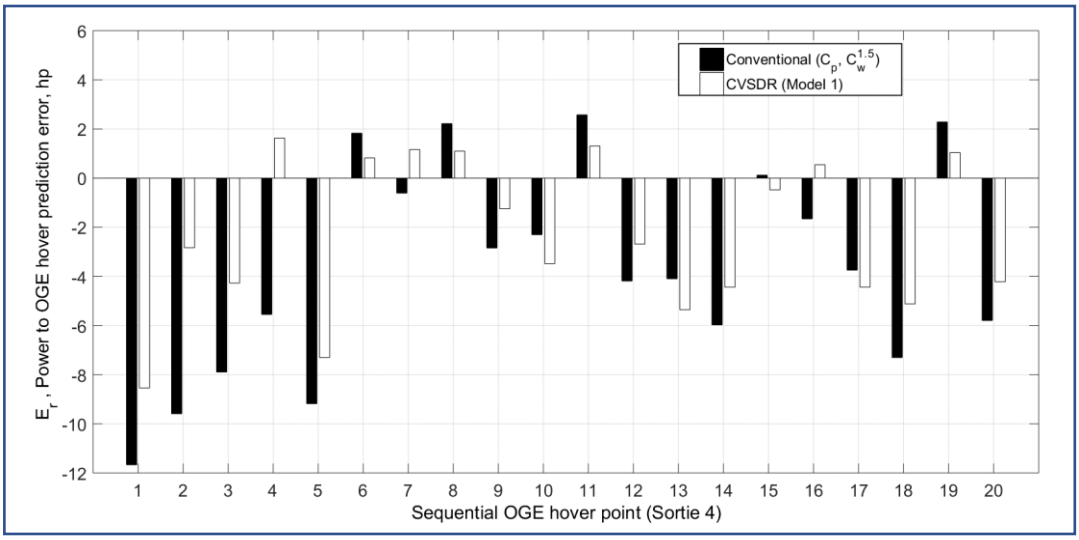

Figure 5.9. The conventional and CVSDR methods prediction comparison. This figure compares the prediction accuracy achieved by both methods (conventional and CVSDR) for the conditions of Sortie 4.

The conventional model predicts the hover points of Sortie 4 with an average error of –3.7 hp and a variance of 18.1 hp^2, whereas the proposed Model 1 yields better predictions with an average error of -2.3 hp and a narrower variance of 9.7 hp^2. Hypothesis testing aimed at projecting from the particular case of Sortie 4 to the general case, shows that at the accustomed 95% confidence level Model 1 predictions deviate ***on-average*** by only 0.9 hp. Power predictions of the conventional model deviate, on average, by a significant 1.7 hp, which is noticeable to the Jet-Ranger helicopter aircrew. This power deviation of 1.7 hp can be translated to a gross-weight difference of about 15 lbs. under the conditions tested (Sorties 1 - 4). The power to hover prediction of the proposed CVSDR method was found to be substantially more accurate than the conventional method as its deviation from the actual power was 1.9 times less than the conventional method.

One might question why is it that Model 1 predicts the power required to hover more accurately than the conventional model? First and foremost, the CVSDR method does not assume beforehand which predictors should be used in the empirical model. Instead, the list of the potential 15 predictors is reduced to the most essential and effective ones based on the specific flight-test data analyzed. This approach by itself provides more flexibility which allows for more accurate modelling. Specifically and as emphasized in the introduction to this chapter, compressibility effects have substantial influence on hover performance of rotors as reported by current CFD analysis. The conventional model neglects compressibility and drag-divergence effects, whereas the multivariable Model 1 employs a predictor to represent the blade tip Mach-number ($\pi_{11}^{*} = \frac{W\omega^2}{\delta\theta}$), therefore capable of representing compressibility and drag-divergence effects. The inherent assumption of the conventional single-variable method for a constant zero-lift drag coefficient (Cd_0) cannot be held valid for a wide range of Mach numbers and for high values of main rotor disk-loading. Hovering at low ambient temperatures (high Mach tip numbers) and at high gross-weights might be responsible for some sections of the main rotor disk to be subjected to drag-divergence conditions.

The two predictors (π_7^*, π_{11}^*) used in Model 1 can provide the extra degree of freedom in modelling compressibility effects, which are absent in the conventional model (the Cp to $(Cw)^{1.5}$ method).

5.7 CONCLUSIONS AND SUMMARY

The proposed CVSDR hover performance flight-testing method requires no modification to the manner helicopter hover performance flight-test sorties are carried out. The change is to the procedure of the data analysis. An original list of 15 corrected variables (predictors) to represent the general hover performance of a helicopter was formulated by means of dimensional analysis. This list is further reduced by applying concepts of dimensionality reduction to include ***only*** the most essential and effective CVs to represent the hover performance problem. For the particular Jet Ranger case demonstrated in this chapter, this list of 15 CVs was reduced to only four essential predictors. Those four CVs represented 98% of variance in the specific hover performance data, and were applied in an empirical model to represent the OGE hover performance of the Jet-Ranger.

The CVSDR method showed great potential as it was used successfully with OGE hover flight-test data. The power predictions of the proposed CVSDR method were compared to those of the conventional single-variable method, and were found to be 1.9 times more accurate. At the 95% confidence level, the CVSDR method deviated by an average of only 0.9 hp from the actual power to hover, whereas the conventional method deviated by an average of 1.7 hp.

Although demonstrated in this chapter using flight-test data of a Bell Jet-Ranger helicopter, the CVSDR method is applicable and can be used for OGE hover flight-testing of any other types of conventional helicopters, which employ a single main rotor and a single tail rotor. The CVSDR method, at its core, is using dimensionality reduction concepts to select the most the most effective and essentials predictors of any physically meaningful problem. This competency of the CVSDR method can also

be applied to other types of helicopter performance testing which seek to relate ND variables. After proved successful for hover performance testing, the following Chapter 6 continues to develop the CVSDR method and expands it further into higher dimensional space of level-flight performance flight-testing.

Philosophy consists mostly of kicking up a lot of dust and then complaining that you can't see anything.

Gottfried Leibniz

6 Level Flight Performance Flight Testing

6.1 Chapter Overview

The evaluation of the power required in level-flight is essential to any new or modified helicopter performance flight-testing effort. The conventional flight-test method is thoroughly discussed in Chapters 1 and 2 (Subsections 1.3.3 and 2.3.3). This testing method is overly simplified as it is based on approximations of the induced and profile power components. The method incorporates several drawbacks which, not only make the execution of the flight-test sorties inefficient and time consuming, but also compromise the level of accuracy one can expect from the empirical model yielded. This chapter proposes an alternative flight test method for level-flight performance of a conventional helicopter that addresses and rectifies all the identified deficiencies of the conventional method, as stated in Subsection 1.4.3 (PS3-PS7). The novel method, referred-to as the 'Corrected-Variables Screening using Dimensionality Reduction' (CVSDR), is practically an expansion of the hover method discussed in Chapter 5. The CVSDR flight-test method for level flight performance can be regarded as an expansion of the hover CVSDR method into a higher dimensional space.

This Chapter 6 was published as the following journal paper: Arush I., Pavel M.D., and Mulder M., "A Dimensionality Reduction Approach in Helicopter Level Flight Performance Flight Testing", Journal of the Royal Aeronautical Society, First View 13 July 2023. https://doi.org/10.1017/aer2023.57

The CVSDR method for level-flight performance uses an original list of 36 corrected-variables (CVs) derived from fundamental dimensional analysis principles. This list of candidate predictors is reduced by means of dimensionality reduction to retain only the most essential and effective predictors. The CVSDR method is demonstrated and evaluated for prediction accuracy level in this chapter by using flight-test data of a MBB BO-105 helicopter. It is shown that the CVSDR method predicts the power required for level-flight about 21% more accurately than the conventional method, while lowering the required flight time by an estimate of at least 60%. Unlike the conventional method, the CVSDR is not bounded by the high-speed approximation associated with the induced power estimation, therefore it is also relevant to the low airspeed regime. This low-airspeed relevancy allows the CVSDR method to bridge between the two important flight regimes of a helicopter, hover and level-flight. The CVSDR method for level-flight performance is applicable to any type of conventional helicopter.

6.2 INTRODUCTION

The helicopter spends most of its flying-time in the level flight regime. The relative time while cruising varies based upon the type and the specific mission the helicopter was designed-for. Porterfield and Alexander [44] analysed data from various types of helicopters and proclaimed that on average the helicopter spends 71% of its flight-time in level-flight. The FAA [45] provides different estimates for two exemplary turbine helicopters. The first example is a utility business type helicopter which estimated to spend 61% of its flight time while cruising and the second example presented is for a transport helicopter which is estimated to spend 73% of its flight time in level-flight. Regardless of where this value for relative time spent in level-flight truly resides, it is fair to say the helicopter spends most of its flight time while cruising.

The helicopter performance flight test team may be tasked to execute a level flight performance test campaign for various reasons; it might be for a limited-scope validation of existing performance charts for certification purposes; or it might be for

the task of updating performance charts due to external configuration modification; or it even be required for a full-scope level flight performance campaign, for which a complete set of charts and/or tables is required to specify the level flight performance of a brand new helicopter type. Whatever the reason is, the performance flight test team has a need for an efficient and accurate method to evaluate the helicopter performance in level-flight.

The conventional flight-test method for helicopter level flight performance is based on a simplification of the equation for the power required to sustain a helicopter in level flight, as already discussed in Chapter 2 (Subsection 2.3.3). This method is further demonstrated in this chapter using flight-test data of a MBB BO-105 helicopter. Although widely used, common practice shows that this flight-testing method is inefficient, time-consuming and includes few drawbacks which seriously compromises the accuracy of the empirical power model it yields. The following is a compilation of the main disadvantages of the conventional flight-testing method, as listed in Chapter 1 (Subsection 1.4.3) as the problem statements (PS3 to PS7).

First, the conventional method reduces a multi-dimensional physical problem into a three non-dimensional variable one. The three non-dimensional variables are the coefficient of power, Cp, the advance ratio, μ, and the coefficient of weight, Cw. The conventional method provides no comprehensive tools for addressing the effect of rotor blades compressibility on the power required for level flight. Boirun [101] addresses the compressibility effect in his work but his approach does not determine a decisive unified empirical model to include compressibility effects. Instead, various curves for different values of main-rotor tip Mach numbers are presented in the format of a 'carpet-plot'. Obtaining an accurate and unified empirical model to predict the level flight performance is highly desirable since it can also be easily used and implemented for real-time applications.

Second, the current method requires executions of various airspeed runs at constant coefficients of weight (Cw). This requirement makes the method inefficient, cumbersome and time consuming. Moreover, the resulting empirical model is prone

to elevated levels of inaccuracy since it is merely a set of single power curves for constant Cw, rather than a unified empirical model which accounts for the entire range of coefficients of weight.

Third, the conventional method takes the high-speed approximation for which the induced velocity of the air through the main-rotor disk is assumed negligible compared to the airspeed the helicopter flies at. By adopting this approximation, the conventional method becomes irrelevant for the low airspeed regime.

Fourth, the current method has no analytical means to account for the helicopter center-of-gravity location although numerous flight-test campaigns show substantial dependency between the helicopter longitudinal center-of-gravity and the power required for level-flight. For example, Buckanin et al. [6] present an increase of about 10 square-feet in the equivalent flat-plate drag area of a Blackhawk helicopter resulting from a 15 inches forward migration of the center-of-gravity in level flight.

Finally, the conventional method requires the flight test crew to precisely control the main rotor-speed. This requirement makes the current flight-test method unsuitable for helicopters which their main-rotor speed control system cannot be easily overridden by the pilot.

Chapters 3-5 presented an alternative and more accurate approach to helicopter performance flight-testing, using multivariable polynomials as empirical models. Chapter 3 discussed this approach for gas-turbine power testing, and demonstrated an increased prediction accuracy (in excess of 300%). This multivariable approach was also used successfully in the prediction of hover performance in Chapter 5; taking this multivariable approach reduced the average prediction error by about 47% as compared to the conventional hover flight test method. The systematic procedure to screen between candidate predictors, which is at the core of the CVSDR method, is discussed in Chapter 4.

The goal of this Chapter 6 is to expand this multivariable polynomial approach for the greater benefit of improving the level-flight test method. The CVSDR method

is stretched to accommodate a more complicated helicopter performance problem than the hover performance discussed in Chapter 5. Abstractly, this Chapter 6 can be regarded as a rigorous expansion of hover CVSDR method into a higher dimensional space of level-flight performance. The proposed CVSDR level-flight performance method is aimed at addressing all identified drawbacks of the conventional method, as specified in this Introduction and specifically listed as the five problem statements PS3-PS7 in Chapter 1 (Subsection 1.4.3).

This chapter is structured as follows: after the short introduction, the conventional level flight performance testing is discussed and demonstrated in Subsection 6.3 by using flight-test data from a MBB BO-105 helicopter. The flight-test data obtained from four distinct sorties totalling 44 data points are used to generate four empirical models to represent the helicopter required power in level-flight. Each empirical model is then used to predict the power required for the other three sorties. This procedure is implemented to assess the accuracy level one can expect by using the conventional flight-test method. Next, in Section 6.4, an alternative method referred to as the 'Corrected-Variables Screening using Dimensionality Reduction' (CVSDR) is proposed. This method is demonstrated by using the same flight-test data used with the conventional method. Section 6.5 provides a summary of the CVSDR method and a practical step-by-step guidance to facilitate the execution of this method by future flight-test crew. Next in Section 6.6, the expected prediction accuracy of the CVSDR method is assessed. This expected accuracy evaluation is executed in few different combinations of sorties to be used as data-base for model building, and sorties to be predicted by those empirical models. Section 6.7 provides a comprehensive comparison between the conventional and the proposed CVSDR methods. Section 6.8 concludes and summarizes the chapter.

6.3 LEVEL-FLIGHT PERFORMANCE TESTING-THE CONVENTIONAL WAY

The conventional flight test method for level flight performance of a helicopter is thoroughly discussed in Chapter 2 (Subsection 2.3.3) and only briefly reminded in this chapter. As per Eq.(6.1), the conventional method attempts to define sets of empirical relationships between the coefficient-of-power (Cp) and the advance-ratio (μ) for various discrete values of coefficient-of-weight (Cw). The different Cw values need to span the entire operational envelope of the helicopter.

$$C_P = \frac{C_W^2}{2\mu} + \frac{1}{8} C_{d_0} \sigma_R \left(1 + k_p \mu^2\right) + \frac{1}{2} \frac{f_e}{A_{disk}} \mu^3$$

$$\left\{ C_P \equiv \frac{P}{\rho_a A_d \left(\omega R\right)^3} \;,\; C_W \equiv \frac{W}{\rho_a A_d \left(\omega R\right)^2} \;,\; \mu = \frac{V_T}{\omega R} \right\} \tag{6.1}$$

For this, the flight-test crew needs to execute numerous 'speed-runs' while maintaining a constant coefficient-of-weight. The technique by-which the coefficient of weight is held constant throughout the speed-runs, defines the specific flight-test method. Ensuring a constant coefficient-of-weight during the speed run can be attained in two ways: (1) the constant "weight over sigma (W/σ)" method; and (2) the constant "weight over delta (W/δ)" method.

6.3.1 Constant Weight over Sigma (W/σ) Method

As previously discussed in Chapter 2, the constant "weight over sigma" is the foremost popular method for level-flight performance of a conventional helicopter. Following this method, the flight-test crew maintains the coefficient-of-weight at a certain value by keeping the main-rotor angular speed (**ω,Ω**) constant *and* maintaining

a constant ratio of weight (W) to the air relative density (σ). As presented in Eq.(6.2), the air relative density is defined as the ratio between the ambient air density (ρ_a) and the standard sea level air density (ρ_o). Maintaining a constant ratio of weight to relative density (W/σ) is achieved by a gradual adjustment of the cruise altitude for the speed runs as the helicopter burns fuel and becomes lighter. The required altitude change in-between test points of a specific speed-run is calculated in real time by the test-crew. It is common to encounter few iterations before the accurate altitude is reached. The extent of altitude climb between consecutive data points relates directly to the fuel consumption of the helicopter and the efficiency of the flight test crew to stabilize the helicopter in the desired conditions. This altitude climb is typically between a few tens to a few hundreds of feet. Once the new altitude is reached, the pilot needs to stabilize the helicopter at the new airspeed and to validate (or to readjust) the main-rotor angular speed remains constant. Note that the pilot is required to 'stay-on-conditions' for the entire duration necessary for the engine(s) to reach thermal equilibrium, followed by the data gathering period of time. Typically, the flight-test campaign for a specific helicopter configuration requires the execution of five sorties, each conducted at a different coefficient-of-weight value. The various coefficient-of-weights shall cover the entire certified envelope of the helicopter. Each speed run consists of *at least* eight different airspeeds, beginning at some 'arbitrary' low airspeed to the maximum level flight airspeed defined either by maximum available power (Vh), or by the manufacturer's definition for the 'never-exceed' airspeed (VNE).

$$C_W \equiv \frac{W}{\rho_a A_{disk}\left(\Omega R\right)^2} = \frac{W}{\sigma \rho_o A_{disk}\left(\Omega R\right)^2} = \underbrace{\frac{W}{\sigma}}_{held} \cdot \underbrace{\frac{1}{\Omega^2}}_{fixed} \cdot \underbrace{\frac{1}{\rho_o A_d R^2}}_{const.} \qquad \left\{ \sigma \equiv \frac{\rho_a}{\rho_o} \right\} \tag{6.2}$$

6.3.2 Constant Weight over Delta (W/δ) Method

The second and less common approach of maintaining a constant coefficient-of-weight during the speed run is called the 'weight over delta' method. This method is demonstrated mathematically in Eq.(6.3). Note that the air relative pressure ratio (δ) is defined as the ambient air static pressure (Pa) over the standard sea level air pressure (P_0). By using the equation of state (Eq.(6.4)), the ambient air density is expressed using the ambient static-temperature (Ta) ambient pressure (Pa) and the specific gas constant of the air (R_{air}). It is evident from Eq.(6.3) that by holding a constant ratio of weight over the relative pressure (W/δ) *and* a constant ratio of static ambient pressure over the angular rotor speed squared (Ta/Ω^2), the flight-test crew assures a constant coefficient-of-weight during the various speed runs. As previously discussed in Chapter 2 (Subsection 2.3.3.3), the only advantage this method has over the W/σ method is that it allows the flight-test crew to gain some limited control over compressibility effect of the main rotor advancing blades.

$$C_W \equiv \frac{W}{\rho_a A_{disk}\left(\Omega R\right)^2} = \frac{W}{\left(\frac{\delta P_o}{R_{air} T_a}\right) A_{disk}\left(\Omega R\right)^2} = \underbrace{\frac{W}{\delta}}_{held} \cdot \underbrace{\frac{T_a}{\Omega^2}}_{fixed} \cdot \frac{R_{air}}{P_o A_{disk} R^2}$$
$$\delta \equiv \frac{P_a}{P_o} \therefore \rho_a = \frac{\delta P_o}{R_{air} T_a} \tag{6.3}$$

$$P_a = \rho_a R_{air} T_a \tag{6.4}$$

This constant W/δ flight-test method requires even more flight-test sorties than the amount required for the W/σ method. This increased number of sorties is mostly attributed to the complexity and cumbersome associated with the continuous adjustments of the main-rotor angular speed.

The following procedure illustrates how cumbersome and time consuming the conventional flight-test method is. For a small size and light helicopter, such as the

BO-105, it takes about five minutes to obtain one data point. One should appreciate that out of those five minutes, only about two are essential for engine(s) thermal equilibrium attaining and data gathering. There is about 60% of time wasted due to the inefficiency of the conventional flight test technique. The requirement of at least eight data points (different airspeeds) for each constant Cw and evaluating five different values of coefficient-of-weight translates into *at least* 3 hours and 20 minutes of flight. This duration should be regarded as an optimistic estimation based on small sized helicopters. Executing level flight performance flight-test campaign on a large and heavy helicopter might even double this time duration. Proposing an alternative flight test method that eliminates the requirement for flying at constant coefficient of weight has the potential for saving at least 2 hours of flight time for the same amount of required data points (60%).

According to the conventional flight-test technique, as long as the helicopter flies straight and level at a constant coefficient-of-weight (Cw), its level flight performance can be ***uniquely*** represented by a single curve of coefficient-of-power (Cp) to advance-ratio (μ). One should question how extensively can the single variables that constitute the coefficient of weight be varied, while keeping the coefficient of weight constant before an effect on the coefficient of power is noticeable? In other words, how realistic is the assumption on which the conventional level-flight test technique is built upon?

6.3.3 Example Application - Constant Weight over Sigma (W/σ) Method

The conventional method (constant weight over sigma approach) is demonstrated within the context of the deficiencies associated with this method, using flight-test data obtained from a MBB BO-105 helicopter. The power required to sustain level flight at various airspeeds was recorded during four distinct sorties. All four sorties, totalling 44 stabilized level flight points, were conducted at a targeted coefficient-of-weight (5.79×10^{-3}) with a tight tolerance between -0.3% to +0.7%. The main-rotor angular

speed was kept constant at 100% (equivalent to 423 RPM for the specific helicopter) throughout the four sorties, as required by the conventional method. All physical values for gross-weight and atmospheric conditions are summarized in Table 6.1. Figure 6.1 presents all 44 data points of Sorties 1-4 as matching pairs of coefficient-of-power (Cp) and advance ratio (μ) accompanied with third order polynomial best-fit curves.

Table 6.1. Summary of flight-test conditions for Sorties 1-4.

Sortie #	Gross weight* [lbs.]	Average Long. C.G. [in.]	Pressure Altitude* [ft.]	Ambient Air Temp.* [°C]	Cw* [x10^{-3}]	Average Cw [x10^{-3}]
1	4890 - 5012	123.8	4000 - 4670	12 to 14	5.78 – 5.80	5.79
2	4760 - 4865	123.9	5040 - 5400	12	5.77 – 5.83	5.80
3	4270 - 4380	123.5	7770 - 8520	9 to 10	5.78 – 5.80	5.79
4	3890 - 3960	124.4	11210 - 11820	0 to 2	5.78 – 5.80	5.79

* values represent the range of change during the sortie

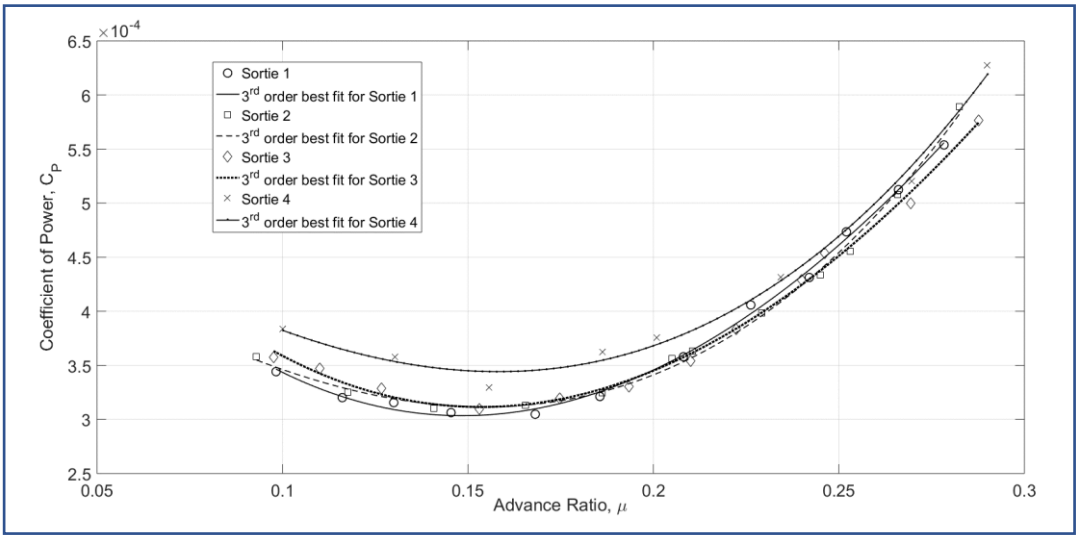

Figure 6.1. Level flight performance (ND) of a BO-105 helicopter. This figure presents the coefficient of power (Cp) against the advance ratio (μ) measured under conditions of four distinct sorties listed in Table 6.1. Data points are accompanied with third order best-fit curves.

The first concern to be discussed is with the uniqueness of the coefficient-of-power (Cp) to advance ratio (μ) curve for the four sorties executed. As previously

noted, all four sorties were conducted at the same coefficient of weight and hence should all generate a unique coefficient-of-power (Cp) to advance-ratio (μ) curve. One can immediately doubt it, just from observing Fig. 6.1. It is quite evident that not all 44 flight-test data points belong to the same (Cp) to (μ) curve. As listed in Table 6.1 the coefficient-of-weight (Cw) was held constant within a tight tolerance range of 1%. The expected variance in the coefficient-of-power (ΔCp) due to the variance in Cw (ΔCw) can be estimated by a sensitivity analysis to Eq.(6.1). This derivation is presented explicitly as Eq. (5).

$$\Delta C_P = \frac{\partial C_P}{\partial C_W}\left(\Delta C_W\right) = \frac{\overline{C_W}}{\mu}\left(\Delta C_W\right) \quad , \quad \overline{C_W} = 5.79\times10^{-3} \tag{6.5}$$

This analysis show that the actual 1% variance in Cw should only be responsible to a ΔCp of 0.02%, under a high advance ratio of 0.3. For a low advance ratio of 0.1 the expected variance in Cp should reach up to only 0.06%. The actual variance in Cp during the four sorties reached 11% in low advance ratios of about 0.1, and 9% for high advance ratios of about 0.3. This variance in (Cp) cannot be entirely explained by the 1% variance in (Cw), therefore casting severe doubts on the soundness of this conventional flight test method.

The level of accuracy achieved using the conventional flight-test method was assessed in two ways. The first and the foremost trivial assessment was to use each single sortie for the prediction of power required in each one of the other three sorties, then comparing the prediction to the actual power measured. This simplistic approach is addressed hereinafter as the ***single sortie approach***. The second approach for accuracy assessment was to base the power prediction of each sortie on a conglomerate of flight-test data from the other three sorties. This approach is referred-to hereinafter as the ***cluster of sorties approach***.

1) ***The single-sortie approach***: linear regressions were performed to retrieve four distinct third order polynomials to describe the non-dimensional level-flight performance of the BO-105 helicopter for the particular tested coefficient of-weight (Eq.(6.6)).

$$C_{P(j)} = a_3^j \mu^3 + a_2^j \mu^2 + a_1^j \mu + a_0^j \quad , \; j = 1,2,3,4 \tag{6.6}$$

Each one of those four third order polynomials ($CP_{(1)}$, $CP_{(2)}$, $CP_{(3)}$, and $CP_{(4)}$) was used to predict the power required for level flight under the conditions of the other three sorties. For example, the third order polynomial based on Sortie 1 was used to predict power required for level flight under the conditions of sorties 2, 3 and 4. The third order polynomial retrieved from Sortie 2 was used to estimate the power required for level flight under the conditions of Sorties 1, 3 and 4 and so on. Power estimations were compared to the actual measured values and prediction errors for each data point were calculated as per Eq.(6.7).

$$\vec{Er}_{(j)_i} = \left\{ C_{P(j)_i} - \left(a_3^j \mu_i^3 + a_2^j \mu_i^2 + a_1^j \mu_i + a_0^j \right) \right\} \rho_i A_d \left(\Omega_i R \right)^3 \quad , i = 1,2,\ldots \tag{6.7}$$

Figure 6.2 presents a summary of all prediction errors retrieved for all four sorties. These errors are presented in horse-power units and as a function of the corresponding advance-ratio (μ). It is worth noting that positive prediction errors mean under estimation of the power required and a negative value represents an over estimation of power. From an operator stand-point, underestimation is the worst-case scenario since the helicopter demands for more power than predicted and planned for. This extra power needed might not be available from the engine or the engines, jeopardizing a successful execution of the mission. On the other hand, overestimation of the power required can only contribute to inefficient planning and execution of the mission.

The prediction errors presented in Fig. 6.2 reveal a dissatisfying accuracy performance of the conventional method. For example, power prediction errors for Sortie 1 ranged between -20 hp (overestimate) to +18 hp (underestimate) using flight-test data from Sortie 2. Using flight-test data from Sortie 4 to predict power levels of Sortie 1 resulted in enormous overestimation errors that ranged between -50 hp to -2 hp. The means of the absolute prediction errors for each sortie were calculated as per Eq.(6.8) and are presented in Fig. 6.3.

$$\overline{E}_{R_{(j)}} = \frac{1}{n}\sum_{i=1}^{n}\left|E_{r(j)_i}\right| \tag{6.8}$$

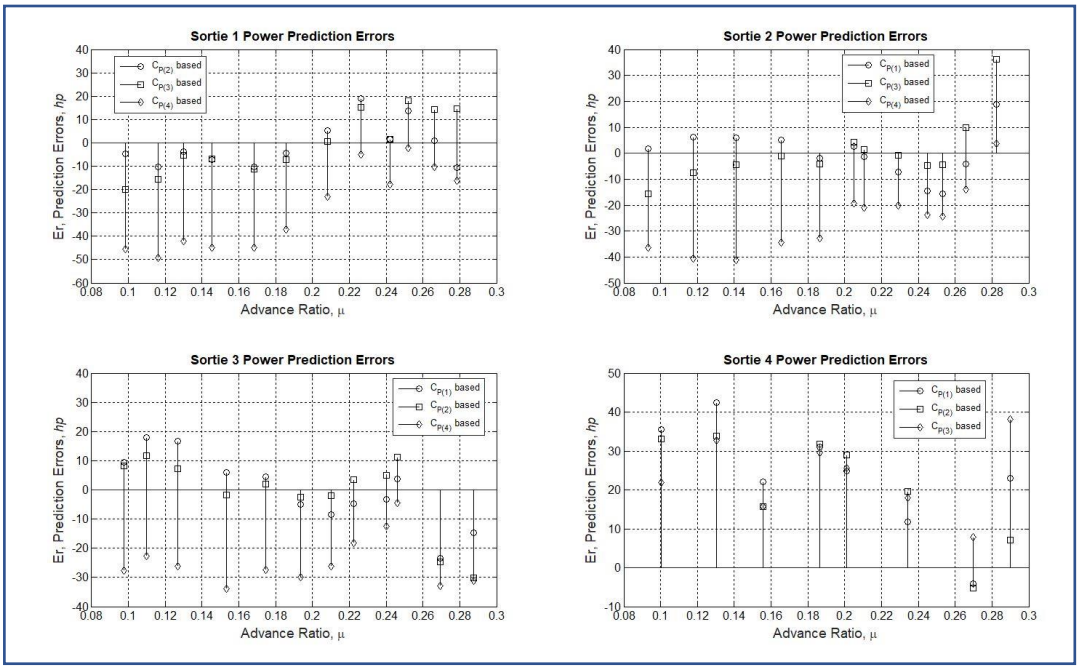

Figure 6.2. Power prediction errors of the BO-105 (single-sortie approach). This figure presents the level-flight power prediction errors yielded by the conventional power models, based on the single-sortie approach.

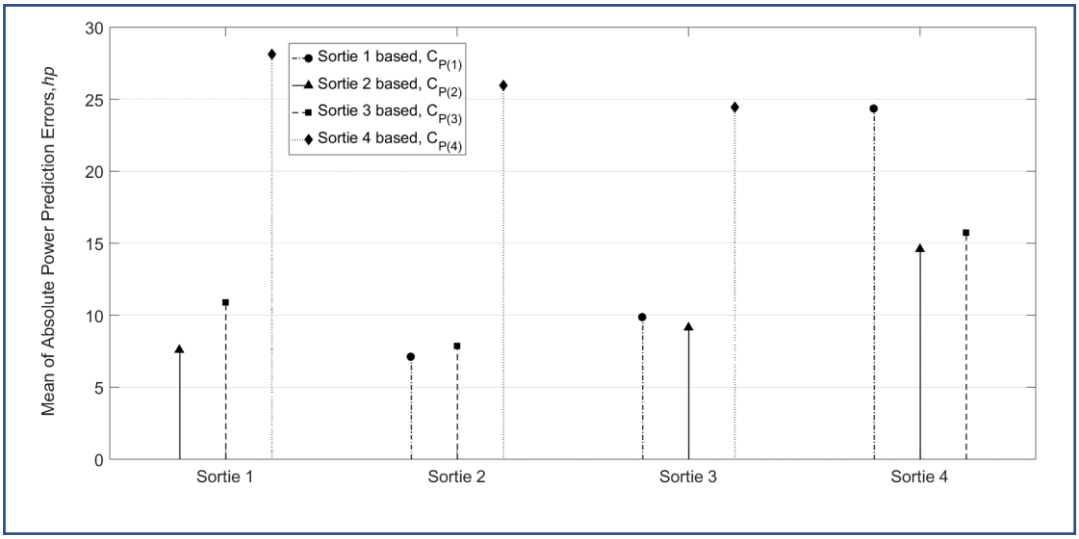

Figure 6.3. Mean of absolute power prediction errors (single-sortie approach). This figure presents the mean of the absolute errors yielded for each sortie by the conventional empirical models and based on the single-sortie approach.

The average power prediction errors range from 7.2 hp to 28 hp and are considered by the author unacceptable for the task of level flight power prediction. It is worth noting that for the specific type of helicopter tested, any power deviation above (or below) 4 hp from the expected value is clearly evident to the aircrew. The BO-105 helicopter (like many other types of helicopters) is not equipped with an instrument that explicitly presents the engines output power in hp units; however, it is equipped with a torque-meter gauge ('steam-gauge' style), installed on the instrument panel, that indicates both engines output shaft torques. The smallest detectable resolution of this gauge translates into a 4 hp quantity.

One might debate whether these samples of prediction errors presented in Fig. 6.2 were drawn from a normally distributed population. For this a Quantile-Quantile (QQ) plot is presented in Fig. 6.4. This plot compares the test data, the prediction errors samples in the case presented, to a theoretical sample drawn from a normally distributed population. A sample of data that comes from a normally distributed population would manifest itself as a straight line on the QQ plot. It is clear from Fig. 6.4 that all sampled prediction errors for sorties 1 through 4 do not come from a normally distributed population. Taking Sortie 1 as an example, the inflection of the curves might indicate that the largest (and smallest) estimate errors are not as extreme as would be expected in a normal distributed population. The QQ plots for Sortie 4 show a different behavior than those of Sortie 1. The curves inflect in a way that might indicate heavier tails of the Probability Density Function (PDF) as compared to a PDF of a normally distributed population. This means more extreme prediction errors are expected from both sides, under-estimation and over-estimation, compared to a normal distributed population.

The correlation between the power prediction level and the advance ratio was studied. For this, the correlation coefficient (r) between the prediction error and the advance ratio was calculated for each combination of sortie predicted and sortie used to base the empirical prediction model on. The correlation coefficient was calculated as per Eq.(6.9), where (n) represents the number of data points (sample size) and (S) stands for the standard deviation of the sample.

$$r_{Er,\mu} = \frac{\frac{1}{n-1}\sum_{i=1}^{n}\left(Er\cdot\mu\right)_i - n\cdot\overline{Er}\cdot\overline{\mu}}{S_{Er}S_{\mu}} \tag{6.9}$$

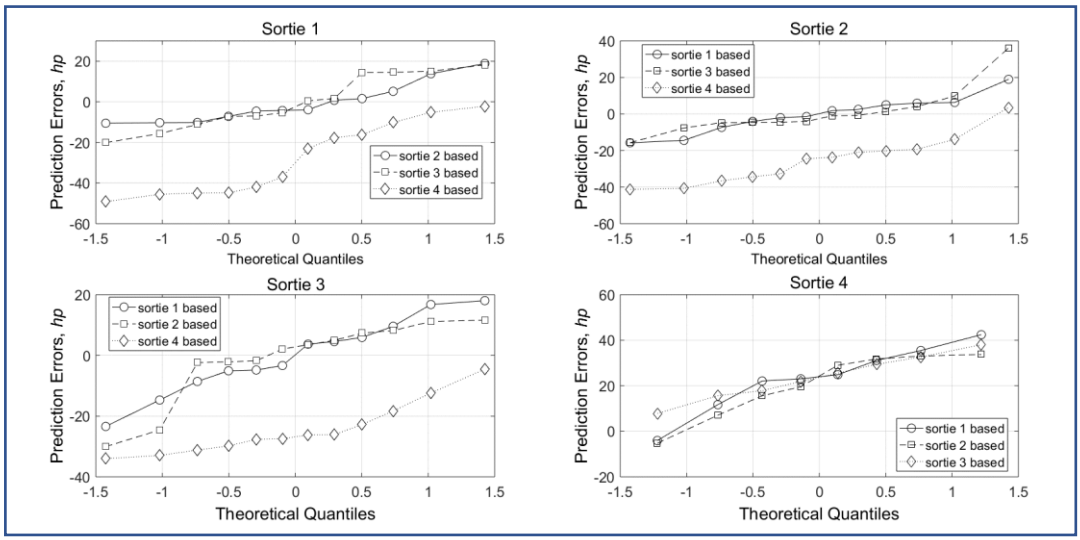

Figure 6.4. Prediction errors quantiles to theoretical normal quantiles ("QQ plot"). This figure shows the sampled prediction errors don't come from a normally distributed population.

Figure 6.5 presents these correlation coefficients for all four Sorties. Sorties 1,2 and 3 had twelve data points and Sortie 4 had only eight. The sample size affects the correlation coefficient value to be considered significant. At the accustomed 95% confidence level and for a sample size of twelve, a correlation coefficient of 0.58 (absolute value) and above indicates significant correlation between the two variables. For a smaller sample size of eight (Sortie 4), significant correlation between two variables (95% confidence level) is indicated by a correlation coefficient of 0.71 and above. Figure 6.5 clearly indicates a significant correlation between the power prediction errors and the advance ratio. The correlation value peaks when Sorties 1 and 2 are used to predict the power levels of sorties 3 and 4 (and vice versa). The conclusion taken from this correlation analysis is there might be one (or few) latent dimensions which is (are) missed by the conventional flight-test method. The empirical prediction models based on the conventional method fail to equally estimate power levels regardless of the advance ratio.

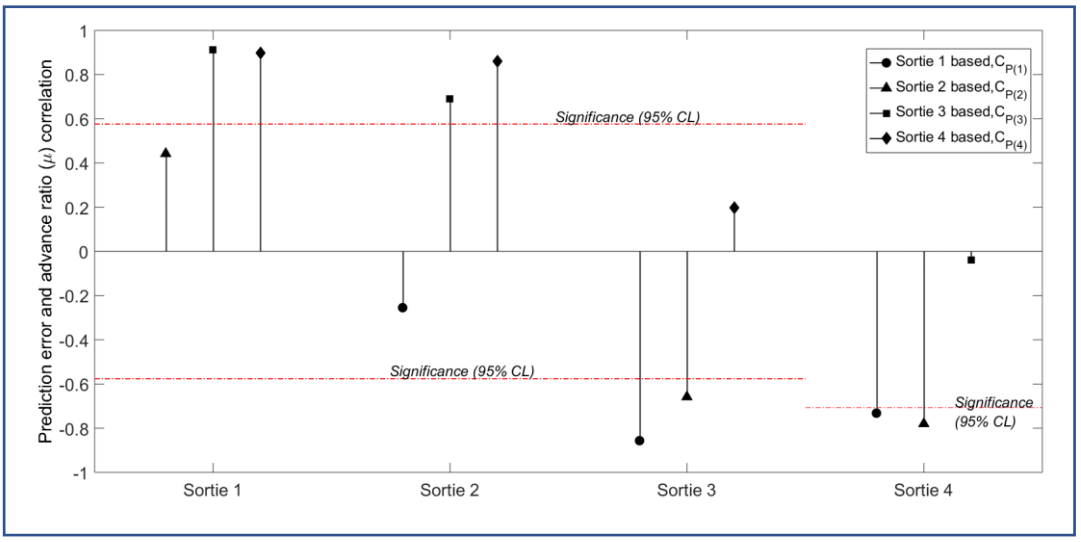

Figure 6.5. Power prediction errors to advance-ratio correlation (single-sortie approach). This figure shows a significant correlation between the prediction errors using the conventional method and the advance-ratio.

2) ***The cluster of sorties approach***: similarly to the single-sortie approach, four linear regressions were performed to retrieve four distinct third order polynomials to describe the non-dimensional level-flight performance of the BO-105 helicopter for the particular tested coefficient of-weight (Eq.(6.6)). The difference from the single-sortie approach is that data used for the regression was based on a conglomerate of three distinct sorties. Each one of these third order polynomials was used to predict the power required for level flight under the conditions of the fourth Sortie, the one not used for the linear regression. For example, data measured in Sorties 1, 2 and 3 was used to regress a third order polynomial which was used to predict the power required of Sortie 4. Power estimation from each third order polynomial were compared with the actual measured values and the estimation errors were calculated as per Eq.(6.7). Figure 6.6 presents a summary of all prediction errors retrieved for all four sorties. The prediction errors are presented in horse-power units and as a function of the corresponding advance-ratio.

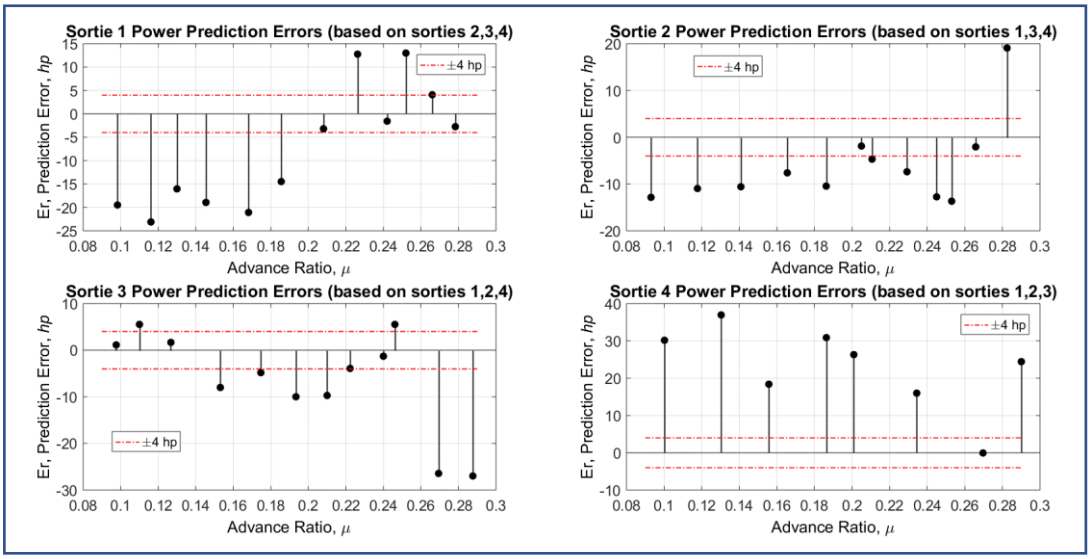

Figure 6.6. Power prediction errors of the BO-105 (cluster of sorties approach). This figure presents the level-flight power prediction errors yielded by the conventional power models, based on the cluster of sorties approach.

Subscribing to the cluster of sorties approach slightly improves the prediction performance. The power prediction errors of Sortie 1 ranged from -23 hp (overestimate) to 13 hp (underestimate). Using flight test data measured in Sorties 1,3 and 4 to predict power levels of Sortie 2 yielded prediction errors between -14 hp to 19 hp. The power predictions errors for Sortie 3 ranged between -27 hp to 5.5 hp and power predictions for Sortie 4 were all underestimating the true measured power by up to 37 hp. The four means of the absolute prediction errors for each sortie were calculated as per Eq.(6.8) and are presented in Fig. 6.7, alongside the absolute prediction errors yielded from the single-sortie approach (Fig. 6.3). The averaged absolute power prediction errors ranged between 8.8 hp to 22.9 hp (mean of 13.4 hp with a standard deviation of 6.5 hp).

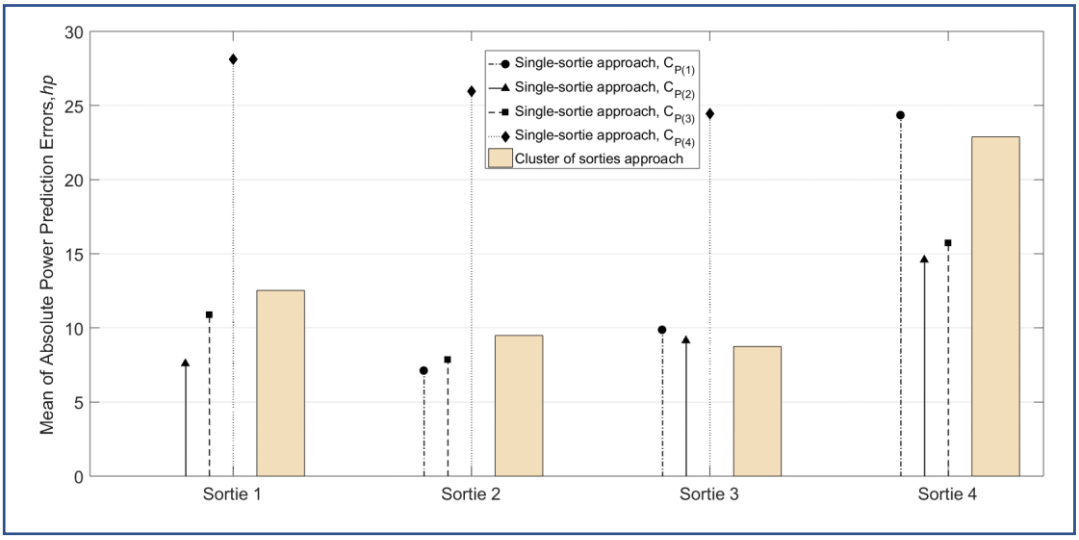

Figure 6.7. Mean of absolute prediction errors (single & cluster of sorties comparison). This figure presents a comparison between the power prediction errors yielded by the two approaches, the single-sortie and cluster of sorties.

Inferring from the specific averaged prediction errors presented in Fig. 6.7 to the general case is based on hypothesis-testing. The null-hypothesis assigned is that on-average the power required for level-flight, as predicted by the conventional flight-test method (using the cluster-of-sorties approach) and the empirical model obtained (Eq.(6.6)) does not differ from the true measured power by more than ±4 hp. This null hypothesis is tested against the alternative that on-average the power required for level-flight as estimated by the conventional method differ from the actual power by more than 4 hp (absolute value). The motivation for setting 4 hp as the threshold for the null-hypothesis is derived from the reasoning that for the BO-105 helicopter any power deviation above (or below) 4 hp is noticeable to the aircrew. As previously explained in this Subsection, the amount of power produced by the engines is (implicitly) presented to the aircrew by the engines torques meter gauge. The smallest detectable resolution of this gauge translates into a 4 hp quantity.

The relevant test-statistic for this hypothesis-testing is calculated per Eq.(6.10) for which the symbol 'n' represents the number of sorties and 'S' stands for the standard

deviation of the averaged power prediction errors that were calculated per Eq.(6.8) and presented in Fig. 6.7.

$$t = \frac{\left|\bar{E}_r\right| - \eta_0}{S/\sqrt{n}} \quad , \; \eta_0 = 4hp \tag{6.10}$$

The calculated value for the test-statistic was 2.89. Inferential statistical analysis shows the probability for making a Type-I error by rejecting the null-hypothesis to be small (3%). This small probability for a Type-I error fall below the 5% significance level accustomed in helicopter performance flight-testing. The practicality of this test is that there is sufficient statistical evidence to reject the null hypothesis and to adopt the alternative hypothesis instead. There is practically no statistical evidence to support the null-hypothesis assigned. Complementary statistical analysis shows that on-average and at the 95% confidence level, the level-flight power predictions based on the current method and Eq. (6) deviate by ±5.8 hp from the actual measured power.

The poor power-prediction performance of the current flight-test method is to be expected. As discussed above, the current level-flight performance method assumes that for a constant coefficient-of-weight the coefficient-of-power is solely dependent on the advance ratio, regardless of any compressibility effects that might be present. Based on data and analysis presented above, this is clearly not a sound assumption to make. Another potential contributor to the unsatisfactory power prediction might be related to the change of the longitudinal center-of-gravity. As mentioned in the introduction to this chapter, a longitudinal migration in the center-of-gravity should have an effect on the total drag area of the fuselage, hence affecting the power required for level flight.

The next section of the chapter presents an alternative flight test method for level-flight performance with an improved prediction accuracy, as compared to the conventional method. This method is based on the SVD concept, first introduced in Section 4.4 for empirical model screening in available power testing. This SVD approach was then reused in Chapter 5, for the novel CVSDR hover performance

flight-testing. The following section continues this course of research with the presentation of the CVSDR method for level flight performance, which can be regarded abstractly as a rigorous expansion of hover CVSDR method into a higher dimensional space.

6.4 THE CVSDR METHOD FOR LEVEL-FLIGHT PERFORMANCE TESTING

The CVSDR method for level-flight performance aims to rectify all identified drawbacks of the existing method, while providing better prediction accuracy as compared to the conventional method. The CVSDR method is implemented in three phases. Employment of this method by flight-testers requires recitation of only the last two phases since the first phase is generic to all conventional helicopters. Phase one deals with the generation of an original list of CVs for a multivariable analysis. In Phase two this list of corrected variables is refined based on concepts of dimensionality reduction through SVD. Phase three of the proposed method focuses on finding an empirical multivariable model using the bare-essential CVs ('predictors') identified in Phase 2. This list of CVs serves as an orthogonal base for the specific helicopter level-flight performance. The complete CVSDR method is demonstrated using the same BO-105 helicopter flight-test data, already presented in Section 6.3. Using the same flight-test data allows for a genuine comparison of the prediction accuracy achieved from each one of the two methods, the conventional and the CVSDR.

A practical and convenient summary of the method is presented in the next section of the chapter (Section 6.5). This summary is intended to serve as a guide for the flight-tester who wishes to evaluate the power required for level flight of a conventional helicopter using the CVSDR method. This Summary provides brief directions with regards to level-flight data base establishment and analysis.

The helicopter spends most of its flying-time in the level flight regime. The relative time while cruising varies based upon the type and the specific mission the helicopter was designed-for. Porterfield and Alexander [44] analysed data from various

6.4.1 Phase One – Original list of corrected variables for level flight performance

The physical problem of the power required to sustain a helicopter in level-flight (out-of-ground effect) was re-evaluated using tools of dimensional analysis [66, 67, and 73]. The procedure starts by proposing variables that are expected to affect the power required in level-flight. These are the ambient static pressure (Pa), the ambient static temperature (Ta), the helicopter gross-weight (W), the true airspeed the helicopter flies at (V_T), the main-rotor disk area (A_d), the main rotor angular speed (ω), and the longitudinal location of the center-of-gravity, Xcg. The power required to hover, P, can be represented mathematically as Eq.(6.11) and Eq.(6.12) in implicit form.

$$P = f(P_a, T_a, W, V_T, A_d, \omega, x_{cg}) \tag{6.11}$$

$$\hat{f}(P, P_a, T_a, W, V_T, A_d, \omega, x_{cg}) = 0 \tag{6.12}$$

The dimensions involved are presented in Table 6.2. 'M' represents mass, 'L' represents length and 'T' represents time.

Table 6.2. Variables and dimensions involved in level-flight performance. This table presents all major variables affecting the level-flight performance problem and associated dimensions.

#	Physical Variable	Notation	Dimension
1	Power Required for Level-Flight	P	$[M][L]^2[T]^{-3}$
2	Ambient static Pressure	P_a	$[M][L]^{-1}[T]^{-2}$
3	Ambient static Temperature	T_a	$[L]^2[T]^{-2}$
4	Helicopter Gross-Weight	W	$[M][L][T]^{-2}$
5	True Airspeed	V_T	$[L][T]^{-1}$
6	Main-Rotor Disk Area	A_d	$[L]^2$
7	Main-Rotor Angular speed	ω	$[T]^{-1}$
8	Longitudinal Center-of-Gravity	Xcg	[L]

The physical problem of power required for level flight involves eight variables with three dimensions (L,M,T). According to the Buckingham Pi-Theorem [66] the complexity of the problem can be reduced from eight dimensional variables to only five Non-Dimensional (ND) variables. Following the methodology presented by Buckingham [20], these 5 ND variables (denoted by ψ) are formed as products of the dimensional variables. Since there are eight dimensional variables to construct five ND variables, three dimensional variables were used as repeating variables in the ND products (ψ). There are 56 different options to choose three variables out of eight for the case where the order does not matter (combinations). This requires a fairly tedious task of screening between 56 different options in order to identify the best way of describing the non-dimensional level-flight performance. The following is a demonstration of only one combination out of the 56 options available. In this particular demonstration, the three repeating variables are the ambient static temperature (Ta), the helicopter gross-weight (W) and the main rotor disk area (Ad). The five ND products (ψ) are defined in Eq.(6.13). According to Buckingham [66], the repeating variables should be raised to some arbitrary powers, those are denoted as $a_1,b_1,c_1,\ldots,c_5$ in Eq.(6.13). As demonstrated hereinafter, these arbitrary powers are identified as those numeric values that make the ψ products non-dimensional.

$$\left\{\begin{array}{l}\psi_i=(T_a)^{a_1}(W)^{b_1}(A_d)^{c_1}(P)\\ \psi_j=(T_a)^{a_2}(W)^{b_2}(A_d)^{c_2}(P_a)\\ \psi_k=(T_a)^{a_3}(W)^{b_3}(A_d)^{c_3}(\omega)\\ \psi_m=(T_a)^{a_4}(W)^{b_4}(A_d)^{c_4}(V_T)\\ \psi_n=(T_a)^{a_5}(W)^{b_5}(A_d)^{c_5}(x_{cg})\end{array}\right\} \tag{6.13}$$

Next, the procedure requires to replace each one of the dimensional-variables with their corresponding dimensions and to enforce each one of the five ψ products to be non-dimensional. This process is demonstrated as per Eq.(6.14). Each one of the ψ products yields three equations with three unknowns, which are the exponents. Solving for the exponents of ψi is demonstrated in Eq.(6.15). The same process is then repeated for each one of the other ND variables, ψ_j , ψ_k , ψ_m and ψ_n.

$$\left\{\begin{array}{l}[\psi_i]=\left[\frac{L^2}{T^2}\right]^{a_1}\left[\frac{ML}{T^2}\right]^{b_1}\left[L^2\right]^{c_1}\left[\frac{ML^2}{T^3}\right]=M^{b_1+1}L^{2a_1+b_1+2c_1+2}\ T^{-2a_1-2b_1-3}\equiv M^0L^0T^0\\ [\psi_j]=\left[\frac{L^2}{T^2}\right]^{a_2}\left[\frac{ML}{T^2}\right]^{b_2}\left[L^2\right]^{c_2}\left[\frac{M}{LT^2}\right]=M^{b_2+1}L^{2a_2+b_2+2c_2-1}\ T^{-2a_2-2b_2-2}\equiv M^0L^0T^0\\ [\psi_k]=\left[\frac{L^2}{T^2}\right]^{a_3}\left[\frac{ML}{T^2}\right]^{b_3}\left[L^2\right]^{c_3}\left[\frac{1}{T}\right]=M^{b_3}L^{2a_3+b_3+2c_3}\ T^{-2a_3-2b_3-1}\equiv M^0L^0T^0\\ [\psi_m]=\left[\frac{L^2}{T^2}\right]^{a_4}\left[\frac{ML}{T^2}\right]^{b_4}\left[L^2\right]^{c_4}\left[\frac{L}{T}\right]=M^{b_4}L^{2a_4+b_4+2c_4+1}\ T^{-2a_4-2b_4-1}\equiv M^0L^0T^0\\ [\psi_n]=\left[\frac{L^2}{T^2}\right]^{a_5}\left[\frac{ML}{T^2}\right]^{b_5}\left[L^2\right]^{c_5}[L]=M^{b_5}L^{2a_5+b_5+2c_5+1}\ T^{-2a_5-2b_5}\equiv M^0L^0T^0\end{array}\right\} \tag{6.14}$$

$$\left\{\begin{array}{l}[M]: b_1+1=0\\ [L]: 2a_1+b_1+2c_1+2=0\\ [T]: -2a_1-2b_1-3=0\end{array}\right\} \Rightarrow \begin{bmatrix}0 & 1 & 0\\ 2 & 1 & 2\\ -2 & -2 & 0\end{bmatrix}\begin{Bmatrix}a_1\\ b_1\\ c_1\end{Bmatrix}=\begin{Bmatrix}-1\\ -2\\ 3\end{Bmatrix} \Rightarrow \begin{Bmatrix}a_1\\ b_1\\ c_1\end{Bmatrix}=\begin{Bmatrix}-1/2\\ -1\\ 0\end{Bmatrix} \tag{6.15}$$

Based on Eq.(6.15), the first ND variable (ψ_i) can be written as Eq.(6.16).

$$\psi_i = \frac{P}{W\sqrt{T_a}} \tag{6.16}$$

This ND variable (Eq.(6.16)) can be further simplified once the ambient static temperature is represented using its relative value (Eq.(6.17)). This gives a simplified expression for ψi (Eq.(6.18)) denoted as ψi*. Since this term indeed carries dimensions and is not a pure ND, it is better defined as a 'corrected' variable (CV).

$$P_a = P_0 \cdot \delta \ , \ T_a = T_0 \cdot \theta \tag{6.17}$$

$$\psi_i = \frac{P}{W\sqrt{T_a}} = \frac{P}{W\sqrt{T_0\theta}} = \frac{1}{\sqrt{T_0}} \cdot \frac{P}{W\sqrt{\theta}} = Const \cdot \frac{P}{W\sqrt{\theta}} \Rightarrow$$
$$\psi_i^* = \frac{P}{W\sqrt{\theta}} \tag{6.18}$$

A similar analysis was conducted to reveal the other four ND variables (ψj, ψ_k, ψ_m and ψ_n). These ND variables were further simplified to represent non-dimensional variables of a particular helicopter, hence referred-to as corrected-variables (CVs). The corresponding CV's are denoted with an asterisk and presented as Eq.(6.19).

$$\psi_j^* = \frac{W}{\delta},\ \psi_k^* = \frac{\omega}{\sqrt{\theta}},\ \psi_m^* = \frac{V_T}{\sqrt{\theta}},\ \psi_n^* = \frac{X_{cg}}{R} \tag{6.19}$$

The procedure demonstrated above was repeated for all other 55 possibilities of choosing three variables out of eight. From all 56 options evaluated, 20 did not yield a unique solution and a few other returned repeating ND variables. Overall, the analysis yielded 36 distinct CVs which can be used for the helicopter level-flight performance. Table 6.3 summarizes all 36 CVs in an array form to indicate which of the five dimensional-variables (power, weight, true airspeed, main-rotor angular speed and\or longitudinal center-of-gravity location) are used in the specific CV. This list of CVs is also presented graphically in Fig. 6.8, where one can clearly observe the number

of dimensional-variables involved in each CV. There are 6 CVs which are based on only one dimensional-variable (1-D), 16 CVs that include two dimensional-variables (2-D), 13 CVs which employ three dimensional-variables (3-D) and only one CV (ψ_{36}*) which involves four dimensional-variables (4-D). Note this ψ_{36}* was omitted from Table 6.3 for reasons of formatting efficiency and is presented as Eq.(6.20)

Table 6.3. Corrected-Variables (CVs) for level-flight performance.

	Power based	***M/R angular-speed based***	***Weight based***	***Airspeed based***	***C.G. based***	***3-D variables***
Power based	$\psi_1^* = \frac{P}{\delta\sqrt{\theta}}$	$\psi_4^* = \frac{P}{\delta\omega}$ $\psi_7^* = \frac{P\omega^2}{\delta\sqrt{\theta^3}}$ $\psi_{20}^* = \frac{P}{\sqrt{\delta\omega}}$ $\psi_{21}^* = \frac{P}{\omega^2\delta\sqrt{\theta^3}}$ $\psi_{24}^* = \frac{1}{\theta}\sqrt[3]{\left(\frac{P\omega^2}{\delta}\right)^2}$	$\psi_5^* = \frac{P}{W\sqrt{\theta}}$ $\psi_{12}^* = \frac{P}{W}$	$\psi_{11}^* = \frac{P}{\delta V_T}$	$\psi_{22}^* = \frac{P}{X_{cg}^2\delta\sqrt{\theta^3}}$ $\psi_{23}^* = \frac{P}{X_{cg}^2\delta\sqrt{\theta}}$	$\psi_6^* = \frac{P}{\omega W}$ $\psi_9^* = \frac{P\sqrt{\delta}}{\omega\sqrt{W^3}}$ $\psi_{25}^* = \frac{P}{WV_T}$ $\psi_{26}^* = \frac{P\cdot\delta}{\omega\sqrt{W^3}}$ $\psi_{27}^* = \frac{V_T\sqrt{\delta}}{\omega\sqrt{W}}$ $\psi_{28}^* = \frac{V_T\omega\sqrt{W}}{\sqrt{\delta}}$ $\psi_{29}^* = \frac{P\omega}{\sqrt{\delta V_T^3}}$ $\psi_{30}^* = \frac{P\omega^2}{\delta V_T^3}$
M/R angular-speed based		$\psi_3^* = \frac{\omega}{\sqrt{\theta}}$ $\psi_{14}^* = \omega^2\sqrt{\theta}$	$\psi_8^* = \frac{W\omega^2}{\delta\theta}$	$\psi_{13}^* = \frac{V_T}{\omega}$	$\psi_{16}^* = \frac{X_{cg}}{\omega\sqrt{\theta}}$ $\psi_{17}^* = \frac{X_{cg}\omega}{\sqrt{\theta}}$	
Weight based			$\psi_2^* = \frac{W}{\delta}$		$\psi_{18}^* = \frac{WX_{cg}^2}{\delta}$ $\psi_{19}^* = \frac{W}{\delta X_{cg}^2}$	$\psi_{31}^* = \frac{P}{\omega X_{cg}\theta}$ $\psi_{32}^* = \frac{P}{\omega X_{cg}^3\delta}$
Airspeed based				$\psi_{10}^* = \frac{V_T}{\sqrt{\theta}}$		$\psi_{33}^* = \frac{V_T}{\omega X_{cg}}$
C.G. based					$\psi_{15}^* = \frac{X_{cg}}{R}$	$\psi_{34}^* = \frac{P}{V_T X_{cg}^2\delta}$ $\psi_{35}^* = \frac{PV_T}{X_{cg}^2\delta}$

$$\psi_{36}^* = \frac{P}{W\omega X_{cg}} \tag{6.20}$$

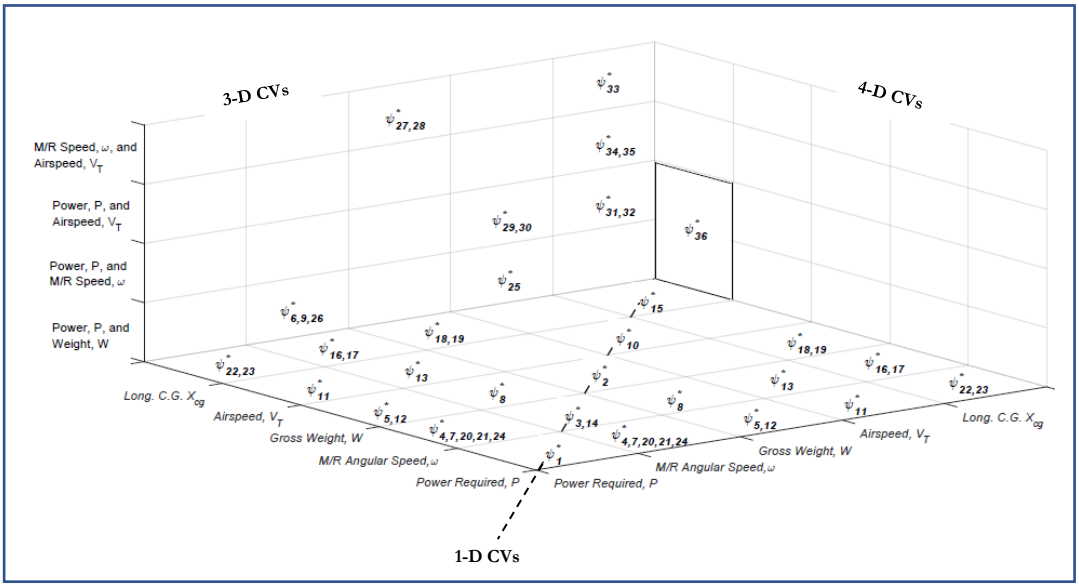

Figure 6.8. Graphical presentation of all 36 CVs for level-flight performance. This figure presents the classification of all determined level-flight performance CVs with their traced dimensionality.

6.4.2 Phase Two – Screening for essential CVs.

Phase Two of the CVSDR method, as already presented for the hover performance in Subsection 5.4.2, focuses on narrowing the list of all candidate CVs (Table 6.3 above) to select only those most essential and effective CVs for the specific helicopter level-flight performance data that is being analysed. A power-based corrected variable needs to be expressed as a function of few other CV's. For this, the flight tester might be asking the following two questions:

(1) How many CVs are required for a sufficient description of the level-flight performance?

(2) Which CVs should be used?

These questions are addressed in this phase of the CVSDR method. The procedure of CVs selection, both the quantity and types of CVs, is based on principals of dimensionality-reduction and the correlated mathematical procedure known as the Singular Value Decomposition (SVD). This phase of the method is demonstrated using the same MBB BO-105 level-flight test data presented and analysed in Subsection 6.3.3 above.

The SVD theorem is thoroughly discussed in Chapter 4 (Subsection 4.4.1), however its fundamentals are briefly reminded to the reader hereinafter. The SVD theorem states that any generic real matrix can be ***uniquely*** decomposed into a set of three matrices as given in Eq.(6.21). Consider a real matrix Z to be of size (m,n) and rank 'r'. This matrix Z can be expressed as a product of the following three ***unique*** matrices: matrix U, an orthonormal matrix of size (m,r) called the "Left-Singular-Vectors" (LSV); matrix Σ, a diagonal matrix which holds along its diagonal the singular-values of Z; and matrix V, an orthonormal matrix of size (n,r) called the "Right-Singular-Vectors" (RSV). From an algebraic point of view, this decomposition is viewed as a convenient way to reveal an orthogonal bases for the column and row spaces of matrix Z (given by matrix U and V^T accordingly).

$$Z = U\Sigma V^T = \begin{bmatrix} u_{1,1} & u_{1,2} & \cdot & u_{1,n} \\ u_{2,1} & u_{2,2} & \cdot & u_{2,n} \\ \cdot & \cdot & \cdot & \cdot \\ \cdot & \cdot & \cdot & \cdot \\ u_{m,1} & u_{m,2} & \cdot & u_{m,n} \end{bmatrix} \begin{bmatrix} \sigma_1 & & & \\ & \sigma_2 & & \\ & & \cdot & \\ & & & \sigma_r \end{bmatrix} \begin{bmatrix} v_{1,1} & v_{2,1} & \cdot & v_{n,1} \\ v_{1,2} & v_{2,2} & \cdot & v_{n,2} \\ \cdot & \cdot & \cdot & \cdot \\ v_{1,r} & v_{2,r} & \cdot & v_{n,r} \end{bmatrix} \tag{6.21}$$

$$\sigma_1 > \sigma_2 > \ldots > \sigma_r \geq 0$$

Alternatively, the SVD decomposition can be regarded as a 'spectral' decomposition of any arbitrary real matrix Z. A generic real matrix Z of rank 'r' can be expressed as a linear combination of 'r' rank-one matrices (Eq.(6.22)).

$$Z = \sigma_1 \begin{bmatrix} u_{1,1} \\ u_{2,1} \\ \cdot \\ \cdot \\ u_{m,1} \end{bmatrix} \begin{bmatrix} v_{1,1} & v_{2,1} & \cdot & v_{n,1} \end{bmatrix} + \sigma_2 \begin{bmatrix} u_{1,2} \\ u_{2,2} \\ \cdot \\ \cdot \\ u_{m,2} \end{bmatrix} \begin{bmatrix} v_{1,2} & v_{2,2} & \cdot & v_{n,2} \end{bmatrix} + \ldots$$
$$\ldots + \sigma_r \begin{bmatrix} u_{1,n} \\ u_{2,n} \\ \cdot \\ \cdot \\ u_{m,n} \end{bmatrix} \begin{bmatrix} v_{1,r} & v_{2,r} & \cdot & v_{n,r} \end{bmatrix} \tag{6.22}$$

The practicality of this approach is that any real matrix Z can be approximated as a lower ranked matrix by using only parts of its rows and columns basis. The 'closeness' between the original matrix and the approximated one can be assessed by comparing the ***norm*** of the two. There is more than one way to measure the 'magnitude' of a matrix (various norms). The preferable norm for the proposed CVSDR method is the Frobenius-norm [106]. This norm is defined as the square root of the sum of all squares of the elements of the matrix. This norm can be expressed, with few simple algebraic passages, as the square root of the sum of all singular-values squares (Eq.(6.23)).

$$\|Z\|_F \equiv \sum_{i=1}^{m} \sum_{j=1}^{n} \sqrt{\left(z_{i,j}\right)^2} = \sqrt{\sigma_1^2 + \sigma_2^2 + \ldots + \sigma_r^2} \tag{6.23}$$

The ability to approximate any arbitrary real matrix of rank 'r' by an increasing sum of rank-one matrices is the essence of the dimensionality reduction concept. Reducing the long list of 36 corrected variables (Table 6.3 and Eq.(6.20)) to a short and practical list of effective CVs for the level-flight performance is precisely based on this concept of dimensionality reduction.

The procedure starts with filling matrix Z with numeral entries of all 36 CV's as measured for the BO-105 level-flight sorties and already presented in Subsection 6.3.3. For this demonstration 36 stabilized level-flight points measured in Sorties 1, 2 and 3 are used. The columns of the matrix represent the various CV's (ψ_1* to ψ_{36}*) and

the 36 rows represent the different test-points measured. Next is to normalize all columns of Z to have a mean of zero and a variance equals 1. This is done by normalizing each entry along the columns of Z by using Eq.(6.24).

$$\psi_i' = \frac{\psi_i^* - \overline{\psi_i^*}}{S_{\psi_i^*}} \quad ,i = 1,2,...,35,36 \tag{6.24}$$

Once matrix Z contains normalized columns it is defined as Z' and can be partitioned into the three unique matrices expressed by Eq.(6.21). The level-flight performance as appears in matrix Z' is represented by all 36 CVs (ψ_1^* to ψ_{36}^*). However, not all CV's possess the same significance in representing the variance captured in the flight-test data. The singular-values (σ_i) which appear along the main diagonal of matrix Σ in a descending order are key to understanding the level of importance each CV ('i') holds. The conceptual interpretation of the SVD of Z' for the specific problem of level-flight performance is illustrated in Fig. 6.9.

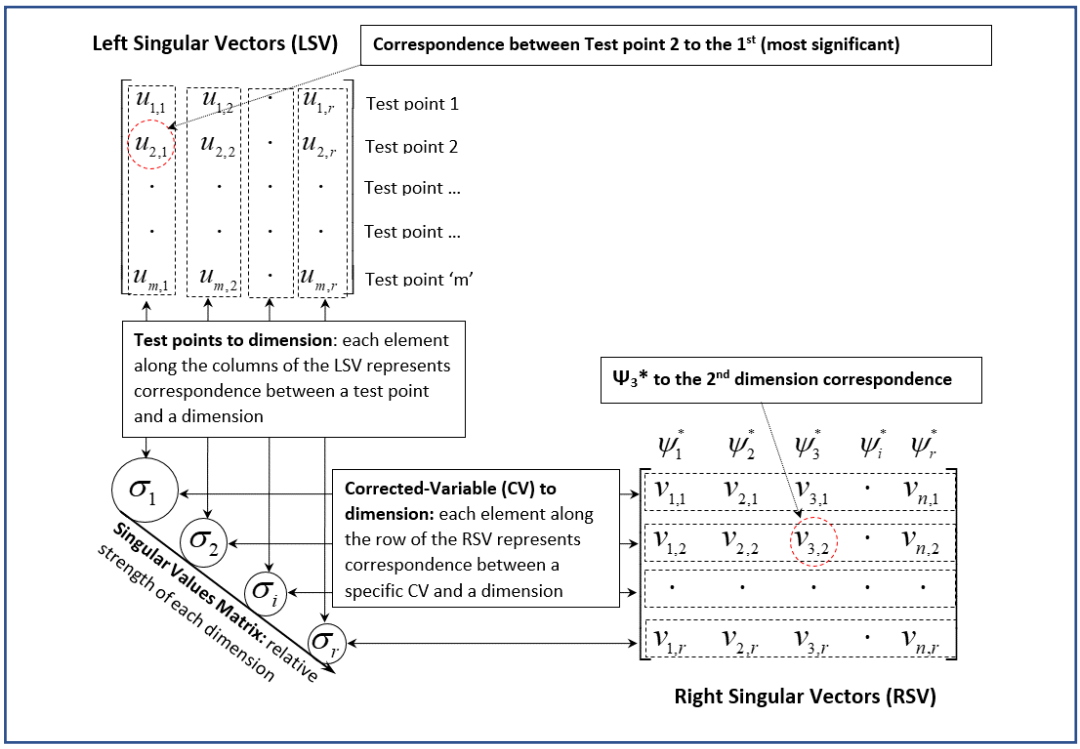

Figure 6.9. The conceptual interpretation of SVD of Z' in level-flight performance. This figure presents how the abstract SVD of matrix Z' (normalized predictors) should be interpreted.

The 36 singular-values of matrix Σ are normalized as per Eq.(6.25) and are presented in Fig. 6.10 alongside a cumulative-sum plot of all normalized singular-values.

$$\hat{\sigma}_i = \frac{\sigma_i}{\sum_{k=1}^{36}\sigma_k} \quad , \; i = 1, 2, \ldots, 35, 36 \tag{6.25}$$

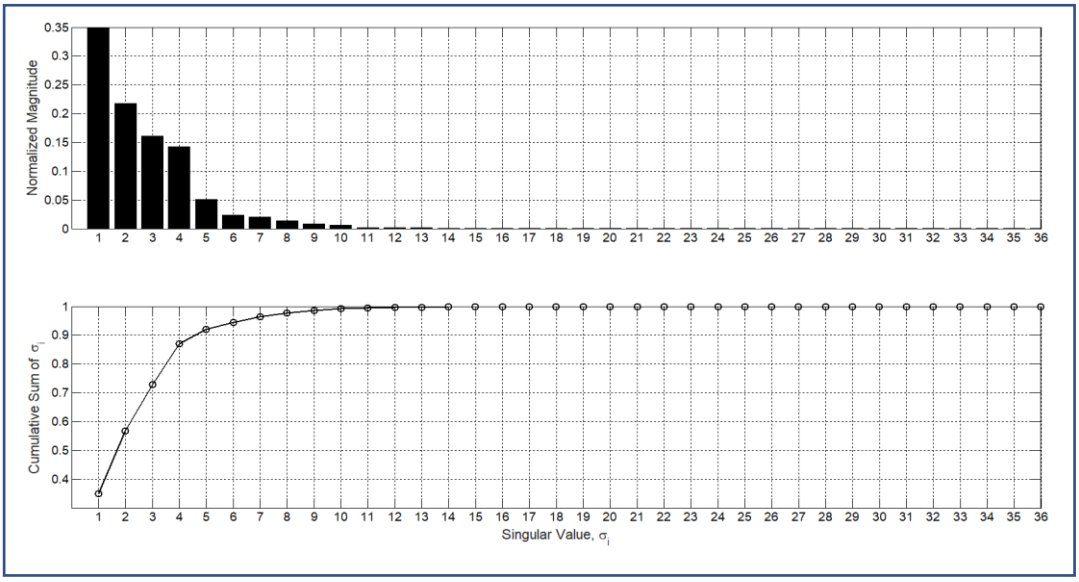

Figure 6.10. The normalized singular values of the level-flight performance. This figure represents the relative magnitude of all 36 dimensions involved in the level-flight performance of the BO-105 helicopter.

One should deduce from Fig. 6.10 that the dimensionality of the level-flight problem can be significantly reduced from a 36-dimension problem to only a 7-dimension one. In linear-algebraic terms, it can be stated that the level-flight performance can be sufficiently described by a basis of only seven orthogonal CVs. The cumulative sum plot presented in Fig. 6.10 shows that 96.7% of the total variance in the flight-test data, as stored in matrix Z, can be presented by using the seven most significant CVs. Also indicated by Fig. 6.10, the most significant dimension of the specific level-flight performance problem analysed holds 35% of the variance in the data. Comparing the Frobenius norm of matrix Z' and its 7th order approximation

(the combination of the first seven rank-1 matrices) reveals a practically similar norm of the two; 34.986 for Z' and 34.983 for its 7th order approximation.

The identity of the seven most important CVs is solely indicated by the right-singular-vector (RSV) matrix. As illustrated in Fig. 6.9, each row of the RSV indicates the level of correspondence to a specific singular-value, or a dimension, of the problem. For example, the first row of the RSV specifies the level of correspondence each one of the 36 CVs has with to first (and most significant) singular-value. The second row of the RSV indicates the correspondence between all 36 CVs to the second most significant dimension of the problem, and so on. Since the dimensionality of the problem is reduced from 36 to seven, it is required to evaluate only the first seven rows of the RSV matrix. For this, the elements along the first seven rows of the RSV matrix are normalized as per Eq.(6.26) and presented in Fig. 6.11. The significance of each CV towards the seven substantial dimensions of the level-flight performance is then concluded.

$$\hat{V}(i,j) = \frac{|V(i,j)|}{\sum_{j=1}^{36}|V(i,j)|} \ , \ i = 1,2,...,6,7 \tag{6.26}$$

The left singular vectors (LSV) matrix has no significant role in the type of analysis addressed in this paper since it only indicates the "level of correspondence" between each one of the level-flight test points and the singular-values of Z. This type of correspondence between particular test-points and the various dimensions of the level-flight performance was deemed irrelevant to the topic analysed.

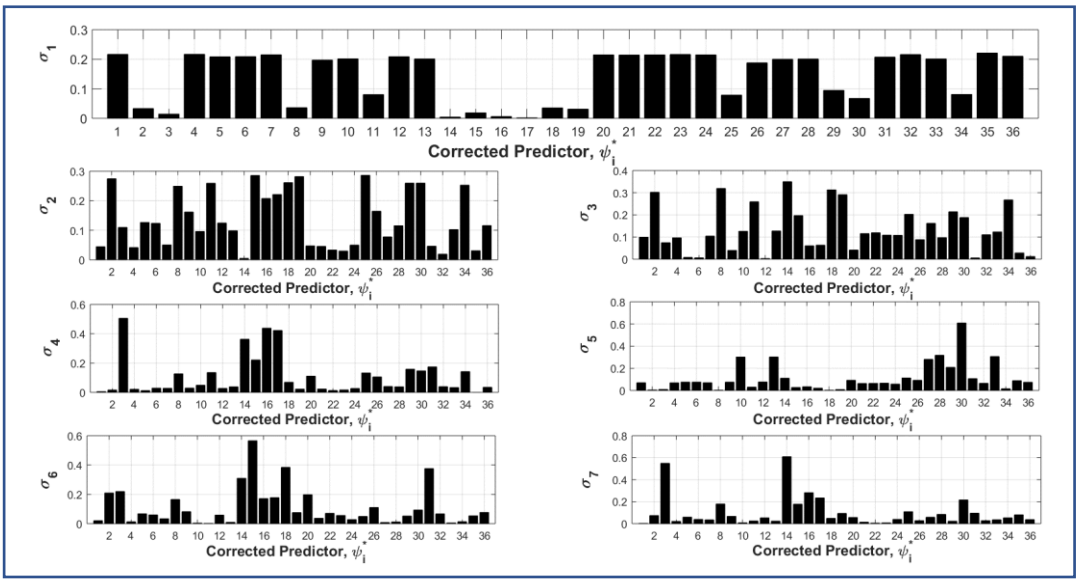

Figure 6.11. Correspondence between CVs and level-flight dimensions. This figure represents the relative correspondence between each CV and each one of the 36 dimensions of the specific BO-105 level flight performance (rows of the RSV).

The following conclusions can be drawn from Fig. 6.10 and 6.11:

(1) The first and most significant dimension of the level-flight performance analysed holds for 35% of variance in the data and is best represented by ψ_1^*. This CV represents variance in power.

(2) The second most significant dimension of the level-flight performance analysed holds for 21.7% of variance in the data and is best represented by ψ_2^*. This CV represents the variance in gross weight of the helicopter.

(3) The third dimension of the level-flight performance analysed holds for 16.1% of variance in the data and is best described by ψ_{14}^*.

(4) The fourth dimension of the problem holds for 14.3% of variance in the data and is best represented by ψ_3^*.

(5) The fifth dimension of the problem holds for 5.1% of variance in the data and is best represented by ψ_{30}*. This ψ_{30}* involves power and since the first dimension already yielded a power-based CV for the role of an independent CV for the physical problem in-hand this CV was renounced. Next in-line (non-power related) to best represent the fifth dimension were the two CVs ψ_{10}* and ψ_{13}* which could not be differentiated with respect to their representation of the fifth dimension.

(6) The sixth dimension of the problem holds for 2.3% of variance in the data and is best represented by ψ_{15}*.

(7) the least significant dimension in the truncated list of seven dimensions holds for only 2% of variance in the data and is best represented by the same CV selected to represent the third dimension, which is ψ_{14}*.

Finally for Phase Two, a conceptual empirical-model to represent the level-flight performance of the MBB BO-105 helicopter, as resulted from the CVSDR method, can be stated as Eq.(6.27). This relation involves six independent corrected variables (CVs) and one power-based dependent CV.

$$\psi_1^* = f(\psi_2^*, \psi_{14}^*, \psi_3^*, \psi_{10}^*, \psi_{13}^*, \psi_{15}^*) \therefore \frac{P}{\delta\sqrt{\theta}} = f\left(\frac{W}{\delta}, \omega^2\sqrt{\theta}, \frac{\omega}{\sqrt{\theta}}, \frac{V_T}{\sqrt{\theta}}, \frac{V_T}{\omega}, \frac{X_{cg}}{R}\right) \quad (6.27)$$

6.4.3 Phase Three – Deriving a practical empirical model

Once the most influential CVs of the level-flight performance problem are exposed, a practical empirical polynomial in the six independent CVs is pursued. The physical nature of the problem (Eq.(6.1)) suggests a third order as the highest degree to represent the power in level-flight. This puts a cap on the order of the empirical polynomials to be explored. As a guideline for simplicity the prospective polynomial needs to refrain from employing any cross-products of CVs as regressors. Numerous configurations involving the six independent CVs were evaluated for their power

estimation accuracy using the 36 stabilized data points from the first three sorties specified in Table 6.1. The particular polynomial presented as Eq.(28, 29) was selected due to its best performance in representing the power measurements in the first three sorties, i.e., yielding the least values for the mean and the variance of the estimation errors. This empirical model is addressed hereinafter as Model 123 (denoted M123) since it is based on flight-test data from sorties 1, 2 and 3.

$$\begin{aligned}\frac{P}{\delta\sqrt{\theta}} &= \gamma_{1_{M123}}\left(\frac{W}{\delta}\right)+\gamma_{2_{M123}}\left(\frac{W}{\delta}\right)^2+\gamma_{3_{M123}}\left(\omega^2\sqrt{\theta}\right)+\gamma_{4_{M123}}\left(\frac{\omega}{\sqrt{\theta}}\right)+\ldots \\ &\ldots+\gamma_{5_{M123}}\left(\frac{V_T}{\sqrt{\theta}}\right)+\gamma_{6_{M123}}\left(\frac{V_T}{\sqrt{\theta}}\right)^2+\gamma_{7_{M123}}\left(\frac{V_T}{\sqrt{\theta}}\right)^3+\gamma_{8_{M123}}\left(\frac{V_T}{\omega}\right)+\ldots \\ &\ldots+\gamma_{9_{M123}}\left(\frac{V_T}{\omega}\right)^2+\gamma_{10_{M123}}\left(\frac{V_T}{\omega}\right)^3+\gamma_{11_{M123}}\left(\frac{X_{cg}}{R}\right)+\gamma_{12_{M123}}\end{aligned} \tag{6.28}$$

$$\begin{Bmatrix}\gamma_{1_{M123}}\\ \gamma_{2_{M123}}\\ \gamma_{3_{M123}}\\ \gamma_{4_{M123}}\\ \gamma_{5_{M123}}\\ \gamma_{6_{M123}}\\ \gamma_{7_{M123}}\\ \gamma_{8_{M123}}\\ \gamma_{9_{M123}}\\ \gamma_{10_{M123}}\\ \gamma_{11_{M123}}\\ \gamma_{12_{M123}}\end{Bmatrix} = \begin{Bmatrix}-6.679\\ 5.85\times10^{-4}\\ -19.475\\ -1019.915\\ 418.52\\ -2.989\\ 8.31\times10^{-3}\\ -19336.47\\ 6189.634\\ -742.462\\ 116.372\\ 102479\end{Bmatrix} \therefore \quad \textbf{M123} \tag{6.29}$$

6.5 PRACTICAL GUIDANCE FOR THE CVSDR METHOD IN LEVEL-FLIGHT

A performance flight-test campaign starts with a careful planning of the required sorties. The power required for level flight using CVSDR is no exception to this rule. The flight tester should plan for a set of level-flight 'speed runs' to cover the applicable and required flight envelope. With the aim of establishing a sound data base to be analysed, the flight tester should gather level-flight performance that covers the entire range of airspeed (V_T), gross-weight (W), center of gravity (Xcg), main-rotor angular speed (ω), and ambient air properties of pressure and temperature. Figure 6.12 provides a methodical approach for sorties planning and execution while using the CVSDR method. The flight test campaign should be executed in three configuration-based stages. Each stage includes a set of various 'speed-runs' (denoted as the numbers 1 to 9 in Fig. 6.12) conducted at various conditions of gross weight, altitude and main-rotor angular speed. Every single 'speed-run' should be conducted from the lowest practicable airspeed (hover if possible) to the highest attainable level flight airspeed, with about eight different intermediate airspeeds.

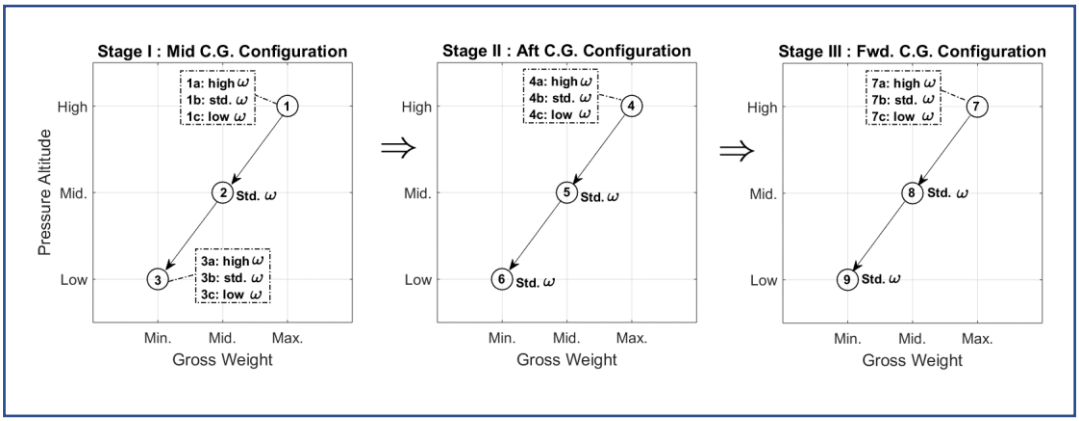

Figure 6.12. CVSDR level flight performance testing- Sorties planning sequence. This figure represents three configuration based stages for planning and execution of level-flight performance testing, based on the CVSDR method.

At each stabilized airspeed point, the flight-tester should gather all data needed to compute the CVs presented in Table 6.3 and Eq.(6.20). The flight-test campaign starts with a middle center of gravity (c.g.) configuration (the left chart in Fig. 6.12), followed by an aft c.g. configuration (the middle chart in Fig. 6.12) and end with a forward c.g. configuration. The first sets of speed-runs should be conducted at high altitude and high gross weight, this would extend the range of many weight-based CVs. For helicopters that allow the crew to adjust the main-rotor speed under standard procedures, few sets of speed runs shall be repeated three times for three distinct values of main rotor speed that span the governed range (see example denoted as 1a, 1b and 1c in Fig. 6.12). Note that by following the directions of Fig. 6.12 closely, the flight-test team are expected to acquire a data base of 17 distinct speed runs, totalling about 136 stabilized level flight data points. This would constitute a sound data base to be analysed. Succeeding the establishment of this data base, the flight test data analysis should be conducted by following the sequential eight steps of Table 6.4. This table is intended to provide a practical, step-by-step guidance, to realize the three phases of the CVSDR method as discussed in Subsections 6.4.1, 6.4.2 and 6.4.3 above.

Table 6.4. A step-by-step guidance for CVSDR level-flight performance testing.

Step	Task Description & Instruction
Phase One – Establish an applicable list of CVs to represent the level-flight performance. This phase is described in Subsection 6.4.1.	
1	Compute all 36 CVs (Table 6.3) for each stabilized level-flight data point measured. There should be 136 stabilized data points, If all sorties of Fig. 6.12 are exactly executed.
2	Arrange the computed CVs in a matrix form (this is matrix Z). The rows of Z should represent the different data points and columns of Z should represent the various CVs. If all sorties of Fig. 6.12 were closely executed, matrix Z should be of size 136x36.
Phase Two – Screening for the most effective CVs using dimensionality reduction. This phase is described in Subsection 6.4.2.	
3	Normalize all columns of matrix Z as per Eq.(6.24) to have a zero mean and a variance equals 1.
4	Decompose the ***normalized*** matrix Z into its three unique matrices (U,Σ and V) using a Singular Value Decomposition (SVD) algorithm. Matrix U is also referred to as the Left Singular Vectors (LSV), matrix Σ is called the singular values and matrix V is called the Right Singular Vectors (RSV).
5	Normalize all singular values (entries along the main diagonal of matrix Σ) as per Eq.(6.25). The normalized values represent the relative strength of the various dimensions exist in the data. Determine the number of ***significant*** dimensions involved in the specific level-flight performance data, based on the cumulative sum of the normalized singular values (as presented in Fig.6.10).
6	Normalize the rows of matrix V^T (RSV) as per Eq.(6.26). This normalization calls for the absolute value of each element along the rows of RSV to be divided by the sum of all elements absolute values along the corresponding row of RSV.
7	Identify the most significant CVs of the specific level-flight performance analysed. The level of correspondence between each CV and an abstract dimension of the level-flight problem is illustrated in Fig. 6.9. Note that only the first significant rows of the normalized RSV should be evaluated. The number of significant rows of RSV equals the number of significant dimensions retrieved in sequential step 5 above. Example for this step is presented in Fig.6.11.
Phase Three – Forming a practical empirical model (Subsection 6.4.3)	
8	Use the most significant CVs identified in sequential step 7 to form a practical polynomial that uses the relevant CVs as regressors in this empirical model.

6.6 THE CVSDR MODEL PREDICTION ACCURACY (LEVEL-FLIGHT)

The prediction accuracy achieved using the CVSDR method is evaluated hereinafter in a build-up manner. First, it is evaluated against the conventional flight-test method by using the flight test data from sorties 1 through 4, all conducted at the same targeted coefficient of weight. Next, the CVSDR method is challenged to predict level flight performance of a new sortie (Sortie 5), which was conducted under arbitrary and varying coefficient-of-weights (Cw). This evaluation is performed only for the purpose of challenging the CVSDR-based empirical model, and to experiment up to what extent it can predict (extrapolate) the level flight performance of the same helicopter but under arbitrary conditions. Note the empirical models retrieved using the conventional method in Section 6.3 (Eq. (6.6)) are irrelevant for the prediction of Sortie 5. These empirical models are representing the level flight performance of the helicopter for a single and specific coefficient of weight (Cw), the one targeted in Sorties 1 through 4. For Sortie 5, the comparison between the conventional and CVSDR methods is trivial since the conventional method immediately fails.

6.6.1 Prediction Accuracy within the same coefficient-of-weight

The latter two phases of the CVSDR method, Phases 2 and 3 as presented in Subsection 6.4.2 and 6.4.3, are repeated by utilizing the three other combinations available from the flight-test data of Sorties 1 through 4. An empirical model based on flight-test data from Sorties 1, 3 and 4 (denoted M134) is used to predict power required under the conditions of Sortie 2. This empirical model which employs nine distinct regressors and a constant is presented in Eq.(6.30) without the numeral coefficient. The same approach was repeated for the derivation of M234 and M124 (empirical models based on sorties 2,3,4 and 1,2,4 accordingly) for power levels predictions of sorties 1 and 3 respectively. The two models, M234 and M124, employ

(each) eight regressors and a constant and are presented in Eq.(6.30). Mind that the four empirical models (M123,M134,M234 and M124) share many of the same regressors but are not exact. This is expected since they are based on slightly different flight test data bases.

$$\frac{P}{\delta\sqrt{\theta}} = \gamma_1\left(\frac{W}{\delta}\right) + \gamma_2\left(\frac{W}{\delta}\right)^2 + \gamma_3\left(\omega^2\sqrt{\theta}\right) + \gamma_4\left(\frac{\omega}{\sqrt{\theta}}\right) +$$
$$+ \gamma_5\left(\frac{V_T}{\sqrt{\theta}}\right) + \gamma_6\left(\frac{V_T}{\sqrt{\theta}}\right)^2 + \gamma_7\left(\frac{V_T}{\sqrt{\theta}}\right)^3 + \gamma_8\left(\frac{V_T}{\omega X_{cg}}\right) + \gamma_9\left(\frac{X_{cg}}{R}\right) + \gamma_{10} \qquad \textbf{M134} \tag{6.30}$$

$$\left\{\textbf{M234}: \gamma_3 \equiv \textbf{0} \;\therefore\; \textbf{M124}: \gamma_4 \equiv \textbf{0}\right\}$$

Power prediction errors were calculated for all four sorties in the same manner demonstrated by Eq.(6.31), specifically for Sortie 4. Figure 6.13 presents these calculated prediction errors against their corresponding advance ratios. For comparison purposes, Fig. 6.13 includes the prediction errors obtained from the conventional flight-test method (cluster of sorties approach).

$$\vec{E}_r = P_i - \delta_i\sqrt{\theta_i}\left(\begin{array}{l} \gamma_{1_{M123}}\left(\frac{W}{\delta}\right)_i + \gamma_{2_{M123}}\left(\frac{W}{\delta}\right)_i^2 + \gamma_{3_{M123}}\left(\omega^2\sqrt{\theta}\right)_i + \gamma_{4_{M123}}\left(\frac{\omega}{\sqrt{\theta}}\right)_i + \\ +\gamma_{5_{M123}}\left(\frac{V_T}{\sqrt{\theta}}\right)_i + \gamma_{6_{M123}}\left(\frac{V_T}{\sqrt{\theta}}\right)_i^2 + \gamma_{7_{M123}}\left(\frac{V_T}{\sqrt{\theta}}\right)_i^3 + \gamma_{8_{M123}}\left(\frac{V_T}{\omega}\right)_i + \\ +\gamma_{9_{M123}}\left(\frac{V_T}{\omega}\right)_i^2 + \gamma_{10_{M123}}\left(\frac{V_T}{\omega}\right)_i^3 + \gamma_{11_{M123}}\left(\frac{X_{cg}}{R}\right)_i + \gamma_{12_{M123}} \end{array}\right) \tag{6.31}$$

$$i = 1, 2, ..., 8$$

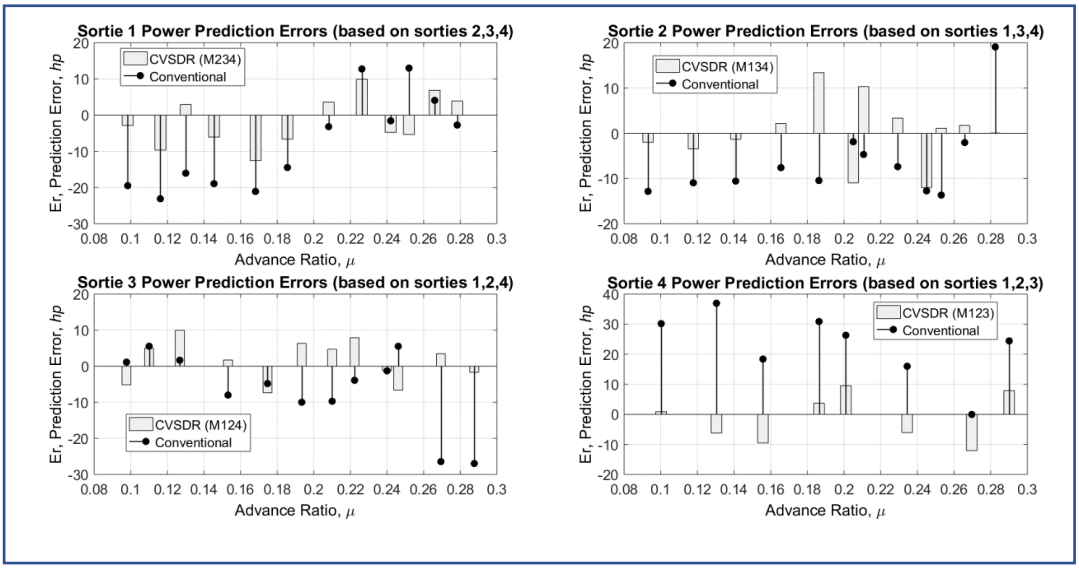

Figure 6.13. Conventional and CVSDR power prediction errors. This figure provides a comparison between the power prediction errors yielded from the CVSDR method and the conventional method (cluster of sorties approach) for all four sorties.

The superiority of the CVSDR over the conventional method is immediately evident from Fig. 6.13. Power prediction of Sortie 1 using M234 resulted in prediction errors that ranged from -12.6 hp (overestimate) to 9.9 hp (underestimate). The prediction errors mean was -1.7 hp with a standard deviation of 7 hp. This compares to prediction errors ranging from -23.1 hp to 12.8 hp (averaged at -7.6 hp with a wide standard deviation of 13 hp) achieved by using the conventional method. Comparing the two methods for the other three sorties reinforces the prediction accuracy advantage of the CVSDR method: for Sortie 2, the CVSDR prediction errors averaged at 0.2 hp with a standard deviation of 7.3 hp as compared to a mean of -6.3 hp with a standard deviation of 9 hp, yielded by the conventional method. For Sortie 3, the respective comparisons were prediction error means of 1.4 hp and -6.4 hp in favor of the CVSDR and standard deviations of 5.8 hp and 10.8 hp in favor of the CVSDR. For Sortie 4, the CVSDR method achieved a prediction error mean of only -1.5 hp, compared to an underestimation average of 22.9 hp. The CVSDR prediction errors for Sortie 4 were also less scattered as demonstrated by the two standard deviations (8.1 hp compared to 11.5 hp).

Figure 6.14 presents an alternative view of the data displayed in Fig. 6.13. The means of the absolute prediction errors for each sortie were calculated as per Eq.(6.8) and are presented alongside the corresponding values retrieved from the conventional method (cluster of sorties approach). Once more, the CVSDR method performed better for this comparison. The means of absolute errors for Sorties 1 through 4 were 6.3 hp, 5.2 hp, 5.1 hp and 7 hp accordingly. These means compare to 12.5 hp, 9.5 hp, 8.7 hp and 22.9 hp resulted from the conventional method.

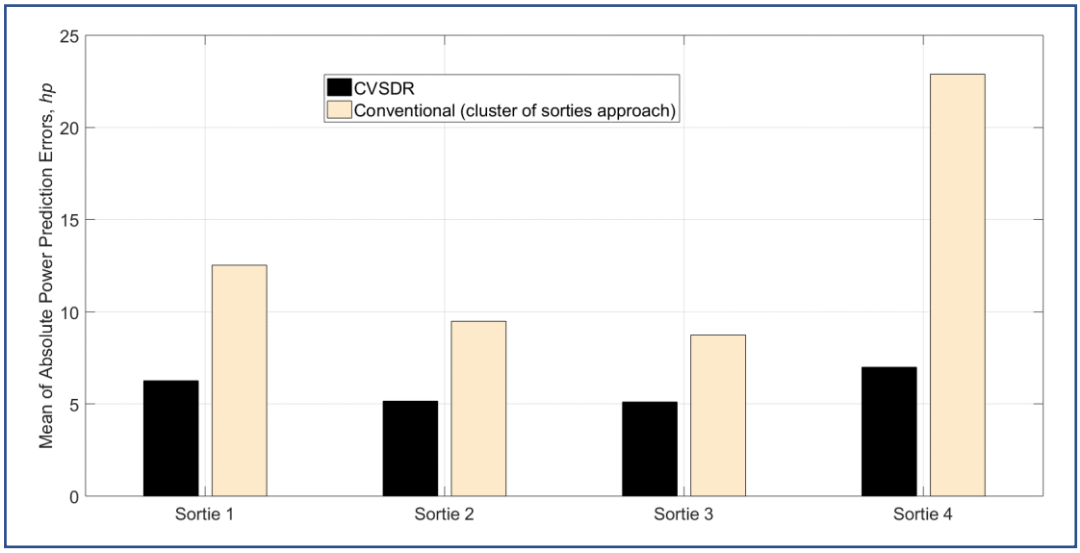

Figure 6.14. Mean of power prediction errors - conventional and CVSDR methods. This figure provides a comparison between the power prediction errors yielded by the CVSDR and the conventional method (cluster of sorties approach) for all four sorties.

Inferring from the particular case of the four sorties to the general case is realized by using the hypothesis testing, as demonstrated in Subsection 6.3.3 for the conventional method. The null hypothesis assigned is that on-average the power required for level-flight as predicted by the CVSDR method does not differ from the true measured power by more than ±4 hp (the smallest deviation noticeable to the BO-105 aircrew). This null hypothesis is tested against the alternative that on-average the CVSDR estimated power for level-flight differ by more than 4 hp (absolute value) from the actual power. The relevant test-statistic for this hypothesis-testing is calculated per Eq.(6.10). The symbol 'n' represents the number of sorties and 'S' stands for the standard deviation of the averaged power prediction errors, calculated per

Eq.(6.8) and presented in Fig. 6.14. The test-statistic was fairly large (4.11), mainly due to the relative low standard deviation. Inferential statistical analysis shows the probability for making a Type-I error by rejecting the null-hypothesis is very small (1.3%) hence does not support the null-hypothesis. On average and at the accustomed 95% confidence level, the CVSDR power predictions deviate from the actual measured power by ±4.8 hp. Although above the 4 hp threshold noticeable to the BO-105 aircrew, this average prediction error is about 17% lower than the ±5.8 hp achieved using the conventional method.

The correlation coefficient between the prediction errors and the advance ratio was calculated for all four sorties per Eq.(6.9). Figure 6.15 presents these coefficients accompanied with those obtained from the conventional method, cluster of sorties approach. It is evident the CVSDR prediction errors are not significantly correlation to the advance ratio. As already explained in Subsection 6.3.3, any correlation coefficient above 0.58 (absolute value) for sorties 1 through 3, and above 0.71 for Sortie 4 indicates a statistically significant correlation.

It can be concluded that based on flight-test data from all four sorties, the power prediction accuracy obtained from the CVSDR method is ***not*** related to the advance ratio. Similar accuracy level is expected from the CVSDR method regardless of the corresponding advance-ratio.

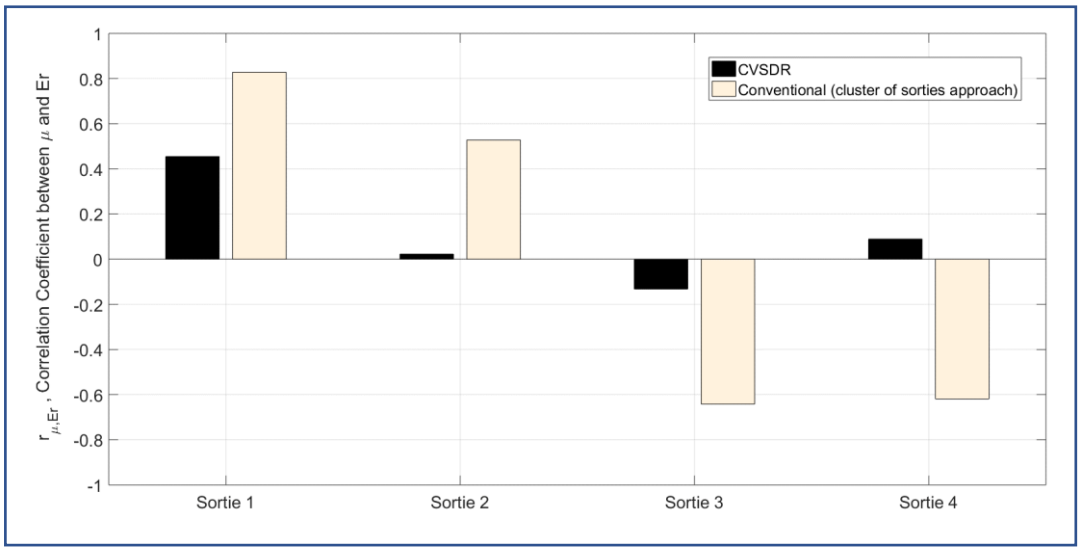

Figure 6.15. Prediction errors to advance ratio correlation. This figure presents the correlation between power prediction errors to the advance ratio using both methods, CVSDR and the conventional (cluster of sorties approach).

6.6.2 Prediction Accuracy within a different coefficient-of-weight

One might inquire whether the adequate performance of the CVSDR method is made possible only due-to the fact the power estimations were made for the same coefficient-of-weight. For this, another Sortie (number 5) was conducted under different values of coefficient-of-weight as specified in Table 6.5. Sortie 5 was executed without the cumbersome restriction imposed by the conventional method for maintaining a constant coefficient-of-weight and a constant main-rotor speed while gathering the power required to sustain level flight at various airspeeds. The coefficient-of-weight varied between $4.8\text{x}10^{-3}$ to $4.95\text{x}10^{-3}$ and was significantly different from the value maintained constant during the first four sorties ($5.79\text{x}10^{-3}$).

Table 6.5. Summary of flight-test conditions for Sortie 5.

Gross weight* [Lbs.]	Long. C.G.* [In.]	Pressure Altitude* [ft.]	Ambient Temp. [°C]	Cw* [x10^{-3}]	Main Rotor speed* [RPM]
3920 - 4080	125.6 – 125.8	5980 - 6050	8	4.81 – 4.95	421 - 425

* values represent the range of change during the sortie

The four empirical models originated from the CVSDR method were used to predict the power levels of ten stabilized data points of Sortie 5. These empirical models are M123 defined in Eq. (6.28) and Eq.(6.29); M234, M134 and M124 specified in Eq.(6.30). Prediction errors were calculated by subtracting the predicted power from the measured value, this way a positive error represents an underestimation of the actual measured power. All power estimation errors for Sortie 5 are presented in Fig. 6.16 against the appropriate advance ratio. This figure also includes a presentation of the average estimation error of the four models for each data point.

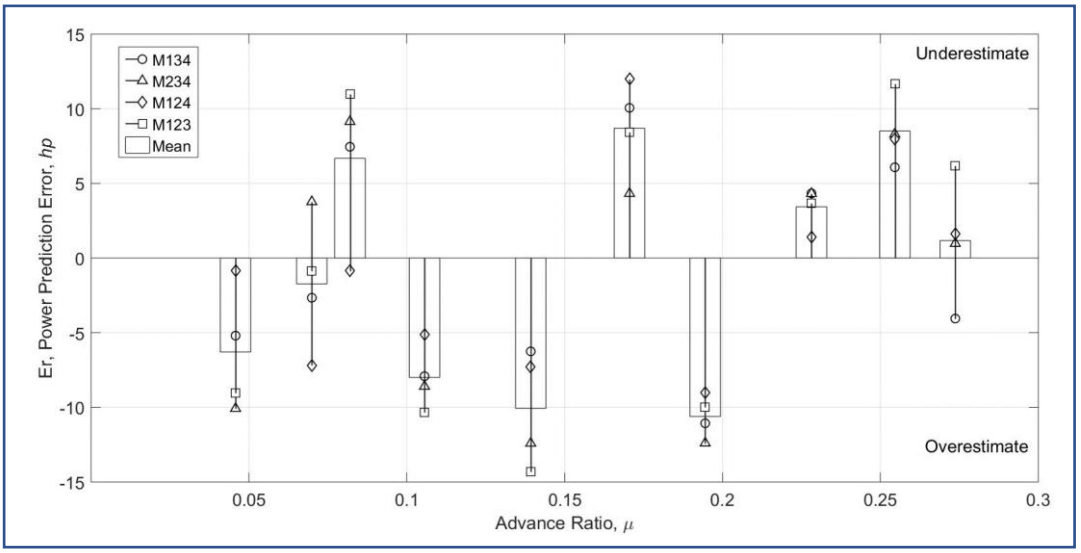

Figure 6.16. Power prediction errors for Sortie 5 (CVSDR method). This figure presents the power estimation errors for Sortie 5 using four distinct CVSDR empirical models.

As expected, all four empirical models provided adequate prediction levels, even for different and varying values of coefficient of weights. Prediction errors ranged

from -11.1 hp to 10.1 hp for M134, -12.4 hp to 9.1 hp for M234, -9 hp to 12 hp for M124 and from -10.6 hp to 8.7 hp for M123. The prediction-error means were all close to zero (-0.9 hp, -1.3 hp, -0.7 hp and -0.4 hp for M134, M234, M124 and M123 accordingly) with relatively narrow standard deviations of 7.3 hp, 8.6 hp, 6.8 hp and 9.8 hp respectively. Hypothesis testing at the 95% confidence level shows no statistically significant difference between the prediction performances of all four empirical models. Moreover, no statistical significance was found between the performance of each empirical model when acted on Sorties 1 to 4 (constant Cw) or when acted on Sortie 5. That means one can expect adequate prediction performance when using the CVSDR method for extrapolating to a different coefficient of weight.

The correlation-coefficients (r) between the power-prediction errors of each empirical model and the advance-ratio were calculated per Eq.(6.9). The values were significantly low; 0.17 for M134, 0.25 for M234, 0.42 for M124 and 0.41 for M123. For the specific number of data points in Sortie 5 (10 data points) and the accustomed 95% confidence level, only a value of 0.632 and above indicates a significant correlation between the two variables. It can be concluded that based on flight-test data of Sortie 5 no significant correlation was found between the power prediction errors using all four empirical models (M134, M234, M124 and M123) and the advance-ratio.

6.7 CONVENTIONAL AND CVSDR METHODS COMPARISON

The conventional flight-test method for level-flight performance is based on a simplification of the physical problem and comprises several drawbacks which affect the accuracy and efficiency of the method. This section draws a comparison between the conventional and the CVSDR methods by dwelling on each one of the conventional method's drawbacks specified in the introduction to this chapter (Section 6.2).

First and foremost, the prediction accuracy to be expected from each method is different. Figure 6.13 shows a comprehensive comparison between the prediction errors attained from each method for all four sorties, totalling 44 flight-test data points. Figure 6.14 compares between the two methods by presenting the mean of the absolute prediction errors for each sortie. The superiority of the CVSDR method over the conventional method is clear. The conventional method generates average absolute prediction errors of 12.5 hp, 9.5 hp, 8.7 hp and 22.9 hp, as compared to 6.3 hp, 5.2 hp, 5.1 hp and 7 hp (respectively) yielded by the CVSDR method. Statistical analysis shows that on-average (at the 95% confidence level) the CVSDR power predictions deviate by up to 4.8 hp (absolute value) from the actual measured power. The corresponding deviation obtained from the conventional method is 5.8 hp, an increase of nearly 21%.

The prediction errors generated from the conventional method were significantly correlated to the advance-ratio, whereas the CVSDR method demonstrated prediction accuracy with no correlation to the advance ratio. This correlation between the prediction error and the advance ratio might suggests there is a latent phenomenon related to the advance ratio which is missed by the conventional method and the empirical model it yields.

The conventional method is aimed at constant coefficient-of-weight data. As such, the empirical models retrieved from the first four sorties were useless for the predictions of Sortie 5. The CVSDR method is more versatile in this manner and was successfully used for the predictions of Sortie 5. Besides the versatility aspect, the constant coefficient-of-weight restriction makes the execution of the conventional flight-test method cumbersome and more time consuming, as compared to the CVSDR method. As discussed in Section 6.3, the conventional method requires the flight-test crew to continuously calculate (in real-time) and adjust the cruise altitude for maintaining a constant coefficient of weight. For a small sized and light helicopter, this inflates the flight time required for each data point from about 2 minutes to about 5 minutes. For large and heavy helicopters this inflation rate is even expected to increase more. For example, on a flight-test campaign that requires five different coefficients of weight, each including eight different airspeeds, the CVSDR method is expected to

save about 2 hours of flight time. This is about 60% reduction in the flight-test duration required by the conventional method. Moreover, losing the requirement for a continuous adjustment of the cruise altitude based on the helicopter weight can free up valuable crew resources and promote flight safety.

There are two approaches of maintaining a constant coefficient-of-weights (Cw) during a speed runs. The first is to keep a constant ratio of weight over relative density (W/σ), and a constant main-rotor angular speed. This approach is discussed Subsection 6.3.1 and thoroughly demonstrated using BO105 data in Subsection 6.3.3. The second approach for maintaining a constant coefficient-of-weight was not demonstrated in the paper but is discussed in Subsection 6.3.2. This second approach requires the flight-tester to maintain a constant ratio of static ambient temperature (Ta) over the main-rotor angular speed squared (Ω^2) during the speed-runs. These requirements dictate a continuous involvement of the flight-test crew with the main-rotor speed. For the first approach of constant main-rotor speed the crew needs to continuously apply fine-tuning, either to compensate for a non-perfect control system (M/R speed governor) functioning, or even to override an inherent scheduling profile dictated by the govern control laws. When executing the second approach the flight tester involvement with main-rotor speed adjustments is even more challenging since they need to maintain a constant value of Ta/Ω^2. Besides the fact this main-rotor speed continuous manipulation during the test imposes inconvenience on the crew, there are types of helicopters (the MD-902 Explorer as an example) which do not allow the crew to adjust the main rotor speed under standard procedures. For these types of helicopters, a precise execution of the conventional level flight performance testing method is questionable, and undesirable scatter in the data is almost inevitable.

The CVSDR method does not force the test crew to follow any kind of main-rotor speed profile, or to keep it fixed. Any variation in the main rotor speed regardless of its initiation source (automatically by the control system or manually by the flight-test crew) can be used as a valid flight-test data point. That said, the flight-tester should be reminded that flight-test data should be collected throughout the flight envelope of

the aircraft. For this reason, performance data should be collected for the entire range of main-rotor angular speed under normal operations (as presented in Fig. 6.12).

Another drawback inherent to the conventional method and efficiently addressed by the proposed CVSDR method is the influence of the center-of-gravity on the power required for level-flight. As mentioned in the chapter introduction (Section 6.2), migration of the center-of-gravity can affect the helicopter attitude, hence alter the drag frontal area of the helicopter. Through this mechanism the power required to sustain level flight is affected as well. Unlike the conventional method which neglects this influence, the CVSDR method identified a corrected variable (ψ_{15}*) which conveys the effect of center-of-gravity migration into the empirical power model. For the specific type of helicopter tested and the limited scope of tests, this center-of-gravity was identified as the 6th concept in the data (σ_6), responsible for 2.3% of variance in the data (as presented in Fig. 6.11). Note that the specific data analyzed covers a limited center-of-gravity travel range (between longitudinal stations 123.5 and 124.4 inch as per Table 6.1), which represents only 6.4% of the allowed longitudinal center-of-gravity of the BO105 helicopter. Expanding the flight-test data base to include level flight performance data measured under a larger center-of-gravity travel range might have resulted in a larger significance of the relevant corrected variable (ψ_{15}*).

The conventional method is bounded by the high-speed approximation, meaning it is relevant only for airspeeds in which the induced velocity through the main-rotor disk is negligible as compared to the airspeed the helicopter flies at. This makes the conventional method irrelevant for modeling and estimating power required in the low-airspeed regime. The CVSDR method is not bounded by this high-speed approximation and is indeed relevant for the low-airspeed regime. As seen in Fig. 6.16, the CVSDR method was also applied to the low-airspeed regime and provided adequate power estimations in this regime. Three power estimations were made for the advance-ratios of 0.05, 0.07 and 0.08 representing true-airspeeds of 19, 30 and 35 kts. respectively. Those estimations were at a similar accuracy level as achieved for the high-speed regime. Nevertheless, statistical analysis for Sortie 5 and the CVSDR

method showed no significant correlation between the power prediction errors and the advance-ratio.

6.8 CONCLUSIONS AND SUMMARY

The conventional flight-test method to evaluate helicopter performance in level-flight includes many drawbacks which seriously compromise its accuracy and its execution efficiency. The proposed CVSDR method aims at addressing those downsides of the conventional flight-test method. The CVSDR method showed great potential as it was used successfully with level-flight test data obtained from a MBB BO-105 helicopter. The power prediction accuracy achieved using the CVSDR method was nearly 21% better than the level of accuracy yielded from the conventional flight-test method. Moreover, the CVSDR method does not require the test crew to follow a strict and binding flight scheduling, as mandated by the conventional method. This potentially makes the CVSDR more efficient and time conserving. The CVSDR is estimated to reduce flight-time for data points gathering by ***at least*** 60%.

The CVSDR method is not restricted by the high-speed approximation and is therefore relevant to the low airspeed regime, as opposed to the conventional flight-test method. This low-airspeed regime relevancy can potentially bridge the empirical-modelling gap between the two most important flight regimes of the helicopter, the hover, and the level-flight.

Although demonstrated using flight-test data from a MBB BO-105 helicopter, the CVSDR method is applicable for any other type of conventional helicopter in level-flight.

No matter how thin you slice it, there will always be two sides.

Baruch Spinoza

7 CONCLUSIONS AND RECOMMENDATIONS

The goal of this dissertation is to develop new and improved flight-testing methods for the available power, the OGE hover and the level-flight performance of a conventional, GT engine(s) powered helicopter. The identified drawbacks of the current flight-test methods are spelled out in the problem statement of this thesis (Subsection 1.4). These shortcomings can be sorted under two core categories of inefficiency and inaccuracy. The two most important properties the performance flight-tester is seeking for are those of efficiency and accuracy. Performance flight-testing is all about acquiring accurate empirical models for the performance of the aircraft by applying efficient methods that minimize time and effort.

7.1 NOVEL VS. CONVENTIONAL FLIGHT TEST METHODS –MAIN DIFFERENCES

The novel flight-test methods presented in this thesis are derived from the same source as the conventional flight-test methods. This is the fundamental approach of dimensional analysis. The performance flight-testing problem is addressed more efficiently by reducing the number of the participating variables. The practicality for the performance flight-tester is that the test matrix and the associated number of planned sorties is immensely reduced. The first substantial difference between the two

performance flight-testing approaches (novel and the conventional) relates to the role dimensional analysis plays within the method. While the conventional flight-test methods are using the Buckingham PI Theorem [66] only as a mean for justification, the novel approach uses it as a genuine tool that provides non-dimensional (ND) variables. These ND variables are used as predictors (regressors) in the empirical models explored.

The conventional dated methods originate from overly simplified physical models that are 'reversed-engineered' to yield ND variables. While the conventional methods are simple to comprehend, and even provide satisfactory interpolation predictions for conservative helicopter and atmospheric conditions ('center of the envelope'), these methods easily fail, when challenged with performance prediction of less benign conditions, where non-linear effects become a factor. The novel flight-test methods employ an original list of ND variables to be used as predictors. This list is reduced using tools of dimensionality reduction (SVD) to retain only the most essential and effective ND variables for the specific performance problem. This method is referred-to as the 'Corrected-Variables Screening using Dimensionality Reduction', or shortly the CVSDR method. Unlike the conventional method, the proposed CVSDR is not bounded by any predetermined simplifications and approximations. This method adjusts and adapts based on the *actual* flight-test data analysed. This flexibility of the CVSDR method allows to accommodate for the various sensitivities each type of helicopter demonstrates and also for any kind of non-linear effects, as they become even more significant while the helicopter operates under extreme conditions and close to the boundaries of its envelope. The proposed CVSDR method accommodates for the exceptionality of each helicopter and for uncommon flight-conditions. This stands opposite to the conventional flight test methods which are bounded by conservative approximations and simplifications.

Another fundamental difference between the two approaches is with respect to multi-variability modelling. The conventional approach consistently avoids dealing with multivariable models and prefers the use of several single-variable mathematical relations over employment of one multivariable relationship. The conventional flight-

testing method for the available power of a gas-turbine (GT) engine is centred on *single-variable* polynomials as discussed in Chapter 1 (Subsection 1.3.1) and demonstrated, using actual flight-test data, in Chapter 2. The conventional approach simplifies a multivariable-type problem by assuming the output power of a GT engine can be treated as a linear combination of single-variable models. This notion of refraining from employing multivariable models also guides the conventional flight-test methods for the required power. Taking the level-flight performance as an example (Subsection 1.3.3), the three-variable empirical model in coefficient-of-power (Cp), advance-ratio (μ) and coefficient-of-weight (C_W) is traded in the name of simplicity for series of two-variable models (Cp to μ), given at various discrete values of coefficient-of- weight (C_W).

7.2 CONCLUSIONS

The main conclusions of this dissertation are summarized and presented hereinafter with respect to the goals and objectives of the research (Section 1.5). All conclusions are numbered for ease of tracking and referencing. This list of conclusions relates to the specific seven Research Questions (RQ's) specified in the problem statement of the dissertation (Section 1.4). Figure 7.1 presents a 'checkers-board' type plot that maps the correspondence between the conclusions and the seven RQ's of this thesis. A dark element in the rectilinear plot of Fig. 7.1 indicates a relationship between the specific conclusion and a particular RQ. Note there are specific conclusions which are related to more than one RQ and vice versa; there are few RQ which are supported by more than one conclusion. Conclusion 22 is not related directly to any RQ's but refers to the conventional level-flight performance method.

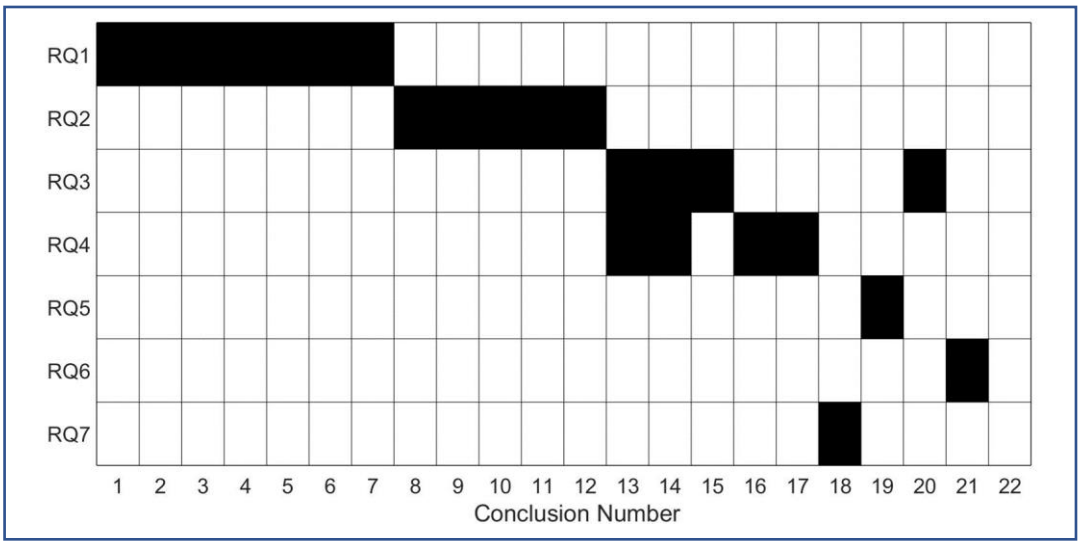

Figure 7.1. Conclusions to RQ's Mapping. This checkers-board type plot presents the correlation between the 7 RQ's and the 22 conclusions of the thesis. A dark element represents a correspondence between a specific conclusion and a specific RQ.

7.2.1 Flight Testing for Power Available

This subsection relates to the first Research Question (RQ1) which is ***Can a novel flight-test method be developed for the available power of a gas-turbine helicopter, which demonstrates enhanced power prediction accuracy as compared to the conventional method?*** For answering RQ1 a novel method, referred to as the 'Multivariable Polynomial Optimization under Constraints' (MPOC), was developed for the available power of a gas-turbine helicopter. The method, which is presented in Chapter 3, seeks for a third order multivariable polynomial to describe the corrected output power of a GT engine (CSHP) as a function of the three engine corrected variables, the corrected compressor speed (CNg), the corrected temperature (CTGT) and the corrected fuel-flow (CW_f). The MPOC method is further developed and tuned in Chapter 4, where a systematic and repeatable methodology to choose in-between various empirical models is discussed. The following seven conclusions, Conclusion (1) to Conclusion (7), are related to RQ1 and were drawn while developing the MPOC method:

(1) The output power of a helicopter GT engine is a multivariable problem that can be adequately described by a third-order multivariable polynomial in corrected compressor speed (CNg), corrected temperature (CTGT) and corrected fuel-flow (CWf).

(2) The prediction of the output power of a GT engine by using a multivariable polynomial in corrected compressor speed (CNg), corrected temperature (CTGT) and corrected fuel-flow (CW_f) is more accurate as compared to single-variable polynomials. For the example BO-105 flight-test data used in Chapter 3, the standard deviation of the output power estimation error is reduced from 13hp using the current single-variable method, to only 4.3hp by using a multivariable polynomial. Expanding the flight-test data base to seven different engines in Chapter 4 reveals that the multivariable polynomials performed much better with all seven engines, as compared to the single-variable approach. The *maximum* average prediction error using a multivariable polynomial model was only 0.2% as compared to a maximum average prediction error of 1.15%, using the single-variable approach.

(3) The maximum available power of a GT engine under various atmospheric conditions can be accomplished by finding the extremum (maximum) of a multivariable polynomial that represents the output power of the engine, subjected to both equalities and inequalities constraints. The novel method called Multivariable Polynomial Optimization under Constraints (MPOC) seeks for optimizing a multivariable polynomial representing the engine output power, while satisfying equalities and inequalities constraints. The equalities constraints are the engine empirical internal rules of operation and the inequalities constraints are the engine operating limitations, i.e., the compressor speed limitation, the maximum allowed engine temperature, and the maximum fuel-flow imposed by the engine fuel pump.

(4) The Karush-Khun-Tucker (KTT) optimization method was used successfully with the MPOC method for the task of evaluating the maximum available power of a GT engine, under various atmospheric conditions. While the current flight-test method yielded unrealistic predictions for certain atmospheric conditions, the

proposed MPOC method demonstrated acceptable predictions for the maximum available power of the engine for a wider range of atmospheric conditions.

(5) The process of empirical models evaluation and screening is at the core business of experimental flight-test data analysis. The flight-test team needs to select the most effective and accurate empirical model to represent the aircraft performance, as reflected by the measured data. The conventional statistical method known as the hypothesis-testing failed to differentiate between the many candidate multivariable polynomials based on their performance in representing the output power of a GT engine.

(6) A singular-value-decomposition (SVD) based procedure was used successfully to distinguish between many candidate multivariable polynomials based on their excellence level in representing the output power of a GT engine. Furthermore, this SVD procedure is capable of exposing latent similarities between different GT engines with respect to their output power models.

(7) No significant correlation was found between the number of predictors used in the multivariable empirical model and the prediction accuracy of the GT engine output power. Two specific multivariable polynomials that employ only 11 predictors (out of 19 available) were identified as the fourth and the fifth best-performing models (out of 512 candidates) for the output power of an example group of seven GT engines.

7.2.2 Flight Testing for Power Required in OGE Hover

This subsection relates to RQ2 which is ***Can a novel flight-test method for OGE hover performance of a conventional helicopter, which demonstrates enhanced prediction accuracy as compared to the conventional OGE hover method be developed?*** For answering RQ2 a novel method, referred to as the

'Corrected Variables Screening using Dimensionality Reduction' (CVSDR), was developed for the power required of a conventional helicopter in OGE hover. The method is presented in Chapter 5 and its explicit steps are summarized in Table 7.1 presented hereinafter. The following five conclusions, Conclusion (8) to Conclusion (12), are related to RQ2 and were drawn while developing the CVSDR method for OGE hover performance:

(8) The power required for OGE hover of a conventional helicopter can be adequately described by a multivariable first order polynomial in corrected variables (predictors) retrieved from a rigorous dimensional analysis.

(9) The identity and number of corrected variables required for the OGE hover multivariable empirical model ('conceptual empirical model') is obtained by the CVSDR method. For the example Bell Jet-Ranger helicopter and the specific OGE hover flight test data base presented in Chapter 5, the CVSDR method propose a list of four corrected variables that represent 98% of the variance in the flight-test data.

(10) The power predictions of the CVSDR method were 1.9 times more accurate than the conventional method, when used with OGE hover flight test data of the example Bell Jet-Ranger helicopter. At the 95% confidence level, the CVSDR method deviated by an average of only 0.9hp (0.3% of the maximum continuous power of the example helicopter) from the actual power required to hover, whereas power predictions from the conventional method deviated by an average of 1.7hp.

(11) Unlike the conventional hover performance flight-testing method, the CVSDR approach is capable of representing non-linear phenomena such as compressibility and drag divergence in its empirical model. The CVSDR method does not determine beforehand which predictors must be used in the empirical model. Instead, it chooses from a list of 15 corrected variables (derived from dimensional analysis) the most essential and effective predictors to represent the specific flight test data analysed. This approach, by itself, provides more flexibility and allows for more accurate empirical modelling, as compared to the conventional method.

(12) The novel CVSDR method for OGE hover performance requires no changes to the manner current OGE hover flight test sorties are carried out. The modification is with the data analysis procedure only.

Table 7.1. A step-by-step guidance for CVSDR OGE hover testing.

Step	Task Description & Instruction
Phase One – Establish an applicable list of CVs to represent the hover performance. This phase is described in Subsection 5.4.1.	
1	Compute all 15 CVs (Table 5.3) for each stabilized OGE hover data point measured.
2	Arrange the computed CVs in a matrix form (this is matrix Z). The rows of Z should represent the different data points and columns of Z should represent the various CVs.
Phase Two – Screening for the most effective CVs using dimensionality reduction. This phase is thoroughly explained in Subsection 5.4.2.	
3	Normalize all columns of matrix Z as per Eq.(5.18) to have a zero mean and a variance equals one.
4	Decompose the ***normalized*** matrix Z into its three unique matrices (U,Σ and V) using a Singular Value Decomposition (SVD) algorithm. Matrix U is also referred to as the Left Singular Vectors (LSV), matrix Σ is called the singular values and matrix V is called the Right Singular Vectors (RSV).
5	Normalize all singular values (entries along the main diagonal of matrix Σ) as per Eq.(5.19). The normalized values represent the relative strength of the various dimensions exist in the data. Determine the number of ***significant*** dimensions involved in the specific hover performance data, based on the cumulative sum of the normalized singular values (as presented in Fig.5.5).
6	Normalize the rows of matrix V^T (RSV) as per Eq.(5.20). This normalization calls for the absolute value of each element along the rows of RSV to be divided by the sum of all elements absolute values along the corresponding row of RSV.
7	Identify the most significant CVs of the specific hover performance analysed. The level of correspondence between each CV and an abstract dimension of the hover problem is illustrated in Fig. 5.4. Note that only the first significant rows of the normalized RSV should be evaluated. The number of significant rows of RSV equals the number of significant dimensions retrieved in sequential step 5 above. Example for this step is presented in Fig.5.6.
Phase Three – Forming a practical empirical model (Subsection 5.4.3)	
8	Use the most significant CVs identified in sequential step 7 to form a practical polynomial that uses the relevant CVs as regressors in this empirical model.

7.2.3 Flight Testing for Power Required in Level Flight

This subsection addresses the five Research Questions (RQ3, RQ4, RQ5, RQ6, and RQ7) which are specified in the problem statement of this thesis (Section 1.4). These five research questions relate to the deficiencies associated with the current level-flight performance flight-testing of a conventional helicopter. The novel CVSDR flight-test method for power required in level flight was developed specifically for addressing the five RQ's (RQ3, RQ4, RQ5, RQ6, and RQ7). This novel method is thoroughly discussed and demonstrated in Chapter 6 and its explicit steps are summarized in Table 7.2 presented hereinafter. Abstractly, the CVSDR method for level flight can be regarded as a rigours expansion of the hover CVSDR method into a higher dimensional-space. The following ten conclusions, Conclusion (13) to Conclusion (22), were drawn while developing the CVSDR method for level flight performance. The detailed mapping of these ten conclusions to the particular five RQ's is presented in Fig. 7.1.

(13) The power required for level flight of a conventional helicopter can be adequately described by a multivariable first order polynomial in corrected variables (predictors) retrieved from a rigorous dimensional analysis. The list of corrected variables includes predictors that represent various coefficient-of-weight and account for non-linear effects. This conclusion relates directly to two research questions; the non-linear effects of RQ3 and the various coefficient-of-weight of RQ4.

(14) The identity and quantity of corrected variables required for the level flight multivariable empirical model ('conceptual empirical model') are established by the CVSDR method. For the example MBB BO-105 helicopter and the specific level flight test data base presented in Chapter 6, the CVSDR method proposed a list of seven corrected variables that represent 96.5% of the measured variance in the data.

(15) The power predictions accuracy achieved using the CVSDR method for level-flight was nearly 21% better (on average and at the 95% confidence level), as

compared to the prediction accuracy yielded from the conventional method. Note this conclusion relates directly to the improved prediction accuracy of the novel CVSDR method as required by RQ3.

(16) The novel CVSDR method for level flight made planning and execution of flight-test sorties more efficient and time conserving. It is estimated to reduce flight-time for data gathering by at-least 60%. Note this conclusion relates directly to the efficiency of the novel CVSDR method as required by RQ4.

(17) The novel CVSDR method for level flight does not require a continuous and accurate adjustment of the flight altitude, as mandated by the conventional method. Renouncing this burdensome requirement can free up valuable crew resources and promote flight safety. Note this conclusion relates directly to the efficiency of the novel CVSDR method as required by RQ4

(18) The novel CVSDR method for level flight does not require to keep the main-rotor angular speed constant throughout the test, as required by the conventional method. This makes the CVSDR method more versatile and relevant for helicopter types, which do not enable pilot-initiated main rotor speed adjustments under standard flight procedures. This conclusion relates directly to RQ7.

(19) The novel CVSDR method for level flight is not restricted by the high-speed approximation like the conventional method. This makes the CVSDR an appropriate method for the low-airspeed regime, and can potentially bridge the empirical modelling gap between the hover and level-flight domains. This conclusion relates directly to RQ5.

(20) The power predication errors yielded by the CVSDR method were not significantly correlated to the advance ratio, as opposed to the prediction errors returned from the conventional method. This might suggest that the CVSDR method is capable of identifying a latent advance-ratio related phenomenon, completely overlooked by the conventional method.

(21) The novel CVSDR flight test method for level flight comprises the effect of center-of-gravity location on the power required. This significant competence adds much value to the CVSDR method over the conventional method. This conclusion relates directly to RQ6.

(22) The soundness of the conventional flight-test method for level flight performance is seriously questionable in light of the research level-flight test sorties. The theoretical uniqueness of the coefficient-of-power (Cp) to advance ratio (μ) curve for four sorties executed at a nominal constant coefficient-of-weight (C_W) was found inaccurate. The measured 11% variance in Cp cannot be entirely explained by the inaccurate flight test execution which resulted in only 1% variance in C_W. Note this conclusion is not related directly to any RQ's but refers to the drawbacks of the conventional level-flight performance method.

Table 7.2. A step-by-step guidance for CVSDR level-flight testing.

Step	Task Description & Instruction
Phase One – Establish an applicable list of CVs to represent the level-flight performance. This phase is described in Subsection 6.4.1.	
1	Compute all 36 CVs (Table 6.3) for each stabilized level-flight data point measured. There should be 136 stabilized data points, If all sorties of Fig. 6.12 are closely executed.
2	Arrange the computed CVs in a matrix form (this is matrix Z). The rows of Z should represent the different data points and columns of Z should represent the various CVs. If all sorties of Fig. 6.12 were closely executed, matrix Z should be of size 136x36.
Phase Two – Screening for the most effective CVs using dimensionality reduction. This phase is described in Subsection 6.4.2.	
3	Normalize all columns of matrix Z as per Eq.(6.24) to have a zero mean and a variance equals 1.
4	Decompose the ***normalized*** matrix Z into its three unique matrices (U,Σ and V) using a Singular Value Decomposition (SVD) algorithm. Matrix U is also referred to as the Left Singular Vectors (LSV), matrix Σ is called the singular values and matrix V is called the Right Singular Vectors (RSV).
5	Normalize all singular values (entries along the main diagonal of matrix Σ) as per Eq.(6.25). The normalized values represent the relative strength of the various dimensions exist in the data. Determine the number of ***significant*** dimensions involved in the specific level-flight performance data, based on the cumulative sum of the normalized singular values (as presented in Fig.6.10).
6	Normalize the rows of matrix V^T (RSV) as per Eq.(6.26). This normalization calls for the absolute value of each element along the rows of RSV to be divided by the sum of all elements absolute values along the corresponding row of RSV.
7	Identify the most significant CVs of the specific level-flight performance analysed. The level of correspondence between each CV and an abstract dimension of the level-flight problem is illustrated in Fig. 6.9. Note that only the first significant rows of the normalized RSV should be evaluated. The number of significant rows of RSV equals the number of significant dimensions retrieved in sequential step 5 above. Example for this step is presented in Fig.6.11.
Phase Three – Forming a practical empirical model (Subsection 6.4.3)	
8	Use the most significant CVs identified in sequential step 7 to form a practical polynomial that uses the relevant CVs as regressors in this empirical model.

7.3 RECOMMENDATIONS

The following are recommendations concerning possible future expansion of the research.

(1) One of the main advantages of the CVSDR method for level flight is that it is unrestricted by the high-speed approximation (Conclusion 19), therefore is applicable to the low-airspeed regime, unlike the conventional method. This opens up an opportunity to provide a unified *empirical* model to describe the power required from hover to the maximum horizontal airspeed of the helicopter. Under the current research limitations for number of flight-hours, availability of aircraft and special flight-test instrumentation it was not feasible to employ the CVSDR method for level flight, from a hover, through the low airspeed regime to the maximum airspeed for level flight. Future research should focus on the applicability and accuracy of the CVSDR method when used as a unified empirical model for the power required from hover to maximum airspeed in level flight.

(2) The current research was limited to out of ground effect (OGE) hover only. Although performance flight testing for in-ground-effect (IGE) was excluded, the derivation of the proposed CVSDR method in Chapter 5 includes provisions to also address the IGE hover. The applicability and accuracy of the CVSDR method for power required to IGE hover should be evaluated in future research.

(3) Future research should expand the CVSDR flight-testing method to include more areas of helicopter performance. These are the power required in a climb (vertical climb and forward climb), and partial-power and unpowered descent performance ('Autorotation').

(4) In recent years we have witnessed an increasing number of vertical lift aircraft types that combine both fixed-wing (FW) and rotary-wing (RW) characteristics. This duality also affects the performance flight-test methods, especially for the transition from RW to FW envelope. The general approach presented in this thesis, of

establishing a generic list of corrected-variables using dimensional analysis, followed by an elimination procedure based on dimensionality reduction to identify the most essential for the specific performance problem analysed and then to establish an empirical multivariable model, can work better for this type of a dual-characteristic aircraft. Future research should be focused on evaluation of the applicability and efficiency of the performance flight-testing method developed in the current research, to relevant vertical-lift aircraft that combine both RW and FW characteristics.

(5) The current research shows that power prediction accuracy for hover and level-flight is better with the proposed empirical models, as compared to the empirical models yielded by the conventional methods. Part of the improved prediction accuracy can be attributed to the increased number and improved quality of the predictors (corrected-variables) used. Using more *appropriate* and *effective* degrees of freedom in the empirical model surely promotes prediction accuracy. That being said, the hover and level-flight research sorties were conducted under relatively moderate flight-conditions. It is believed the *full* potential of the proposed performance flight-testing methods was not entirely exposed by the relatively moderate flight conditions tested. Future research should apply the novel CVSDR method for hover and level flight under extreme conditions of atmosphere and configuration. This includes high altitude and low ambient temperatures to expose the helicopter to severe compressibility effects, and for all corners of gross-weight/center-of-gravity envelope.

(6) Future research should look into the potential and feasibility of employing the CVSDR method for empirical modelling by the Health and Usage Monitoring Systems (HUMS) installed in helicopters. For example, the novel CVSDR method for performance flight testing could be entirely automated and integrated into HUMS to provide real time performance empirical modelling for and prediction of the *specific* helicopter (not just the type). The CVSDR algorithm can also be used to flag exceptional prediction discrepancies that might be indicative of potential helicopter malfunctions and hazards.

7.4 CLOSING REMARKS

The performance flight-tester needs practical and efficient flight-test methods with the purpose of producing accurate empirical models for aircraft performance prediction. The novel flight-test method presented in this dissertation fits into this need for a practical, efficient and accurate performance flight-testing method. The novel method developed and tested in this research, yielded better prediction accuracy as compared to the accuracy level of conventional methods. The available power prediction using the novel method was on average 5.75 times more accurate than the conventional flight-test method. The novel method predicted power required for OGE hover, about 1.9 times more accurately than the conventional method. Superior performance prediction of the novel method was also demonstrated for power required for level flight (about 21% more accurate). It is believed the main reason for superior prediction accuracy is mainly attributed to the flexibility of the novel method. It is capable to adjust and to adapt to specific flight-test data reflecting various helicopter types, aircraft configurations and ambient conditions. This flexibility does not exist to the same extent within the conventional flight-test methods. The efficiency and practicality of the novel method is mostly demonstrated in level flight performance flight-testing. As thoroughly discussed in Chapter 6, the novel method is estimated to reduce flight-time for data gathering by at-least 60%, while at the same time decreasing the complexity in flight-test execution, hence promoting safety of flight.

Alongside the many advantages of the novel flight-test method, there is one drawback. At the core of this novel method lies an analytical procedure that starts with fundamental dimensional analysis, followed by dimensionality reduction procedure, based on the concept of singular-value-decomposition (SVD). This dimensionality reduction procedure requires for more analysis effort, both in terms of flight-test data reduction and a supporting software package, capable of performing the SVD algorithm.

The scope of this research was limited to the power available of gas-turbine engines and the power required for a conventional helicopter in OGE hover and in

level-flight. Despite focusing on limited flight-testing areas only, it is believed the novel method presented in this dissertation is applicable to other areas of performance flight-testing and can be employed outside of the conventional helicopter configuration. It is recommended the novel performance flight-test method be evaluated in the future under extreme flight and ambient conditions, for other areas of performance flight-testing and also for unconventional helicopters, those which do not conform to the single main-rotor and a single tail-rotor configuration.

A. GAS-TURBINE ENGINE DIMENSIONAL ANALYSIS

This appendix provides the generic gas-turbine engine dimensional analysis. The classical Buckingham Pi theorem [66] is used to demonstrate how the gas-turbine engine dimensional physical problem is converted into a non-dimensional (ND) problem and how should the dimensional variables involved in the gas-turbine engine performance problem be non-dimensionalized or 'corrected' in order to reduce the number variables involved in the problem. The method of parameter correction presented here is the classical approach that follows from the theorem. Note there are few turbine engine manufacturers that tweak or 'fine-tune' these classical correction factors to better work with their specific engine types.

Consider first the dimensional variables that affect the ***generic*** gas turbine engine output power problem. The practice would suggest that these should be the ambient static pressure, Pa, ambient static temperature, Ta, engine compressor speed, Ng, engine temperature, TGT, fuel-flow (weight flow), Wf and the physical size of the engine. Consider a descriptive cross section area, Ae, to represent the physical size of the engine. The engine output power, SHP, can be mathematically represented as in Eq.(A.1) or equivalently implicitly as in Eq.(A.2).

$$SHP = f(P_a, T_a, Ng, TGT, W_f, Ae) \tag{A.1}$$

$$f(SHP, P_a, T_a, Ng, TGT, W_f, Ae) = 0 \tag{A.2}$$

The dimensions involved in this physical problem are presented in Table A.1. The notation M represents mass, L represents length and T represents time.

Table A.1 – Gas turbine engine - summary of variables and dimensions involved.

#	Physical Variable	Notation	Dimension
1	Shaft Output Power	SHP	$[M][L]^2[T]^{-3}$
2	Ambient Air static Pressure	Pa	$[M][L]^{-1}[T]^{-2}$
3	Ambient Air static Temperature	Ta	$[L]^2[T]^{-2}$
4	Engine Compressor Speed	Ng	$[T]^{-1}$
5	Engine Temperature	TGT	$[L]^2[T]^{-2}$
6	Engine Cross Section Area	Ae	$[L]^2$
7	Fuel (Weight) Flow	w_f	$[M][L][T]^{-3}$

There are seven dimensional variables involved in the problem with three dimensions (L, M, and T). According to the Buckingham Pi Theorem, the complexity of the physical problem can be reduced from seven dimensional variables to four Non-Dimensional (ND) variables. This is the number of dimensional variables minus the number of dimensions involved in the problem, i.e., seven minus three equals four.

The next phase is to build those four ND variables as products of the dimensional variables. The four ND variables will be denoted by π_i (hence the origin of the name of this Pi theorem). Since there exist seven dimensional variables to be used for the construction of the four ND variables, three dimensional variables out of the seven must be used as repeating variables in the ND products.

There are 35 different options to choose three variables out of seven for the case where the order does not matter (combinations) as shown by Eq.(A.3), for which N represents the number of options.

$$N = \binom{7}{3} = \frac{7!}{(3!)(4!)} = 35 \tag{A.3}$$

It is a fairly tedious task of screening between 35 different combinations. This phase usually involves some trial and error rounds before obtaining the most suitable configuration. The following is a demonstration of only one combination out of the 35 options available. In this particular example presented in Eq.(A.4), the three repeating variables were chosen as the ambient air static pressure, Pa, the ambient air static temperature, Ta, and the engine cross-sectional area, Ae.

$$\left\{\begin{aligned}
\pi_1 &\equiv \left(P_a\right)^{a_1}\left(T_a\right)^{b_1}\left(Ae\right)^{c_1}\left(SHP\right)\\
\pi_2 &\equiv \left(P_a\right)^{a_2}\left(T_a\right)^{b_2}\left(Ae\right)^{c_2}\left(Ng\right)\\
\pi_3 &\equiv \left(P_a\right)^{a_3}\left(T_a\right)^{b_3}\left(Ae\right)^{c_3}\left(TGT\right)\\
\pi_4 &\equiv \left(P_a\right)^{a_4}\left(T_a\right)^{b_4}\left(Ae\right)^{c_4}\left(W_f\right)
\end{aligned}\right\} \tag{A.4}$$

According to Buckingham [66], the repeating variables should be raised to some arbitrary powers, those are denoted as $a_1,b_1,c_1,\ldots,c_4$ in Eq.(A.4). As demonstrated hereinafter, these arbitrary powers are identified as those numeric values that make the π_i products non-dimensional.

The next step in this process of non-dimensionalizing the problem is to enforce all four π_i products to be non-dimensional. First, each variable is replaced with its equivalent dimensions representation, then a system of linear equations is produced. Each non-dimensional variable produced a set of three equations in three unknowns as presented in Eq.(A.5).

$$\left\{\begin{aligned}
\pi_1 &= \left(\frac{M}{LT^2}\right)^{a_1}\left(\frac{L^2}{T^2}\right)^{b_1}\left(L^2\right)^{c_1}\left(\frac{ML^2}{T^3}\right) = M^{a_1+1}L^{-a_1+2b_1+2c_1+2}T^{-2a_1-2b_1-3} \triangleq M^0L^0T^0 \\
\pi_2 &= \left(\frac{M}{LT^2}\right)^{a_2}\left(\frac{L^2}{T^2}\right)^{b_2}\left(L^2\right)^{c_2}\left(T^{-1}\right) = M^{a_2}L^{-a_2+2b_2+2c_2}T^{-2a_2-2b_2-1} \triangleq M^0L^0T^0 \\
\pi_3 &= \left(\frac{M}{LT^2}\right)^{a_3}\left(\frac{L^2}{T^2}\right)^{b_3}\left(L^2\right)^{c_3}\left(\frac{L^2}{T^2}\right) = M^{a_3}L^{-a_3+2b_3+2c_3+2}T^{-2a_3-2b_3-2} \triangleq M^0L^0T^0 \\
\pi_4 &= \left(\frac{M}{LT^2}\right)^{a_4}\left(\frac{L^2}{T^2}\right)^{b_4}\left(L^2\right)^{c_4}\left(\frac{ML}{T^3}\right) = M^{a_4+1}L^{-a_4+2b_4+2c_4+1}T^{-2a_4-2b_4-3} \triangleq M^0L^0T^0
\end{aligned}\right\} \tag{A.5}$$

Realizing the exponents for each ND variable π_i is done through solving the four sets of three equations with three unknowns. This procedure is demonstrated for for π_1 in Eq.(A.6):

$$\left\{\begin{aligned}
&[M]: a_1 + 1 = 0 \\
&[L]: -a_1 + 2b_1 + 2c_1 + 2 = 0 \\
&[T]: -2a_1 - 2b_1 - 3 = 0
\end{aligned}\right\} \Rightarrow \begin{pmatrix} 1 & 0 & 0 \\ -1 & 2 & 2 \\ -2 & -2 & 0 \end{pmatrix}\begin{pmatrix} a_1 \\ b_1 \\ c_1 \end{pmatrix} = \begin{pmatrix} -1 \\ -2 \\ 3 \end{pmatrix} \Rightarrow \begin{pmatrix} a_1 \\ b_1 \\ c_1 \end{pmatrix} = \begin{pmatrix} -1 \\ -1/2 \\ -1 \end{pmatrix} \tag{A.6}$$

Once the exponents of π_1 are found, the first ND variable is revealed (Eq.)

$$\pi_1 \equiv \left(P_a\right)^{a_1}\left(T_a\right)^{b_1}\left(Ae\right)^{c_1}\left(SHP\right) = \left(P_a\right)^{-1}\left(T_a\right)^{-1/2}\left(Ae\right)^{-1}\left(SHP\right) = \frac{SHP}{P_a\sqrt{T_a}}\frac{1}{Ae} \tag{A.7}$$

The static ambient pressure, Pa, and the static ambient temperature, Ta, can be replaced with the pressure and temperature ratios as respectively appears in Eq.(A.8) and (A.9) to constitute Eq.(A.10)

$$\delta \equiv \frac{p_a}{p_o}\ , p_o = 14.7\,psi \tag{A.8}$$

$$\theta \equiv \frac{T_a}{T_0} \ , \ T_0 = 288K \tag{A.9}$$

$$\pi_1 = \frac{SHP}{\delta\sqrt{\theta}} \cdot \frac{1}{P_o A e \sqrt{T_o}} = \frac{SHP}{\delta\sqrt{\theta}} \cdot K_1 \tag{A.10}$$

Since K_1 in Eq.(A.10) is a constant for a specific helicopter (the engine cross sectional area does not change and P_0 and T_0 represent the standard sea level values for static air pressure and static air temperature respectively) it is evident that the first ND variable involved in the problem (π_1) is the expression presented in Eq.(A.11).

$$\pi_1^* = \frac{SHP}{\delta\sqrt{\theta}} \tag{A.11}$$

Note that the term defined in Eq.(A.11) is not a pure ND parameter and it carries units. For this it is better defined as a "corrected-variable" and is symbolized with an asterisk (*) to differentiate it from the true ND variable in Eq.(A.10).

From the second equation in Eq.(A.4), one can extract the following set of equations (Eq.(A.12)) to yield the second ND (Eq.(A.13),(A.14)) and corrected variable (Eq.(A.15)) by following the same procedure presented above for π_1.

$$\left.\begin{cases} [M]: a_2 = 0 \\ [L]: -a_2 + 2b_2 + 2c_2 = 0 \\ [T]: -2a_2 - 2b_2 - 1 = 0 \end{cases}\right\} \Rightarrow \begin{pmatrix} 1 & 0 & 0 \\ -1 & 2 & 2 \\ -2 & -2 & 0 \end{pmatrix} \begin{pmatrix} a_2 \\ b_2 \\ c_2 \end{pmatrix} = \begin{pmatrix} 0 \\ 0 \\ 1 \end{pmatrix} \Rightarrow \begin{pmatrix} a_2 \\ b_2 \\ c_2 \end{pmatrix} = \begin{pmatrix} 0 \\ -1/2 \\ 1/2 \end{pmatrix} \tag{A.12}$$

$$\pi_2 \equiv \left(P_a\right)^{a_2}\left(T_a\right)^{b_2}\left(Ae\right)^{c_2}\left(Ng\right)=\left(P_a\right)^{0}\left(T_a\right)^{-1/2}\left(Ae\right)^{1/2}\left(Ng\right)=\frac{Ng}{\sqrt{T_a}}\sqrt{Ae} \tag{A.13}$$

$$\pi_2=\frac{Ng}{\sqrt{\theta}}\cdot\sqrt{\frac{Ae}{T_0}}=\frac{Ng}{\sqrt{\theta}}\cdot K_2 \tag{A.14}$$

$$\pi_2^*=\frac{Ng}{\sqrt{\theta}} \tag{A.15}$$

From the third equation in Eq.(A.4), one can extract the following set of equations (Eq.(A.16)) to yield the third ND (Eq.(A.17),(A.18)) and corrected variable (Eq.(A.19)) by following the same procedure presented above for π_1, π_2.

$$\left.\begin{cases}\left[M\right]: a_3=0\\ \left[L\right]: -a_3+2b_3+2c_3+2=0\\ \left[T\right]: -2a_3-2b_3-2=0\end{cases}\right\}\Rightarrow\begin{pmatrix}1&0&0\\-1&2&2\\-2&-2&0\end{pmatrix}\begin{pmatrix}a_3\\b_3\\c_3\end{pmatrix}=\begin{pmatrix}0\\-2\\2\end{pmatrix}\quad\Rightarrow\begin{pmatrix}a_3\\b_3\\c_3\end{pmatrix}=\begin{pmatrix}0\\-1\\0\end{pmatrix} \tag{A.16}$$

$$\pi_3 \equiv \left(P_a\right)^{a_3}\left(T_a\right)^{b_3}\left(Ae\right)^{c_3}\left(TGT\right)=\left(P_a\right)^{0}\left(T_a\right)^{-1}\left(Ae\right)^{0}\left(TGT\right)=\frac{TGT}{T_a} \tag{A.17}$$

$$\pi_3=\frac{TGT}{\theta}\frac{1}{T_0}=\frac{TGT}{\theta}\cdot K_3 \tag{A.18}$$

$$\pi_3^*=\frac{TGT}{\theta} \tag{A.19}$$

From the fourth equation in Eq.(A.4), one can extract the following set of equations (Eq.(A.20)) to yield the third ND (Eq.(A.21),(A.22)) and corrected variable (Eq.(A.23)) by following the same procedure presented above for π_1, π_2 and π_3.

$$\left.\begin{array}{l}[M]: a_4 + 1 = 0 \\ [L]: -a_4 + 2b_4 + 2c_4 + 1 = 0 \\ [T]: -2a_4 - 2b_4 - 3 = 0\end{array}\right\} \Rightarrow \begin{pmatrix} 1 & 0 & 0 \\ -1 & 2 & 2 \\ -2 & -2 & 0 \end{pmatrix}\begin{pmatrix} a_4 \\ b_4 \\ c_4 \end{pmatrix} = \begin{pmatrix} -1 \\ -1 \\ 3 \end{pmatrix} \Rightarrow \begin{pmatrix} a_4 \\ b_4 \\ c_4 \end{pmatrix} = \begin{pmatrix} -1 \\ -1/2 \\ -1/2 \end{pmatrix} \quad \text{(A.20)}$$

$$\pi_4 \equiv (P_a)^{a_4} (T_a)^{b_4} (Ae)^{c_4} (W_f) = (P_a)^{-1} (T_a)^{-1/2} (Ae)^{-1/2} (W_f) = \frac{W_f}{P_a\sqrt{T_a}} \frac{1}{\sqrt{Ae}} \quad \text{(A.21)}$$

$$\pi_4 = \frac{W_f}{\delta\sqrt{\theta}} \cdot \frac{1}{P_o\sqrt{T_o Ae}} = \frac{W_f}{\delta\sqrt{\theta}} \cdot K_4 \quad \text{(A.22)}$$

$$\pi_4^* = \frac{W_f}{\delta\sqrt{\theta}} \quad \text{(A.23)}$$

Finally, Eq.(A.2) can be rewritten in its corrected form (ND for a specific engine) as in Eq.(A.24). The gas-turbine engine output power problem is now reduced to be a function of only four corrected variables, π_1*, π_2*, π_3* and π_4*. Another way to present Eq.(A.24) is in its explicit form as Eq.(A.25). The corrected output power of the engine is a function of three corrected variables i.e., the corrected compressor speed, the corrected engine temperature and the corrected engine fuel flow.

$$f^*(\pi_1^*, \pi_2^*, \pi_3^*, \pi_4^*) = f^*\left(\frac{SHP}{\delta\sqrt{\theta}}, \frac{Ng}{\sqrt{\theta}}, \frac{TGT}{\theta}, \frac{W_f}{\delta\sqrt{\theta}}\right) = 0 \quad \text{(A.24)}$$

$$\pi_1^* = f^{**}(\pi_2^*, \pi_3^*, \pi_4^*) \rightarrow \frac{SHP}{\delta\sqrt{\theta}} = f^{**}\left(\frac{Ng}{\sqrt{\theta}}, \frac{TGT}{\theta}, \frac{W_f}{\delta\sqrt{\theta}}\right) \quad \text{(A.25)}$$

B. High Speed Approximation, 10K Ft., Standard Day

This appendix provides a graphical tool to assess the inaccuracy introduced by using Glauert's high-speed approximation, as compared to the CMIV under standard day conditions, 10K ft. pressure altitude. A similar graph for Standard Sea Level (SSL) conditions is presented in Chapter 2 (Subsection 2.2.1) as Fig. 2.12.

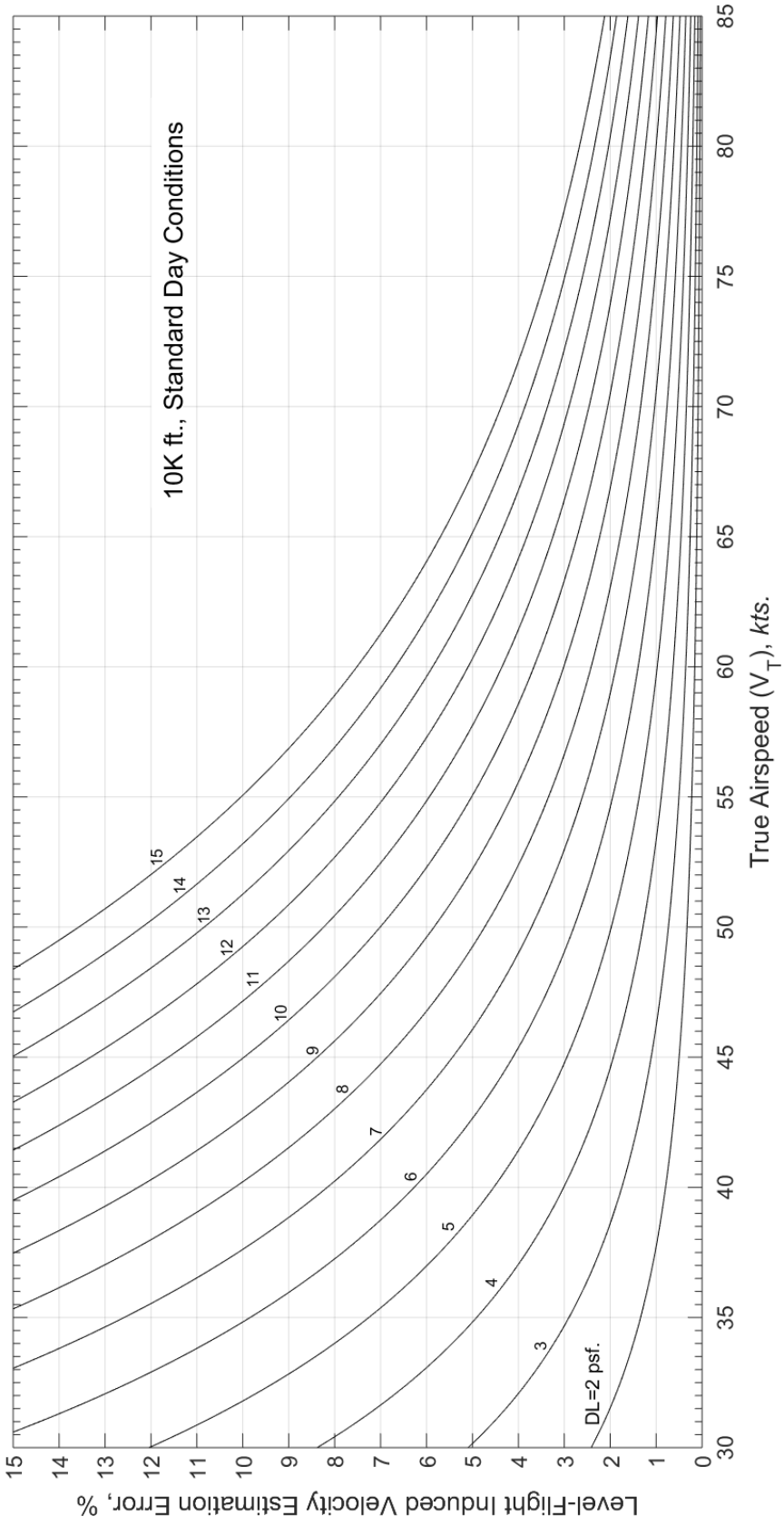
10K ft., Standard Day Conditions
DL=2 psf.
3
4
5
6
7
8
9
10
11
12
13
14
15
True Airspeed (V_T), *kts.*
Level-Flight Induced Velocity Estimation Error, %

C. Research Helicopters Description

This appendix provides a more detailed description of the two helicopters used for this research; the Bell Jet Ranger and the MBB BO-105 helicopters used for training at the National Test Pilot School (NTPS) in Mojave, California.

The Bell Jet-Ranger Helicopter

The Bell Jet-Ranger helicopter used for the research is a single-engine light observation helicopter, designed for day and night, visual flight rules (VFR) and instrument flight rules (IFR) operations. The helicopter is designed for landing and take-off from prepared or unprepared surfaces with a skid-type landing gear. The helicopter can be flown by a single pilot from the right-hand seat and has a place for three passengers in the back. The helicopter has an overall length of 12.5 m (main rotor fore to aft end of tail) and a maximum allowed take-off gross weight of 3,200 lbs. (1,452 kg.). The helicopter conforms to the definition of a 'conventional' helicopter, as it has a single main-rotor (M/R) and a single tail-rotor (T/R). The M/R assembly is a two-bladed, semi-rigid, teetering type also known as underslung feathering axis hub. The M/R rotates counter-clockwise, when viewed from above, at a standard angular speed of 354 RPM. An audio warning tone and a RPM warning light are designed to come on and alert the pilot when the M/R angular speed decreases below 335 RPM. The M/R blades are all metal and consist of extruded aluminium

alloy nose block and trailing edge, filled with aluminium honeycomb structure filler. The T/R configuration is two bladed teetering with 30° delta-three flapping hinge offset. The T/R is mounted on the left side of the tail-boom structure, and rotates with the bottom blade traveling forward. The T/R operates as a 'pusher' type, i.e., it generates an anti-torque force which pushes the tail structure of the helicopter to the right.

The helicopter is powered by a single Allison T63-A-720 gas-turbine engine, which is installed immediately behind the main transmission as shown in Fig. C.1. The engine uninstalled maximum output power is rated at 420 shaft horsepower (shp) under standard day, sea level conditions. Once installed in the Jet-Ranger helicopter, the engine performance is de-rated due to drivetrain limitations to a maximum output power of 317 hp (5 minutes take off rating limit) and of 270 hp (continuous operation). The dry weight of this engine is 158 lbs. The engine power is transmitted through a freewheeling unit to the main transmission, which drives both the main and the tail rotors. The freewheeling unit is designed to disconnect both rotors drive shafts from the engine, enabling rotation of the main and the tail rotors through the main transmission in case of an emergency engine-out auto-rotational descent. The maximum output power (take-off rating) is attained with a 100% engine indicated torque and 100% N2 (power turbine angular speed). The engine incorporates a compressor section with six axial stages followed by a centrifugal stage, a gas-turbine section with two axial stages and a two axial stages power-turbine. This engine configuration is of a reverse-flow annular type, for which the exhaust gases follow a reverse path to the compressor gasses, before passing through the turbine section.

Figure C.1. The Allison T63-A-720 gas turbine engine. This photo shows the engine, as installed on the Jet Ranger helicopter.

The output power of the engine is controlled by the turbine power governor through means of varying the amount of fuel that flows to the engine. The power turbine speed (N2) is selected by the pilot, and the output power required to maintain this speed is commanded by the power-turbine hydro-mechanical governor. With the throttle rotated to full-open position, the power-turbine governor works to maintain a constant N2 speed. Rotating the throttle towards the idle position causes the N2 speed to be manually selected, instead of automatically controlled. A droop-compensator unit, within the power-turbine governor, maintains a constant N2 speed as power demand is increased (or decreased) by main-rotor collective stick manipulation. This function is implemented through a mechanical linkage that connects between the collective stick to the speed selector lever on the N2 governor.

The dual flight controls of the helicopter (for the pilot and for another crew member) consist of mechanical type non reversible cyclic-stick, collective-stick, and reversible directional pedals to control the helicopter in yaw. Figure C.2 shows the pilot station (right-hand side) flight controls. The flight controls pass-on the pilot inputs to the three main-rotor hydraulic servo cylinders and to the tail-rotor forged

aluminium alloy yoke. An electrically operated mechanical unit provide cyclic stick force trim function which helps in providing artificial force gradient to the pilot and to hold the cyclic stick in place and prevent it from migrating due to vibrations and mass imbalance. The collective stick incorporate no means of 'trimming' capabilities besides a simple adjustable mechanical friction.

The helicopter features a rectangular fixed-position horizontal stabilizer. This stabilizer is mounted approximately at the middle of the tail-boom and has a span of 6 ft. and 5 inches (195.6 cm.) and a chord of 45cm. This rectangular shaped horizontal stabilizer (shown in Fig. C.3) is designed to generate a down force with forward airspeed. A fixed position vertical fin is located to the right of the tail-boom.

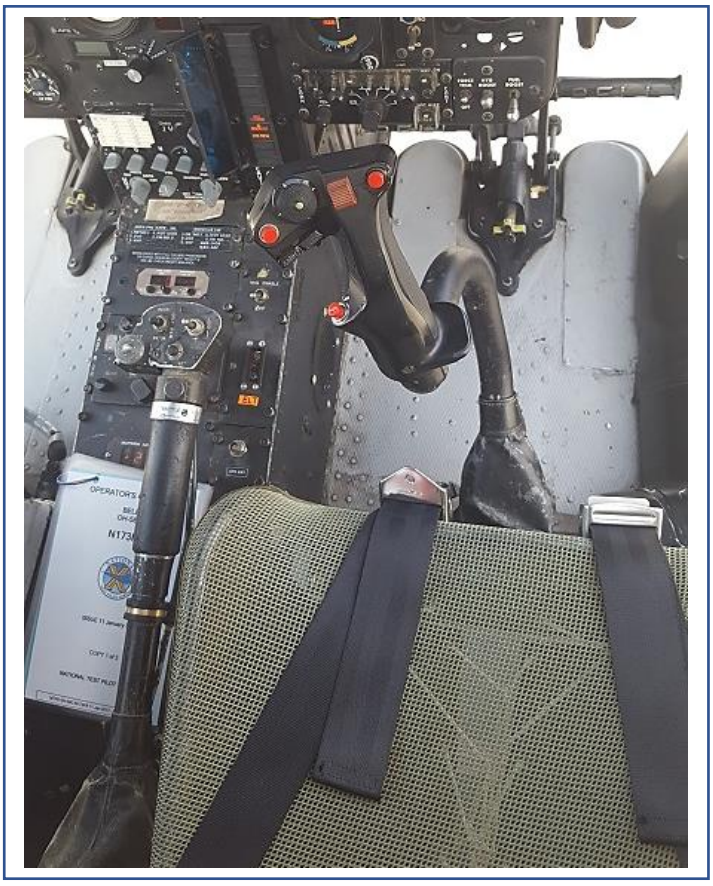

Figure C.2. The Jet-Ranger flight-controls. This photo shows the pilot seat (right-hand side) flight-controls; the cyclic-stick, the tail-rotor pedals (only the right pedals is shown) and the collective stick mounted to the left of the pilot seat.

The pitot-static system is used to measure airspeed, pressure-altitude and vertical rate of climb and descent. This system is made-up of two ports (static pressure ports) mounted on either side of the helicopter, forward of the pilot and the co-pilot doors, a single Pitot port mounted on the nose of the aircraft, plastic tubing and analogue instruments of (1) airspeed indicator (ASI), (2) altimeter and (3) vertical velocity indicator (VVI) all three located on the instrument panel as shown in Fig. C-4. The Pitot tube which is a heated type and is mounted approximately four inches to the right of the helicopter centreline. The static pressure is fed by means of plastic tubing to all three pneumatic analogue instruments. The total pressure is fed from the Pitot tube to the airspeed indicator only.

Figure C.3. The horizontal stabilizer. The horizontal stabilizer is designed to generate a down-loaded aerodynamic force in forward flight.

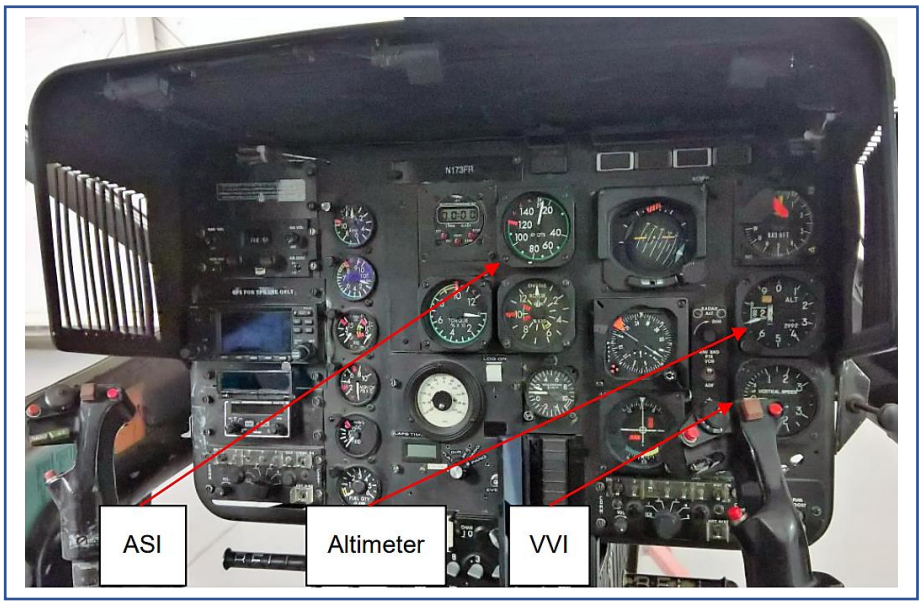

Figure C.4. The Jet-Ranger flight instruments fed by the Pitot system. The pneumatic flight instruments that present to the flight crew the airspeed (ASI), pressure altitude (Altimeter) and the vertical velocity (VVI).

The Jet-Ranger's important specifications pertaining to its performance are summarized in Table C.1.

Table C.1 – The Bell Jet Ranger performance specifications.

Parameter	Value
M/R (T/R) diameter [ft.]	35.3 (5.2)
M/R (T/R) standard angular speed (RPM)	354 (2,670)
M/R (T/R) number of blades (b)	2 (2)
M/R (T/R) blade chord [ft.]	1.08 (0.43)
M/R (T/R) solidity ratio (σ_R)	0.039 (0.105)
Take-off (continuous) power rating [hp.]	317 (270)
Take-off (continuous) max. TGT [°C]	810 (738)
Max. take-off gross weight [lbs.]	3,200
Never Exceed Airspeed, VNE [KCAS]	120

THE MBB BO-105 HELICOPTER

The Messerschmitt-Bölkow-Blohm (MBB) BO-105 helicopter used for the research is a dual-engine light observation and utility helicopter, designed for day and night, visual flight rules (VFR) and instrument flight rules (IFR) operations. The helicopter is designed for landing and take-off from prepared or unprepared surfaces with a skid-type landing gear. The helicopter can be flown by a single pilot from the right-hand seat and has a place for three passengers in the back. The helicopter has an overall length of 11.86 m (main rotor fore to aft end of tail) and a maximum allowed take-off gross weight of 5,512 lbs. (2,500 kg.). The helicopter conforms to the definition of a 'conventional' helicopter, as it has a single main-rotor (M/R) and a single tail-rotor (T/R). The M/R assembly is a four-bladed, hinge less, rigid type with an effective flapping offset of 14%. The M/R blades motion in flapping in lead/lagging was enabled through a flexible blade root. The M/R rotates counter-clockwise, when viewed from above, at a standard angular speed of 423 RPM. The M/R blades are constructed of fiberglass reinforced plastic with a NACA 23012 aerofoil and a geometric pitch angle twist of -8° between the root and the tip. As shown in Fig. C.5, each one of the four M/R blades is fitted with appended pendulum absorber ('pendab') designed to reduce the 4/rev. vertical vibration transferred to the fuselage. These pendabs are installed on the roots of the M/R blades, at about 16.2% of the blade length (M/R radius). The T/R configuration is a two-bladed semi-rigid, teetering with 45° delta-three flapping hinge offset. The tail-rotor is mounted on the left side of the tail-boom structure, and rotates at a standard 2,219 RPM with the bottom blade traveling forward. The tail-rotor operates as a 'pusher' type, i.e., it generates an anti-torque force which pushes the tail structure of the helicopter to the right.

Figure C.5. The main-rotor assembly of the BO-105 helicopter. Each one of the blade is fitted with a pendulum absorber designed to alleviate vertical vibrations.

The BO-105 helicopter is powered by two Allison 250-C20B gas-turbine engines, each with independent drive-train systems. These engines are very similar to the Bell Jet-Ranger gas-turbine engine. The maximum (uninstalled) output power of each engine is rated at 420 shaft horsepower under standard-day sea-level conditions. Due to drive-train limitations of the helicopter, each one of the 158 lbs. (dry) engines, is de-rated to a maximum output power of 400 hp (5 minutes take off rating limit) and of 344 hp (continuous operation). Each engine incorporates a compressor section with six axial stages followed by a centrifugal stage, a gas-turbine section with two axial stages and a two axial stages power-turbine. This engine configuration is of a reverse-flow annular type, for which the exhaust gases follow a reverse path to the compressor gasses, before passing through the turbine section

The dual flight controls of the helicopter (for the pilot and for another crew member) consist of mechanical type non-reversible cyclic-stick, collective-stick, and reversible directional pedals to control the helicopter in yaw. The helicopter is equipped with a dual-redundant, 103 bar hydraulic power supply system that is used

to boost the cyclic-stick and the collective stick controls. The T/R pedals are not hydraulically boosted. The helicopter features a trim-system designed to provide artificial cyclic-stick force gradient and to reduce opposing control forces to zero. This is activated by a four-way switch located on top of the cyclic stick grip.

The airframe consists of the fuselage, the cabin and the cargo compartment. The fuselage is a conventional "semi-monocoque" structure. The floor of the helicopter runs through both the cabin and the cargo compartment at the same level. The engines deck forms the roof of the cargo compartment and acts as a firewall for the engines. The engines deck also provides mounting for the main transmission, the two engines and the dual-redundant hydraulic boost system. The two cabin doors are sliding doors which allow them to be opened during flight. As shown in Fig. C.6, access to the cargo compartment is via two clam-shell doors, opening sideways at the rear end of the fuselage. The aft fuselage incorporates a spoiler designed to assist in increasing stability by imposing a flow separation over the clamshell doors.

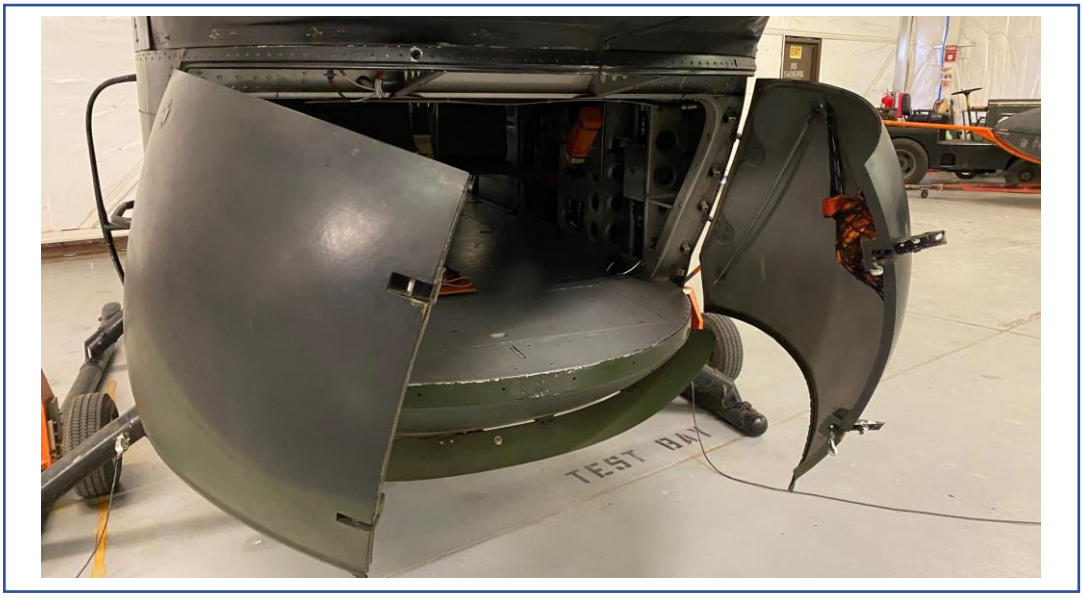

Figure C.6. The rear end of the BO-105 fuselage. Access to the cargo compartment in via two clamshell doors.

The BO-105 helicopter incorporates a horizontal stabilizer with vertical endplates installed symmetrically on both sides of the tail boom as shown in Fig. C.7. The horizontal stabilizer has a span of 2.5 m with an aspect ratio of 5.2 and extends beyond the maximum width of the fuselage.

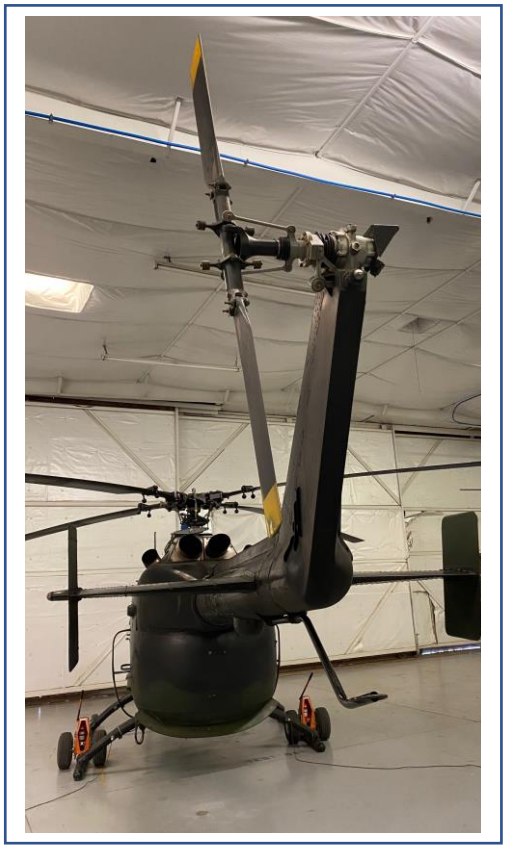

Figure C.7. The tail section of the BO-105 helicopter. The 2.5 m span horizontal stabilizer extends beyond the fuselage width.

The pitot-static system is used for measuring airspeed, pressure-altitude and vertical rate of climb and descent. This system is made-up of two static ports mounted on either side of the helicopter, below the pilot and the co-pilot doors, a single Pitot port mounted in proximity and below the right static port, plastic tubing and analogue instruments of airspeed indicator, altimeter and vertical velocity indicator located on the instrument panel (see Fig. C.8). The BO-105 helicopter basic specifications pertaining to its performance are summarized in Table C.2.

Table C.2 – The MBB BO-105 performance specifications.

Parameter	Value
M/R (T/R) diameter [ft.]	32.3 (6.28)
M/R (T/R) standard angular speed (RPM)	423 (2,219)
M/R (T/R) number of blades (b)	4 (2)
M/R (T/R) blade chord [ft.]	0.86 (0.59)
M/R (T/R) solidity ratio (σ_R)	0.07 (0.12)
Take-off (continuous) power rating [hp.]	800 (688)
Take-off (continuous) max. TGT [°C]	810 (738)
Max. take-off gross weight [lbs.]	5,512
Never Exceed Airspeed, VNE [KCAS]	145

Figure C.8. The BO-105 Instrument Panel. The pneumatic flight instruments are located first from the right (pressure altitude on the top row and vertical rate of climb/descent on the bottom). The airspeed indicator is located on the top row, third from the right.

REFERENCES

[1] Pavlok, K. M., Flight Test Engineering, Edwards California: NASA Dryden [Armstrong] Flight Research Center, NASA Report #DRFC-E-DAA-TN11035, September 19, 2013

[2] Knoth, Florian, and Christian Breitsamter. "Aerodynamic Testing of Helicopter Side Intake Retrofit Modifications." *Aerospace* 4, no. 3 (2017): 33–33. https://doi.org/10.3390/aerospace4030033.

[3] M. Nowakowski. 2011. "Flight Tests of Upgraded Helicopters." *Journal of Kones* 18 (4): 317–24.

[4] Flemming, Robert J, Kimberly W Hanks, M. Lynn Hanks, 2007 SAE Aircraft and Engine Icing International Conference Seville, Spain 2007-09-24. "US Army UH-60M Helicopter Main Rotor Ice Protection System." *SAE Technical Paper* (20070924) (2007). https://doi.org/10.4271/2007-01-3301

[5] M. Wojtas, Ł. Czajkowski, and A. Sobieszek. "The Influence of the Blades Leading Edge Anti-Erosion Protection on Main Rotor Performances." *Journal of Kones* 25, no. 2 (2018). https://doi.org/10.5604/01.3001.0012.2866.

[6] Buckanin, R.M. et. al., 'Level Flight Performance Evaluation of the UH-60A Helicopter with the Production External Stores Support System and Ferry Tanks

Installed', US Army Aviation Engineering Flight Activity, Project 86-01, September 1986.

[7] (ASA), Federal Aviation Administration (FAA)/Aviation Supplies & Academics. 2016. *Pilot's Handbook of Aeronautical Knowledge: FAA-H-8083-25b*. FAA Handbooks Series. Newcastle: Aviation Supplies and Academics.

[8] Prouty RW. *Helicopter Performance, Stability, and Control*. Boston: PWS Engineering; 1986, Chapter 4, "Performance Analysis".

[9] Gessow A., Myers GC, Aerodynamics *of the Helicopter*. Third printing, Frederick Ungar Publishing Company, New York, 1967, Chapter 4, "Hovering and Vertical Flight Performance Analyses".

[10] Leishman JG. *Principles of Helicopter Aerodynamics*. 2nd ed. Cambridge: Cambridge University Press; 2006, Chapter 5, "Helicopter Performance".

[11] Anonymous "Sikorsky Introduces 'Project Firefly(TM)' Electric Helicopter Demonstrator," *PR Newswire,* 2010. Available: https://www.proquest.com/wire-feeds/sikorsky-introduces-project-firefly-tm-electric/docview/613400680/se-2?accountid=27026.

[12] Moon K, et al. "A Comparative Statistical Analysis of Global Trends in Civil Helicopter Accidents in the U.S., the EU, and the CIS." *Iop Conference Series: Materials Science and Engineering*, vol. 868, no. 1, 2020, doi:10.1088/1757-899X/868/1/012020.

[13] Turczeniuk, Bohdan. 1982. "Exhaust Gas Reingestion Measurements." *Journal of the American Helicopter Society* 27 (3): 4–10. https://doi.org/10.4050/JAHS.27.4.

[14] Jackson, Michael E, and Richard L House. 1982. "Exhaust Gas Reingestion during Hover in-Ground-Effect." *Journal of the American Helicopter Society* 27 (3): 74–79. https://doi.org/10.4050/JAHS.27.3.74.

[15] Taslim, M. E, and S Spring. 2010. "A Numerical Study of Sand Particle Distribution, Density, and Shape Effects on the Scavenge Efficiency of Engine Inlet Particle Separator Systems." *Journal of the American Helicopter Society* 55 (2): 22006–220069. https://doi.org/10.4050/JAHS.55.022006.

[16] M. Paszko. 2017. "Infrared Signature Suppression Systems in Modern Military Helicopters." *Prace Instytutu Lotnictwa* 3 (248).

[17] Nidhi Baranwal, and Shripad P. Mahulikar. "Review of Infrared Signature Suppression Systems Using Optical Blocking Method." *Defence Technology* 15, no. 3: 432–39. Accessed July 31, 2022.

[18] Cooke AK, and Fitzpatrick EWH., Helicopter Test and Evaluation, 1st ed. AIAA Education Series, Wright Patterson Air Force Base, Ohio, USA, 2002.

[19] National Test Pilot School, Professional Course Textbook Series, Chapter 5, Vol. VII, Rotary Wing Performance Flight Testing, Mojave, 2017.

[20] U.S. Naval Test Pilot School, Flight Test Manual No. 106, Rotary Wing Performance, Naval Air Warfare Center, Patuxent River, Maryland, USA, 1996.

[21] US Army Material Command (AMC), Engineering Design Handbook, Helicopter Performance Testing, AMCP 706-204, August 1974.

[22] Leishman, J. G., *Principles of Helicopter Aerodynamics*, 2nd ed., Cambridge University Press, 2006, Chapter 1, "Introduction- A History of Helicopter Flight".

[23] Gessow A, and Myers G., *Aerodynamics of the Helicopter*, Third printing, Frederick Ungar Publishing Company, New York, 1967, Chapter 1, "The Development of Rotating-Wing Aircraft".

[24] Richards RB, Naval Test Pilot School Textbook, USNTPS-T-No.1, Principles of Helicopter Performance, Naval Air Test Center, Patuxent River, Maryland, USA, 1968.

[25] Lewicki D. G., Coy J. J., "Helicopter Transmission Testing at NASA Lewis Research Center", NASA Technical Memorandum 89912, US Army Aviation Research and Technology Activity, AVSCOM Technical Report 87-C-10, Lewis Research Center, Cleveland, Ohio, June 1987.

[26] Coy J. J., Townsend D. P. et al., "Helicopter Transmission Testing at NASA Lewis Research Center", NASA Technical Memorandum 100962, US Army Aviation Research and Technology Activity, AVSCOM Technical Report 88-C-003, Lewis Research Center, Cleveland, Ohio, November 1988.

[27] Rankine, W. J. M. 1865. "On the Mechanical Principles of the Action of Propellers", Transactions of the institute of Naval Architects, 6, pp. 13-39.

[28] Froude, W. 1878. "On the Elementary Relation between Pitch, Slip and Propulsive Efficiency", Transactions of the institute of Naval Architects, 19, pp. 47-57.

[29] Glauert, H. 1935. "Airplane Propellers", in division L of Aerodynamic Theory, edited by W. F. Durand, Springer Verlag, Berlin Germany. Reprinted by Peter Smith, Glouster, MA, 1976.

[30] Prandtl, L., "Applications of Modern Hydrodynamics to Aeronautics", NACA 116, June 1921.

[31] Gessow, Alfred, Langley Aeronautical Laboratory, and United States. National Advisory Committee for Aeronautics. 1948. Effect of Rotor-Blade Twist and Plan-Form Taper on Helicopter Hovering Performance. National Advisory Committee for

Aeronautics Technical Note, 1542. Washington, D.C.: National Advisory Committee for Aeronautics. https://digital.library.unt.edu/ark:/67531/metadc54535.

[32] Prouty RW. *Helicopter Performance, Stability, and Control*. Boston: PWS Engineering; 1986. Chapter 10, "Preliminary Design".

[33] Prouty RW. *Helicopter Performance, Stability, and Control*. Boston: PWS Engineering; 1986. Chapter 1, "Aerodynamics of Hovering Flight".

[34] Leishman, J. G., *Principles of Helicopter Aerodynamics*, 2nd ed., Cambridge University Press, 2006, Chap. 2, "Fundamentals of Rotor Aerodynamics".

[35] Gessow A, and Myers G., *Aerodynamics of the Helicopter*, Third printing, Frederick Ungar Publishing Company, New York, 1967, Chapter 3, "An Introduction to Hovering Theory".

[36] Shahmiri, Farid, Maryam Sargolzehi, and Mohammad Ali Shahi Ashtiani. "Systematic Evaluation of the Helicopter Rotor Blades: Design Variables and Interactions." *Aircraft Engineering and Aerospace Technology* 91, no. 9 (2019): 1223–37. https://doi.org/10.1108/AEAT-06-2018-0163.

[37] Harris, Franklin D, and Michael A McVeigh. "Uniform Downwash with Rotors Having a Finite Number of Blades." *Journal of the American Helicopter Society* 21, no. 1 (1976): 9–20. https://doi.org/10.4050/JAHS.21.9.

[38] Carpenter, Paul J. *Lift and Profile-Drag Characteristics of an Naca 0012 Airfoil Section As Derived from Measured Helicopter-Rotor Hovering Performance*. National Advisory Committee for Aeronautics Technical Note, 4347. Washington: NACA, 1958.

[39] Boatwright, "Measurements of Velocity Components in the Wake of a Full-Scale Helicopter Rotor in Hover", United States Army Air Mobility Research and Development Laboratories (AMRDL), Technical Report 72-33, 1972.

[40] Cheeseman, I.C. and Bennett, W.E. *The Effect of the Ground on a Helicopter Rotor in Forward Flight*. A.A.E.E. Report Ray./288 3021, Aeronautical Research Council (1955).

[41] Hayden, J.S., The effect of the ground on helicopter hovering power required. In, proceedings of the American Helicopter Society, 32nd annual forum, 1976.

[42] Kutz, Benjamin M, Manuel Keßler, and Kraïmer Ewald. "Experimental and Numerical Examination of a Helicopter Hovering in Ground Effect." *Ceas Aeronautical Journal: An Official Journal of the Council of European Aerospace Societies* 4, no. 4 (2013): 397–408. https://doi.org/10.1007/s13272-013-0084-x.

[43] Griffiths, Daniel A, Shreyas Ananthan, and J. Gordon Leishman. "Predictions of Rotor Performance in Ground Effect Using a Free-Vortex Wake Model." *Journal of the American Helicopter Society* 50, no. 4 (2005): 302–14. https://doi.org/10.4050/1.3092867.

[44] Porterfield, J. D., and Alexander W. T., "Measurements and Evaluation of Helicopter Flight Loads Spectra Data", Journal of the American Helicopter Society, Vol. 15, Number 3, 1 July 1970, pp. 22-34(13).

[45] U.S. Department of Transportation, Federal Aviation Administration, Certification of Normal Category Rotorcraft, AC 27-1B, Change 3, Subpart C, Strength Requirements, AC 27.571, September 2008.

[46] Glauert, H., "On the Horizontal Flight of a Helicopter", Aeronautical Research Committee, Reports & Memoranda 1157, 1928.

[47] Prouty RW. *Helicopter Performance, Stability, and Control*. Boston: PWS Engineering; 1986, Chapter 3, "Aerodynamics of Forward Flight".

[48] Vil'dgrube, L.S, Vozhdayev Y.S, and National Aeronautics and Space Administration. Vertol Division. 1976. *Theory of the Lifting Airscrew*. NASA Technical Translation, F-823. Washington: NASA.

[49] Stepniewski, W.Z., and Keys, C.N., Rotary Wing Aerodynamics, Two Volumes Bounded as One, Dover Publication Inc., New York, 1984, Chapter 3,"Blade Element Theory- Forward Flight".

[50] Leishman JG. *Principles of Helicopter Aerodynamics*. 2nd ed. Cambridge: Cambridge University Press; 2006. Chapter 6, "Aerodynamic Design of Helicopters".

[51] Noonan KW and Bingman GJ, Two-Dimensional Aerodynamic Characteristics of Several Rotorcraft Airfoils at Mach Numbers from 0.35 to 0.9, NASA TM X-73990, Langley Research Center, Virginia, January 1977.

[52] McCloud, John L, James C Biggers, Robert H Stroub, and National Aeronautics and Space Administration. *An Investigation of Full-Scale Helicopter Rotors at High Advance Ratios and Advancing Tip Mach Numbers*. Nasa Technical Note, D-4632. Washington: NASA, 1968

[53] Caradonna, Franck X, Jean-Jacques Philippe, "*The Flow Over a Helicopter Blade Tip in the Transonic Regime",* Proceedings of the 2nd European Rotorcraft and Powered Lift Aircraft Forum, Buckeburg, Germany, 1976.

[54] Paul, William F. "A Self-Excited Rotor Blade Oscillation at High Subsonic Mach Numbers." Journal of the American Helicopter Society 14, no. 1 (1969): 38–48. https://doi.org/10.4050/JAHS.14.1.38.

[55] Abbott, Ira H, and Abert E Von Doenhoff. 1999. Theory of Wing Sections: Including a Summary of Airfoil Data. Mineola: Dover Publications.

[56] Thwaites, Bryan, ed. Incompressible Aerodynamics: An Account of the Theory and Observation of the Steady Flow of Incompressible Fluid Past Aerofoils, Wings, and Other Bodies. Fluid Motion Memoirs. Oxford: Clarendon Press, 1960.

[57] McCroskey, W. J, K. W McAlister, L. W Carr, S. L Pucci, O Lambert, and R. F Indergrand. "Dynamic Stall on Advanced Airfoil Sections." Journal of the American Helicopter Society 26, no. 3 (1981): 40–50. https://doi.org/10.4050/JAHS.26.40.

[58] Carr, Lawrence W, Kenneth W Mcalister, and William J McCroskey. Analysis of the Development of Dynamic Stall Based on Oscillating Airfoil Experiments. NASA Technical Note, D-8382. Washington: NASA, 1977.

[59] Martin, J. M, R. W Empey, W. J McCroskey, and F. X Caradonna. "An Experimental Analysis of Dynamic Stall on an Oscillating Airfoil." Journal of the American Helicopter Society 19, no. 1 (1974): 26–32. https://doi.org/10.4050/JAHS.19.26.

[60] Merz, Christoph B, et al. "New Results in Numerical and Experimental Fluid Mechanics X : Contributions to the 19th Stab/Dglr Symposium Munich, Germany, 2014." *Experimental Investigation of Dynamic Stall on a Pitching Rotor Blade Tip*, Cham: Springer International Publishing: Springer, 2016, pp. 339–348.

[61] Johnson, Wayne, and Norman D Ham. "On the Mechanism of Dynamic Stall." *Journal of the American Helicopter Society*, vol. 17, no. 4, 1972, pp. 36–45., https://doi.org/10.4050/JAHS.17.36.

[62] Dommasch, D.O., Sherby S.S. and Connoly T.F., "Airplane Aerodynamics", Fourth Edition, Pitman Publishing Corporation, 1967. Chapter 2, "Fundamental Dynamics, and Thermodynamics of Air".

[63] Rosenstein, H., Stanzione, K. 1981. "Computer-Aided Helicopter Design", 37th Annual Forum of the American Helicopter Society, Washington D.C., May 17-20.

[64] Sheehy, Thomas W. 1977. "A General Review of Helicopter Rotor Hub Drag Data." *Journal of the American Helicopter Society* 22 (2): pp. 2–10. https://doi.org/10.4050/JAHS.22.2.2.

[65] Arnold, J.R, and Skinner, G.L. '*Army Preliminary Evaluation YOH-58A Helicopter with a Flat-Plate Canopy: Final Report',* US Army Aviation Engineering Flight Activity, Project 75-20, December 1975.

[66] Buckingham, E., "On Physically Similar Systems; Illustrations of the Use of Dimensional Equations", Physical Review, Vol IV, No. 4, 1914, pp. 345 – 376, doi:10.1103/PhysRev.4.345.

[67] Evans, HJ, "Dimensional Analysis and the Buckingham PI Theorem", American Journal of Physics 40, 1815 (1972); doi: 10.1119/1.1987069.

[68] Gratton, J, "Applying Dimensional Analysis to Wave Dispersion", American Journal of Physics 75, 158 (2007); doi: 10.1119/1.2372471.

[69] Jensen, JH, "Introducing Fluid Dynamics using Dimensional Analysis", American Journal of Physics 81, 688 (2013); doi: 10.1119/1.4813064.

[70] Robinett, RW, "Dimensional Analysis as the other Language of Physics", American Journal of Physics 83, 353 (2015); doi: 10.1119/1.4902882.

[71] G. Maheedhara Reddy, V. Diwakar Reddy, Theoretical Investigations on Dimensional Analysis of Ball Bearing Parameters by Using Buckingham Pi-Theorem, Procedia Engineering, Volume 97, 2014, Pages 1305-1311,ISSN 1877-7058, https://doi.org/10.1016/j.proeng.2014.12.410.

[72] Lawal, Abiodun Ismail, Seun Isaiah Olajuyi, Sangki Kwon, and Moshood Onifade. 2021. "A Comparative Application of the Buckingham Π (Pi) Theorem, White-Box Ann, Gene Expression Programming, and Multilinear Regression Approaches for Blast-Induced Ground Vibration Prediction." Arabian Journal of Geosciences 14 (12). https://doi.org/10.1007/s12517-021-07391-x.

[73] Knowles, P. *The Application of Non-dimensional Methods to the Planning of Helicopter Performance Flight Trials and Analysis Results,* Aeronautical Research Council ARC CP 927, 1967.

[74] Zohuri B, *Dimensional Analysis beyond the Pi Theorem*, Chap. 1, Cham, Switzerland: Springer; 2017. doi:10.1007/978-3-319-45726-0.

[75] Jackson ME, House RL. Exhaust gas reingestion during hover in-ground-effect. *Journal of the American helicopter society*. 1982;27(3):74-79. doi:10.4050/JAHS.27.3.74.

[76] U.S. Naval Test Pilot School, Flight Test Manual No. 106, Rotary Wing Performance, Chapter 7, Naval Air Warfare Center, Patuxent River, Maryland, USA, 1996.

[77] Nagata JI, Piotrowski JL, Young CJ, et al. Baseline Performance Verification of the 12th Year Production UH-60A Black Hawk Helicopter. Final Report, US Army Aviation Engineering Flight Activity, Edwards AFB, California, USA, January 1989.

[78] Belte D, Stratton MV. Fuel Conservation Evaluation of U.S. Army Helicopters, Part 4, OH-58C Flight Testing. Final Report, US Army Aviation Engineering Flight Activity, Edwards AFB, California, USA, August 1982.

[79] Advisory Group for Aerospace Research & Development (AGARD), *Flight Test Techniques Series*. Vol 14 on Introduction to Flight Test Engineering. AGARD-AG-300, September 1995.

[80] Ulbrich, N., Regression Model Optimization for the Analysis of Experimental Data, AIAA 2009–1344, paper presented at the 47th AIAA Aerospace Sciences Meeting and Exhibit, Orlando, Florida, January 2009.

[81] Ulbrich, N., Optimization of Regression Models of Experimental Data using Confirmation Points, AIAA 2010–930, paper presented at the 48th AIAA Aerospace Sciences Meeting and Exhibit, Orlando, Florida, January 2010.

[82] Zhao, D. and Xue, D., A multi-surrogate approximation method for metamodeling, Engineering with Computers, Vol. 27, No. 2, pp. 139-153, 2011.

[83] Strang, G., Introduction to Linear Algebra, 5th ed., Wellesley-Cambridge Press, Wellesley MA, 2016, Chap. 4.

[84] Guttman, I., Wilks, S., and Hunter, J., Introductory Engineering Statistics, 2nd ed., John Wiley & Sons, Inc., New York, 1971, Chap. 10, 'Statistical Tests'.

[85] Singiresu, R., Engineering Optimization Theory and Practice, 4th ed., John Wiley & Sons, Inc., New Jersey, 2009, Chap. 2.

[86] Benson TP, Buckanin RM, Mittag CF, et al. Evaluation of a OH-58A Helicopter with an Allison 250 C-20B Engine. Final Report, US Army Aviation Engineering Flight Activity, Edwards AFB, California, USA, April 1975.

[87] Kreyszig E. Advanced Engineering Mathematics, 3rd ed., John Wiley & Sons, Inc., New York, 1972, Chap. 19.

[88] Strang, G. Introduction to Linear Algebra, 4th ed., Belmont, CA: Thomson Brooks/Cole, 2006, Chap. 6.

[89] Gomez A, Arantes J, De Andrade D, et al. Helicopter Engine Performance Determination using Analysis of Variance. In: AHS 71st Annual Forum, Virginia Beach, Virginia, USA, May 5-7 2015.

[90] MacMillan WL. Development of a modular-type computer program for the calculation of gas-turbine of design performance, Ph.D. Dissertation, School of Engineering, Cranfield University, Cranfield, Bedford, 1974.

[91] Goulos I, Giannakakis P, Pachidis V. et al. Mission Performance Simulation of Integrated Helicopter-Engine Systems using an Aeroelastic Rotor Model, Journal of Engineering for Gas Turbines and Power, Volume 135, September 2013, Vol. 135.

[92] Heng W, Shufan Z, Jijun Z, et al. Gas Turbine Power Calculation Method of Turboshaft based on Simulation and Performance Model, MATEC Web of Conferences 189, 02003, 2018. DOI:10.1051/matecconf/201818902003.

[93] Zhang C, Gummer V. The potential of helicopter turboshaft engines incorporating highly effective recuperators under various flight conditions. Aerospace Science and Technology, 6 March 2019. http://doi.org/10.1016/j.ast.2019.03.008.

[94] Savelle SA, Garrard GD. Application of transient and dynamic simulations to the US Army T55-L-712 helicopter engine. In: International Gas Turbine and Aeroengine Congress and Exhibition, Birmingham, UK, June 10-13 1996.

[95] Yeo H, Bousman WG and Johnson W. Performance analysis of a utility helicopter with standard and advanced rotors. In: AHS Aerodynamics, Acoustics and Test and

Evaluation Technical Specialist Meeting, San Francisco, California, USA, January 23 – 25 2002.

[96] Bousman, W. G., "Out-of-Ground Effect Hover Performance of the UH-60A", UH-60A Airloads Program Occasional Note 2001-01, US Army Aeroflight dynamics Directorate (AMCOM) Ames Research Center, February 2001.

[97] Siva, C., Murugan, M. S., Ganguli, R., "Uncertainty Qualification in Helicopter Performance Using Monte Carlo Simulations", Journal of Aircraft, Vol. 48, No. 5, 2011, pp. 1503-1511, DOI: 10.2514/1.C000288.

[98] Jacobson, K. E., Smith, M., J., "Carefree Hybrid Methodology for Rotor Hover Performance Analysis", Journal of Aircraft, Vol. 55, No. 1, 2018, pp. 52-65, DOI: 10.2514/1.C034112.

[99] Garcia, A. J., Barakos, G., N., "Accurate Predictions of Rotor Hover Performance at Low and High Disc Loadings", Journal of Aircraft, Vol. 55, No. 1, 2018, pp. 89-110, DOI: 10.2514/1.C034144.

[100] Matayoshi, N., Asaka, K., Okuno, Y., "Flight-Test Evaluation of a Helicopter Airborne Lidar", Journal of Aircraft, Vol. 44, No. 5, 2007, pp. 1712-1720, DOI: 10.2514/1.28338.

[101] Boirun, B. H., "Generalizing Helicopter Flight Test Performance Data (GENFLT), The 34th Annual National Forum of the American Helicopter Society, May 1978.

[102] Abraham, M., Costello, M., "In-Flight Estimation of Helicopter Gross Weight and Mass Center Location", Journal of Aircraft, Vol. 46, No. 3, 2009, pp. 1042-1049, DOI: 10.2514/1.41018.

[103] Scmitz S., Bhagwat M., Moulton M. A., et al. The Prediction and Validation of Hover Performance and Detailed Blade Loads, Journal of the American Helicopter Society 54, 032004, May 2009.

[104] Wang, Q., and Zaho Q., Rotor aerodynamic shape design for improving performance of an unmanned helicopter. Aerospace Science and Technology, 3 March 2019, DOI: 10.1016/j.ast.2019.03.006.

[105] Peterson, R. L., and Warmbrodt, W., Hover Performance and Dynamics of a Full-Scale Hingeless Rotor. In: The Tenth European Rotorcraft Forum, The Hague, The Netherlands, August 1984.

[106] Horn, RA., and Johnson CR., Matrix Analysis, 2nd edition, Cambridge University Press, New York, NY, 2012, Chap. 5.

ACKNOWLEDGEMENTS

In April 2010, I started to work at the National Test Pilot School (NTPS) in Mojave, California as a rotary wing flight test engineer instructor. I would like to thank Mr. Sean C. Roberts (RIP) for offering me this position and giving me the privilege of educating and training many remarkable individuals who belong to the international community of flight-testers. The idea of pursuing a Ph.D. research in the field of helicopter performance flight testing has been a goal of mine for several years and became a reality in February of 2018. I would like to thank Dr. Lester Ingham who together with Dr. Marilena Pavel made this Ph.D. research possible as a collaboration between the NTPS and TU Delft.

Many scholars have already said before, that you never really know something until you teach it to someone else. To all my past and future students, thank you for everything you taught me so far, and for the things you are about to teach me in the future. Spending valuable time with you in class and in the air fills me with scholastic satisfaction and a sense of fulfilment. Thanks to you, I have found my own fountain of youth. A special appreciation goes to test pilot Stefan Hanekom, an NTPS class of 2011 student member who became an instructor colleague and a true friend in 2016. Thank you Stefan for your support in flying data points during this Ph.D. research. It has been great working with you and I hope our professional paths merge again in the future.

I wish to extend my gratitude and appreciation to my two extraordinary promotors, Dr. Marilena Pavel and Professor Max Mulder. When I started the Ph.D. research, Marilena resided in California, just a few miles away from me. Frequent meetings took place in the neighbourhood 'Starbucks' where fruitful professional discussions were accomplished and resolutions were made. The first paper was written and the frame for the second one was laid down. Those were the early days that built

a strong foundation which allowed for the continuation of the research, following Marilena's return to the Netherlands. The in-person meetings were replaced with coffee-less Skype conferences. Thank you Marilena for your intelligent and compassionate guidance throughout this research. You have always practiced one of Newton's famous quotes: 'Tact is making a point without making an enemy'. My first in-person encounter with Professor Max Mulder took place in September 2018, while I came to present a paper during the European Rotorcraft Forum that took place in TU Delft. I met an impressive professor who listens to you very carefully, quickly processes the information, and communicates back in the most efficient manner. Max, your exceptional ability to say so much in a few words is remarkable. Your ratio of content to number of words used, can only be surpassed by the lift to drag ratio of a modern competition glider…Thank you very much for sharing your wisdom with me. Although this research was done remotely being an external Ph.D. student, Marilena and Max's support and guidance have travelled over the Atlantic Ocean and most of the US continent, all the way to California.

Many thanks are in order to the helpful staff of the Aerospace Engineering faculty, especially Ms. Bertine Markus, and of the graduate school of TU Delft. You were always happy to assist and you have made my personal experience as pleasant as possible.

I was born and raised in Israel, the second child among three. The importance of good education and striving for excellence in this walk of life, are qualities that both my parents worked to instil in me. I would like to express my infinite gratitude to my first ever two teachers, my mother Raymonde and my father Armand of blessed memory. Much of my motivation to pursue a Ph.D. in this later phase of my life, and the need to 'finish the job' was fuelled by these two greatest supporters. I would also like to thank my older brother David, who was my first successful Mathematics teacher. My personal Mathematics 'light-bulb' lit up thanks to you and has remained on ever since.

I would like to thank the educational institution I consider as my 'alma mater'. It is the Israeli Institute of Technology ('Technion'). This excellent institution has prepared me well to the many engineering and scientific challenges I have faced to date. The high standards and knowledgeable professors have made me suffer… but also made me proud to be a graduate of this prestigious institute. I can't mention my aeronautical engineering alma mater without including my flight-testing alma mater. Much appreciation and many thanks go to the US Naval Test Pilot School (USNTPS) in Patuxent River, Maryland. I still consider the yearlong rigorous training back in 1993, as the most challenging and rewarding year of my life.

Last but definitely not least, my upmost appreciation and many thanks go to my immediate family. This Ph.D. research is dedicated to you. To my son and daughter, Ofek and Maya, thank you for challenging me with the most fundamental question of what do I need this Ph.D. for, especially in this advanced phase of my life? Thank you both for keeping me current with the fundamental and advanced concepts of Calculus while seeking for help, even in the middle of the night... This helped me during my research and promoted few ideas. To my wife and life-long partner, Shoshi, thank you very much for your endless support during this unorthodox quest I have embarked on. You have always been there to support me pursuing this dream of mine, although many of our weekends and holidays were consumed by this research. My dearest wife and friend, this Ph.D. research is yours as much as it is mine. THANK YOU!

Ilan Arush

Lancaster, California
September 2023

CURRICULUM VITÆ

Ilan Arush was born on November 11th, 1966, in the town of Rehovot, Israel. After graduating with a Bachelor's in Science in aeronautical engineering from the Israel institute of technology ("Technion") in 1989, he joined the Israeli Air Force.

Ilan served in the IAF for 21 years in a wide range of positions and roles. The majority of his time in the IAF was spent in the flight test center where he planned, conducted and analysed numerous flight test campaigns on both fixed wing and rotary wing aircraft. In 1993 he attended a yearlong course at the US naval test pilot school in Patuxent River, Maryland where he was qualified as a flight test engineer (FTE). Ilan accumulated over 1200 flight hours in various helicopters and jet fighters in a role of a FTE. Amongst his various positions within the IAF, he was the head of rotary wing section in the flight test centre, the program officer for the Sikorsky CH-53 upgrade program and the lead liaison officer for the Sikorsky S70A-55 program. For the later position he was officially commended by the US Army for exemplary performance of duties. Ilan holds a Master's in science in industrial and management engineering from the Ben-Gurion University in Israel.

Since April 2010, Ilan works as a flight test engineer instructor at the National Test Pilot School (NTPS) in Mojave, California. He teaches a variety of graduate level classes in helicopter performance, stability and flying qualities, vibrations, system command and control, and fundamental topics in Mathematics and Physics. He is also the NTPS chief academic officer, a position he was appointed in 2018. Ilan has instructed and trained hundreds of international test pilots and FTEs since 2010.

When not working, Ilan enjoys road and mountain biking, and long hikes. He is married to Shoshi and the couple has two children; Ofek (born March 1998) and Maya (born May 2002).

LIST OF PUBLICATIONS

Journal Publications

1. **Arush, I.**, and Pavel, M. D., "Helicopter Gas Turbine Engine Performance Analysis: A Multivariable Approach", Proceedings of the Institute of Mechanical Engineers, Part G: Journal of Aerospace Engineering, Vol. 223, No. 3, March 2019. https://doi.org/10.1177/0954410017741329

2. **Arush, I.**, and Pavel, M. D., and Mulder, M., "A Singular Value Approach in Helicopter Gas Turbine Engine Flight Testing Analysis", Proceedings of the Institute of Mechanical Engineers, Part G: Journal of Aerospace Engineering, April 2020. https://doi.org/10.1177/0954410020920060

3. **Arush I.**, Pavel M.D., and Mulder M., "A Dimensionality Reduction Approach in Helicopter Hover Performance Flight Testing", Journal of the American Helicopter Society 67, no. 3 (2022): 129–41. https://doi.org/10.4050/JAHS.67.032010

4. **Arush I.**, Pavel M.D., and Mulder M. "A Dimensionality Reduction Approach in Helicopter Level Flight Performance Flight Testing", Journal of the Royal Aeronautical Society, published as First View 13 July 2023. https://doi.org/10.1017/aer.2023.57

Conference Publications

1. **Arush, I.**, "Lateral Center of Gravity Envelope Development for the UH-1N Helicopter", 39th Israel Annual Conference on Aerospace Sciences, Israel, March 1999.

2. **Arush, I.**, & Pavel, M.D., "Flight testing and analysis of gas turbine engine performance: A multivariable approach." In C. Hermans (Ed.), Proceedings of the 44th European Rotorcraft Forum: Delft, The Netherlands, September 2018.